NOTICE

The quality of this microform is heavily dependent upon the quality of the original thesis submitted for microfilming. Every effort has been made to ensure the highest quality of reproduction possible.

If pages are missing, contact the university which granted the degree.

Some pages may have indistinct print especially if the original pages were typed with a poor typewriter ribbon or if the university sent us an inferior photocopy.

Reproduction in full or in part of this microform is governed by the Canadian Copyright Act, R.S.C. 1970, c. C-30, and subsequent amendments.

AVIS

La qualité de cette microforme dépend grandement de la qualité de la thèse soumise au microfilmage. Nous avons tout fait pour assurer une qualité supérieure de reproduction.

S'il manque des pages, veuillez communiquer avec l'université qui a conféré le grade.

La qualité d'impression de certaines pages peut laisser à désirer, surtout si les pages originales ont été dactylographiées à l'aide d'un ruban usé ou si l'université nous a fait parvenir une photocopie de qualité inférieure.

La reproduction, même partielle, de cette microforme est soumise à la Loi canadienne sur le droit d'auteur, SRC 1970, c. C-30, et ses amendements subséquents.

Canada

RIDE DYNAMIC ANALYSIS OF TRACKED VEHICLES

Manuel F. R. Afonso

A Thesis

in

The Department

of

Mechanical Engineering

Presented in Partial Fulfillment of the Requirements
for the Degree of Master of Engineering at
Concordia University
Montreal, Quebec, Canada

April 1989

ISBN 0-315-49108-6

ABSTRACT

RIDE DYNAMIC ANALYSIS OF TRACKED VEHICLES

Manuel F. R. Afonso

Tracked vehicles, such as military battle tanks and personnel carriers, designed for mobility over rough terrains impose severe ride environment. The driver and the crew members of such vehicles are exposed to a comprehensive magnitude of low frequency ride vibrations arising from the vehicle-terrain interactions. Large amplitude low frequency ride vibrations of tracked vehicles limit the performance abilities of the driver and thus the vehicle mobility. Furthermore, prolonged exposure to such ride vibrations imposes health and safety hazards to the driver and the crew members. In this thesis, the ride quality of a military armoured personnel carrier (M113 APC) is investigated through a systematic study of the ride dynamics of the tracked vehicle.

The ride dynamics is investigated through four mathematical models characterizing the dynamics of the wheeled as well as tracked vehicles. The mathematical models include nonlinearities due to damping characteristics of the shock absorbers, Coulomb friction and bump stops. The kinematics and dynamics of the independent trailing arm road wheel suspension is incorporated in the mathematical models, assuming small angles. The ride dynamics of multi-wheeled and tracked vehicles is investigated for deterministic and random terrain excitations. Transient acceleration response at the driver's location is evaluated

for deterministic excitations, arising from semicircle and block obstacles, via direct integration of the nonlinear differential equations of motion.

A frequency dependent linearization technique, based on dissipation of energy, is employed to represent the suspension nonlinearities by an array of local equivalent linear coefficients. The linearized system of equations is solved in the frequency domain to determine the vibration transmission performance of various configurations of road wheel suspension. The random roughness of various terrains is expressed in terms of their displacement and acceleration power spectral density and the ride response of multi-wheeled and tracked vehicles due to the random terrain excitations is evaluated, using local equivalent linearization technique. The sensitivity of response characteristics of the vehicle models to variations in running gear parameters is investigated. Ride quality due to random excitation is assessed based on absorbed power at the driver's location.

ACKNOWLEDGEMENTS

The author wishes to thank his supervisors, Dr. S. Sankar and Dr. S. Rakheja for continued guidance and encouragement in the preparation of this thesis.

The author also wishes to thank members of faculty and staff of the CONCAVE (Concordia Computer-Aided Vehicle Engineering) Research Center, Department of Mechanical Engineering, Concordia University for their time and assistance during the progression of this project.

Support provided by the Department of National Defence in sponsoring this project is gratefully acknowledged.

This thesis is dedicated to the author's parents, Firmino and Gilda, his sister, Linda and niece, Melanie Fatima for their love, patience and understanding for if not for them, this thesis would not have been possible.

Thanks are also due to Jayne Claassen, Suchit Nayak and Arlene Zimmerman for their assistance in typing this manuscript.

TABLE OF CONTENTS

Page

CHAPTER 6

CONCLUSIONS AND RECOMMENDATIONS FOR FUTURE WORK

LIST OF FIGURES

LIST OF TABLES

NOMENCLATURE

SYMBOL	*DESCRIPTION*
a_{dr}	Horizontal distance between hull c.g. and driver's location, (m)
a_{Id}	Horizontal distance between hull c.g. and idler, (m)
a_i	Horizontal distance between hull c.g. and road wheel 'i', (m)
a_{Sp}	Horizontal distance between hull c.g. and sprocket, (m)
a_{si}	Horizontal distance between hull c.g. and shock absorber 'i' at hull chassis, (m)
a_{ti}	Horizontal distance between hull c.g. and torsion bar 'i', (m)
$\bar{a}_j$	RMS acceleration at frequency 'j', (m/sec^2)
b_{dr}	Vertical distance between hull c.g. and driver's location, (m)
b_{Id}	Vertical distance between hull c.g. and idler, (m)
b_{Sp}	Vertical distance between hull c.g. and sprocket, (m)
b_s	Vertical distance between hull c.g. and shock absorber at hull chassis, (m)
b_t	Vertical distance between hull c.g. and torsion bars, (m)
$c_b, c_{\theta b}$	Bump stop contact factors
C_i	Viscous damping coefficient of 'i'th shock absorber, (N·sec/m)
$C_{ji}, \bar{C}_{ji}$	High/low damping coefficients of the 'i'th shock absorber, corresponding to the 'j'th gradient of the force-velocity power curve, (N·sec/m)
$C_i^*(\omega_j)$	Equivalent damping coefficient representing nonlinear damping of 'i'th shock absorber at a frequency ω_j, (N·sec/m)
[C]	Damping matrix, (N x N)
$[C_{eq}^*(\omega_j)]$	Equivalent damping coefficient matrix representing nonlinear damping at a given frequency ω_j, (N x N)
d_c	Permissible clearance between road wheel and bump stop, (m)
d_s, d_I	Clearances of the leading and trailing portions of the track, respectively, with reference to the ground, (m)

d	Peak displacement amplitude, (In inches for Janeway limit ; in mm for Dieckmann's constant)
D_o	Semicircle obstacle diameter, (m)
D_s, D_w, D_I	Diameters of sprocket, road wheel and idler, respectively, (m)
ΔE	Energy dissipated per cycle by the nonlinear shock absorber
f	Temporal frequency, (Hz)
f_o	Frequency constant - German k-factor, (Hz)
F_{bi}	Force due to wheel-to-bump stop contact at wheel 'i', (N)
F_{Di}, F_{di}	Dissipative forces due to shock absorber at wheel 'i', (N)
F_{fi}	Force due to friction of the suspension at wheel 'i', (N)
F_{fLi}, F_{fsi}	Friction force due to 'i'th suspension linkage and shock absorber, (N)
F_L, F_{sa}	Friction force magnitudes, (N)
F_{Ki}, F_{Ci}, F_{sui}	Total suspension spring/damping forces at wheel 'i', (N)
F_{tri}, F_{ti}	Force due to track and/or road wheel tire flexibility, (N)
$F_{\theta bi}$	Force due to road arm/bump stop contact, (N)
$\mathcal{F}_1, \mathcal{F}_2, \mathcal{F}_3, \mathcal{F}_4$	Polynomial functions of frequency for determining absorbed power quantities
$\{F_C\}$	Suspension damping force vector, (N x 1)
$\{F_G\}$	Vector of gravitational forces, (N x 1)
$\{F_K\}$	Suspension stiffness force vector, (N x 1)
$\{F_o\}$	Excitation force vector, (N x 1)
$\{F_{tr}\}$	Track/tire force vector, (N x 1)
g	Gravitational constant, (m/sec^2)
h_o, h_B	Semicircle and block obstacle heights, respectively, (m)
$\mathcal{H}_{pj}(j\omega)$	Complex frequency response function between 'p'th output and 'j'th input variable
$[\mathcal{H}(j\omega)]$	Frequency response function matrix, (N x N)
I_h	Pitch mass moment of inertia of the hull, ($kg \cdot m^2$)

J	Janeway's safe limit
k	Dieckmann's constant
k	German k-factor
K_b, K_p, K_{wi}	Stiffness coefficient of bump stop, track pad, and 'i'th road wheel tire, respectively, (N/m)
K_i	Spring constant of the 'i'th road wheel suspension, (N/m)
K_{tri}	Effective spring constant for the road wheel tire and track pad, (N/m)
$K_{\theta b}$	Equivalent torsional stiffness coefficient representing bump stop, (N·m/rad)
$K_{\theta i}$	Stiffness coefficient of 'i'th torsion bar, (N·m/rad)
$\mathcal{K}_j, \mathcal{K}_o, \mathcal{K}_1$	Absorbed power constants of the human body, $\left(\frac{N \cdot sec/m}{(m/sec^2)^2}\right)$
$[K]$	Suspension stiffness matrix, (N x N)
$[K_b], [K_c]$	Stiffness matrices representing bump stops (N x N)
$[K_f]$	Forced stiffness matrix, (N x n)
L_B	Block obstacle length, (m)
L_S, L_w, L_I	Horizontal distances between the sprocket & the first road wheel, consecutive road wheels, and idler & the last road wheel, respectively, (m)
m_{wi}	Mass of the 'i'th road wheel, (kg)
$[m]$	Mass/inertia matrix, (N x N)
n	Number of road wheels / Number of excitation variables
n_x	Number of longitudinal variables
N	Number of degrees of freedom
$\vec{P}, \vec{P}_T$	Absorbed power associated with vertical and horizontal vibrations, (Watts)
R	Road arm length, (m)
S, S_L, S_P	Overhang Lengths, (m)
$\Phi_a(f)$	Temporal acceleration spectral density of terrain roughness, $((m/sec^2)^2/Hz)$

$\Phi_p(f), \Phi_p(\Omega)$	Temporal/spatial displacement spectral density of terrain roughness, (m^2/Hz, m^2/cycle/m)
$\Phi_{jk}(f)$, $\Phi_{jk}(\omega)$	Temporal/radial spectral density of input variables (CSD for $j \neq k$, PSD for $j=k$), (m^2/Hz, m^2/rad/sec)
$\Phi_d^p(\omega)$	Power spectral density displacement of the 'p'th response variable, (m^2/rad/sec)
$[\mathcal{S}_d(\omega)]$	Spectral density matrix of response variables, (N x N)
$[\mathcal{S}_{dd}(\omega)]$	General spectral density matrix of response variables other than the generalized coordinate variables
$[\mathcal{S}_w(f)]$	Temporal spectral density displacement input matrix, (n x n)
t, t_f	Time coordinate and predetermined time, respectively, (sec)
t_{oS}, t_{oi} t_{oI}	Time corresponding to instantaneous positions of leading portion of track, consecutive road wheels, and trailing portion of track, respectively, with respect to approaching obstacle, (sec)
t_{st}	Time corresponding to starting position of vehicle, (sec)
T_i^l, T_i^r	Forces due to tension of the track acting on the left and right of road wheel 'i', respectively, (N)
T_I, T_S	Forces due to tension of the track between road wheels '5' & idler, and between sprocket & road wheels '1', respectively, (N)
$\mathcal{T}_{\theta bi}$	Torque due road arm/bump stop contact, (N·m)
$[T_D], [T_L]$	Transformation matrices established from constraint equations representing relative displacements across the shock absorbers and suspension linkages, respectively, (n x N)
$[T_\theta], [T_{\theta H}]$	Transformation matrices established from constraint equations representing road arm/wheel absolute and relative rotation response, respectively, (n x N)
$[T_X]$	Transformation matrix established from constraint equations representing longitudinal response, (n_x x N)
V	Vehicle speed, (m/sec)
x	Distance travelled by vehicle, (m)
x_{dr}, x_{wi}	Longitudinal displacement at the driver's location, & 'i'th road wheel, respectively, (m)
x_{oi}, x_{oI}, x_{oS}	Instantaneous horizontal location of the 'i'th road wheel, trailing and leading track segment, respectively, with respect to approaching obstacle, (m)

x_{st}	Starting position of vehicle with respect to obstacle , (m)
$\{X_W(j\omega)\}$	Fourier transform of vector containing longitudinal response variables
y_{dr}, y_h, y_{wi}	Vertical displacement of the driver's location, hull c.g., & 'i'th road wheel, respectively, (m)
y_{hs}, y_{trs}, y_{ws}	Static deflection of wheel suspension, track pads/tires, and road wheel tires, respectively, (m)
y_{oi}, y_{oI}, y_{oS}	Vertical coordinate of terrain at 'i'th road wheel, trailing and leading track segments, respectively, (m)
$\bar{y}_{oi}(\omega_j)$	RMS excitation amplitude due to terrain roughness at the 'j'th discrete frequency, (m)
$\psi_{ij}, \mathcal{Y}_{ij}$	Relative displacement and peak amplitude across the 'i'th shock absorber at the 'j'th frequency, (m)
$\{y\}$	Vector of response variables, (N x 1)
$\{Y(j\omega)\}$	Fourier transform of vector containing bounce and pitch response variables, (N x 1)
$\{Y_O(j\omega)\}$	Fourier transform of vector containing excitation variables, (n x 1)
$\{\mathcal{Y}\}, \{\mathcal{Y}_L\}$	Relative displacement vectors, (n x 1)
w	Waviness of terrain
α	RMS acceleration, German *k*-factor, (m/sec^2)
β_o	Shock absorber inclination, (rad)
χ_1, χ_2, χ_3	Constants, ($k/m/sec^2, k/mm/sec^2, k/mm/sec^2$)
δ	Conversion factor
ε	Error parameter
ϕ_h	Pitch rotation of the hull c.g., (rad)
γ_o	$= \theta_o + \beta_o + \zeta_o - \frac{\pi}{2}$
$\{\Psi_i\}, \{\Psi_{Di}\}$	Eigenvectors of undamped and damped vehicle models, (N x 1)
η	Number of discrete frequencies
λ_i, λ_{Di}	Eigenvalues of undamped and damped vehicle models for the 'i'th vibration mode

θ_c Permissible angular clearance between road arm and bump stop (rad)

θ_o, θ_s Initial and static inclinations of road arm, respectively, (rad)

θ_{wi} Pitch rotation of the 'i'th road-arm, (rad)

$\{\Theta(j\omega)\}$ Fourier transform of vector containing road arm/wheel rotation response variables, (n x 1)

$\{\Theta_L\}$ Response vector of relative rotation of the road arm with respect to hull chassis, (n x 1)

μ_I, μ_S, μ_w Stiffness coefficients for trailing and leading portions of the track, and track portions between road wheels, respectively, (N/m)

v, σ RMS velocity & displacement, (mm/sec, mm)

τ_S, τ_w, τ_I Time delays between sprocket & first road wheel, consecutive road wheels, and idler & last road wheel, (sec)

v_i Relative velocity across the 'i'th shock absorber of the wheel suspension, (m/sec)

v_{Ai}, v_{Bi} Velocities of the 'i'th shock absorber link, (m/sec)

v_f Infinitesimal velocity band in the friction force-velocity characteristics, (m/sec)

v_p Velocity corresponding to transition of high/low damping coefficient of shock absorber power curve, (m/sec)

ω Radial frequency, (rad/sec)

ω_{ni}, ω_{Di} Undamped and damped natural frequencies of the 'i'th vibration mode, respectively, (rad/sec)

Ω Spatial frequency of road roughness, (cycle/m)

ξ_i Damping ratio of the underdamped 'i'th vibration mode

ζ_o Angle between line bisecting overhang and road arm centerline, (rad)

$(\cdot)$ designates differentiation with respect to time

$*$ designates complex conjugate

T designates transpose

Re designates real part

CHAPTER 1

INTRODUCTION AND LITERATURE SURVEY

1.1 INTRODUCTION

The performance of off-road vehicles, either wheeled or tracked, is assessed by their power and mobility. In view of rough off-road terrains, an increasing demand on larger power-to-weight ratio and higher speeds, research and development efforts have been mounted to improve suspension systems to achieve efficient utilization of power, and safety and ride comfort of the vehicle operator(s). Tracked vehicles, such as military battle tanks and personnel carriers, designed for mobility over rough terrains, impose severe ride environment due to vehicle-track-terrain interactions. A typical armoured personnel carrier (APC), as shown in Figure 1.1, comprises of a hull supported by a number of road wheels and suspension. The number of road wheels, enveloped by a track driven by the sprocket, are selected depending upon the power required for combat. The operating performance of the armoured tracked vehicle depends primarily on the power and mobility of the vehicle.

In view of the increased power-to-weight ratio and mobility requirements, the driver and the crew are inevitably exposed to a comprehensive magnitude of ride vibrations, arising from dynamic terrain-vehicle interactions. The crew members are affected adversely due to the low frequency nature of the terrain-induced vibrations, transmitted to the hull through the track and vehicle suspension. Prolonged exposure to such low frequency and large amplitude ride vibrations of tracked vehicles causes operator bodily discomfort, physiological damage and increased inefficient performance, and thus the

mobility performance of the vehicle is limited. Poor performance rate of the vehicle operator has been attributed to various effects of vehicle vibration; namely, operator's slow reaction time, errors in compensatory tracking, loss of foot pressure constancy and visual acuity [1].

In view of detrimental effects of ride vibration on the health and safety of vehicle drivers, the ride dynamics of wheeled vehicles has drawn extensive research and development efforts [2,3,4]. However, only a few similar studies on the ride dynamics of tracked vehicles have been reported in the literature. A number of experimental and analytical studies have been conducted to develop effective wheel suspension to achieve improved mobility performance of the tracked vehicles. A brief review of the relevant literature is presented in the following section.

1.2 REVIEW OF RELEVANT LITERATURE

Recent trends toward increased power-to-weight ratio and mobility of military ground vehicles has drawn significant efforts in development of effective running gear for such vehicles. However, the requirements of increased vehicle mobility performance have lead to considerable increase in the magnitude of ride vibrations due to vehicle-track-terrain dynamics. Previous investigations on these vehicles include a diversity of emphasis concerning the tractive performance, gradability, steering response, stability, braking, etc. Numerous analytical and experimental studies have been carried out to assess the performance of running gear and vehicle mobility. However, the studies on ride dynamics of these vehicles have been limited.

Investigations on dynamics of tracked vehicles in view of the running gear have established that dynamics of tracks contribute

considerably to the dynamic response of the vehicle. Eppinger *et al.* [5] developed and analyzed an in-plane model of the tracked vehicle to illustrate the effects of the track loads on the dynamic response of the vehicle. A six-wheeled tracked vehicle is modeled as a two-degree-of-freedom (hull bounce and pitch) dynamical system, incorporating suspension bump stops, wheel lift-off, and nonlinear suspension damping, as shown in Figure 1.2. Influence of running gear components, such as the road wheel suspension and the track on the dynamic response of the hull is investigated. The analytical model was validated against the laboratory measured response of a prototype vehicle with and without the track. The analytical and experimental acceleration response at the hull center of gravity of the vehicle with and without the track tension, due to excitation from a trapezoidal-shaped bump revealed that the addition of the track increases the severity of the ride.

Lessem and Murphy [6] developed a mathematical model based on data compiled from field tests of four tracked vehicles of different weights and running gear. The mathematical model incorporates the degrees-of-freedom associated with the bounce and pitch motion of the hull as well as the vertical motion of each road wheel. The number of degrees of freedom of the system depends on the number of wheels of the vehicle considered. Figure 1.3 illustrates an eight-degree-of-freedom model of the six-wheeled M60 A1 battle tank. Dynamic tension of the track is represented by interconnecting linear springs between each road wheel, where the spring constant is determined based on the weight of each road wheel against the track. The spring constant of the track segment between the sprocket and the first road wheel is determined using three

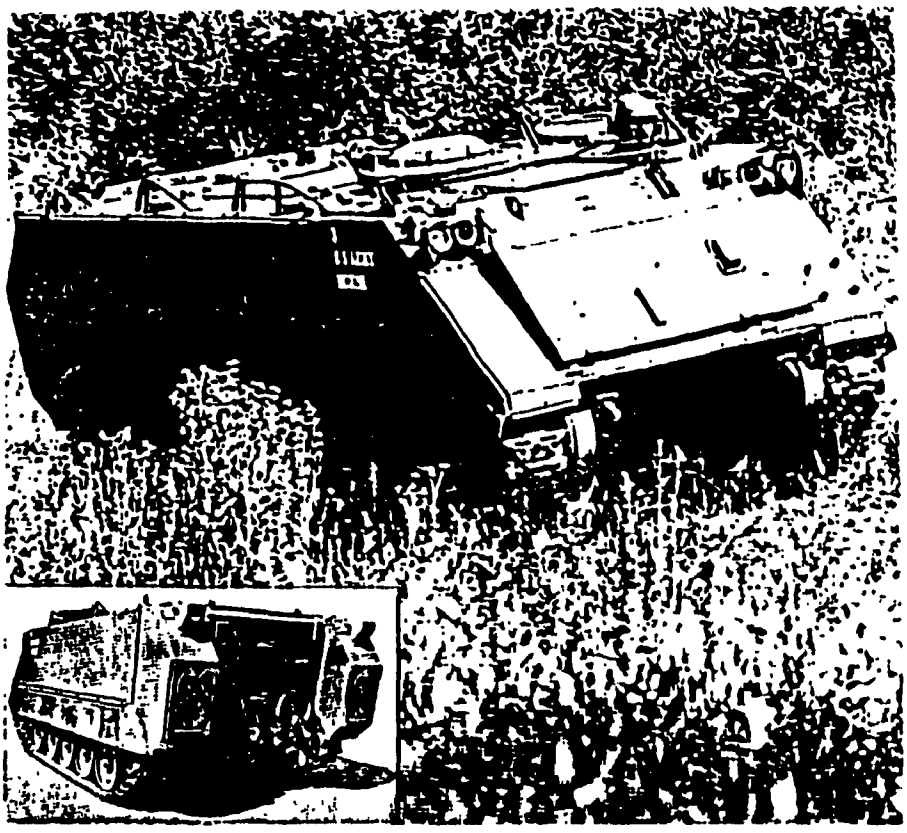

Figure 1.1 The M113 (APC) Personnel Carrier (COURTESY OF FMC).

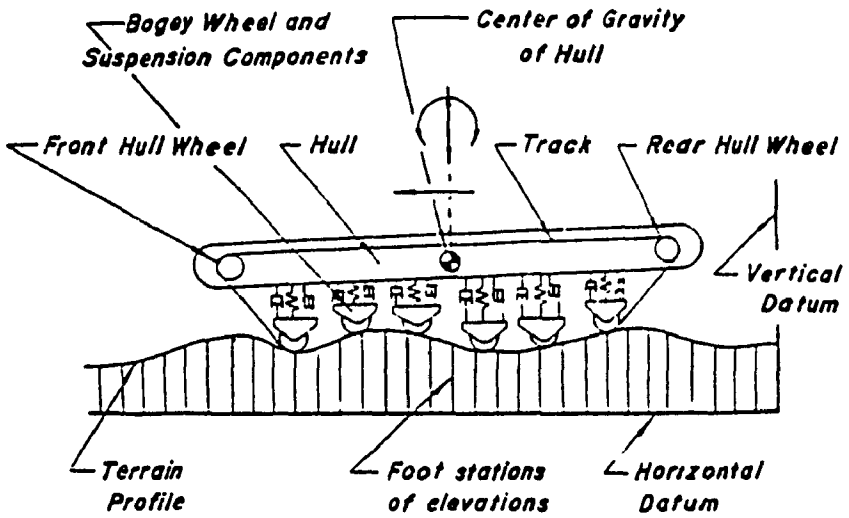

Figure 1.2 Schematic Representation of an In-Plane Tracked Vehicle Model [5].

I = pitch moment of inertia

M, M_i = mass of main frame and ith bogie assembly, respectively

$K(\Delta_i)$ = force-deflection relation for ith bogie suspension

$C(\Delta_i)$ = force-velocity relation for ith bogie suspension

μ_i = spring constant for ith track spring

z = vertical motion at c.g. of main frame

z_i = vertical motion at c.g. of ith bogie

θ = angular motion at c.g of main frame

x = horizontal motion at c.g. of main frame

Δ_i = relative motion between main frame and ith bogie c.g.

l_i = horizontal distance from c.g. of main frame to contact point of ith bogie

s = vertical distance from c.g. of main frame to bogie c.g.

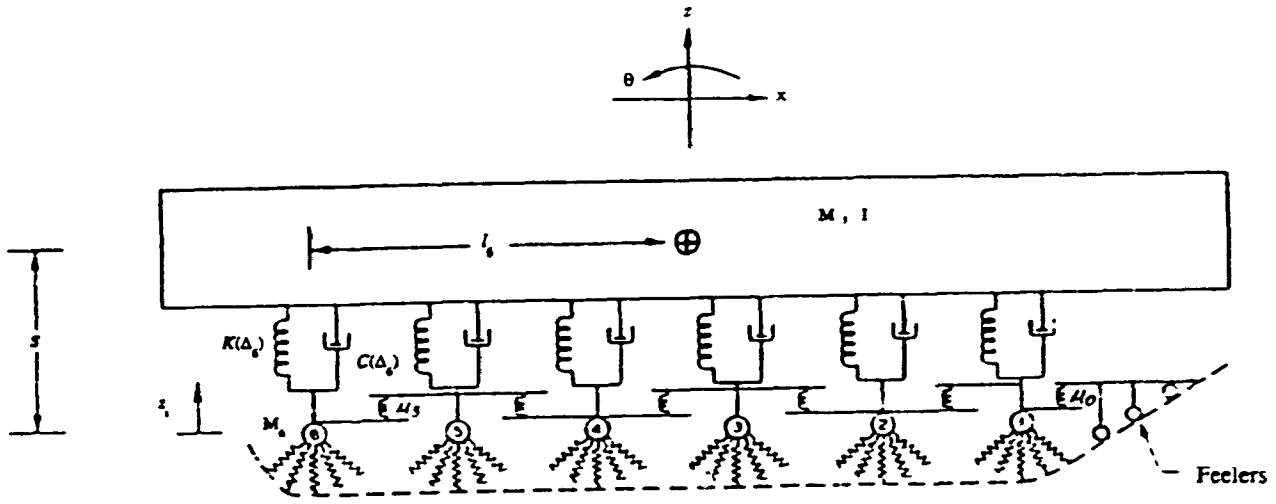

Figure 1.3 Schematic Representation of M60 A1 Battle Tank Model [6].

massless feelers placed against the track. The road wheel tires are modeled as radial springs, and the horizontal tire forces are used to determine the longitudinal response at the hull. Results obtained via computer simulations are compared to the experimental results involving M29, M113, M114, and M4 vehicles. The test vehicles with and without the track were towed over an array of half-round rigid obstacles and a sequence of ditches, and the corresponding acceleration response was recorded. The analytical and experimental studies revealed that the interactions of the track are strongly dependent on vehicle speed. The track produced a smoothing effect at low speeds while the ride quality at higher speeds is deteriorated due to track interactions.

Hoogterp [7] developed a mathematical model of a two-wheeled vehicle for evaluating the ride dynamic response of a tracked vehicle due to terrain undulations, as shown in Figure 1.4. The ride dynamic response of the vehicle is evaluated in terms of pitch and vertical motion of the hull, and the vertical motion of the road wheels, while the dynamic interactions of the track is neglected. The model may be adapted for a multi-wheeled vehicle. The road wheel tires are represented by 'point-follower' springs and dampers. Driver comfort limiting velocity, the velocity at which the absorbed power of vibration levels at the driver's location approaches six watts is determined as a function of terrain roughness. Results showed that comfort limiting velocity, decreases for rougher terrains.

The above studies describe linear mathematical models using vibration theory at its most basic. The primary objective of the studies conducted by Eppinger *et al.* [5], and Lessem and Murphy [6], was merely to determine the contribution of track tension to the dynamic

response of the vehicle. However, the model developed by Hoogterp [7], emphasizes on the ride comfort and ride quality of tracked vehicles. A number of analytical techniques have been proposed to describe the complex phenomena associated with the vehicle-track-terrain interactions. Lee [8] presented a method of analysis for describing the cyclic chordal action of the track, defined as variation in velocity of the track as it passes over a sprocket or the road wheel, using a receptance technique. It has been established that low frequency noise and vibration is experienced in the vehicle compartment when the track leaves the last road wheel to engage with the idler and the sprocket due to cyclic chordal action of the track [9]. These studies on dynamic forces acting on the idler supports have been employed to describe favourable idler wheel configuration, compliance of the idler arm and geometry of the track shoe assembly to minimize the vibrations arising from the track-idler interactions. Galaitsis [10] outlined a method for predicting dynamic loads due to the track, that occur in high speed M113 vehicles. A mathematical model was developed emphasizing the interactions between the track shoes and road wheels of the tracked vehicle. The two-dimensional model incorporates dynamics of all the road wheels, the track loop, rigid suspension and flat ground profile. The equations of motion for the track loop were developed by considering the inertias of the shoes, and stiffness and damping characteristics of the rubber bushings inserted between each shoe as shown in Figure 1.5. The shoe-wheel interactions are taken into account by considering the properties of shoe pads and the friction forces exerted by the wheel on the pads. The track tension and track bending moment established by the analytical model are validated via experimental investigations.

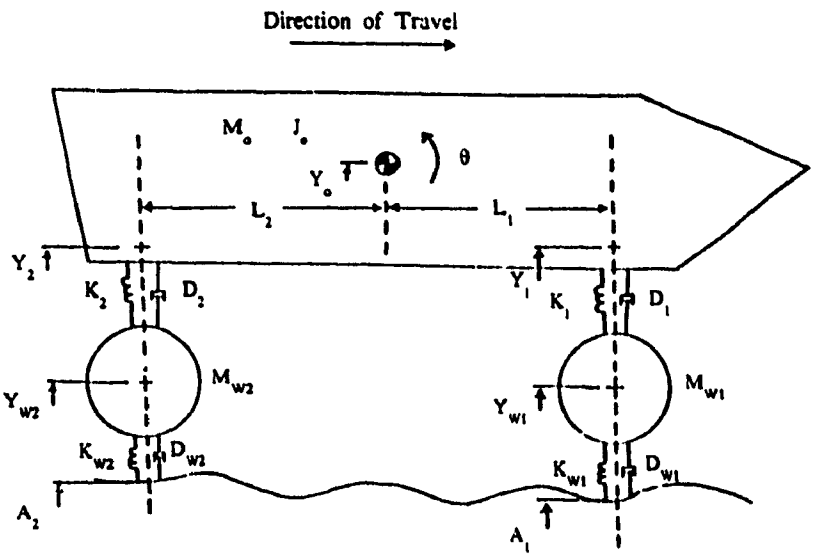

M_o = 1/2 the sprung mass of the vehicle

J_o = 1/2 the sprung pitch moment of inertia of the vehicle

M_{Wi} = the mass of wheel i

K_i = the spring rate at wheel i

D_i = the damping rate at wheel i

K_{Wi} = the spring rate of wheel i

D_{Wi} = the damping rate of wheel i

Y_i = the hull reference position of wheel i

Y_{Wi} = vertical position of wheel i

θ = the pitch angle of the vehicle (front end up is positive)

Y_o = the vertical position of the CG

A_i = the terrain elevation at wheel i

L_i = the horizontal distance from the CG to wheel i

Figure 1.4 Schematic Representation of Vehicle Model with Two Wheels per Side [7].

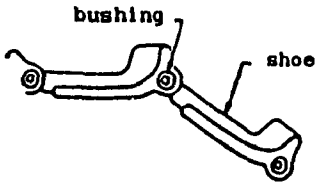

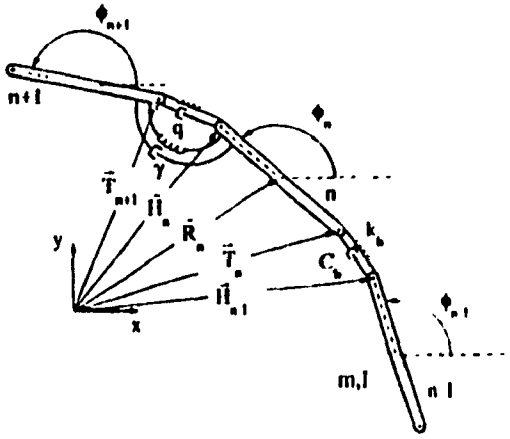

m = mass of shoe

I = moment of inertia of shoe

k_b = shoe-shoe coupling spring rate

C_b = shoe-shoe coupling damping rate

T_n, H_n = tail and head displacement on nth shoe

ϕ_n = angular displacement of nth shoe

q = shoe-shoe coupling torsional spring rate

γ = shoe-shoe coupling torsional damping rate

Figure 1.5 Track Shoe and Bushing Models [10].

Garnich and Grimm [11] developed an in-plane model of the M60 A1 tracked vehicle with trailing arm suspension. The M60 A1 battle tank is modeled as an eight-degree-of-freedom discrete dynamic system, incorporating the motions of each road arm and road wheel assemblies, and vertical and pitch motions of the main frame of the vehicle, as shown in Figure 1.6. The torsion bars connecting the road arm and road wheel to the hull chassis are modeled as constant rate torsional springs, while the shock absorbers mounted at the first and last road wheels are represented by linear torsional dampers. The tires are represented by radial springs and dampers while overloading springs are used to represent bump stops. The contribution of the track loads to the vehicle dynamics is accounted for by considering four different types of track tension (Figure 1.7): global track tension, drive sprocket induced tension, track bridging effect, and tension due to track compensating linkage. The global track tension is determined from the change in the overall track length and thus the track tension is assumed to be uniform over the entire track. The bridging effect involves the track creating a flexible bridge spanning terrain concavities. The drive sprocket induced tension is determined from the sprocket torques as the vehicle passes over an obstacle, while the slack in the track is taken up by the compensating linkage next to the idler. The analytical results established for deterministic excitations are validated via an array of experimental investigations, varying from simple static deflection checks to track effects which influence the individual road wheels. Simulation inputs included undeformable level ground and discrete rigid half round obstacles.

McCullough and Haug [12] extended the concept of superelement

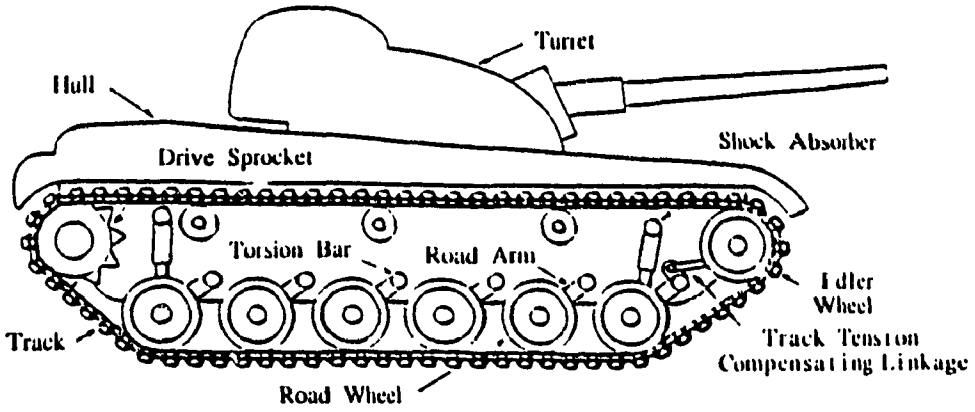

(a). M60 battle tank

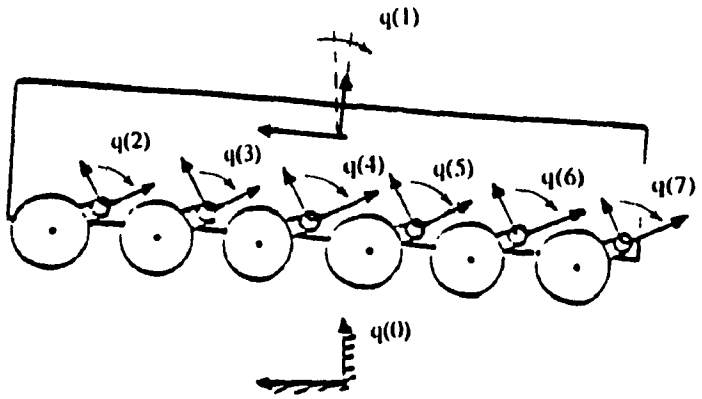

q(0), q(1) = translational and rotational motion of the hull, respectively

q(i), i=1,...,7 = rotational motion of road wheel assemblies relative to the hull

(b). Generalized coordinates and frames of reference

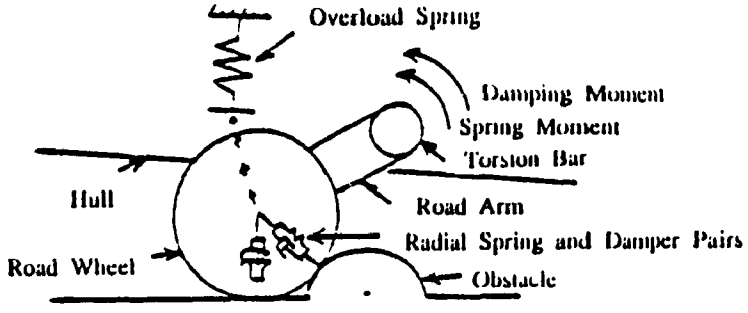

(c). Road wheel model

Figure 1.6 Schematic Representation of the M60 Tank Model [11]

representation of recurring subsystems in mechanical system modeling to a military vehicle. The running gear subsystem, including the track, sprocket, idler, road wheels and road arms, is defined as a superelement. The model incorporates the track forces, suspension forces, track-wheel-ground contact forces, and connectivity and bridging of the track. The track tension is approximated by catenary equations. The absorbed power of the vertical accelerations at the driver's location is established via simulation and experimentation, when the vehicle is traversing obstacles. The absorbed power due to driver acceleration indicated that track bridging contributes to an improved ride quality. Krupka [13] developed a comprehensive three-dimensional mathematical model for the tracked vehicles. The equations of motion for a military battle tank, are derived using Lagrange's formulation. The tank is represented by three distinct bodies; the hull, turret and main gun, each having six degrees of freedom. The gun bending effects are also included in the model.

Numerous computer programs have been developed to carry out the dynamic analysis of military tracked vehicles. Galaitsis [10] developed the TRAXION software to compute the dynamic track loads. Hoogterp [7] developed an integrated computer package consisting of four modules: vehicle parameters and terrain characteristics; request of output information; dynamic simulation over cross-country terrains; and dynamic simulation over discrete obstacles. Wheeler [14] developed a comprehensive simulation package to simulate for in-plane dynamics of the vehicle subjected to terrain inputs. The program was developed for the XM1 tank although it has been applied to a 3/4-ton truck and the combat tracked vehicle signature duplicator, CTVSD. The simulation

model considers two degrees of freedom (pitch and bounce) associated with the vehicle sprung weight with an additional degree of freedom for each road wheel, as shown in Figure 1.8. The package employs MIMIC simulation language for the solution of equations of motion, and thus allows for variation in parameters such as; number and location of road wheels, spring rates, damping characteristics, road arm lengths, vehicle speed, sprung weight, pitch moment of inertia, etc.

A comprehensive analytical and experimental study of track dynamics was undertaken by Meachom *et al.* [15]. Analytical techniques are developed to predict vibration modes of the track, chordal effects, dynamic track tension and path, energy dissipation, tension during negotiation of an obstacle, distribution of track tension, pin/bushing stresses and deflections, temperature buildup, and end connector tightening effectiveness. Various computer codes, developed to simulate for track dynamics are listed in Table 1.1. Of the various computer software developed, the TRACKOB, based on finite-element methods, is perhaps the most comprehensive one, which predicts the dynamic tension of the track. TRACKOB II simulates an in-plane vehicle model, formulated to predict track tension when the track is deflected uniformly across its width by an obstacle. The model is formulated for the M60 tank, based upon the track segment that crosses over the obstacle, as shown in Figure 1.9. A three-dimensional model, TRACKOB III, was developed to simulate the instance when an obstacle falls under only one edge of the track.

Beck and Wehage [16] conducted a study to investigate the use of force feedback servo control mechanisms to improve the man-machine interaction and the response of an articulated tracked vehicle. The

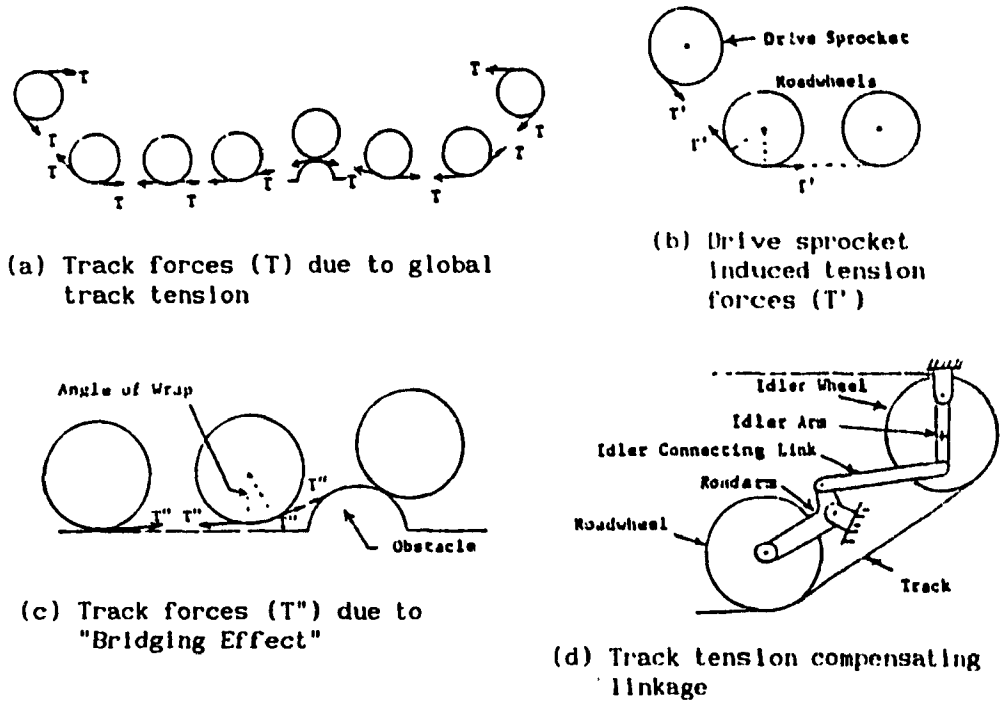

(a) Track forces (T) due to global track tension

(b) Drive sprocket induced tension forces (T')

(c) Track forces (T") due to "Bridging Effect"

(d) Track tension compensating linkage

Figure 1.7 Track Forces due to Global Track Tension, Drive Sprocket Induced Tension, Track Bridging Effect, and Track Compensating Linkage [11].

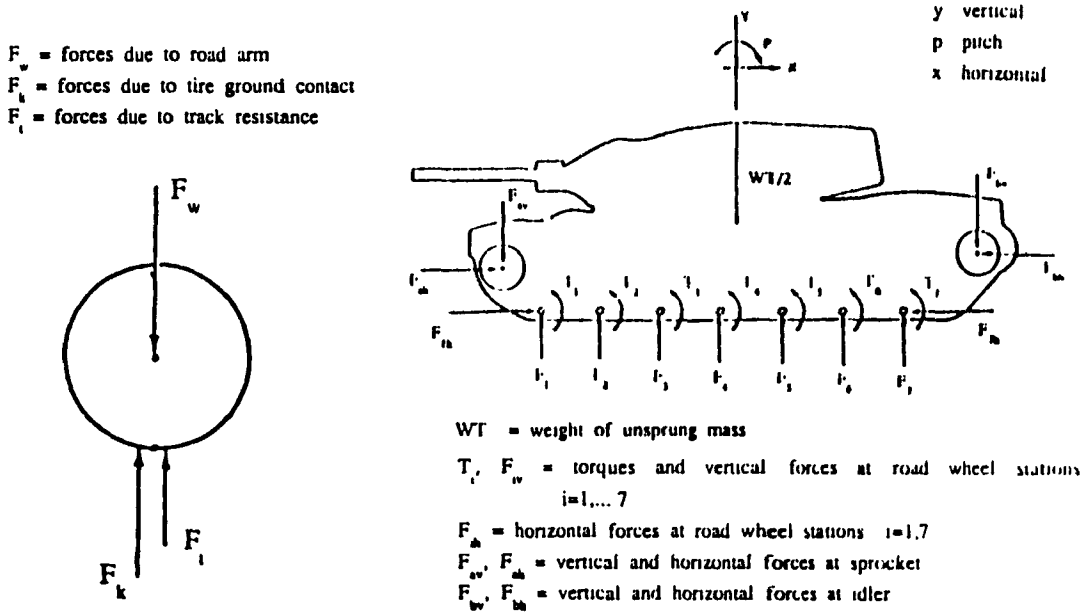

Figure 1.8 Schematic of a Multi-Degree-of-Freedom XM1 Tank Model [14]

TABLE 1.1

TRACK DYNAMICS ANALYSES SOFTWARE [15]

	Analysis	Type	Main Output	Condition
(1)	BUSHSTRESS	Computer	Rubber bushing stresses	Track assembled, no tension (2D)
(2)	PINSTRESS II	Hand	Pin stresses and deflections, bushing deflections	Static condition--uniform or nonuniform tension across track width (3D)
(3)	TRACKOB II	Computer	Localized track path and tension	Uniform obstacle across track width (2D)
(4)	TRACKOB III	Computer	Localized track path and tension	Nonuniform obstacle across track width (3D)
(5)	TRACKVIBE	Computer	Vibration frequencies and amplitudes	Track sections free vibration
(6)	CHORDACT	Computer	Localized tensions and deflections	Track moving over sprocket or front idler
(7)	TRACKCENT	Hand	Overall track path and tension	Track moving (centrifugal force effects)
(8)	TRACKDYNE	Computer	Localized tension, path, energy loss, force	Track moving over front idler and road wheel (2D)
(9)	WEDGEND	Hand	End connector bolt torque versus bushing torque	Tightening wedge-type end connector
(10)	SHOETEMP II	Computer	Track shoe temperature distribution	Vehicle moving on smooth, hard surface (2D)
(11)	SHOETEMP III	Computer	Track shoe temperature distribution	Vehicle moving on smooth, hard surface (3D)

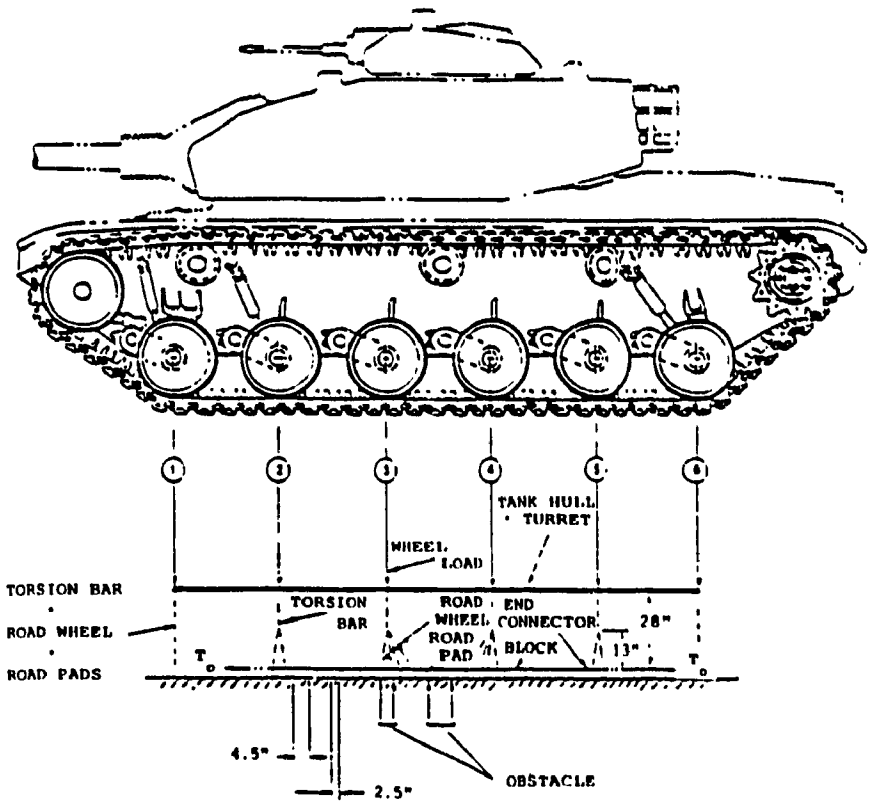

(a) TRACKOB model used to predict track loads and deflections over obstacle.

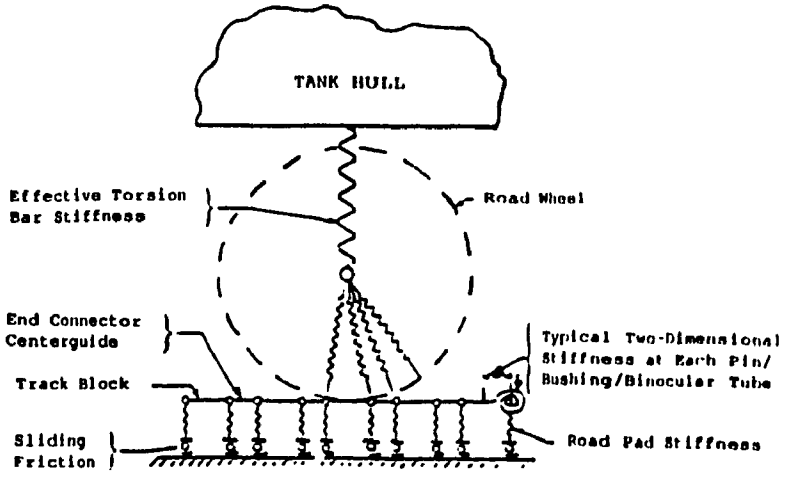

(b) Two-dimensional finite-element model of third road wheel and track.

Figure 1.9 Model Representation of M60 Tank used in TRACKOB II [15]

general purpose DADS (Dynamic Analysis and Design System) Software, was utilized to formulate the equations and geometric constraints describing two identical M113 tracked vehicles coupled by an electro-hydraulic servo-controlled articulation joint. The primary objective in this study was to investigate the potential of the controlled articulation and to compare mobility performances of the articulated and the single vehicle, specifically in view of obstacle crossing characteristics. In view of improving suspension performance of tracked vehicles, feasibility analyses involving fluidically-controlled suspension systems have also been conducted by various researchers [17,18].

A comprehensive computer code, referred to as NRMM (Nato Reference Mobility Model), is extensively used by the military to evaluate the off-road mobility performance of armoured vehicles. Selected submodels are integrated to predict maximum cross-country speed of tracked or wheeled vehicles in any terrain environment [19]. The NRMM package includes the VEHDYN (Vehicle Dynamics) module to simulate dynamics of the tracked vehicles with rigid, independent, walking-beam, and bogie type suspensions. VEHDYN [20] describes the state (accelerations, velocities, and displacements) at any point of the vehicle as it travels over a given profile. The U.S. Army Engineer Waterways Experiment Station (WES) [21] has employed the AMC (Army Mobility Code) to predict cross-country vehicle performance and to investigate effects of design changes on the performance of existing vehicles, namely the M35 A2, 6X6 $2\frac{1}{2}$ ton truck and the M113 A1 personnel carrier. The AMC model, an earlier version of the NRMM, was specifically designed to predict mobility performance of ground vehicles for various terrains [22]. The influence of suspension characteristics on the vehicle mobility is

investigated for three types of suspension: the standard torsion bar, hydropneumatic, and modified torsion bar suspensions. The results revealed that these suspension systems have only insignificant effects on the mobility performance.

Maclaurin [23] described a computer system used by British researchers for military tracked vehicle simulation. The AD (Applied Dynamics) digital computer with multiprocessing capability, specifically designed for high speed simulation of complex dynamic systems was used which allows for analysis of suspension models including active suspensions. The vehicle is modeled in the pitch and bounce plane and accounts for the various nonlinearities in springs, dampers, Coulomb friction, tire stiffness, wheel/terrain separation, sprocket and idler terrain contact. The track is modeled by equating the peripheral length, catenary action and track tension. The vehicle models can be simulated for deterministic as well as random profiles. Maclaurin [23] conducted analytical and experimental studies to determine the influence of suspension characteristics on mobility performance of battle tanks. An MCV (Mechanised Combat Vehicle), fitted with torsion bars and rotary vane hydraulic dampers, and the Challenger, fitted with the hydrogas suspension were tested for various terrains. Results revealed that the Challenger exhibited higher limiting speeds with acceptable vibration levels than the MCV.

A number of experimental studies on vehicle suspensions have been carried out by various researchers [24,25,26,27]. Murphy [24] investigated the experimental ride and shock response of a tracked vehicle fitted with improved suspensions. Ride and shock responses were obtained for an M60 tank fitted with three types of suspensions: a

hydropneumatic suspension (HSS); an advanced torsion bar suspension (ATB); and a combination of hydropneumatic and advanced torsion bar. The experimental study concluded that the M60 HSS/ATB hybrid vehicle offers better ride quality. Austin *et al.* [25] conducted tests on shock absorbers installed on IFV (Infantry Fighting Vehicle) tanks and M113 personnel carriers to establish the force-velocity characteristics of the various shock absorbers. Giguere [26] investigated five different suspension configurations as possible solutions to track/suspension interference problems, which is often encountered in M113 A2 APCs equipped with Diehl tracks. The track/suspension interference primarily arises from the repetitive hitting of track end connectors against the suspension guards due to excessive relative dynamic motion, thus leading to rapid track wear. The track/suspension interference performance of an M113 A2 APC, fitted with the stiffer A1 torsion bar, has been evaluated in relation to conventional M113 A1 and M113 A2 configurations, via field tests. Field tests involving the ride and handling characteristics were conducted for an unladen and combat-loaded vehicle traversing various test courses. Results showed that the M113 A2 fitted with A1 torsion bars can eliminate the track/suspension interference problem. Mobility performance evaluation of the new M113 A1$\frac{1}{2}$ vehicle configurations revealed that average maximum speed on selected test courses is similar to that of the M113 A2 vehicle [27].

Terramechanics involving track-ground interactions such as sinkage and ground compaction for military tracked vehicles has also drawn considerable attention in the study of vehicle mobility. Vodyanik [28] developed a set of force equations describing the soil-track interaction. Kogure [29] dealt with the external motion resistance of a tracked

vehicle caused by rut formation (sinkage) or compaction of soil under the tracks. Kitano and Kuma [30] presented a theoretical analysis of non-stationary motion of a tracked vehicle on level grounds. An analytical model that includes track slippage, inertial forces, and moment of inertia was developed to analyze and predict steering dynamics and steerability of the vehicle. Bekker [31,32] presented insight on the theory of soil mechanics and the interrelationship with tracked vehicles such as rut making and ground compaction including snow, and how these constraints result in higher locomotive resistance which lowers fuel economy. More recently, Wong *et al.* [33] presented an analytical framework for predicting the ground pressure distribution and tractive performance of tracked vehicles. The prediction of ground pressure distribution under the track has become of vital importance since vehicle sinkage and motion resistance is critical to vehicle mobility. It is also important to the steering dynamics of the vehicle since turning resistance depends on the ground pressure. The above terramechanics studies have concentrated on vehicle mobility and environmental protection, however, information pertaining to track-terrain interactions may be acquired and may be useful to ride dynamic response analysis of the vehicle crossing over deformable terrains.

1.3 SCOPE OF THE PRESENT RESEARCH WORK

The primary objectives of this thesis research are to evaluate the ride dynamics of a tracked military personnel carrier (M113 APC) via computer simulation and to investigate the significance of the running gear in view of the ride vibration levels at the driver's location. The specific objectives of the proposed research are as follows:

1) To develop a comprehensive mathematical model of a multi-wheeled and tracked vehicle to carry out the ride dynamic analyses.

2) To analyze the vibration transmission performance of various multi-wheeled/tracked vehicle suspension configurations.

3) To evaluate the ride vibration response of the multi-wheeled and tracked vehicles subject to deterministic obstacles and random terrains.

4) To assess the ride quality at the driver's location.

5) To carry out parametric sensitivity analyses to illustrate the influence of vehicle suspension and track parameters on the ride dynamics of the multi-wheeled and tracked vehicles.

In Chapter 2, various configurations of the tracked vehicle, M113 APC are described. Mathematical models of the multi-wheeled and tracked vehicle are formulated based on a building block approach. Dynamic loads arising from the track, road wheels, suspension, and terrains are identified and incorporated into the mathematical models to determine the ride vibration levels at the vehicle hull. Major assumptions associated with model formulations are discussed.

In Chapter 3, the military test courses are briefly reviewed and the excitations arising from the deterministic as well as random terrains are discussed. The roughness of selected random terrains is expressed by its displacement and acceleration power spectral densities (PSDs) as a function of vehicle speed. The deterministic excitations arising from half-round and block obstacles are presented.

In Chapter 4, the analytical techniques for solving the differential equations of motion characterizing the dynamics of the

multi-wheeled/tracked vehicle models are discussed. Eigenvalue analysis of the vehicle models is carried out to evaluate the free vibration response. The various techniques for solving the nonlinear differential equations are summarized. The nonlinear equations of motion are linearized using local equivalent linearization technique based on dissipation of energy. Transmissibility characteristics of the linearized system are obtained and compared to that of the nonlinear model established via numerical integration. The sensitivity of the hull response to variations in suspension and track parameters is investigated. The ride dynamic response of the multi-wheeled and tracked vehicles to random terrains, and discrete semicircle and block obstacles is presented.

In Chapter 5, the proposed ride assessment techniques are discussed and the ride quality of the tracked vehicle is presented in terms of absorbed power of the vibration levels at the driver's seat location for M113 vehicles traversing selected terrains. Parametric sensitivity analysis is carried out to study the influence of running gear parameters on the ride quality of M113 vehicles.

In Chapter 6, the conclusions and recommendations for future work are presented.

CHAPTER 2

DEVELOPMENT OF VEHICLE RIDE MODELS

2.1 INTRODUCTION

The dynamic behaviour of tracked vehicles is primarily dominated by the track-terrain interactions and vehicle suspension. Thus, a comprehensive mathematical model of the tracked vehicle must identify and characterize the dynamics associated with the track and wheel suspension. During the modeling stage, it is usually desirable to develop a simple and credible model such that the dynamics of the vehicle is fully described. Simplicity of the model is determined by its degree-of-freedom whereas the credibility of the vehicle model is demonstrated by its capability to simulate the vehicle behaviour realistically within the desired accuracy.

In the case of tracked vehicles, there exists a high degree of complexity associated with track-terrain interactions, track pull, suspension spring loads, Coulomb and viscous damping forces, and road arm linkage mechanisms. A building block modeling approach is used to develop four ride dynamic models of the tracked vehicle with varying complexities. Various suspension forces and track loads are identified and incorporated in the mathematical models to evaluate the ride vibration response. In this chapter, the running gear of an armoured personnel carrier (M113 APC) is described and dynamic loads arising from the track, road wheels, suspension and terrains are identified. The systematic development of various multi-wheeled/tracked vehicle models is presented along with underlying assumptions.

2.2 THE M113 APC PERSONNEL CARRIER

Figure 2.1 illustrates a typical M113 armoured personnel carrier

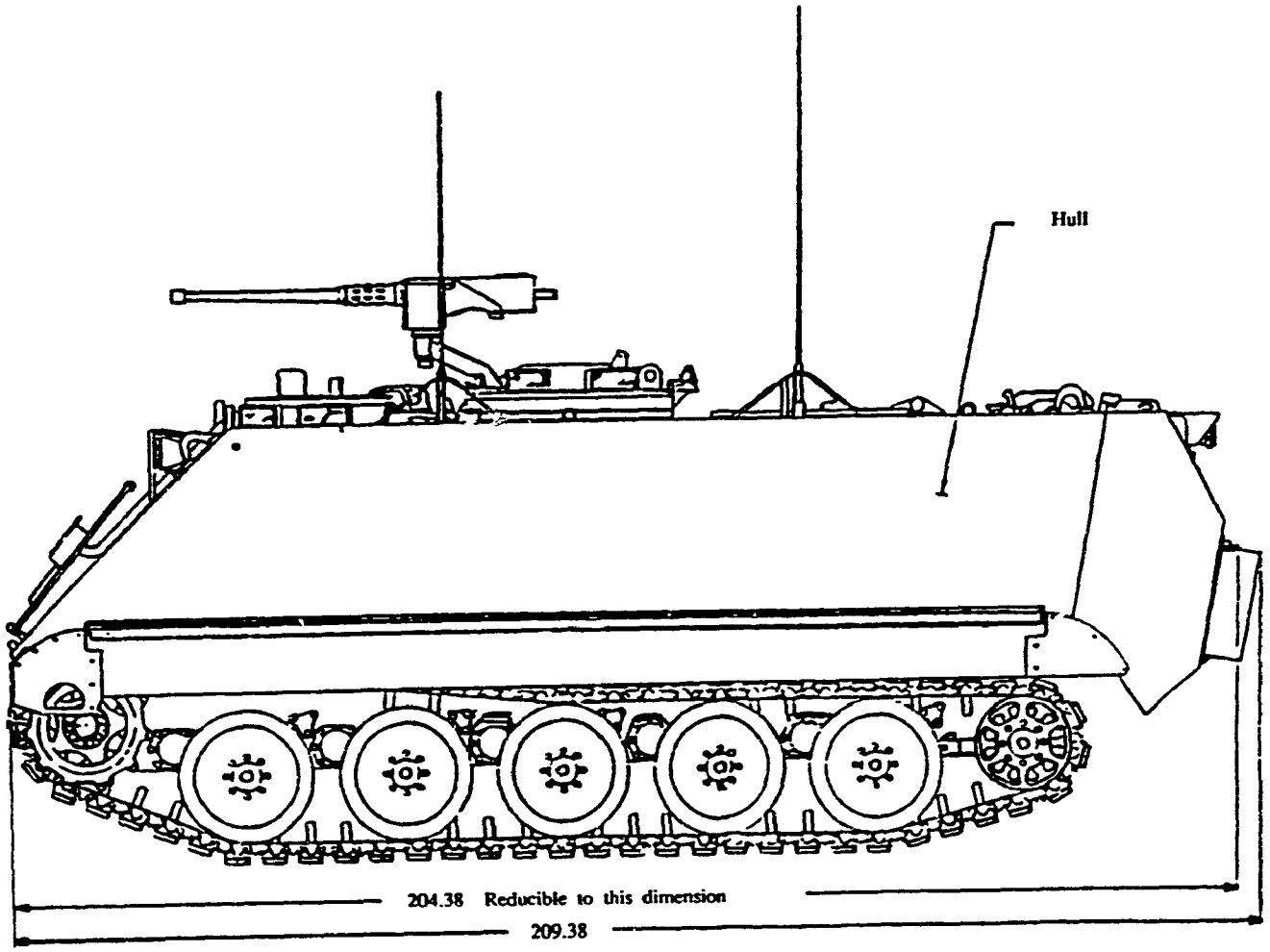

Figure 2.1 Schematic of a Typical M113 Armoured Personnel Carrier (COURTESY OF DND).

(APC) supported by five road wheels on each track. The M113 tracked vehicle consists of a sprung crew compartment, referred to as the hull, and a running gear. The running gear consists of drive sprockets, idlers, independent road wheel suspension and tracks. The road wheels are attached to the hull through a trailing arm suspension while the tracks are extended around the wheels by the sprocket and idler wheel at the front and rear ends, respectively, on each side of the vehicle.

The hull is the primary superstructure of the vehicle which contains the engine room, driver's chamber, and the personnel compartment. Figure 2.2 shows the various cross-sections of the tracked vehicle. The engine room, located by the side of the driver's chamber, contains the vehicle power plant and power train. The power plant consists of 210 hp V6 Diesel engine and the transmission, which drives the sprocket, provides one reverse and three forward speeds. Steering manoeuvres are achieved via a differential mechanism while the braking is performed by pivot disc brakes. The fuel tanks may be mounted either externally or internally. The driver's chamber contains the steering, braking, and fuel controls. The personnel compartment of the hull has a capacity of twelve persons not including the driver. The compartment also allows for stowage of ammunition and other cargo necessary for combat. On top of the hull, a machine gun and turret is mounted near the commander's cupola.

The suspension for the M113 APC is an independent trailing arm torsion bar type. Each road wheel is mounted on a road arm splined to a torsion bar. The torsion bars extend over the width of the chassis, as shown in Figure 2.3. The shock absorbers are mounted between the road arms and the hull chassis at an inclined position. At the upper and

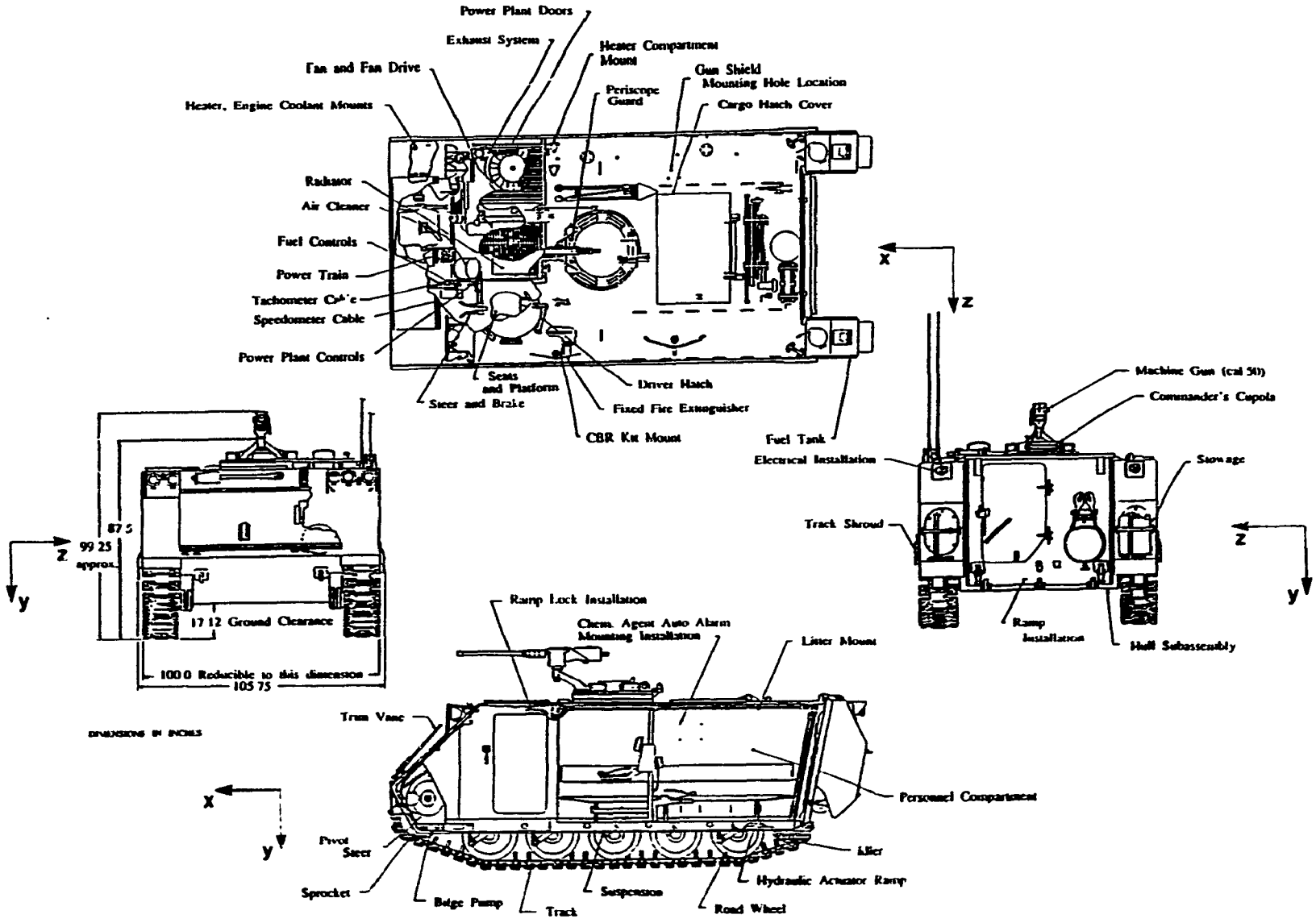

Figure 2.2 Cross-Sections of the M113 Vehicle (COURTESY OF DND).

lower bounds of road arm travel, rubber bumpers are mounted to prevent the road wheel from hitting the hull chassis and driving the track into the ground. The schematics of suspension components are presented in Figures 2.4, 2.5. and 2.6.

The M113 APC, in general, employs three types of suspension configurations, referred to as A1, A2, and A1$\frac{1}{2}$. All the three suspension designs consist of a trailing arm torsion bar suspension, however, the number and location of shock absorbers differ in each design. An A1 suspension design utilizes inclined shock absorbers at the first and fifth road wheel per track; A2 and A1$\frac{1}{2}$ configurations employ shock absorbers at the first, second and fifth road wheels. Apart from the different number of shock absorbers utilized, the M113 A1, M113 A2 and M113 A1$\frac{1}{2}$ vehicles exhibit certain variations in vehicle geometry, and considerable variations in the torsion bar stiffness and shock absorber damping characteristics, wheel mass, and total vehicle weight. The A1$\frac{1}{2}$ suspension configuration is identical to that of the M113 A2 vehicle with an exception that A2 torsion bars are replaced by the A1 counterparts.

The tracks of M113 APCs are of steel construction with detachable rubber pads. Two types of track, the single-pin and the double-pin track, are used extensively in military vehicles. The single-pin track is made up of adjacent track shoes which partially overlap like door hinges, and are connected by a single pin, as shown in Figure 2.7a. The double-pin track is constructed of adjacent track shoes joined by a set of connectors and two pins, as shown in Figure 2.7b. Most M113 vehicles are equipped with the German-made double-pin Diehl track, as shown in Figure 2.7c. The right track on the M113 APC consists of 64 metal track

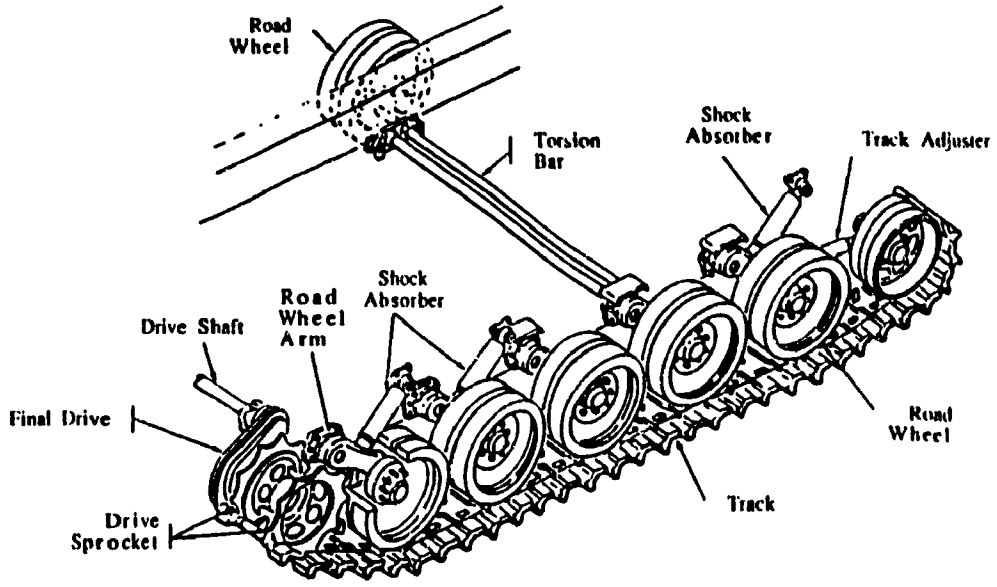

Figure 2.3 Schematic of the Tracked M113 APC Suspension System (COURTESY OF FMC).

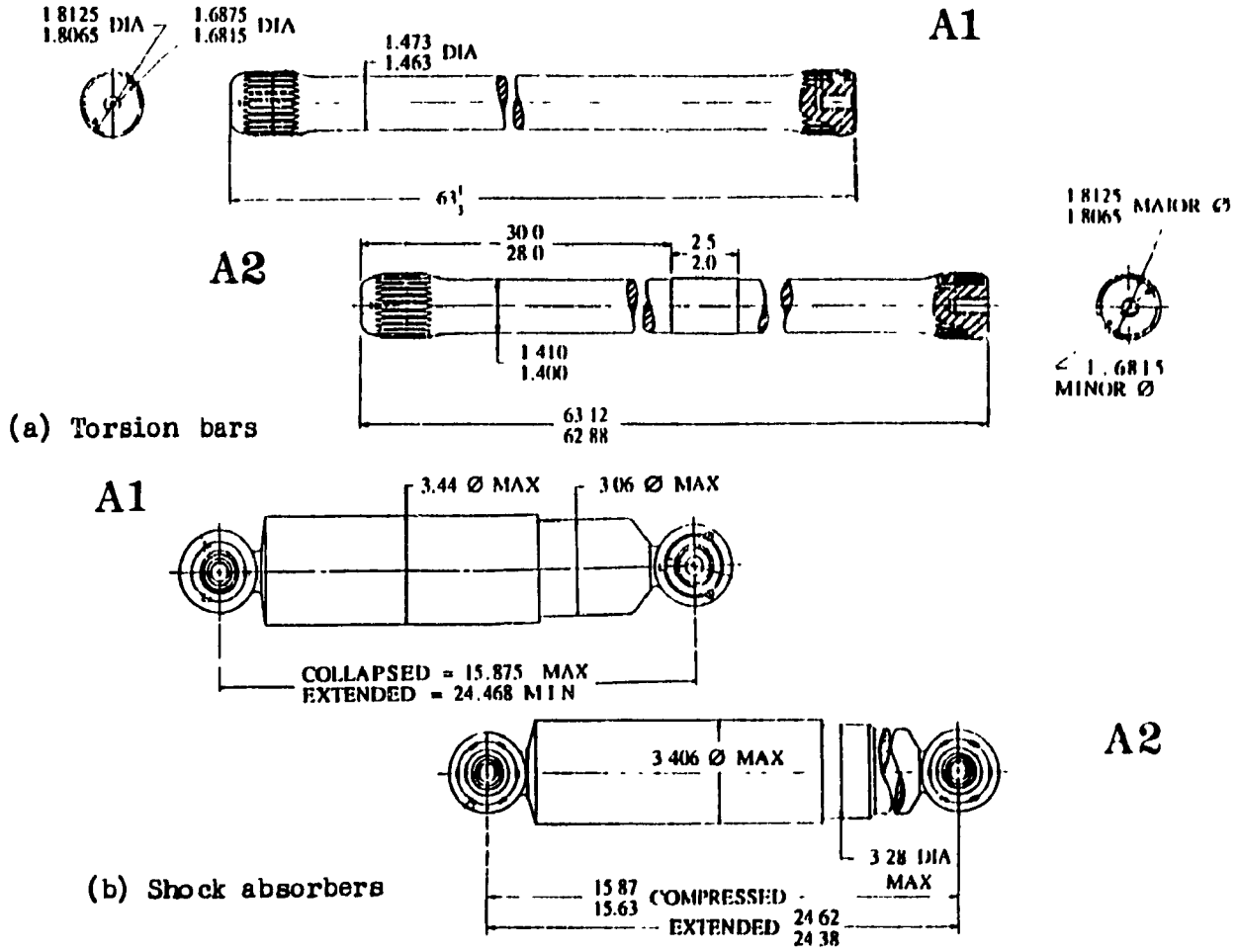

Figure 2.4 Schematic Representation of the Torsion Bars and Shock Absorbers of the M113 APC (COURTESY OF DND)

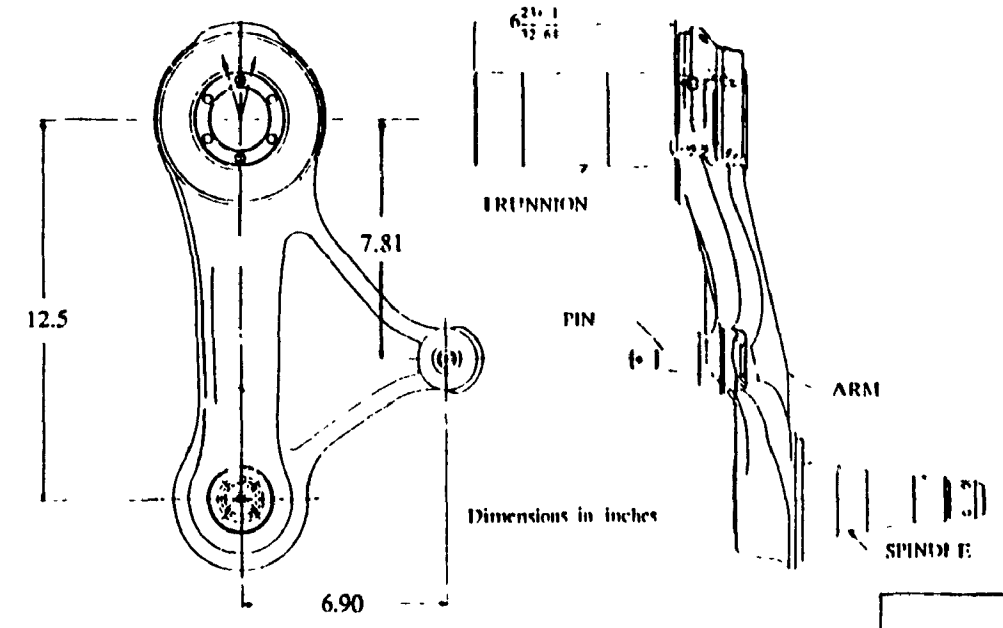

(a) Road arm with overhang for A1 shock absorber

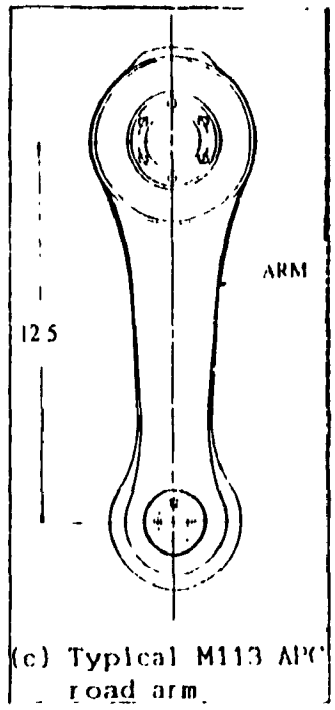

(c) Typical M113 APC road arm.

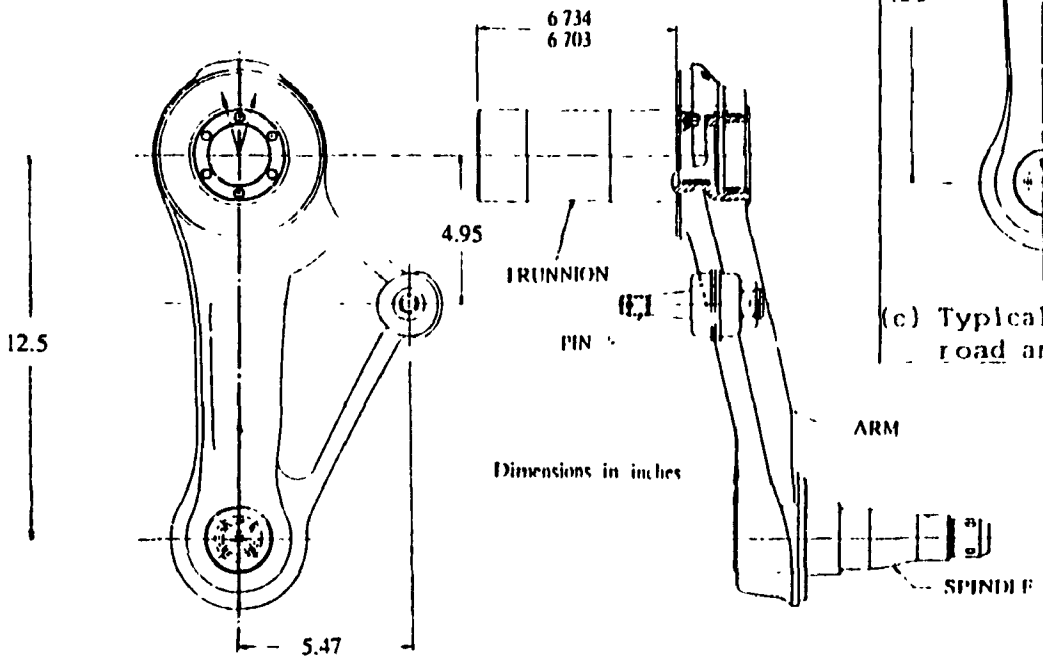

(b) Road arm with overhang for A2 shock absorber

Figure 2.5 Schematic of the Road Arms employed in A1 and A2 Suspensions (COURTESY OF DND).

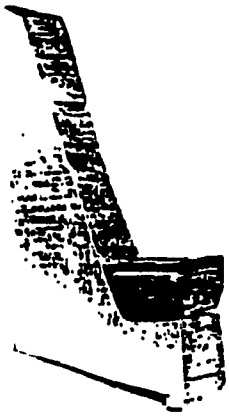

(a) Bump stop with rubber pad

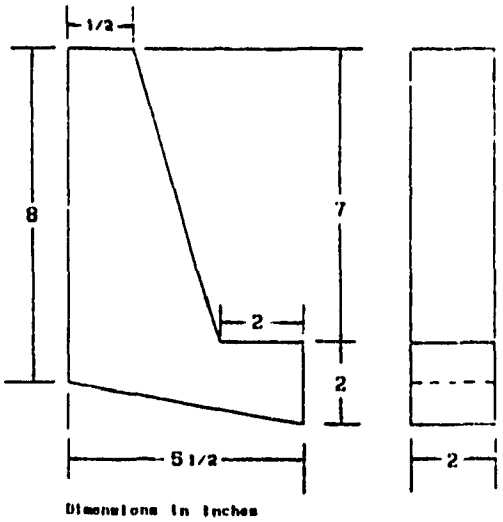

(b) Lower bump stop dimensions

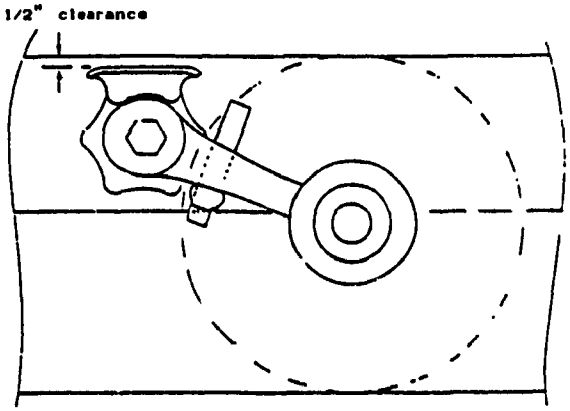

(c) Location of lower bump guard

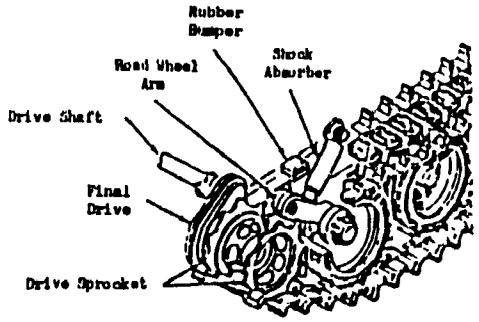

(d) Location of upper bump guard

Figure 2.6 Bump Stops of the M113 Suspension [26].

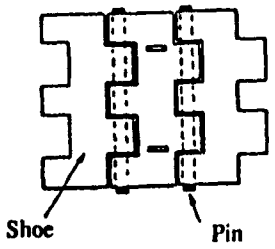

(a). Single-pin track

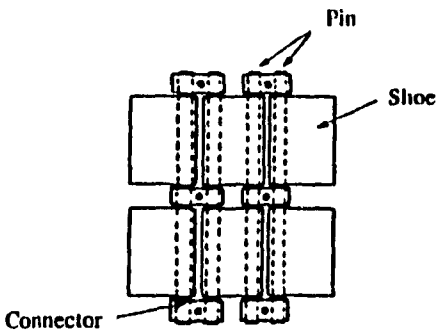

(b). Double-pin track

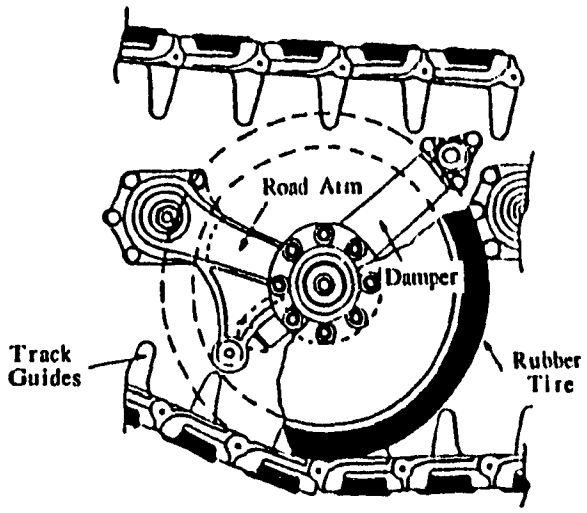

(d). Road arm/wheel and track

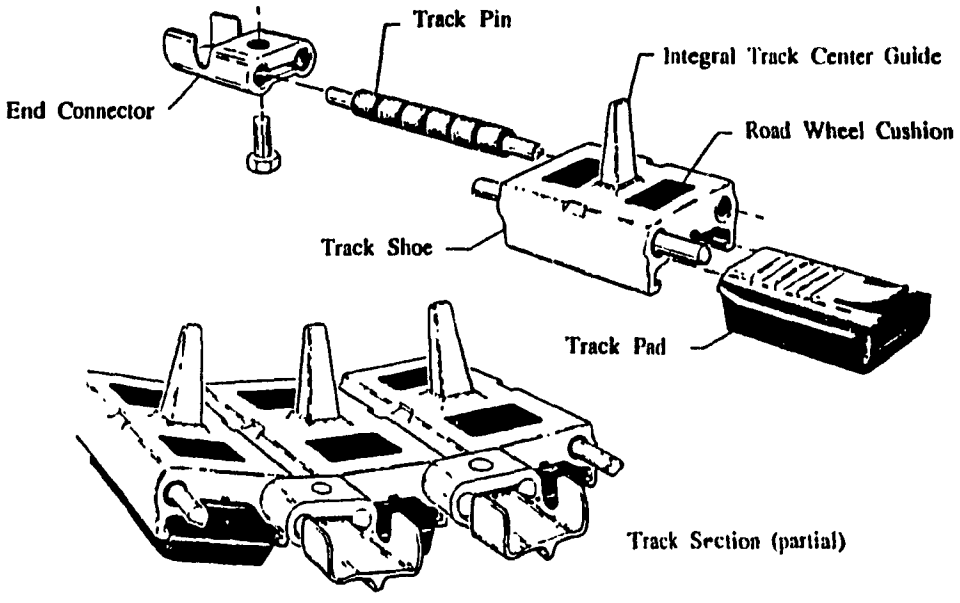

(c). Diehl 213B track components

Figure 2.7 Schematic of the Track and Road Wheel [10,44].

shoes while the left track consists of 63; the track shoes have rubber pads on the inner and outer surfaces. The inner pads prevent metal-to-metal contact during shoe-wheel interaction, while the outer pads soften shoe-ground interaction and protect paved roads from premature wear during vehicle operations. The road wheels have an all-metal body (hub, web, and tread) with a rubber tire vulcanized to the metal tread for vibration isolation, as shown in Figure 2.7d. To prevent track disengagement, the track consists of track guides which mesh into the circumferences of the road wheels, sprocket and idler. The idler stabilizes the motion of the upper track strand and maintains the track segment past the last road wheel at a desirable slope. Adjustment of the idler wheel position can be achieved by a hydraulic actuator to increase or reduce track pre-tension. The sprocket, which is connected to the vehicle engine through a drive train, develops the track tension necessary to set the vehicle in motion.

2.3 DEVELOPMENT OF RIDE DYNAMIC MODELS FOR THE M113 TRACKED VEHICLE

The development of a ride dynamic model involves the identification of suspension elements such as the springs and shock absorbers connecting the wheels to the vehicle superstructure; unsprung and sprung masses and inertias; and elastic properties of tires, bump stops, etc. In the case of tracked vehicles, the track effects such as track pull and track pad elasticity are taken into account to study the ride dynamic behaviour of the tracked vehicle. The track loads along with the various suspension forces are then incorporated to develop a ride dynamic model to evaluate the ride vibration levels at the vehicle hull, and driver and crew compartments. Four vehicle ride models of varying complexities are developed using a building block modeling approach

The mathematical ride models along with the associated simplifying assumptions are presented in the following subsections:

2.3.1 Development of Ride Dynamic Model of a Multi-Wheeled Vehicle with Idealized Suspension (*MODEL I*)

The initial model in the development process is formulated, while neglecting track loads and the kinematics of the linkage suspension. The generalized coordinates of the seven-degree-of-freedom model, thus formulated, comprise of the vertical motion of the vehicle hull, pitch motion of the vehicle hull, and the vertical motion of each road wheel, as shown in Figure 2.8. Various assumptions associated with the model are as follows:

(a) The trailing arm road wheel suspension is idealized by a parallel combination of a linear spring and a viscous damper. Thus, the kinematics of the road arm and shock absorber linkages are neglected.

(b) The suspension springs and dampers are constrained to translate along the vertical coordinates only.

(c) Nonlinearities due to orifice damping are neglected.

(d) Road wheel tires are represented by point contact springs.

(e) Bump stops, which prevent the road wheels from hitting the hull chassis, are represented by springs in parallel to the road wheel suspension.

(f) Dynamics due to the track are neglected.

(g) The road wheels are assumed to be in contact with the ground at all times.

(h) Magnitude of vehicle motion along the generalized coordinates is assumed to be small.

The damping and stiffness characteristics of the road wheel

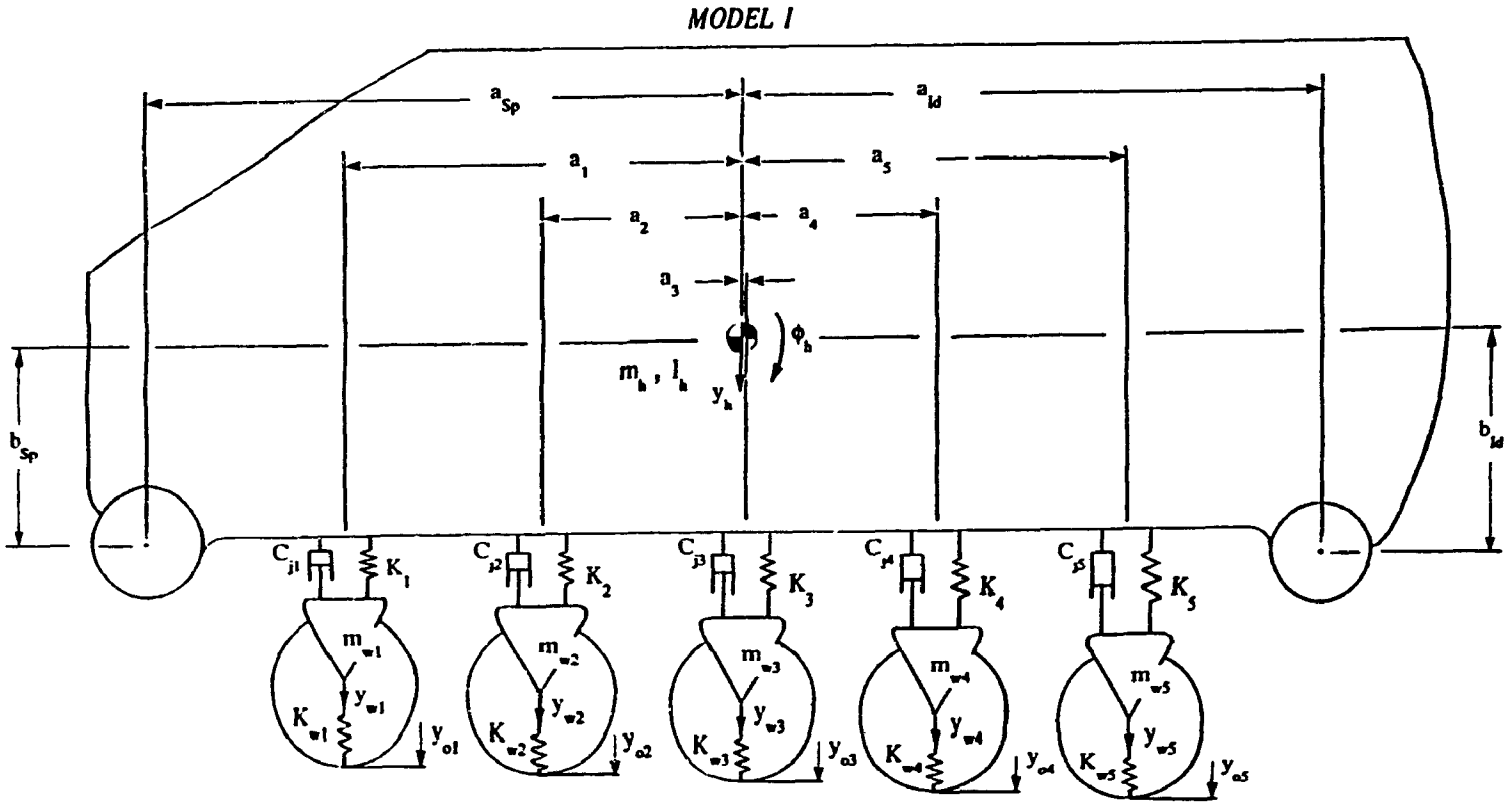

Figure 2.8 Schematic of the M113 Multi-Wheeled Vehicle Model with Idealized Suspension (*Model I*).

suspension are established from the force-velocity and force-displacement relationships, respectively. The spring rate due to torsional springs is computed using basic theory of torsion. The bump stop stiffness coefficient is determined from the typical force-displacement characteristics shown in Figure 2.9. An idealized model of the suspension bump stops is presented in Figure 2.10. The damping coefficient of the wheel suspension is determined from the force-velocity characteristics of the shock absorbers. Typical force-velocity characteristics of the shock absorbers employed in M113 vehicle suspensions are presented in Figure 2.11. The cross-section of a typical shock absorber is shown in Figure 2.12. The force-velocity power curve shown in Figure 2.11 is composed of two segments: bleed-control, and blow-off region. The force-velocity characteristics of the shock absorbers indicate high damping constant corresponding to low piston velocities and the damping coefficient decreases significantly as the piston velocity exceeds certain break velocity.

The differential equations of motion of the vehicle model are derived by identifying the various forces acting on the hull and the road wheels. The static deflections of the suspension springs, tires (and track pads where applicable), due to the vehicle sprung and unsprung weights are computed from the static force balance, assuming that the sprung weight is uniformly distributed over the ten road wheels. A free body diagram of the multi-wheeled vehicle is shown in Figure 2.13. The equations of motion, derived using d'Alembert's Principle, are expressed as follows:

Bounce Motion of the Hull

$$m_h \ddot{y}_h + 2\sum_{i=1}^{n} (F_{Di} + F_{fi}) + 2\sum_{i=1}^{n} K_i (y_h - a_i \phi_h - y_{wi} + y_{hs})$$

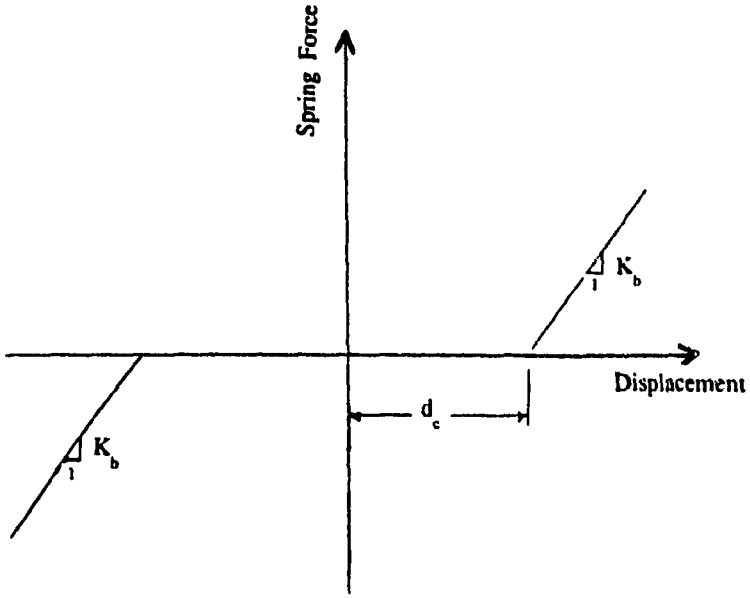

Figure 2.9 Force-Displacement Characteristics of the Bump Stops.

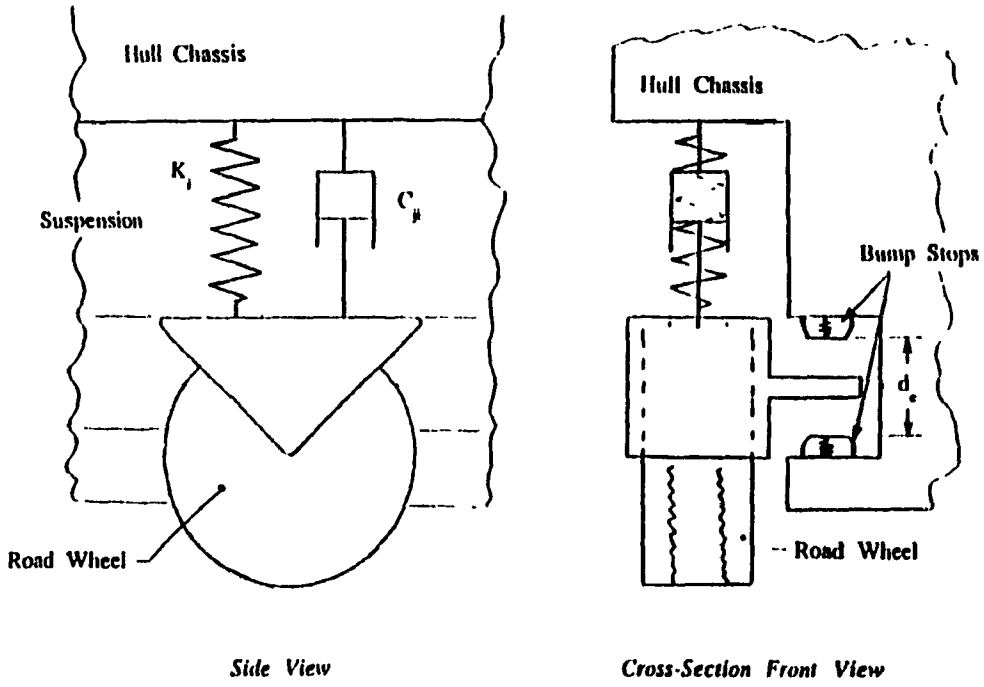

Figure 2.10 Idealized Representation of the Bump Stops.

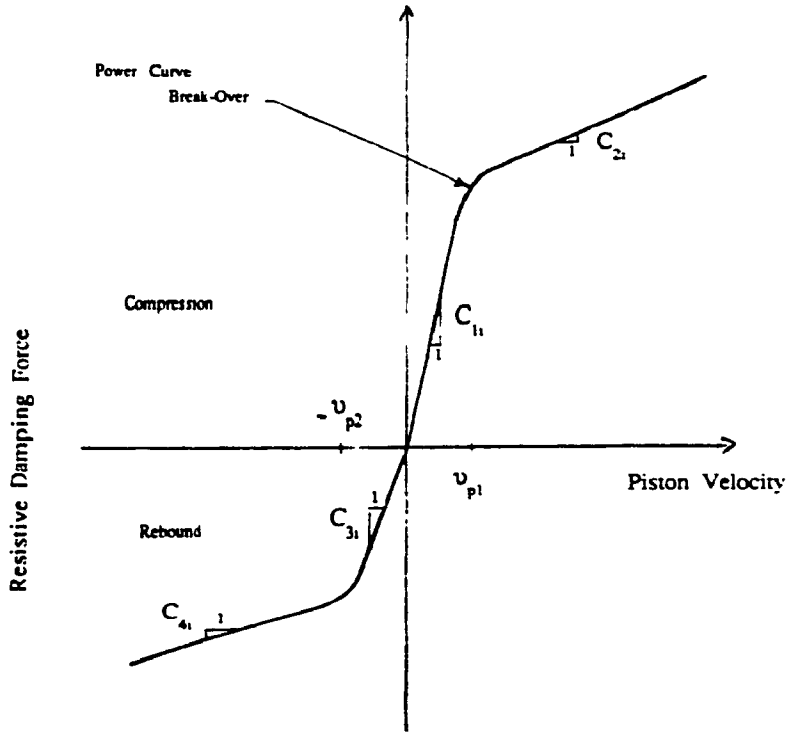

Figure 2.11 Typical Force-Velocity Characteristic of the Shock Absorbers.

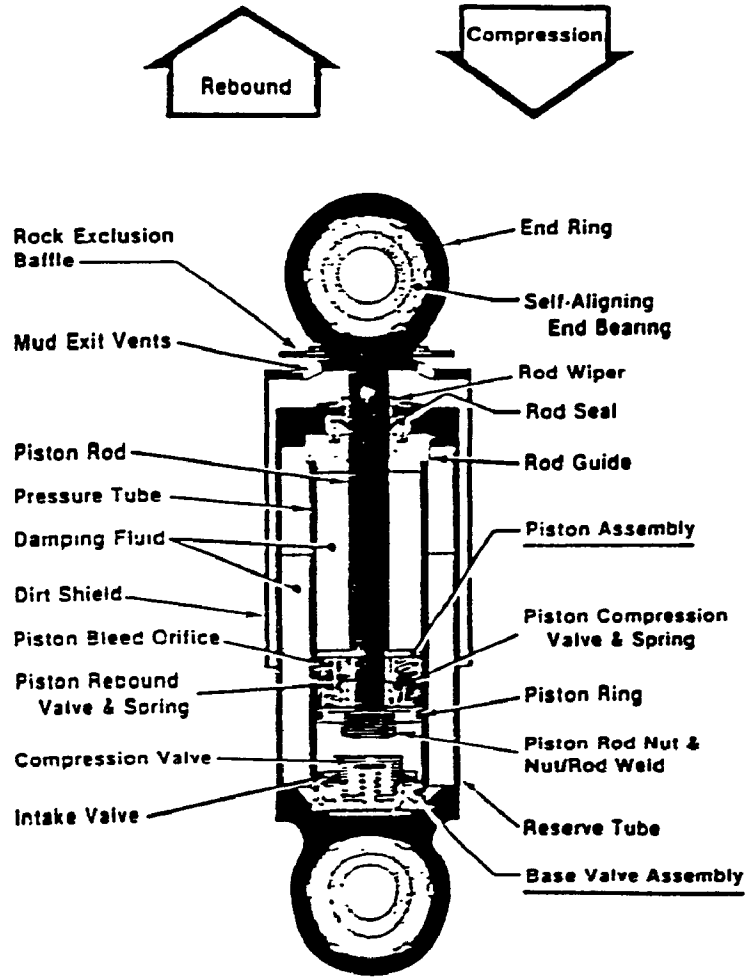

Figure 2.12 Schematic of a Typical Military Vehicle Shock Absorber [25].

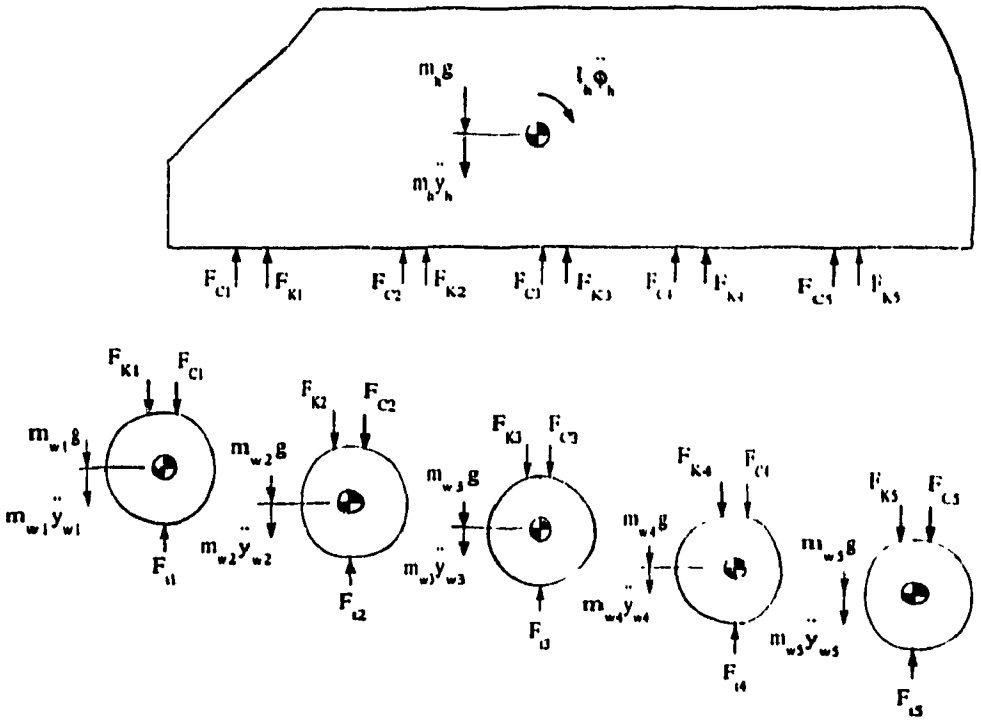

F_{Ci} = total suspension damping forces

F_{Ki} = total suspension spring forces

F_{ti} = total tire forces

Figure 2.13 Free-Body Diagram of the Multi-Wheeled Vehicle (*Model 1*).

$$+ 2\sum_{i=1}^{n} F_{bi} = m_h g \qquad (2.1)$$

Pitch Motion of the Hull

$$I_h \ddot{\phi}_h - 2\sum_{i=1}^{n} a_i (F_{Di} + F_{fi}) - 2\sum_{i=1}^{n} a_i K_i (y_h - a_i \phi_h - y_{wi} + y_{hs})$$

$$- 2\sum_{i=1}^{n} a_i F_{bi} = 0. \qquad (2.2)$$

Bounce Motion of the Road Wheels

$$m_{wi} \ddot{y}_{wi} - F_{Di} - F_{fi} - K_i (y_h - a_i \phi_h - y_{wi} + y_{hs})$$

$$- F_{bi} + K_{wi} (y_{wi} - y_{oi} + y_{ws}) = m_{wi} g \ ;$$

$$(i = 1,2,\ldots,n) \qquad (2.3)$$

where

m_h = sprung mass of the hull

m_{wi} = mass of the road wheel 'i'

I_h = pitch mass moment of inertia of the hull about its c.g.

K_i = stiffness coefficient of the suspension at road wheel 'i'

K_{wi} = stiffness coefficient for the tire of road wheel 'i'

a_i = horizontal distance between the hull center of gravity and the road wheel 'i' (a_i is positive when the suspension is located ahead of the c.g. and negative when the suspension is located behind the c.g.)

y_h = vertical motion of the hull c.g.

ϕ_h = pitch rotation of the hull

y_{wi} = vertical motion of the road wheel 'i'

y_{oi} = input displacement at road wheel 'i'

g = gravitational constant

y_{hs} = static deflection of the wheel suspension

y_{ws} = static deflection of the tires

n = number of road wheels

$(\cdot)$ = $\frac{d}{dt}$

F_{bi} = force due to wheel-to-bump stop contact at road wheel 'i'

F_{Di} = force due to suspension damping at road wheel 'i'

F_{fi} = force due to friction of the suspension at road wheel 'i'

The bump stop force is expressed as:

$$F_{bi} = K_b \cdot c_b \left[y_h - a_i \phi_h - y_{wi} - d_c \, \mathrm{sgn}(y_h - a_i \phi_h - y_{wi}) \right] \qquad (2.4)$$

where K_b is the bump stop stiffness coefficient, d_c is the permissible wheel travel, and c_b is the contact factor given as:

$$c_b = \begin{cases} 1 \; ; & \text{if} \quad |y_h - a_i \phi_h - y_{wi}| \geq d_c \\ 0 \; ; & \text{if} \quad |y_h - a_i \phi_h - y_{wi}| < d_c \end{cases}$$

and the function sgn $(\circ)$ is expressed as:

$$\mathrm{sgn}(\circ) = \begin{cases} 1 & \text{if} \quad \circ \geq 0. \\ -1 & \text{if} \quad \circ < 0. \end{cases}$$

The damping forces F_{Di} are determined from the force-velocity power curves of the shock absorbers, presented in Figure 2.11. In general, the power curve for a particular shock absorber on the M113 vehicle can be approximated by the following relation:

$$F_{Di} = \begin{cases} C_{1i} v_{p1} + C_{2i} \left[v_i - v_{p1} \right] & \text{if} \quad v_i > v_{p1} \\ C_{1i} v_i & \text{if} \quad 0. \leq v_i \leq v_{p1} \\ C_{3i} v_i & \text{if} \quad v_{p2} \leq v_i < 0. \\ C_{3i} v_{p2} + C_{4i} \left[v_i - v_{p2} \right] & \text{if} \quad v_i < v_{p2} \end{cases} \qquad (2.5)$$

where C_{jl} represents the high/low damping coefficients corresponding to the 'j'th gradient of the force-velocity curve, and v_l is the relative velocity across the shock absorber given by:

$$v_l = \dot{y}_h - a_l \dot{\phi}_h - \dot{y}_{wl} \tag{2.6}$$

Friction forces due to shock absorber and suspension linkage, F_{fl}, are expressed as:

$$F_{fl} = (F_{sa} + F_L)\ \mathrm{sgn}(v_l) \tag{2.7}$$

where F_{sa} and F_L are the magnitudes of friction force of the shock absorber and suspension linkage, respectively.

Equations (2.1), (2.2), and (2.3) describe the motion of the seven-degree-of-freedom multi-wheeled vehicle model with idealized suspension, while neglecting the dynamics of the track and the suspension linkages. For a ten wheeled vehicle, equation (2.3) yields five coupled differential equations of motion. The equations of motion for the in-plane vehicle model are developed assuming that each road wheel is equipped with a shock absorber. However, the ride dynamics of M113 A1 and M113 A2 vehicles can be simulated using equations (2.1) to (2.3) by setting the damping coefficient at the undamped road wheel stations to zero.

2.3.2 Development of Ride Dynamic Model of the Tracked Vehicle with Idealized Suspension (*MODEL II*)

The previous model (*Model I*), described in section 2.3.1, represents the ride dynamics of a multi-wheeled vehicle with idealized suspension. Although the dynamics of the track are entirely ignored, significant information pertaining to the road wheel and hull dynamics due to suspension forces can be achieved. The track does however,

provide a cushion under the road wheels by virtue of the track pads and thus the elastic properties of the track should be incorporated into the model. Furthermore, a number of analytical and experimental studies on the dynamics of tracked vehicles have established that dynamic track tension influences the vehicle dynamics, considerably [6]. The ride dynamics model of the tracked vehicle is developed assuming the track tension as restoring forces acting on the road wheels, as shown in Figure 2.14. Various simplifying assumptions associated with the tracked vehicle model are as follows:

(a) The track is assumed to be a continuous belt, which remains in contact with the terrain at all times.

(b) The elastic properties of the road wheel-track interface are represented by point contact springs in series.

(c) Inertia due to the track is neglected, however, a portion of the mass of the track is lumped with the sprung mass of the vehicle.

(d) The road wheels are assumed to be in contact with the track at all times.

Tension due to each track segment between consecutive road wheels is represented by a restoring force due to linear relative springs placed between the consecutive road wheels, as shown in Figure 2.14. The track tension caused by the relative displacement of a road wheel with respect to the adjacent road wheel, is thus modeled as a restoring force proportional to the relative motion of the wheel. The spring constants due to each track segment is established from the suspension forces acting on the road wheel and the unsprung weight, as shown in Figure 2.15. The spring constant, μ_w, is expressed as:

$$\mu_w = \frac{F_{sui} + m_{wi} g}{\psi_w} \qquad (2.8)$$

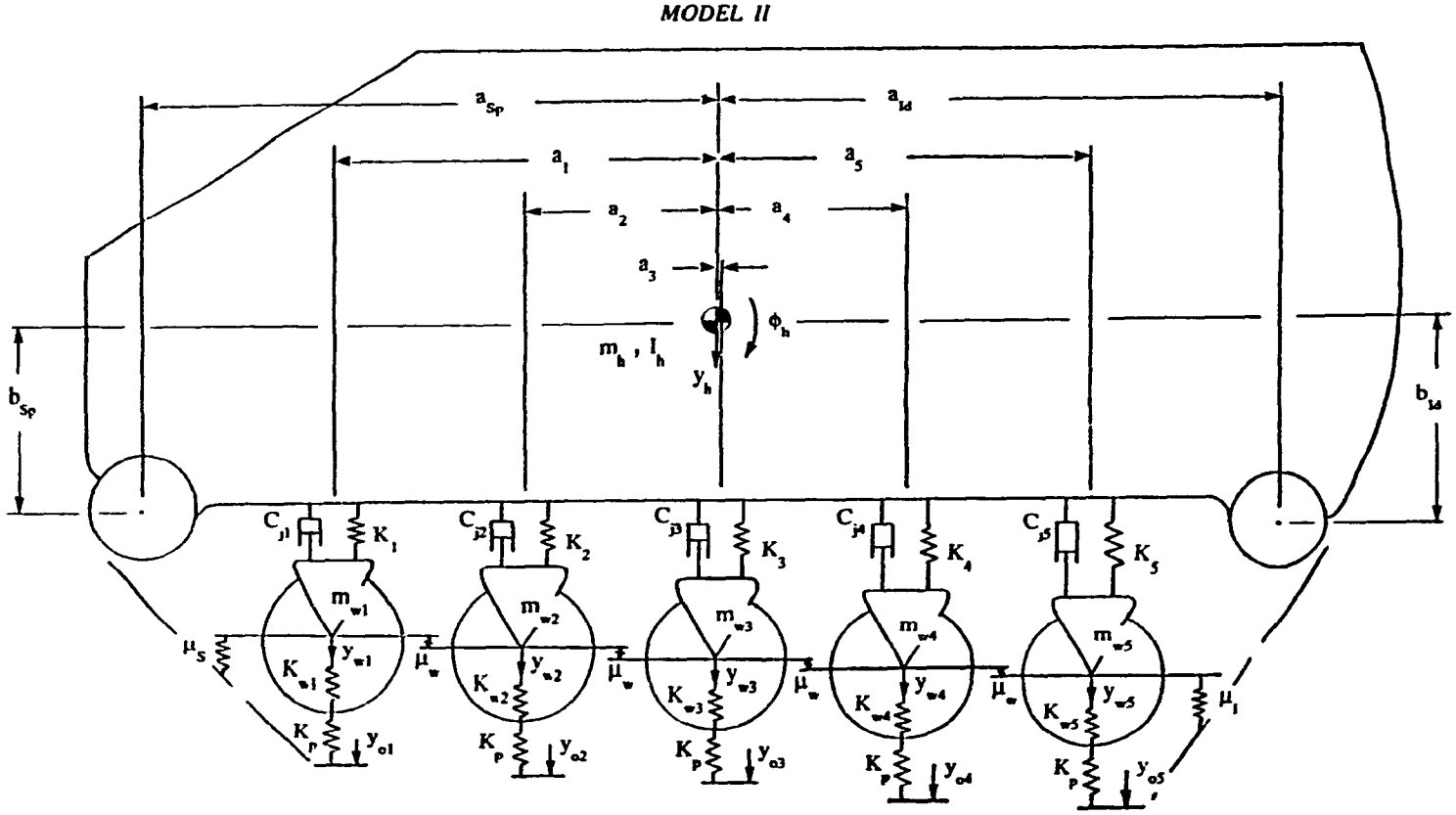

Figure 2.14 Schematic of the M113 Tracked Vehicle Model with Idealized Suspension (*Model II*).

where F_{sui} is the resultant suspension force acting on the road wheel, and ψ_w is the relative displacement with respect to the adjacent road wheel.

Track forces due to the leading and trailing portions of the track may be considered when there is track/terrain contact along these track segments. It is safe to assume that the forces due to tension in the leading and trailing segments of the track influence the first and last road wheels, respectively, since any tensile force acting near the sprocket or idler or both take up slack from the upper strand of the track between the sprocket and the idler. Spring constants for track tension of the leading and trailing portions of the track are established by computing the vertical component of tension due to the maximum deflection of the track in contact with the terrain profile. Measurement of the spring constants due to leading and trailing segments of the track are usually performed through massless feelers positioned on the surface of the tracks [6,20]. The restoring forces due to the track acting on the road wheels, sprocket and idler are illustrated in the free body diagram presented in Figure 2.16. Using d'Alembert's Principle, the differential equations of motion of the tracked vehicle model with idealized suspension are expressed as follows:

Bounce Motion of the Hull

$$m_h\ddot{y}_h + 2\sum_{i=1}^{n}(F_{Di} + F_{fi}) + 2\sum_{i=1}^{n}K_i(y_h - a_i\phi_h - y_{wi} + y_{hs}) + 2\sum_{i=1}^{n}F_{bi} = m_h g \qquad (2.9)$$

Pitch Motion of the Hull

$$I_h\ddot{\phi}_h - 2\sum_{i=1}^{n}a_i(F_{Di} + F_{fi}) - 2\sum_{i=1}^{n}a_iK_i(y_h - a_i\phi_h - y_{wi} + y_{hs})$$

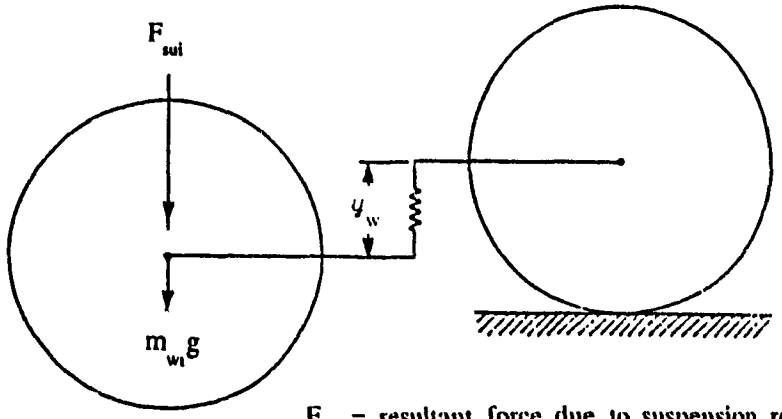

F_{sui} = resultant force due to suspension reaction

Figure 2.15 Schematic Representation of the Track Segment Model.

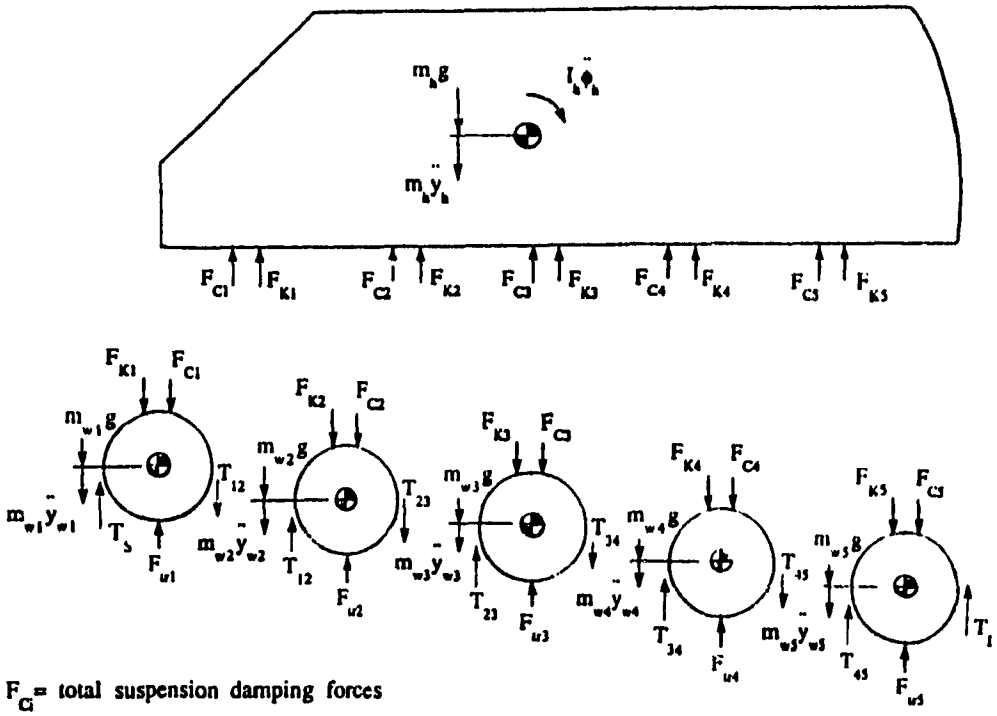

F_{Ci} = total suspension damping forces

F_{Ki} = total suspension spring forces

F_{ui} = total tire-track forces

T_s, T_y, T_t = forces due to track tension

Figure 2.16 Free-Body Diagram of the Tracked Vehicle (*Model II*).

$$- 2\sum_{i=1}^{n} a_i F_{bi} = 0. \qquad (2.10)$$

Bounce Motion of the Road Wheels

$$m_{wi}\ddot{y}_{wi} - F_{Di} - F_{fi} - K_i(y_h - a_i\phi_h - y_{wi} + y_{hs}) - F_{bi} + K_{tri}(y_{wi} - y_{oi} + y_{trs}) - T_i^l - T_i^r = m_{wi}g \qquad (2.11)$$

where y_{trs} represents the static deflection of the tires/track interface. The forces generated due to the wheel-terrain interactions are expressed in terms of the equivalent stiffness coefficient K_{tri} given by:

$$K_{tri} = \frac{K_p K_{wi}}{K_p + K_{wi}} \qquad (2.12)$$

where K_p and K_{wi} are the spring rates of the track pads and road wheel tires, respectively. Vertical forces due to tension of the track , T_i^l and T_i^r , acting on the left and right of each road wheel are expressed as:

$$T_i^l = \begin{cases} - T_S & \text{for } i = 1 \\ - \mu_w(y_{wi} - y_{wi-1}) & \text{for } i = 2, \ldots, n \end{cases}$$

$$T_i^r = \begin{cases} \mu_w(y_{wi+1} - y_{wi}) & \text{for } i = 1, \ldots, n-1 \\ - T_I & \text{for } i=n \end{cases} \qquad (2.13)$$

where μ_w is the spring coefficient of the track segments between consecutive road wheels. For equally spaced road wheels, the spring constants are all equal reflecting uniform track tension.

T_S is the vertical component of the tension of the leading portion of the track (sprocket-to-first road wheel), when in contact with the terrain profile or obstacle. It may be expressed as:

$$T_S = \mu_S(y_{oS} - y_{w1}) \tag{2.14}$$

where μ_S is the spring constant of the leading track segment, and y_{oS} is the corresponding vertical deflection.

Similarly, T_I is the vertical component of the tension of the trailing portion of the track (last road wheel-to-idler), when in contact with the terrain, and is expressed as:

$$T_I = \mu_I(y_{oI} - y_{w5}) \tag{2.15}$$

where μ_I is the spring constant of the trailing track segment, and y_{oI} is the corresponding vertical deflection.

Equations (2.9) thru (2.15) yield seven coupled, second order, non-homogeneous differential equations of motion characterizing the ride dynamics of the tracked vehicle model assuming idealized suspension.

2.3.3 Development of Ride Dynamic Model of a Multi-Wheeled Vehicle with Trailing Arm Torsion-Bar Suspension (*MODEL III*)

In previous models, the suspension system of the M113 APC vehicle is modelled as a parallel combination of spring and damping elements, constrained to translate along the vertical coordinate alone. The road wheels are assumed to experience vertical motion only. The M113 APC suspension comprises of the M113 APC road wheels supported by swing arms individually splined to torsion bars which extend over the width of the hull chassis, as illustrated in Figure 2.4. The shock absorbers are mounted at inclined positions linking the road arms to the chassis. Thus, the road wheels will not only experience vertical motion but also rotation. Therefore, a vehicle model incorporating the kinematics and dynamics of the trailing arm torsion-bar suspension is vital for a more realistic and accurate simulation of ride behaviour of M113 tracked

vehicles.

A seven-degree-of-freedom ride dynamic model of the multi-wheeled vehicle is developed, incorporating the kinematic relations as implied by the linkage assembly comprising of the torsion bars, road arms, and shock absorbers, while neglecting the dynamics of the track . Figure 2.17 illustrates the seven degree-of-freedom ride dynamic model of the wheeled M113 vehicle. The model is very similar to that of *Model 1* except for the kinematics and dynamics of the trailing arm suspension. Various simplifying assumptions associated with the vehicle model are specified as follows:

(a) Each road wheel is attached to the hull chassis through a trailing arm suspension.

(b) Kinematics of the road arm and shock absorber linkage are taken into consideration and the suspension elements are characterized by linear or piecewise linear stiffness and damping coefficients.

(c) Nonlinearities due to orifice damping are neglected.

(d) The elastic properties of the road wheel tires are represented by point contact springs .

(e) Bump stops are represented by equivalent torsional springs in parallel with the torsion bar springs.

(g) Dynamics due to the track are neglected.

(h) The road wheels are assumed to be in contact with the ground at all times.

(i) Magnitude of vehicle motion along the generalized coordinates is assumed to be small.

The tracked vehicle suspension configuration (Figure 2.17) reveals that the trailing arm torsion bar suspension induces spring torques as well as vertical and horizontal damping forces to the sprung mass of the

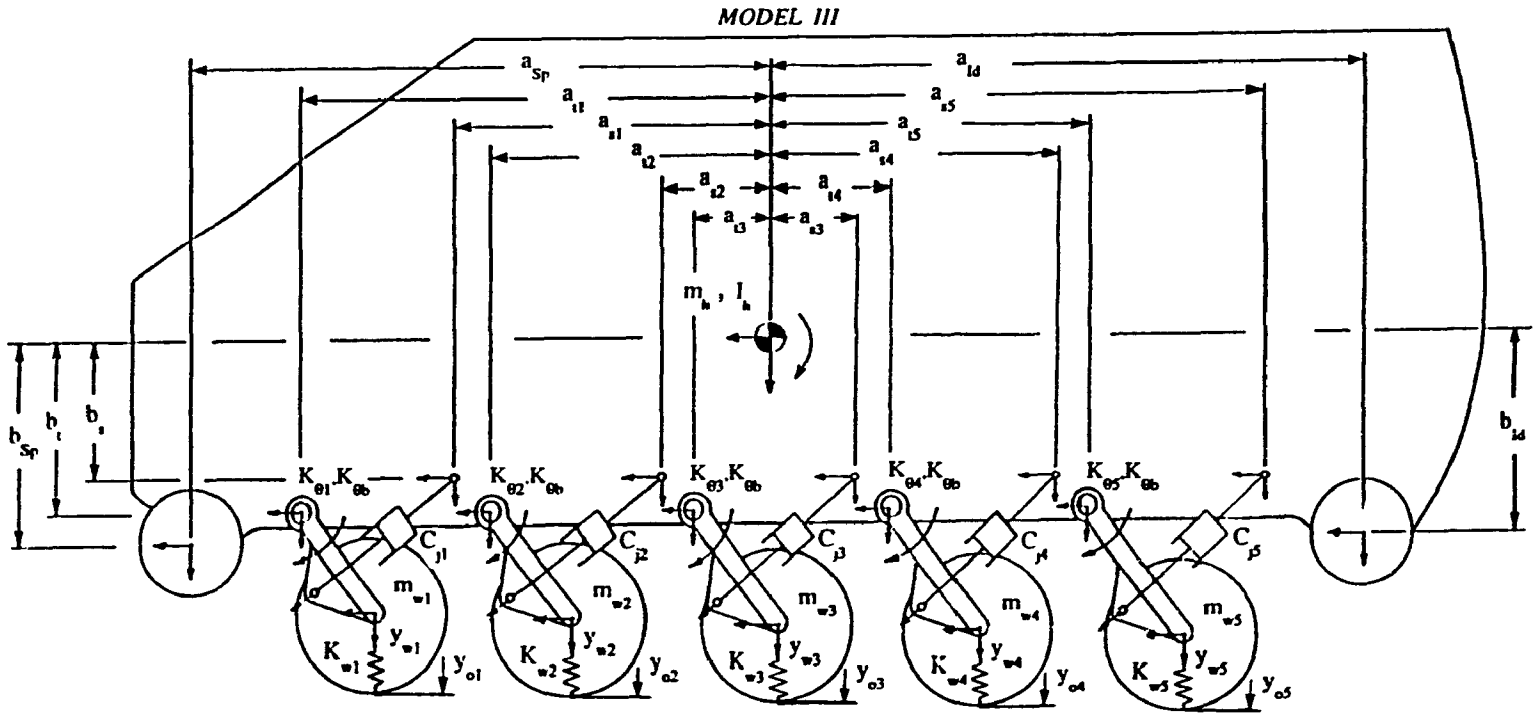

Figure 2.17 Schematic of the M113 Multi-Wheeled Vehicle Model with Linkage Suspension (*Model III*).

vehicle. The differential equations of motion for the in-plane seven degree-of-freedom vehicle model incorporating hull bounce, hull pitch and bounce motion of each road wheel are developed using Lagrange's energy method. For convenience of analysis and comparison purposes, the vertical motions of the road wheels are selected as the generalized coordinates. The rotational and longitudinal motions of the road arm and road wheel assemblies are described by constraint equations involving road wheel bounce, hull bounce and hull pitch. Using Lagrange's technique, the equations of motion for the vehicle *Model III* are formulated as follows:

Hull Bounce Motion

$$\left[m_h + 2\sum_{i=1}^{n} m_{wi}\tan^2\theta_o\right]\ddot{y}_h - \left[2\sum_{i=1}^{n} m_{wi}(b_t + a_{ti}\tan\theta_o)\tan\theta_o\right]\ddot{\phi}_h$$
$$- 2\sum_{i=1}^{n} m_{wi}\tan^2\theta_o\,\ddot{y}_{wi} + 2\sum_{i=1}^{n}(F_{Di} + F_{fsi})\frac{S}{R}\frac{\cos\gamma}{\cos\theta_o}$$
$$+ 2\sum_{i=1}^{n}\frac{K_{\theta i}(\phi_h - \theta_{wi} - \theta_s)}{R\cos\theta_o} + 2\sum_{i=1}^{n}(F_{b\theta i} + F_{fLi}) = m_h g \qquad (2.16)$$

Hull Pitch Motion

$$\left[I_h + 2\sum_{i=1}^{n} m_{wi}(b_t + a_{ti}\tan\theta_o)^2\right]\ddot{\phi}_h - \left[2\sum_{i=1}^{n} m_{wi}(b_t + a_{ti}\tan\theta_o)\tan\theta_o\right]\ddot{y}_h$$
$$+ 2\sum_{i=1}^{n}(F_{Di} + F_{fsi})\left[(a_{ti} - a_{si})\sin\beta_o + (b_s - b_t)\cos\beta_o - \frac{S}{R}a_{ti}\frac{\cos\gamma}{\cos\theta_o}\right]$$
$$+ 2\sum_{i=1}^{n} K_{\theta i}(\phi_h - \theta_{wi} - \theta_s)\left[1 - \frac{a_{ti}}{R\cos\theta_o}\right]$$
$$+ \sum_{i=1}^{n}(F_{\theta bi} + F_{fLi})\left[1 - \frac{a_{ti}}{R\cos\theta_o}\right] = 0. \qquad (2.17)$$

Road Wheel Bounce

$$[m_{wi}(1 + \tan^2\theta_o)]\,\ddot{y}_{wi} - [m_{wi}\tan^2\theta_o]\,\ddot{y}_h + [m_{wi}(b_t + a_{ti}\tan\theta_o)\tan\theta_o]\,\ddot{\phi}_h$$
$$- (F_{Di} + F_{fsi})\frac{S}{R}\frac{\cos\gamma}{\cos\theta_o} - \frac{K_{\theta i}(\phi_h - \theta_{wi} - \theta_s)}{R\cos\theta_o} - F_{\theta bi} - F_{fLi}$$

$$+ K_{wi}(y_{wi} - y_{oi} + y_{ws}) = m_{wi}g \qquad (2.18)$$

where,

$K_{\theta i}$ = Stiffness coefficient of torsion bar 'i'

a_{ti} = horizontal distance from torsion bar 'i' to the hull center of gravity

a_{si} = horizontal distance from shock absorber end 'Bi' to the hull center of gravity

b_t = vertical distance from torsion bars to the hull c.g.

b_s = vertical distance from shock absorber end 'Bi' to the hull c.g.

R = road arm length

S = distance from road arm hinge to the shock absorber end 'Ai'

θ_o = initial angle of inclination of road arm to the hull chassis

$\gamma_o = \beta_o + \theta_o + \zeta_o - \frac{\pi}{2}$

β_o = initial angle of inclination of shock absorber to the hull chassis

ζ_o = angle between the road arm centerline and the line bisecting the road arm hinge and shock absorber end 'Ai'

Assuming small motions, the pitch and longitudinal motion of the road arm and road wheel assembly, as shown in Figure 2.18, are derived from the following constraint equations:

$$\theta_{wi} = \frac{(y_{wi} - y_h + a_{ti}\phi_h)}{R \cos \theta_o} \qquad (2.19)$$

$$x_{wi} = b_t\phi_h + (y_{wi} - y_h + a_{ti}\phi_h)\tan \theta_o \qquad (2.20)$$

$$x_{fi} = b_t\phi_h \qquad (2.21)$$

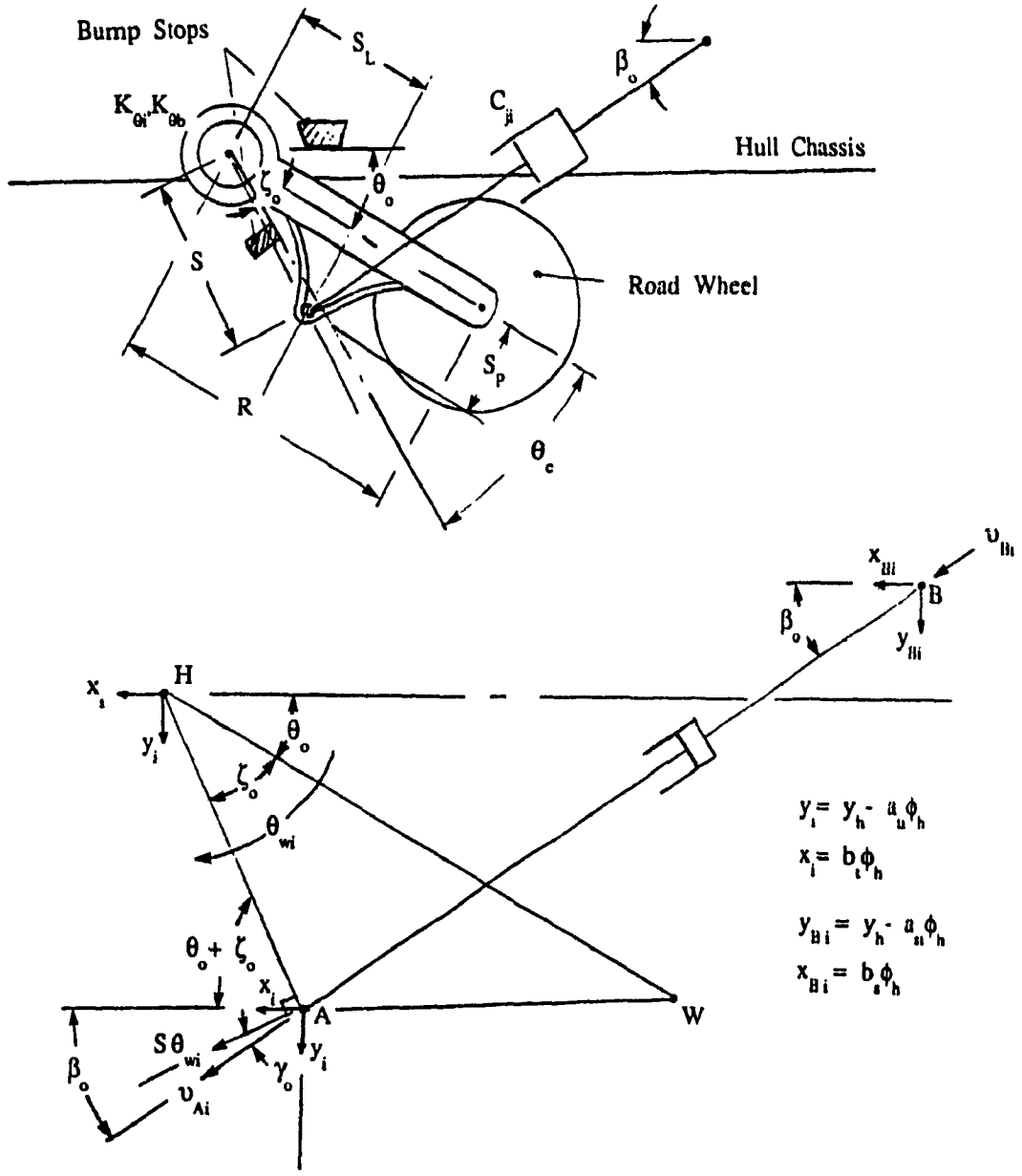

Figure 2.18 Schematic of the Linkage Suspension Model.

where θ_{wi} is the rotation of the road arm, x_{wi} is the longitudinal motion of the road wheel and x_{fl} is the longitudinal motion at the hull floor. The static deflection of the road arm, θ_s, is computed from the static suspension deflection:

$$\theta_s = \frac{y_{hs}}{R \cos \theta_o} \tag{2.22}$$

The damping force F_{Di} is expressed as a function of the relative velocity across the shock absorber mounted at road wheel 'i'. The damping force due to the shock absorber is assumed to be asymmetric, as illustrated in the force-velocity curve (Figure 2.11):

$$F_{Di} = \begin{cases} C_{1i} v_{p1} + C_{2i}\left(v_{Bi} - v_{Ai} - v_{p1}\right) & \text{if } \left(v_{Bi} - v_{Ai}\right) > v_{p1} \\ C_{1i}\left(v_{Bi} - v_{Ai}\right) & \text{if } 0. \le \left(v_{Bi} - v_{Ai}\right) \le v_{p1} \\ C_{3i}\left(v_{Bi} - v_{Ai}\right) & \text{if } v_{p2} \le \left(v_{Bi} - v_{Ai}\right) < 0. \\ C_{3i} v_{p2} + C_{4i}\left(v_{Bi} - v_{Ai} - v_{p2}\right) & \text{if } \left(v_{Bi} - v_{Ai}\right) < v_{p2} \end{cases} \tag{2.23}$$

where v_{p1} and v_{p2} are the break relative velocities, and v_{Bi} and v_{Ai} are the velocities of the damper links, established from the kinematics of the linkage presented in Figure 2.18:

$$v_{Ai} = (\dot{y}_{wi} - a_{ti}\dot{\phi}_h)\sin \beta_o + b_t \dot{\phi}_h \cos \beta_o + \frac{S}{R}(\dot{y}_{wi} - \dot{y}_h + a_{ti}\dot{\phi}_h)\frac{\cos \gamma}{\cos \theta_o} \tag{2.24}$$

$$v_{Bi} = (\dot{y}_h - a_{si}\dot{\phi}_h)\sin \beta_o + b_s \dot{\phi}_h \cos \beta_o \tag{2.25}$$

Friction forces due to shock absorber and suspension linkage, respectively, are expressed as:

$$F_{fsi} = F_{sa}\,\mathrm{sgn}(v_{Bi} - v_{Ai}) \tag{2.26}$$

$$F_{fLi} = F_L \text{sgn}(\phi_h - \theta_{wi}) \tag{2.27}$$

where F_{sa} and F_L are the magnitudes of friction force of the shock absorber and suspension linkage, respectively.

The forces due to bump stops are derived from the schematic presented in Figure 2.18. The force due motion limiting elastic stop is expressed by an equivalent torsional spring at the road arm hinge:

$$F_{\theta bi} = \frac{\mathcal{T}_{\theta bi}}{R \cos \theta_o} \tag{2.28}$$

where $\mathcal{T}_{\theta bi}$ is the torque due to road arm/bump stop contact given by,

$$\mathcal{T}_{\theta bi} = K_{\theta bi} \cdot c_{\theta b}\left[\phi_h - \theta_{wi} - \theta_c \text{sgn}(\phi_h - \theta_{wi}) \right] \tag{2.29}$$

where θ_c is the permissible angular clearance between the road arm and elastic stop, $K_{\theta b}$ is the equivalent torsional stiffness coefficient representing the elastic bump stop, and $c_{\theta b}$ is the contact factor given by,

$$c_{\theta b} = \begin{cases} 1 & \text{for } |\phi_h - \theta_{wi}| \geq \theta_c \\ 0. & \text{for } |\phi_h - \theta_{wi}| < \theta_c \end{cases}$$

Equations (2.16), (2.17) and (2.18) provide seven second order coupled differential equations of motion describing the ride dynamics of a multi-wheeled vehicle with trailing arm suspension (*Model III*). The rotational and longitudinal motion of the road arm and wheel assembly is determined from constraint equations (2.19) and (2.20), respectively

2.3.4 Development of Ride Dynamic Model of the Tracked Vehicle with Trailing Arm Torsion-Bar Suspension (*MODEL IV*)

In the previous model (*Model III*), described in section 2.3.3, the dynamics of the track are assumed to be negligible, thus the model represents the ride dynamics of a vehicle with linkage suspension The

dynamic effects of the track on the ride performance of the tracked vehicle are investigated by introducing the track model, similar to that discussed in section 2.3.2. Dynamics of the track are modelled via relative springs between the feeler and first road wheel, between adjacent road wheels, and between the last road wheel and the feeler, as illustrated in Figure 2.19. The differential equations of motion for the tracked vehicle incorporating dynamics of the trailing arm suspension and the track (*Model IV*), are derived using Lagrange's formulation and are expressed as follows.

Hull Bounce Motion

$$\left[m_h + 2\sum_{i=1}^{n} m_{wi}\tan^2\theta_o\right]\ddot{y}_h - \left[2\sum_{i=1}^{n} m_{wi}(b_t + a_{ti}\tan\theta_o)\tan\theta_o\right]\ddot{\phi}_h$$
$$- 2\sum_{i=1}^{n} m_{wi}\tan^2\theta_o\,\ddot{y}_{wi} + 2\sum_{i=1}^{n}(F_{Di} + F_{fsi})\frac{S}{R}\frac{\cos\gamma_o}{\cos\theta_o}$$
$$+ 2\sum_{i=1}^{n}\frac{K_{\theta i}(\phi_h - \theta_{wi} - \theta_s)}{R\cos\theta_o} + 2\sum_{i=1}^{n}(F_{b\theta i} + F_{fLi}) = m_h g \qquad (2.30)$$

Hull Pitch Motion

$$\left[I_h + 2\sum_{i=1}^{n} m_{wi}(b_t + a_{ti}\tan\theta_o)^2\right]\ddot{\phi}_h - \left[2\sum_{i=1}^{n} m_{wi}(b_t + a_{ti}\tan\theta_o)\tan\theta_o\right]\ddot{y}_h$$
$$+ 2\sum_{i=1}^{n} m_{wi}(b_t + a_{ti}\tan\theta_o)\tan\theta_o\,\ddot{y}_{wi}$$
$$+ 2\sum_{i=1}^{n}(F_{Di} + F_{fsi})\left[(a_{ti} - a_{si})\sin\beta_o + (b_s - b_t)\cos\beta_o - \frac{S}{R}a_{ti}\frac{\cos\gamma_o}{\cos\theta_o}\right]$$
$$+ 2\sum_{i=1}^{n} K_{\theta i}(\phi_h - \theta_{wi} - \theta_s)\left[1 - \frac{a_{ti}}{R\cos\theta_o}\right]$$
$$+ \sum_{i=1}^{n}(F_{\theta bi} + F_{fLi})\left[1 - \frac{a_{ti}}{R\cos\theta_o}\right] = 0. \qquad (2.31)$$

Road Wheel Bounce

$$[m_{wi}(1 + \tan^2\theta_o)]\ddot{y}_{wi} - [m_{wi}\tan^2\theta_o]\ddot{y}_h + [m_{wi}(b_t + a_{ti}\tan\theta_o)\tan\theta_o]\ddot{\phi}_h$$

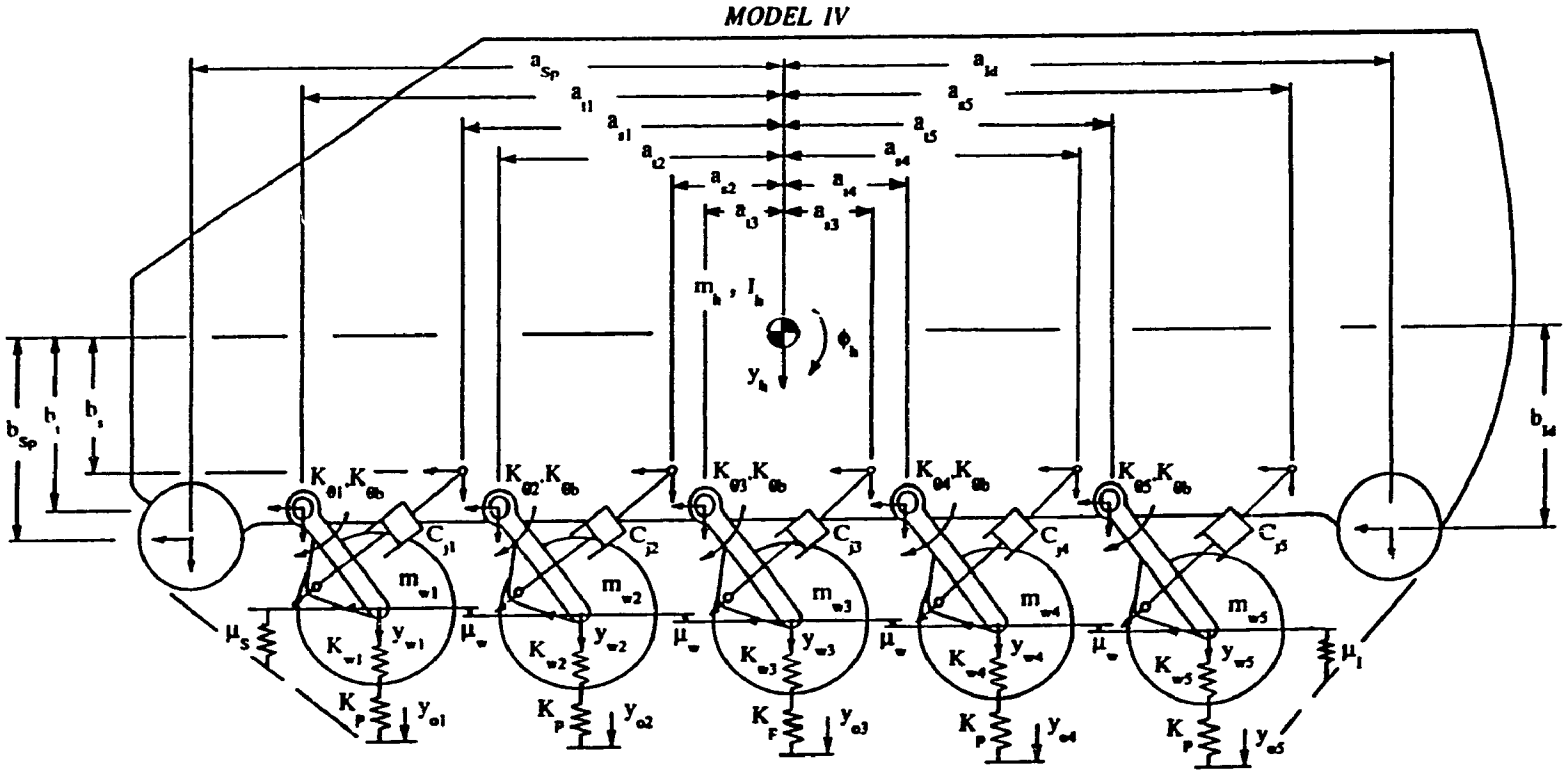

Figure 2.19 Schematic of the M113 Tracked Vehicle Model with Linkage Suspension (*Model IV*).

$$- (F_{Di} + F_{fsi}) \frac{S}{R} \frac{\cos \gamma_o}{\cos \theta_o} - \frac{K_{\theta l}(\phi_h - \theta_{wi} - \theta_s)}{R \cos \theta_o}$$

$$- F_{\theta bi} - F_{fLi} - K_{tri}(y_{wi} - y_{oi} + y_{trs})$$

$$- T_i^r - T_i^l = m_{wi} g \qquad (2.32)$$

The static and dynamic angular deflections of the road arm (θ_s and θ_{wi}), are described by equations (2.22) and (2.19), respectively, and y_{trs} is the static deflection of the track and tires. The velocities of the shock absorber links, v_{Ai} and v_{Bi}, are computed from equations (2.24) and (2.25). The forces due to damping, elastic limit stops and track tension are computed from equations (2.23), (2.26) thru (2.28), and (2.13) thru (2.15), respectively.

2.4 SUMMARY

In this chapter, four mathematical models of the wheeled and tracked vehicle are developed to study the ride dynamic performance of the vehicle. Each model represents a seven-degree-of-freedom dynamic system comprising of generalized coordinates: vertical motion of the hull, pitch motion of the hull and vertical motion of each road wheel. The highlights of each model are summarized as follows:

Model I: The trailing arm road wheel suspension is idealized by a parallel combination of linear spring and viscous damper. The Kinematics due to suspension linkage and dynamics due to the track are neglected. The ride dynamic performance of a multi-wheeled vehicle can be investigated using this model.

Model II: The kinematics and dynamics due to suspension linkage are neglected, however, the dynamics of the track are incorporated via restoring force generated by relative springs between the sprocket and first road wheel, adjacent road wheels, and idler and last road wheel. The elastic properties

of the track are represented by point contact springs in series with road wheel tire springs.

Model III: Kinematics of the trailing road arm linkage suspension are taken into consideration involving torsional stiffness due to the torsion bars and damping force due to inclined shock absorber. The dynamics due to the track are neglected.

Model IV: This suspension model is similar to *Model III*, however, the dynamics due the to track and elastic properties of track pads are incorporated via the track model established for *Model II*.

In the tracked vehicle models the track is assumed as a continuous belt, and to remain in contact with the road wheels and terrain at all times, while neglecting inertia due to the track. For the multi-wheeled vehicles, the road wheels are assumed to remain in contact with the ground at all times. Damping characteristics of the shock absorbers are represented by piecewise linear power curves, and friction forces due to suspension linkage and shock absorber are modelled as ideal Coulomb friction. The torsion bars are represented by torsional springs for the vehicle models with trailing arm suspension and by equivalent linear rates in the models with idealized suspension. The bump stops are represented by symmetric contact springs for *Models I* and *II*, and by equivalent torsional springs for *Models III* and *IV*.

CHAPTER 3

DESCRIPTION OF TERRAIN EXCITATIONS

3.1 INTRODUCTION

Ride vibrations of tracked vehicles, primarily, originate from random terrain undulations. Thus evaluation of ride performance characteristics of the vehicle models developed in Chapter 2, requires description of vibration excitations arising from the terrains. The input data must be representative of the terrain and it must also be concise in order to minimize computations. Vibration excitations arising from random terrain profiles are often expressed in terms of their displacement and acceleration power spectral densities (PSDs) as well as cross spectral densities (CSDs), assuming the terrain to be undeformable. Input excitations may also be expressed in the form of deterministic undeformable obstacles and deformable soil models incorporating soil compaction and sinkage due to vehicle-terrain interaction.

3.2 DETERMINISTIC INPUTS

Discrete undeformable ground profiles, such as half round obstacles, sinusoidal course, granite blocks etc., have been used to assess the vibration isolation performance of vehicle suspension and track dynamics [6,12,20,25,26]. The various researchers have used these ground profiles to evaluate vehicle mobility performance. In most cases, the deterministic ground profiles have been used for comparison of computed and measured results to validate their analytical models. Table 3.1 gives a summary of profiles utilized by the various researchers for simulation and field testing of wheeled and tracked vehicles.

TABLE 3.1

STATE OF THE ART SURVEY ON GROUND PROFILES UTILIZED FOR SIMULATION SOFTWARE AND TESTING OF TRACKED VEHICLES

Researcher(s)	Study	Test Vehicle	Obstacle	Terrain
Eppinger *et al* [5]	Ride simulation & prototype testing	Experimental six-wheel tracked vehicle	Trapezoidal bump	Mild, rough, plowed fields
U S. Army Engineer Waterways Exper. Station [21] Nutall *et al* [22]	Mobility performance, AMC (AMC'71, AMC'74) model simulation & vehicle field testing	M35A2, M113A1	-------	Terrain units 20in fine grained, 10in coarse grained soils
Lessem & Murphy [6]	Ride performance model simulation & vehicle field testing	M4, M113, M114 M29	Semicircle obstacles: 6-,8-,12-,14-,16- & 18-inch heights; Ditches: 8 inch deep and 12-,24-,36- & 48-in. wide	- - - -
Wheeler [14]	Ride performance simulation & testing	XM1, CTVSD, 3/4-ton truck	Random obstacle, bump courses (see Figure 3.6)	Cross country terrain
Hoogterp [7]	Ride performance simulation & testing	M60A1, MICV	Semicircle bumps: 3-,6-,8-,& 12-inch heights Trapezoidal bumps: 3- & 6-inch heights	Spectral density ground profiles and surveyed courses; flat level road, hood trail, & APG course
Meachom *et al.* [15]	TRACKOB II & III obstacle negotiation test and simulation	M60, XM1	Block obstacles: 5-, & 9-inch height	----- --
Murphy [24]	Ride performance field testing	M60	Semicircle obstacles: 12- & 16-inch heights	Terrain courses of varying surface roughness: 1.1, 1.9, 2.8, 5.8 RMS inches
Beck & Rehage [16]	Test & graphics simulation of articulated vehicles	M113	Water obstacles	Flat terrain
Austin *et al* [25]	Shock absorber & vehicle field testing	IFV, M113	Ramp obstacle course	Washboard terrain course
Petrick *et al* [19] Creighton [20]	NNNM, VEHDYN (VEHDYN II) mobility models of tracked vehicles	M60, M113, XM1	Discrete rigid obstacles, ditches, & streams	Cross country field, road, and trail courses
Giguere [26]	Ride performance field testing of tracked vehicle with different suspension configurations	M113	Granite block obstacle course	Selected standard courses: cross-country, sinewave
Maclaurin [23]	Ride performance AD-Model simulation, & vehicle field testing	British MCV, Challenger	Ramp course	Random, rocky and sinewave courses
Garnich & Grimm [11]	Ride performance model simulation, & vehicle field testing	M60	Semicircle obstacles: 8-, 12-inch heights	-
Galaitsis [10]	Track model simulation & vehicle field testing	M113	-------	Flat ground profile
McCullough & Haug [12]	Superelement model simulation and vehicle testing	M113	Semicircle obstacle 8-inch height	Soil storage model profiles

Lessem & Murphy [6] and Garnich & Grimm [11] conducted field tests with semicircle and ditch obstacles to validate the analytical models. Eppinger *et al.* [5] used the trapezoidal bump to test a six-wheeled prototype model. Meachom *et al.* [15] validated the TRACKOB II and TRACKOB III with block discrete obstacles. Simpler ground profiles were flat terrains as used by Galaitsis [10] to study the track dynamics and by Beck & Wehage [16] for analyzing dynamics of coupled vehicles. Field research on dynamic performance of tracked vehicles traversing discrete obstacles was conducted by Murphy [24], Austin *et al.* [25] and Giguere [26]. Murphy [24] studied the ride and handling characteristics of a vehicle traversing over semicircle obstacles. Figure 3.1 illustrates typical vehicle test runs over semicircle and ditch obstacles. Figures 3.2 and 3.3 illustrate the washboard and ramp courses used to evaluate the shock absorbers for military vehicles [25]. Giguere [26] conducted field tests of an M113 tracked vehicle, with different suspension configurations using the granite block course, shown in Figure 3.4.

For analysis of the vehicle models presented in Chapter 2, the semicircle and block obstacles are selected as deterministic inputs for transient response analyses. Figure 3.5 depicts the schematics of the semicircle and block obstacles. Displacement input due to wheel/track-obstacle contact is characterized by the obstacle geometry. The displacement excitation due to a semicircle obstacle is computed as a function of the obstacle height (h_0), obstacle diameter (D_0) and the location of wheel/track contact point. In the case of a block obstacle, the displacement excitation is expressed as a function of block height (h_B), length (L_B) and the location of wheel/track contact point

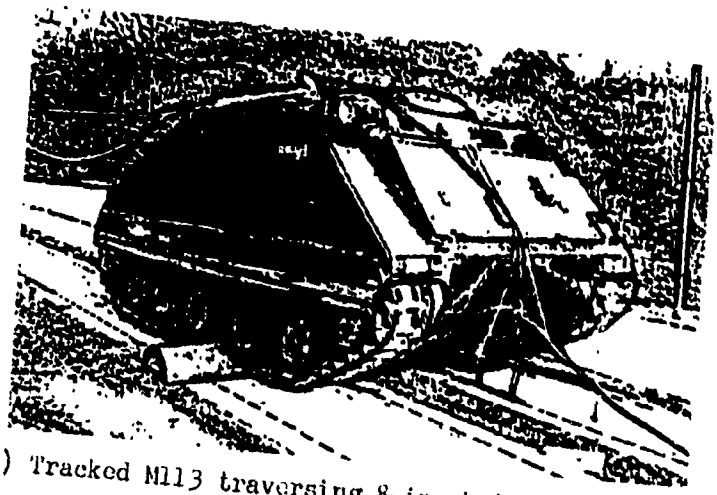

(a) Tracked M113 traversing 8-in. half-round obstacle

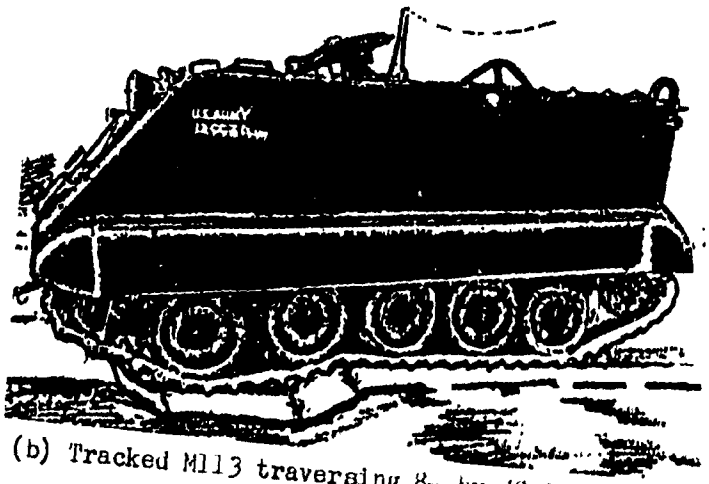

(b) Tracked M113 traversing 8- by 48-in. ditch

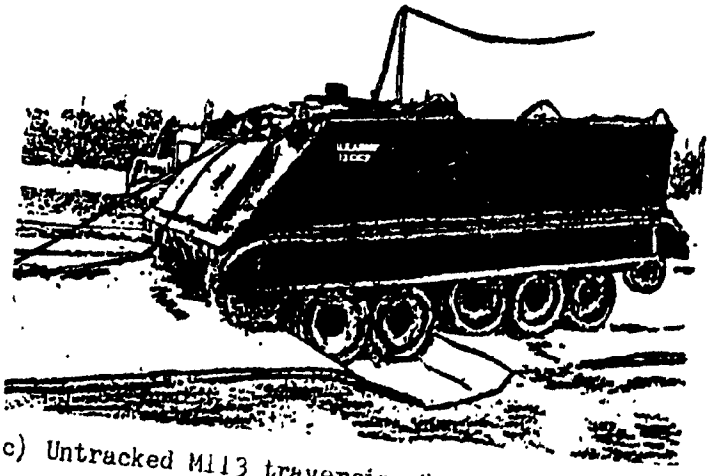

(c) Untracked M113 traversing 8- by 48-in. ditch

Figure 3.1 M113 Vehicles Traversing Various Obstacles [6].

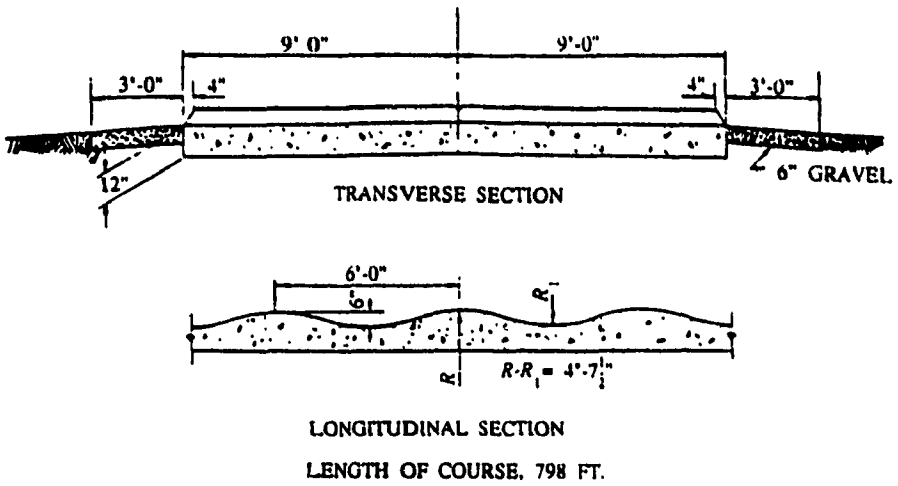

Figure 3.2 Sections of Six-Inch Washboard Course [25].

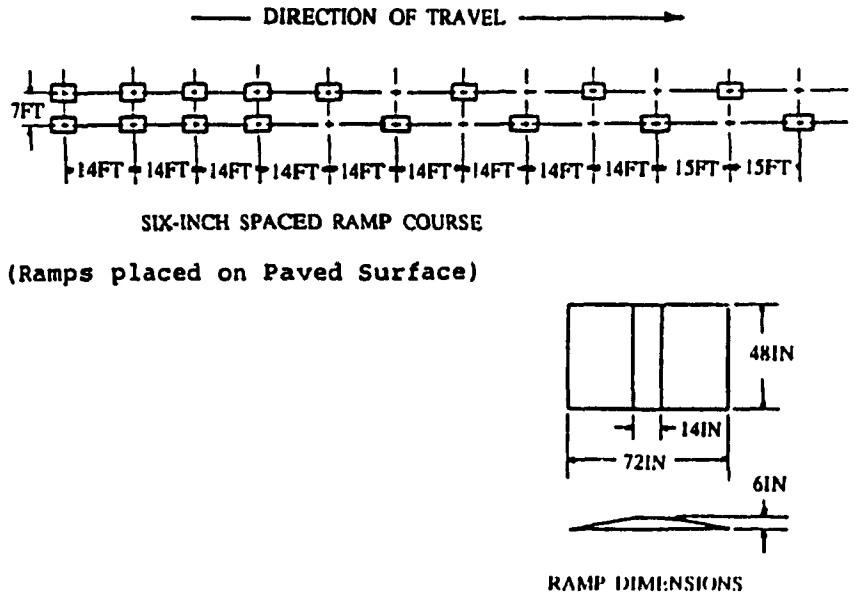

Figure 3.3 Diagram of Spacing for Ramp Course [25].

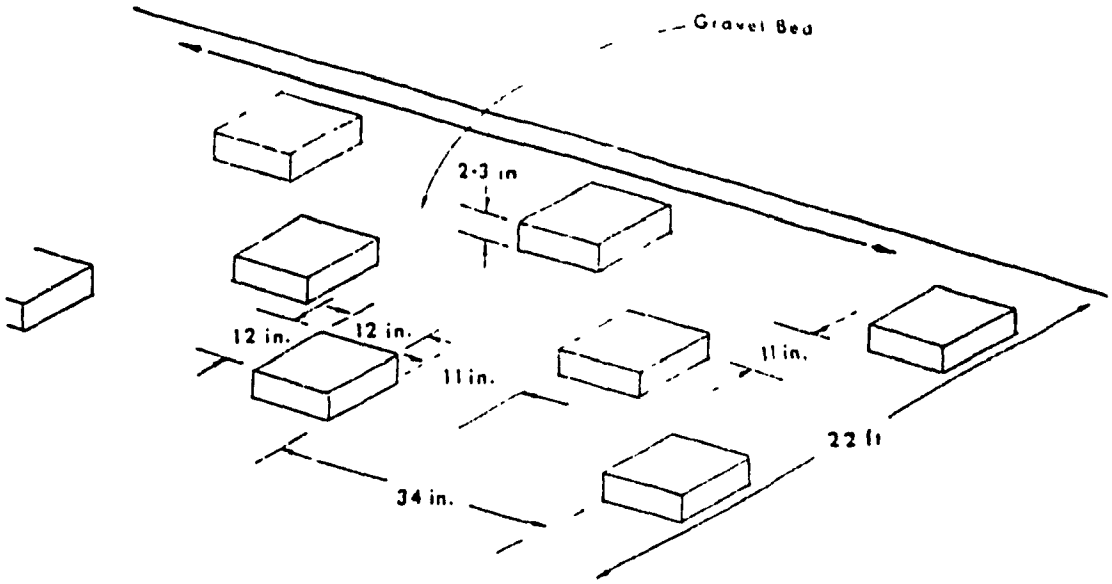

(a) Technical specifications for the Granite Block Course - The course is 200 m long and is designed to provide shock inputs alternately to opposite vehicle suspension components. The effect on the vehicle varies with speed and suspension design.

(b) The Iltis on the Granite Block Course.

Figure 3.4 Granite Block Course (COURTESY OF LETE).

3.3 RANDOM TERRAINS

While deterministic inputs have been utilized to determine maximum speeds for vehicle mobility and ride dynamics, various studies have emphasized the significance of realistic terrain conditions. Numerous studies on mobility performance of tracked vehicles have been conducted on random off-road terrains [6,24,26]. Hoogterp [7], Wheeler [14], and WES [21] used elevations of various random terrains to validate their models. Hoogterp [7] utilized hood trail and surveyed courses while factors representing the roughness of various courses have been assigned by WES [21]. A bumpy terrain course, as shown in Figure 3.6, was established by Wheeler [14] to evaluate vehicle mobility.

Terrains which are random in nature are conveniently expressed in terms of power spectral density. Generally, terrains traversed by vehicles are assumed rigid and the profiles measured under no-load conditions, represent the disturbances to the vehicle running gear. It has been established that terrain roughness is normally distributed and can be accurately represented as a stationary random process [36]. Since the power spectral density of the input random process is a quantity suitable for analysis of the dynamic behaviour of the vehicle, the disturbances due to irregular terrains are readily described by power spectral densities.

Various profiles of random undeformable terrains have been reported in the form of PSDs. Bogdanoff *et al.* [34] provided an atlas of roughness of various off-road grounds representing the test areas for military tracked vehicles. Maclaurin [23] established PSD representations of random course and rocky terrains. The MVEE (Military Vehicles & Engineering Establishment) random course is utilized for ride

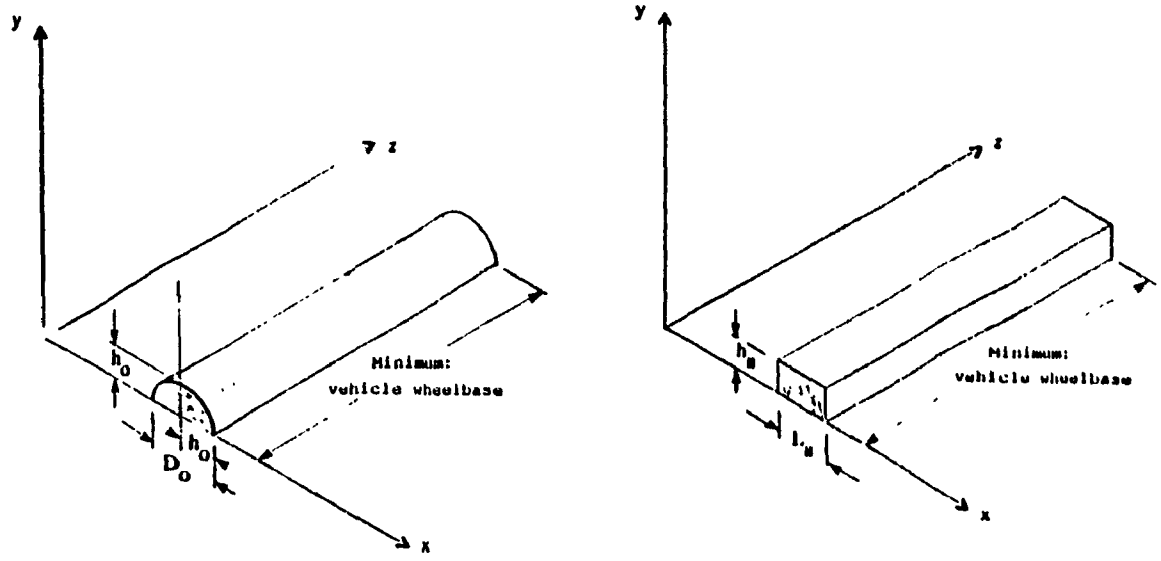

Figure 3.5 Geometry of Semicircle and Block Obstacles.

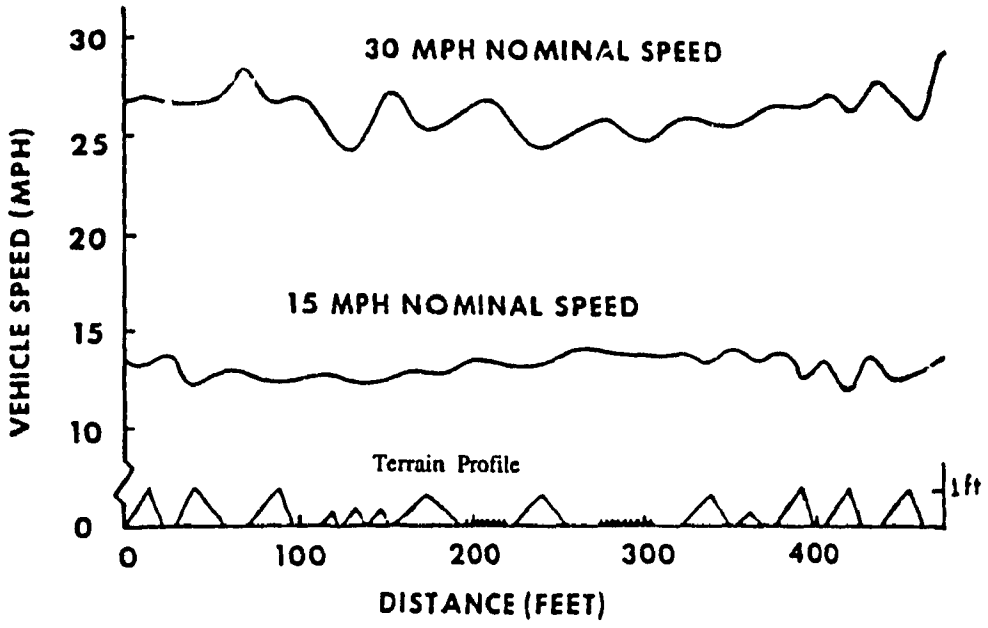

Figure 3.6 XM1 Speed Record Over Terrain Profile [14].

and mobility performance analysis while the rocky course is suitable for vehicle durability testing. The spatial power spectral densities of typical terrains, used to evaluate the tracked vehicle performance are shown in Figure 3.7. Power spectral densities of roads and agricultural terrains, suitable for ride performance testing of various vehicles including military tracked vehicles, have also been established. Wong [38] established the spatial spectral density of pasture and plowed fields, as shown in Figure 3.8. The spectral densities of various road surfaces, which have been established by MIRA (Motor Industry Research Association) [35], are shown in Figure 3.9.

Ordinarily, power spectral densities of road or off-road terrains are established via measurements of the terrain profiles, statistical manipulation of the random data, and analytical techniques converting the statistical data to power spectrum quantities. Measurements are performed by means of rod and level instruments or profilometers which provide ground elevations over certain wavelength. Most of the terrains overrun by tracked vehicles are of deformable nature and significant amount of sinkage is experienced by the track and road wheels. Wong *et al.* [33] conducted a study on ground pressure distribution under the running gear of the tracked vehicle establishing track-terrain sinkage relationships. McCullough & Haug [12] made use of soil models for the simulation of their superelement model. Soil models may represent sand, snow, or mud including muskeg. However in this study, the influence of sinkage on terrain-track interactions is neglected and the ride performance of multi-wheeled and tracked vehicles is evaluated for selected undeformable terrains, represented by their PSDs.

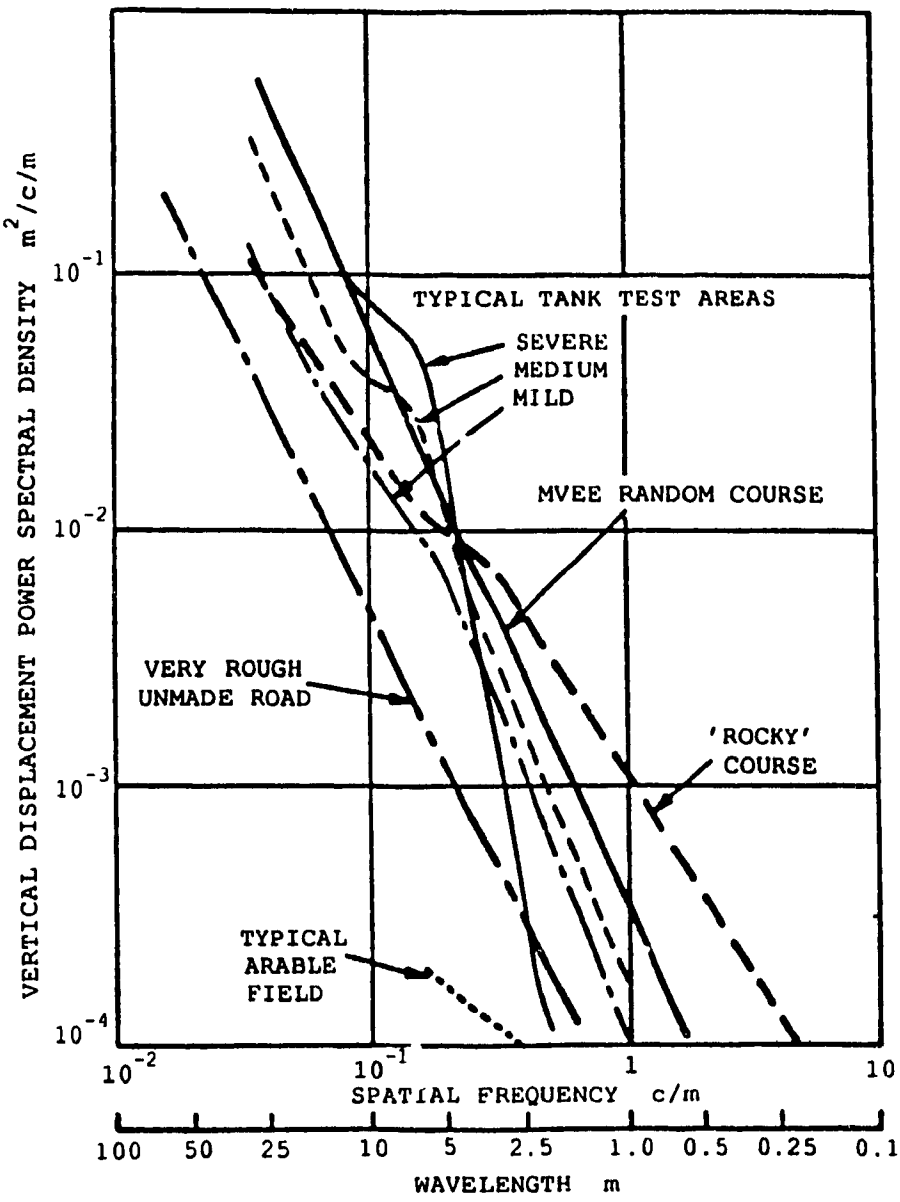

Figure 3.7 Vertical Displacement PSDs of Typical Tank Test Areas [23].

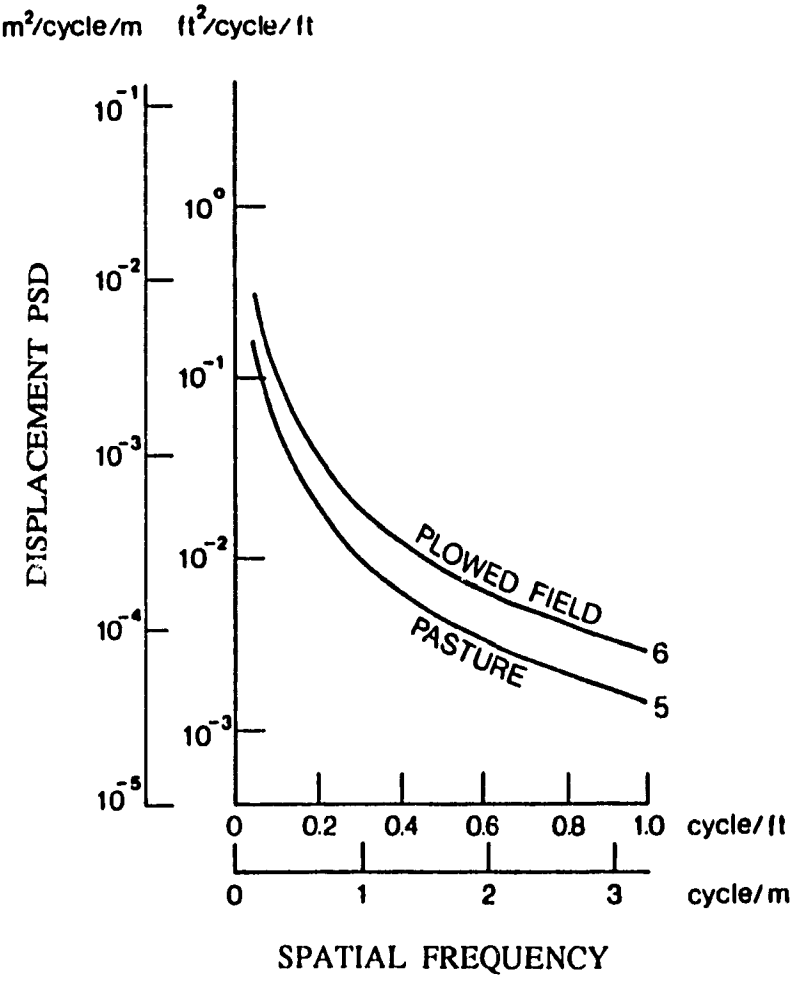

Figure 3.8 Spectral Densities as Functions of Spatial Frequency for Two Types of Unprepared Terrains [38].

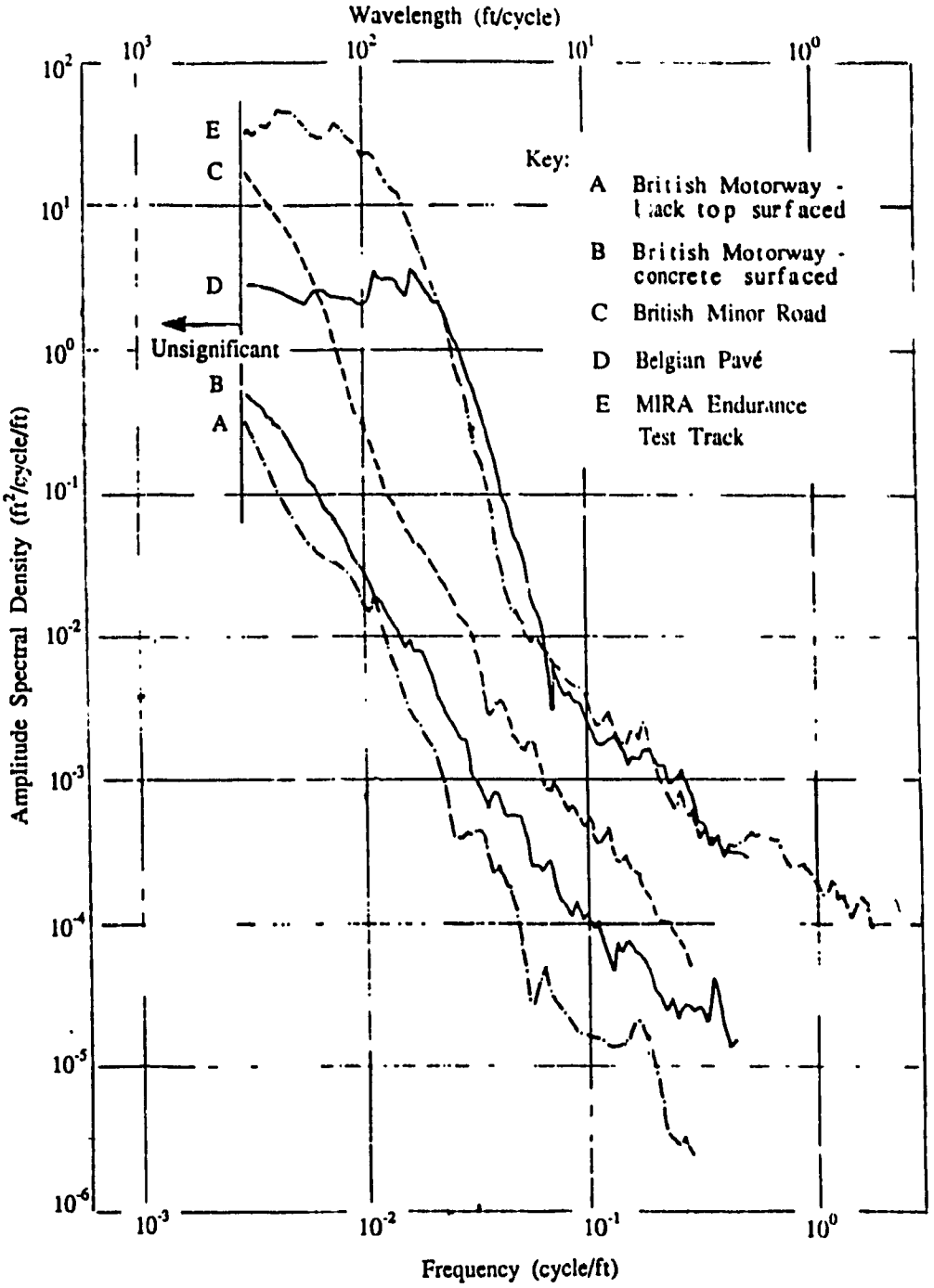

Figure 3.9 Displacement Spectra of Various Roads [35].

3.3.1 Description of Random Terrains

Spectral densities of various road and off-road surfaces that closely approximate the experimental terrain roughness data are described by [36,37]:

$$\Phi_p(\Omega) = \Phi_p(\Omega_o)\left[\frac{\Omega}{\Omega_o}\right]^{-w} \qquad (3.1)$$

where

$\Phi_p(\Omega)$ = spatial spectral density of the terrain roughness

$\Phi_p(\Omega_o)$ = roughness coefficient (value of the spectral density at the discontinuity frequency, Ω_o)

Ω = spatial frequency of road roughness

Ω_o = spatial frequency at which a discontinuity occurs (Ω_o=1 for continuous spectral density)

w = waviness of the terrain

Four terrain profiles, namely, the Belgian pavé [35], the MVEE random test course [23], and pasture and plowed fields [38], are selected to evaluate the ride dynamic response of the vehicle models. It has been established that the spectral density of the measured random road/off-road terrains can be expressed by equation (3.1), where the roughness coefficient, $\Phi_p(\Omega_o)$, and waviness of the terrain w, are estimated from the spectral density curve. The spectral density of the Belgian Pavé reveals two discontinuities, as shown in Figure 3.10, thus the equation (3.2) is modified to represent the spectral density of three continuous bands:

$$\Phi_p(\Omega) = \begin{cases} \Phi_p(\Omega_{o1})\left[\dfrac{\Omega}{\Omega_{o1}}\right]^{-w_1} & \text{for } \Omega \le \Omega_{o1} \\ \Phi_p(\Omega_{o1})\left[\dfrac{\Omega}{\Omega_{o1}}\right]^{-w_2} & \text{for } \Omega_{o1} < \Omega \le \Omega_{o2} \\ \Phi_p(\Omega_{o2})\left[\dfrac{\Omega}{\Omega_{o2}}\right]^{-w_3} & \text{for } \Omega > \Omega_{o2} \end{cases} \qquad (3.2)$$

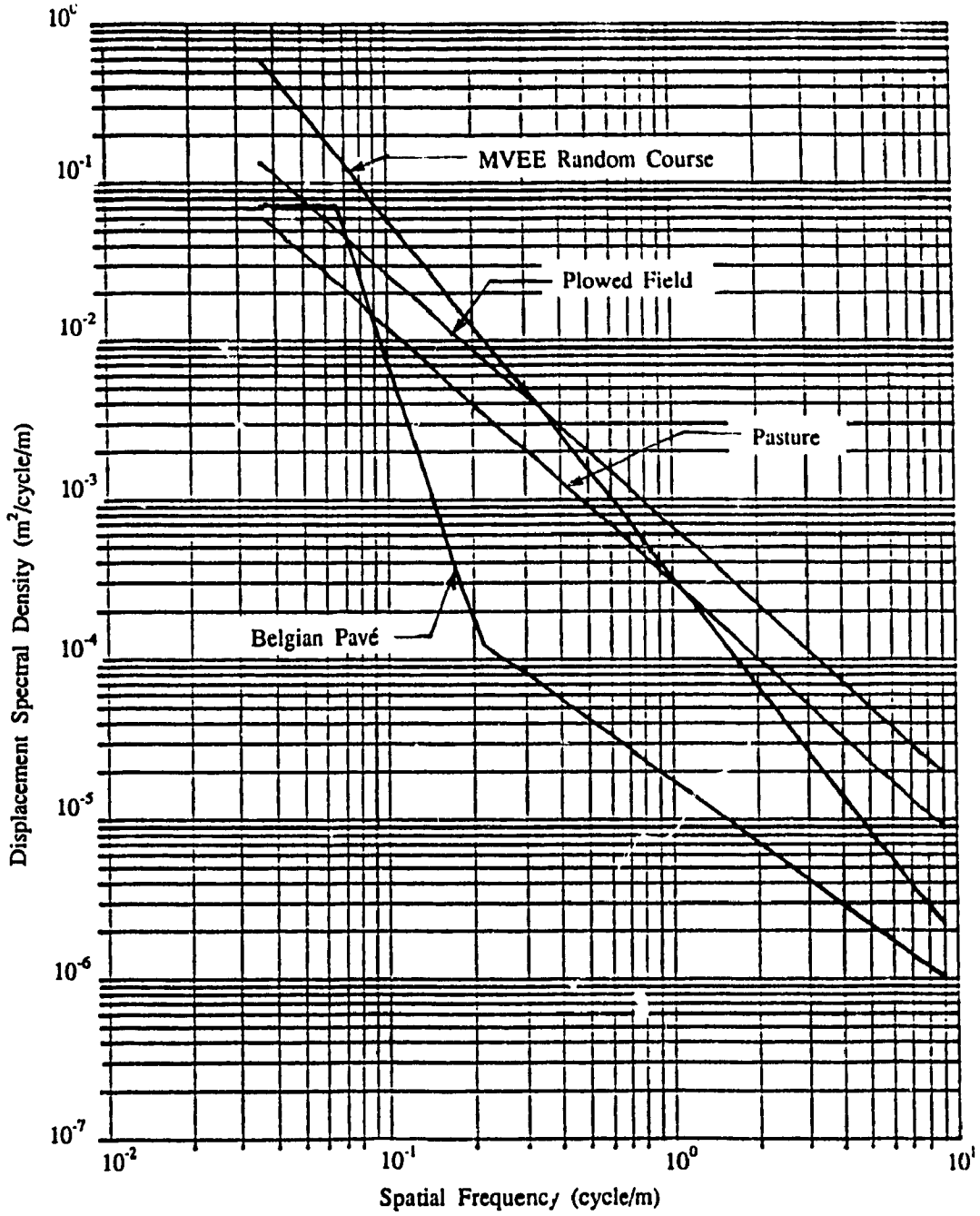

Figure 3.10 Comparison of Displacement Spectra for Selected Road and Off-Road Terrains.

TABLE 3.2

ROUGHNESS PARAMETERS OF SELECTED ROAD AND OFF-ROAD TERRAINS

Terrain	Waviness Number	Ω_o	$\Delta(\Omega_o)$
Belgian Pavé	$w_1 = 0.0$ $w_2 = 5.664$ $w_3 = 1.290$	$\Omega_{o1} = 0.0656$ $\Omega_{o2} = 0.207$	$\Delta(\Omega_{o1}) = 7.113 \times 10^{-4}$ $\Delta(\Omega_{o2}) = 1.295 \times 10^{-4}$
Pasture	$w = 1.6$	1	3.0×10^{-4}
Plowed Field	$w = 1.6$	1	6.5×10^{-4}
MVEE Random Course	$w = 2.27$	1	3.1622×10^{-4}

The spectral density of unprepared terrains, such as the pasture and plowed field, and the MVEE random test course are expressed by equation (3.1) with $\Omega_o = 1$. The spatial spectral density of these terrains along with the road surface Belgian pavé is presented in Figure 3.10. The values of roughness coefficients and waviness of the terrains are listed in Table 3.2.

3.3.2 Input Spectral Density Matrix

As the M113 vehicle traverses along a randomly rough course, it is subjected to five vertically imposed spatial displacement functions, one at each road wheel per track. Temporal frequency of vehicle vibration, f, is related to the spatial frequency and the vehicle speed:

$$f = \Omega V \tag{3.3}$$

where V is the vehicle speed. The temporal spectral density, $\Phi(f)$, is then related to spatial spectral density as:

$$\Phi_p(f) = \frac{1}{V} \Phi_p(\Omega) \tag{3.4}$$

where $\Phi_p(f)$ is the spectral density of direct input displacement to the vehicle at the road wheel and track contact point. The input acceleration power spectral density is then expressed as:

$$\Phi_a(f) = (2\pi f)^4 \Phi_p(f) \tag{3.5}$$

where $\Phi_a(f)$ is the spectral density of acceleration input to the vehicle at the road wheel and track contact point. Figures 3.11 to 3.14 present the displacement and acceleration spectral densities of Belgian pavé, pasture and plowed field, and MVEE random course profiles, respectively, for various vehicle speeds.

Assuming that all the road wheels follow the same path and are

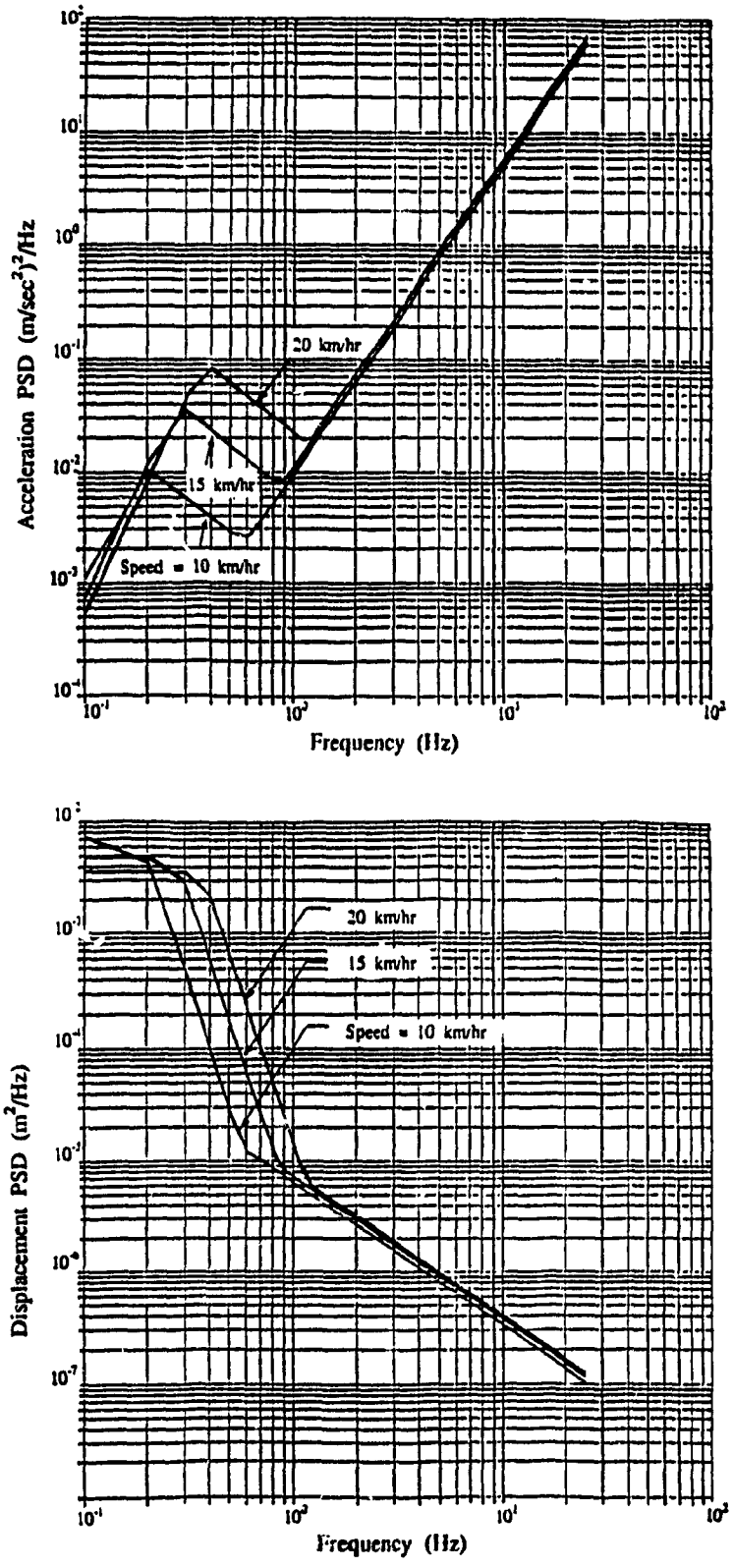

Figure 3.11 Displacement and Acceleration Spectral Densities of Belgian Pavé for Various Speeds.

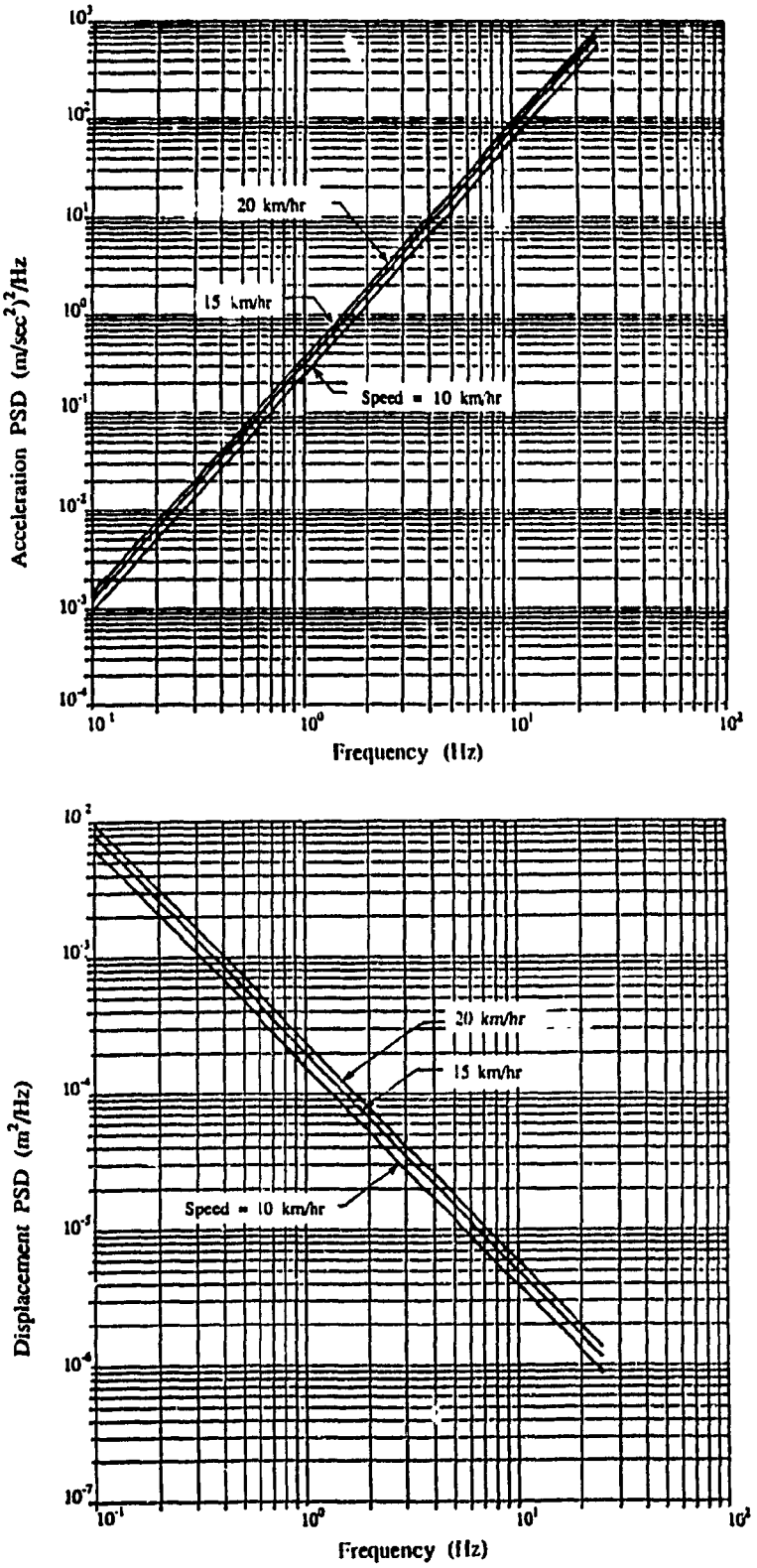

Figure 3.12 Displacement and Acceleration Spectral Densities of Pasture for Various Speeds.

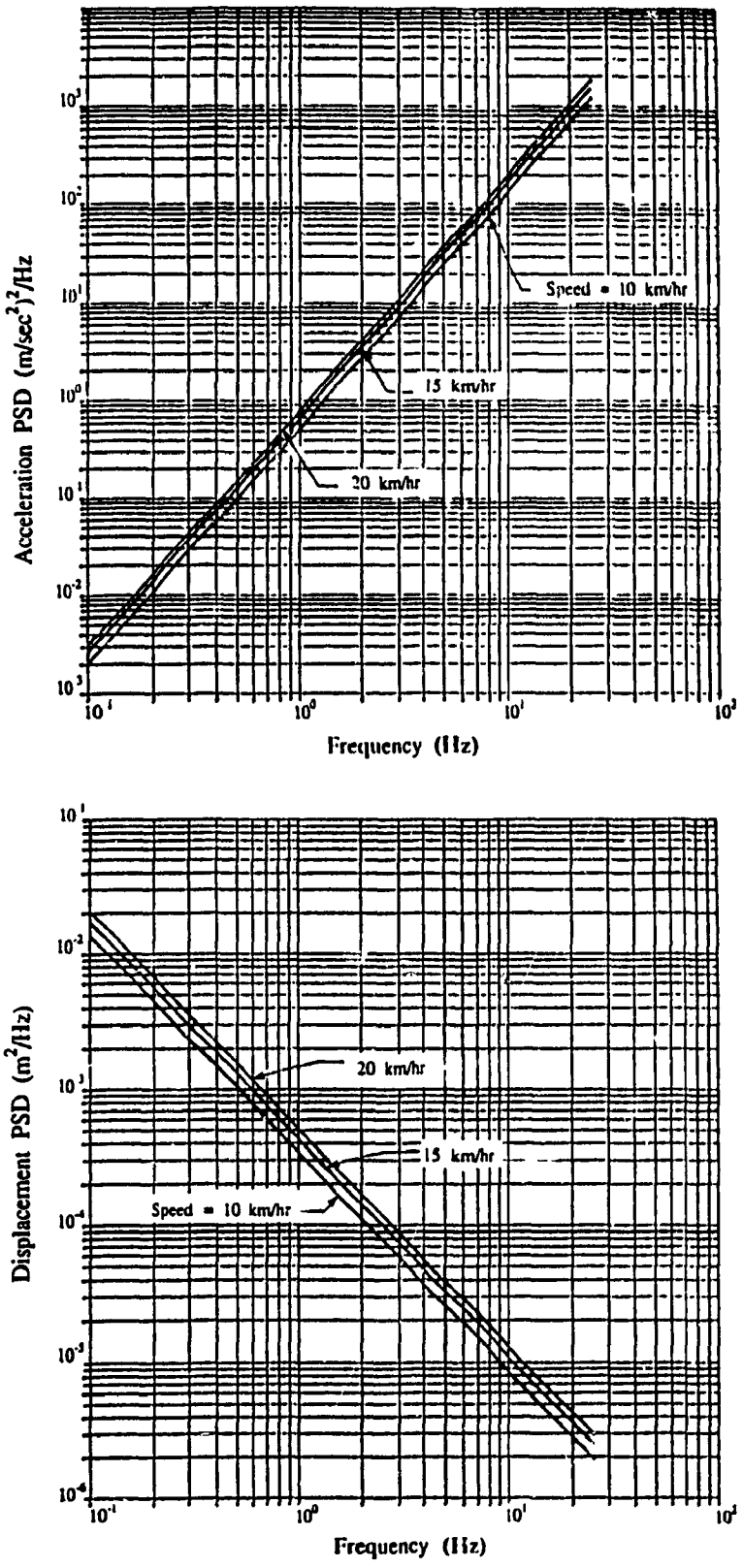

Figure 3.13 Displacement and Acceleration Spectral Densities of Plowed Field for Various Speeds.

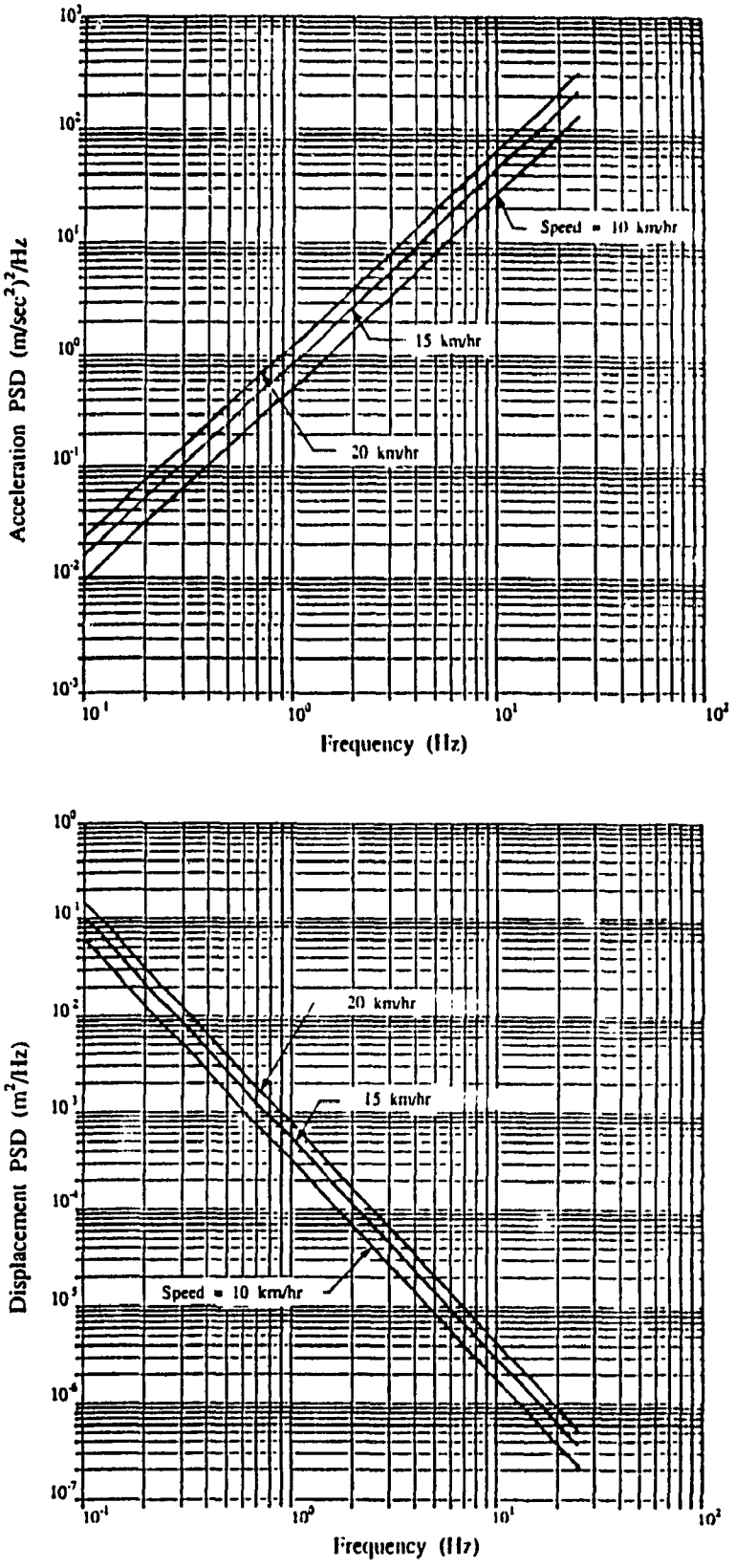

Figure 3.14 Displacement and Acceleration Spectral Densities of MVEE Random Course for Various Speeds.

subjected to the same profile as the first road wheel, the cross-spectral densities can be established as a function of the time delay. The time delay is related to the vehicle speed and spacing of the road wheels, given by:

$$\tau_{jk} = L_{jk} / V \tag{3.6}$$

where τ_{jk} is the time delay of road wheels 'j' and 'k', L_{jk} is the distance between road wheels 'j' and 'k'. The cross spectrum of road wheels 'j' and 'k', is given by [39]:

$$\Phi_{jk}(f) = \Phi_{jj}(f) \exp(-j2\pi f L_{jk}/V) \tag{3.7}$$

where $\Phi_{jk}(f)$ is the cross spectral density and $\Phi_{jj}(f)$ represents the direct power spectral density determined from equation (3.4). The input spectral density matrix for the M113 vehicle models is then obtained from equations (3.4) and (3.7), considering the property of cross-spectra:

$$\Phi_{jk}(f) = \Phi_{kj}^{*}(f) \tag{3.8}$$

and in matrix form:

$$\left[\Phi_{w}(f)\right] = \frac{\Phi(\Omega)}{V} \begin{bmatrix} 1 & e^{-ju_{12}} & e^{-ju_{13}} & e^{-ju_{14}} & e^{-ju_{15}} \\ e^{ju_{21}} & 1 & e^{-ju_{23}} & e^{-ju_{24}} & e^{-ju_{25}} \\ e^{ju_{31}} & e^{ju_{32}} & 1 & e^{-ju_{34}} & e^{-ju_{35}} \\ e^{ju_{41}} & e^{ju_{42}} & e^{ju_{43}} & 1 & e^{-ju_{45}} \\ e^{ju_{51}} & e^{ju_{52}} & e^{ju_{53}} & e^{ju_{54}} & 1 \end{bmatrix} \tag{3.9}$$

where $u_{jk} = 2\pi f L_{jk}/V$; $j = 1,2,\ldots,5$; $k = 1,2,\ldots,5$,

and '*' denotes the complex conjugate.

3.4 SUMMARY

The ground profiles utilized by various researchers for simulation and field testing of military vehicles are reviewed. The excitations arising from deterministic as well as random terrains are discussed. The semicircle and block obstacles are the deterministic inputs selected for transient response analyses of the vehicle models. Displacement input due to wheel/track-obstacle interaction is characterized by obstacle geometry and location of wheel/track contact point. The Belgian Pavé, pasture, plowed fields and MVEE random course are selected as random terrain excitations for dynamic analyses of the vehicle models. The roughness of the selected terrains is expressed by its displacement and acceleration PSDs which are dependent on vehicle speed.

CHAPTER 4

RESPONSE EVALUATION OF MULTI-WHEELED/TRACKED VEHICLE MODELS

4.1 INTRODUCTION

A number of options are available for solving the differential equations characterizing the dynamics of the wheeled and tracked vehicle models, presented in Chapter 2. The usual approach is to obtain the dynamic response of the vehicle, when the vehicle is traversing a non-deformable terrain, as a function of time. However, off-road terrains used by tracked vehicles are deformable in nature and thus significant amount of track and road wheel sinkage may be experienced. Although the road wheel and track sinkage is the primary factor that affects the mobility performance of the vehicle, the sinkage also influences the track-terrain interactions and thus the vehicle ride. Objective of this study is to establish an understanding of the tracked vehicle ride in view of dynamics of the vehicle and its suspension systems. Thus, the ride response of vehicle models is evaluated for undeformable terrains, while neglecting track and road wheel sinkage.

In this chapter, the analytical techniques employed to simulate the vehicle models, developed in Chapter 2, are described. The dynamic response of the M113 vehicle subjected to non-deformable terrains, described in Chapter 3, is evaluated. The relative ride performance of M113 A1, M113 A2 and M113 A1$\frac{1}{2}$ vehicles is evaluated via comparing the bounce and pitch response characteristics of the vehicle models.

4.2 ANALYTICAL TECHNIQUES

Two options are available for simulating the vehicle models developed in Chapter 2, namely: the time-domain and frequency-domain techniques. The time-domain analysis utilizes variables as functions of

time and uses numerical integration algorithms to solve the differential equations of motion of the tracked vehicle. The frequency-domain approach utilizes Fourier transform to represent the time dependent variables as frequency dependent variables. Frequency-domain technique is suitable for either linear or linear equivalent models, whereas the time-domain technique can simulate both linear as well as nonlinear models. Both analytical techniques are described in the following subsections.

4.2.1 Time Domain Analysis

Time-domain analysis is primarily a direct solution of the equations of motion, such as differentiation or integration of the equations. Numerous numerical integration algorithms exist to solve either linear or non-linear set of differential equations [40]. In particular, the Runge-Kutta fourth order method is utilized to solve the coupled differential equations of motion of the tracked vehicle.

The differential equations of motion of the vehicle models, developed in Chapter 2, may be represented in the following matrix form:

$$[m]\{\ddot{y}\} + \{F_C\} + \{F_K\} + \{F_{tr}\} = \{F_G\} + \{F_o\} \qquad (4.1)$$

where [m] is the (N x N) mass/inertia matrix. $\{F_C\}$, $\{F_K\}$, $\{F_{tr}\}$, $\{F_G\}$ and $\{F_o\}$ are (N x 1) vectors of suspension damping, suspension stiffness, track/tire, gravitational and excitation forces, respectively. N is the number of degrees of freedom and $\{y\}$ is the vector of response coordinates, given by,

$$\{y\} = \{y_h,\ \phi_h,\ y_{w1},\ y_{w2},\ y_{w3},\ y_{w4},\ y_{w5}\}^T$$

Equation (4.1) is re-arranged as

$$\{\ddot{y}\} = [m]^{-1}\left\{\{F_G\} + \{F_o\} - \{F_C\} - \{F_K\} - \{F_{tr}\}\right\} \qquad (4.2)$$

The set of N second order differential equations are then transformed into 2N first order differential equations utilizing the following substitution:

$$\dot{y}^i = y^{i+N} \qquad i = 1,\ldots,N$$
$$\ddot{y}^i = \dot{y}^{i+N} \qquad i = 1,\ldots,N \tag{4.3}$$

The resulting first order differential equations are thus expressed in the following form:

$$[\mathcal{P}]\ \{\dot{y}\} + [Q]\ \{y\} = \{F\} \tag{4.4}$$

where $[\mathcal{P}]$ and $[Q]$ are coefficient matrices of $\{\dot{y}\}$ and $\{y\}$, respectively, and $\{F\}$ is the forcing function matrix. Equation (4.4) is then rearranged into a prescribed numerical integration format by premultiplying by the inverse of matrix $[\mathcal{P}]$ as,

$$\{\dot{y}\} = -[\mathcal{P}]^{-1}\ [Q]\ \{y\} + [\mathcal{P}]^{-1}\ \{F\} \tag{4.5}$$

The first order expressions are then solved for velocities and displacements using the Runge Kutta Order-Four algorithm [40]. The differential equations of motion of the vehicle models incorporating nonlinearities arising from shock absorbers and bump stops are solved in the time domain.

4.2.2 Frequency Domain Analysis

In the frequency domain analysis the time dependent equations of motion are Fourier transformed to frequency dependent variables. In general, the linear or linearized equations of motion for the vehicle models are expressed in matrix form as:

$$[m]\ \{\ddot{y}\} + [C]\ \{\dot{y}\} + [K]\ \{y\} = [K_f]\ \{y_o\} \tag{4.6}$$

where [C] and [K] are (N x N) damping and stiffness matrices,

respectively, and $[K_f]$ is (N x n) forcing matrix. Equation (4.6) is Fourier transformed to yield:

$$\{Y(j\omega)\} = [\mathcal{H}(j\omega)]\ \{Y_0(j\omega)\} \tag{4.7}$$

where

$\{Y(j\omega)\}$ is the Fourier transform of vector containing response variables.

$\{Y_0(j\omega)\}$ is the Fourier transform of vector containing excitation variables.

and

$[\mathcal{H}(j\omega)]$ is the complex matrix representing the frequency response function of the system, given by:

$$[\mathcal{H}(j\omega)] = \left[[K] - \omega^2[m] + j\omega\ [C]^{-1}\ [K_f]\right] \tag{4.8}$$

Equation (4.8) yields the frequency response characteristic of the vehicle model along the generalized coordinates. The dynamic characteristics of the multi-wheeled/tracked vehicle along the coordinates other than generalized coordinates, such as fore-aft motion of the hull, road arm rotation, and fore-aft motion of the wheels, are determined via constraint equations. The longitudinal response of the vehicle hull and the road wheels and the road arm rotation are determined from the following:

$$\{X_w(j\omega)\} = [T_X]\ \{Y(j\omega)\} \tag{4.9}$$

$$\{\Theta(j\omega)\} = [T_\theta]\ \{Y(j\omega)\} \tag{4.10}$$

where $[T_X]$ and $[T_\theta]$ are transformation matrices of dimension (n_x x N) and (n x N), respectively, (n_x = 1, for *Model I & II*, n_x = 6, for *Model III & IV*). $\{\Theta(j\omega)\}$ is (n x 1) vector of the Fourier transform of road arm rotational coordinates.

The frequency domain solution technique thus reduces simulation

time considerably as compared to the time domain analysis. However, the frequency domain method is limited to linear or linearized systems of equations only. Therefore, the nonlinear differential equations of motion characterizing the multi-wheeled/tracked vehicle models, must be linearized to be solved in the frequency domain.

4.3 VEHICLE PARAMETERS

Vehicle parameters, such as vehicle geometry; masses and inertias; static characteristics of torsion bars, road wheel tires and track pads; force-velocity characteristics of shock absorbers; and force-displacement characteristics of bump stops, are determined from the design drawings [42], published literature [6,20], and experimental studies carried out by Ford Motor Company [43], DEW Engineering and Development [44], and Austin *et al.*[25].

Table 4.1 lists the mass/inertia and running gear parameters of the M113 A1 and M113 A2 vehicles. Sprung mass of the vehicle hull represents the gross vehicle weight less the road wheel masses, suspension masses and half the weight of the tracks. Road wheel mass includes half the mass of the road arm. The torsional stiffnesses of A1 and A2 suspension systems are represented by their equivalent spring rates to be employed in the vehicle *Model I* and *II* with idealized vertical suspension.

Force-velocity power curves for A1 and A2 shock absorbers have been established via laboratory testing [25]. The force-velocity characteristics of shock absorbers used in A1 and A2 suspension configurations, as shown in Figure 4.1, reveal a power curve composed of segments of varying slopes associated with the damping generated through bleed-control, blow-off, and orifice control. The force-velocity

TABLE 4.1

PARAMETERS OF MULTI-WHEELED/TRACKED M113 VEHICLE MODEL
[25,42,43]

Description	Symbol	Vehicle Configuration	
		M113 A1	M113 A2
Mass/Inertia			
Hull mass, kg (lb)			
untracked vehicle	m_h	8351 (18380)	8484 (18653)
tracked vehicle		8869 (19520)	9006 (19790)
Hull pitch moment of Inertia, $kg \cdot m^2$ ($lb \cdot sec^2 \cdot in$)			
untracked vehicle	I_h	17360 (153664)	14155 (125359)
tracked vehicle		18437 (163195)	15026 (133000)
Road wheel mass, kg (lb);			
wheel station 1	m_{w1}	113.5 (250)	92.6 (204)
wheel station 2	m_{w2}	113.5 (250)	92.6 (204)
wheel station 3	m_{w3}	113.5 (250)	87.0 (192)
wheel station 4	m_{w4}	113.5 (250)	87.0 (192)
wheel station 5	m_{w5}	113.5 (250)	92.6 (204)
Tire Parameters			
Tire spring rate, N/m (lb/in)	K_{wi}	612900 (3500)	612900 (3500)

(Table 4.1...cont'd)

Note: Running gear parameters (wheel mass, tire stiffness, independent suspension properties, etc.) represent single units from both sides of the vehicle.

TABLE 4.1 (continued)

Description	Symbol	Vehicle Configuration	
		M113 A1	M113 A2
Suspension Parameters			
Torsion bar spring rate, N·m/rad (lb·in/rad)	$K_{\theta i}$	9884 (87462)	8350 (73888)
Equivalent vertical spring rate, N/m (lb/in)	K_i	115675 (660)	97722 (558)
Shock absorber damping rate, N·sec/m (lb·sec/in)	C_{1i}	22520 (128.6)	55629 (317.7)
	C_{2i}	5126 (29.27)	7135 (40.74)
	C_{3i}	22520 (128.6)	39146 (223.5)
(i=1,5 for A1; i=1,2,5 for A2)	C_{4i}	4187.5(23.91)	4536 (25.9)
Breakpoint velocity*, m/s (in/s)	υ_{p1}	0.4064 (16)	0.216 (8.0)
	υ_{p2}	-0.4064 (-16)	-0.216(-8.0)
Friction Force Magnitude,			
linkage, N (lb)	F_L	222.4 (50)	222.4 (50)
shock absorber, N (lb)	F_{sa}	222.4 (50)	222.4 (50)
Bump stop stiffness coef., N/m (lb/in)	K_b	1500000 (8565)	1500000 (8565)
Bump stop equivalent torsional stiffness coef., N·m/rad (lb·in/rad)	$K_{\theta b}$	151250 (1338400)	151250 (1338400)

*Velocity at which transition from high value of damping coefficient to a low value occurs.

characteristics exhibit high damping coefficient corresponding to low piston velocities and the damping coefficient is reduced considerably when the piston velocity exceeds certain velocity, as shown in Figure 4.1. Coulomb damping due to dry friction within the linkage suspension and shock absorber is also listed in Table 4.1.

The geometric parameters of M113 A1 and M113 A2 vehicle models are presented in Tables 4.2 and 4.3, and the properties of the track are presented in Table 4.4. Mass, stiffness and damping properties of the running gear, listed in Tables 4.1 and 4.4, represent individual independent suspension road wheel assembly, and the track on each side of the vehicle.

The A1$\frac{1}{2}$ suspension configurations employ shock absorbers used in A2 suspension and torsion bars of A1 suspension system. Thus, the parameters of M113 A1$\frac{1}{2}$ vehicle are identical to those of M113A2 vehicle with the exception of torque-deflection characteristics of torsion bars.

4.4 FREE VIBRATION ANALYSIS OF THE VEHICLE MODELS

Multi-wheeled/tracked vehicle vibrations comprise of various deflection modes associated with the hull, chassis, road wheels, tracks and the driver. The amplitude, frequency and the direction of ride vibrations are strongly related to the free-vibration characteristics of the vehicle models. Hence an eigenvalue analysis [41] is carried out to establish the natural frequencies and principal deflection modes of the vehicle models.

4.4.1 Free-Vibration Analysis of the Undamped Vehicle Models

The equations of free-motion of the undamped vehicle models are expressed in the matrix form as:

$$[m]\{\ddot{y}\} + [K]\{y\} = \{0\} \qquad (4.11)$$

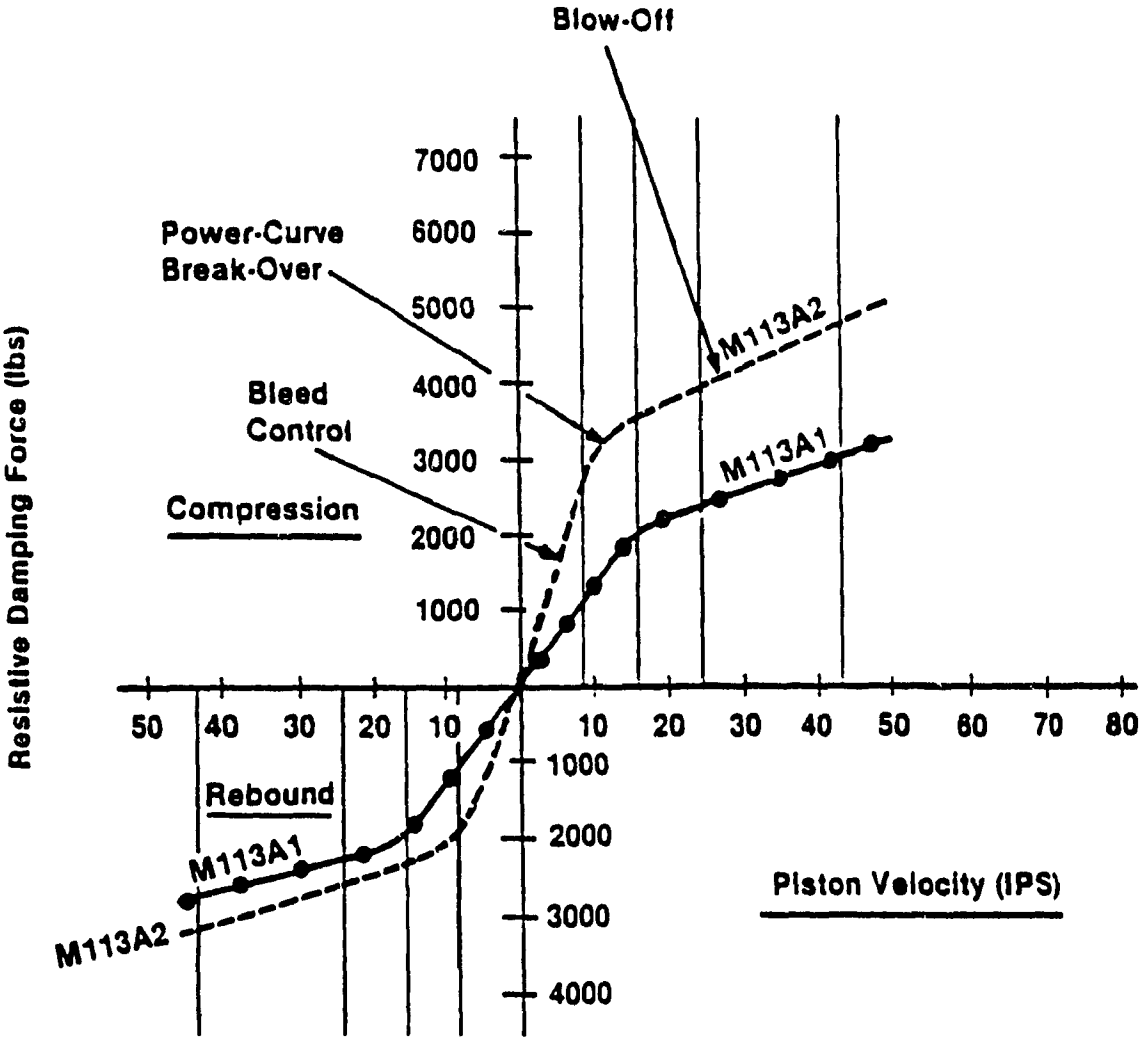

Figure 4.1 Force-Velocity Curves for M113 A1 and M113 A2 Shock Absorbers, [25].

TABLE 4.2

VEHICLE GEOMETRY - *MODEL I & II*
[42]

Description	Symbol	Vehicle Configuration	
		M113 A1	M113 A2
Suspension Location			
Horizontal distance from c.g. to:			
sprocket, m (in)	a_{Sp}	1.939 (76.35)	1.942 (75.45)
idler, m (in)	a_{Id}	-2.037 (80.18)	2.047 (80.60)
suspension 1, m (in)	a_1	1.285 (50.6)	1.288 (50.7)
suspension 2, m (in)	a_2	0.618 (24.35)	0.621 (24.45)
suspension 3, m (in)	a_3	-0.048 (-1.90)	-0.046 (-1.80)
suspension 4, m (in)	a_4	-0.715(-28.15)	-0.712(-28.05)
suspension 5, m (in)	a_5	-1.382 (-54.4)	-1.379(-54.30)
Bump stop clearance, m (in)	d_c	0.1254 (4.9)	0.1254 (4.9)
Driver position			
horizontal, m (in)	a_{dr}	0.9997 (39.4)	0.9652 (38.0)
vertical, m (in)	b_{dr}	-0.356 (-14.0)	-0.356 (-14.0)

TABLE 4.3

VEHICLE GEOMETRY - *MODEL III & IV* [42,43]

Description	Symbol	Vehicle Configuration	
		M113 A1	M113 A2
Suspension Location			
Horizontal distance from c.g. to:			
sprocket, m (in)	a_{Sp}	1.939 (76.35)	1.942 (76.45)
idler, m (in)	a_{Id}	-2.037(-80.18)	-2.047(-80.60)
torsion bar 1, m (in)	a_{t1}	1.577 (62.10)	1.580 (62.20)
torsion bar 2, m (in)	a_{t2}	0.911 (35.85)	0.913 (35.95)
torsion bar 3, m (in)	a_{t3}	0.244 (9.60)	0.246 (9.70)
torsion bar 4, m (in)	a_{t4}	-0.423(-16.65)	-0.420 (16.55)
torsion bar 5, m (in)	a_{t5}	-1.089(-42.90)	-1.087(-42.80)
shock absorber end B1, m (in)	a_{s1}	1.048 (41.27)	1.051 (41.37)
shock absorber end B2, m (in)	a_{s2}	0.381 (15.02)	0.384 (15.12)
shock absorber end B3, m (in)	a_{s3}	-0.286(-11.23)	-0.283(-11.13)
shock absorber end B4, m (in)	a_{s4}	-0.952(-37.49)	-0.949(-37.38)
shock absorber end B5, m (in)	a_{s5}	-1.619(-63.73)	-1.616(-63.63)
Vertical distance from c.g. to:			
sprocket, m (in)	b_{Sp}	0.518 (20.40)	0.518 (20.40)
idler, m (in)	b_{Id}	0.650 (25.61)	0.617 (24.31)
torsion bars, m (in)	b_t	0.606 (23.84)	0.606 (23.84)
shock absorber ends Bi, m (in)	b_s	0.506 (19.93)	0.518 (20.40)

(Table 4.3...cont'd)

TABLE 4.3 (continued)

Description	Symbol	Vehicle Configuration	
		M113 A1	M113 A2
Bump stop-road arm radial clearance, rad (deg)	θ_c	0.401 (23)	0.401 (23)
Road arm length, m (in)	R	0.3175 (12.5)	0.3175 (12.5)
Arm overhang length;			
point Ai to road arm hinge, m (in)	S_L	0.198 (7.81)	0.126 (4.95)
point Ai to road arm centerline, m (in)	S_P	0.175 (6.90)	0.139 (5.47)
Road arm inclination, rad (deg)	θ_o	0.401 (23)	0.401 (23)
Shock absorber inclination, rad (deg)	β_o	0.698 (40)	0.524 (30)
Road arm overhang angle, rad (deg)	ζ_o	0.724 (41.5)	0.834 (48)
Diameters			
sprocket, m (in)	D_S	0.498 (19.6)	0.498 (19.6)
road wheel, m (in)	D_W	0.610 (24)	0.610 (24)
idler, m (in)	D_I	0.498 (19.6)	0.498 (19.6)
Driver seat location:			
horizontal, m (in)	a_{dr}	0.9997 (39.4)	0.9652 (38.0)
vertical, m (in)	b_{dr}	-0.356 (-14.0)	-0.356 (-14.0)

TABLE 4.4

TRACK GEOMETRY & PROPERTIES [6,33,42,44]

Parameter Type	symbol	Vehicle Configuration	
		M113 A1	M113 A2
Track pad stiffness, N/m (lb/in)	K_p	1500000 (8565)	1500000 (8565)
Track effects equivalent stiffness coefficient;			
leading portion of track, N/m (lb/in)	μ_s	105075 (600)	105075 (600)
portion between wheels, N/m (lb/in)	μ_w	65672 (375)	65672 (375)
trailing portion of track, N/m (lb/in)	μ_I	51622.5 (295)	79857 (456)
Track length between;			
sprocket and adjacent wheel, m (in)	L_s	0.654 (25.75)	0.654 (25.75)
consecutive road wheels, m (in)	L_w	0.667 (26.25)	0.667 (26.25)
idler and adjacent wheel, m (in)	L_I	0.655 (25.78)	0.668 (26.30)
Track inclination to Ground:			
leading portion of track, rad (deg)	α_s	0.419 (24)	0.419 (24)
trailing portion of track, rad (deg)	α_I	0.209 (12)	0.314 (18)
Track weight per unit length N/m (lb/in)	m_{tr}	560 (3.2)	560 (3.2)
Track clearance:			
leading portion; midpoint to ground, m (in)	d_s	0.146 (5.73)	0.146 (5.73)
trailing portion; midpoint to ground, m (in)	d_I	0.0696 (2.73)	0.120 (4.73)

The eigenvalue problem for the undamped vehicle model is formulated as:

$$[A - \lambda I]\{\Psi\} = \{0\} \tag{4.12}$$

where $[A] = [m]^{-1}[K]$ is the system matrix, and $[I]$ is the identity matrix, λ_i are the eigenvalues, $\{\Psi_i\}$ is the eigenvector corresponding to eigenvalue λ_i. The undamped natural frequencies, ω_{ni}, are then computed from the eigenvalues:

$$\lambda_i = \omega_{ni}^2 \tag{4.13}$$

4.4.2 Free-Vibration Analysis of the Damped Vehicle Models

Assuming linear damping characteristics, the damped free-vibration system of equations for the multi-wheeled and tracked vehicle models is presented in matrix form as:

$$[m]\{\ddot{y}\} + [C]\{\dot{y}\} + [K]\{y\} = \{0\} \tag{4.14}$$

The damped resonant frequency and deflection modes are established from the following damped eigenvalue analysis:

$$[A_D - \lambda_{Di} I]\{\Psi_{Di}\} = 0 \tag{4.15}$$

where $[A_D] = [m^*]^{-1}[K^*]$, and

$$[m^*] = \left[\begin{array}{c|c} [I] & 0 \\ \hline 0 & [m] \end{array}\right] \quad ; \quad [K^*] = \left[\begin{array}{c|c} 0 & [I] \\ \hline -[K] & -[C] \end{array}\right]$$

λ_{Di} are the complex eigenvalues, and $\{\Psi_{Di}\}$ are the eigenvectors corresponding to the damped eigenvalue λ_{Di}. The damped natural frequency, ω_{Di}, of the 'i'th deflection mode is determined from the corresponding complex eigenvalue. The damping ratio, ξ_i, of the underdamped 'i'th mode of vibration is then determined by:

$$\xi_i = \sqrt{1 - \left[\frac{\omega_{Di}}{\omega_{ni}}\right]^2} \tag{4.16}$$

4.4.3 Free-Vibration Response Evaluation

Free-vibration analyses of vehicle *Model I* thru *IV* are carried out by solving the eigenvalue problems of equations (4.11) and (4.14). The undamped natural frequencies and the dominant deflection modes of the tracked vehicle models are presented in Table 4.5a. Undamped natural frequencies of the hull bounce and pitch modes of the vehicle models incorporating suspension linkage (*Model III* & *IV*) are quite close to those of the vehicle models with idealized suspension (*Model I* & *II*). The pitch resonant frequency of the A2 and A1$\frac{1}{2}$ vehicle models is slightly larger than that of the A1 vehicle models, while the hull bounce resonant frequency of A2 and A1$\frac{1}{2}$ vehicle models is slightly lower than that of the A1 vehicle models. Hull bounce and pitch resonant frequencies of A1$\frac{1}{2}$ vehicle models are larger than those of the A2 vehicle models due to stiffer A1$\frac{1}{2}$ torsion bars. The principal deflection modes of multi-wheeled and tracked vehicle models are quite similar as shown in Figures 4.2 and 4.3, respectively. The damped natural frequencies for the A2 vehicle are given in Table 4.5b which depicts overdamped wheels for heavily damped shock absorbers.

4.5 DYNAMIC RESPONSE OF MULTI-WHEELED/TRACKED VEHICLES SUBJECTED TO DISCRETE OBSTACLES

Dynamic response of a tracked vehicle due to excitations arising from discrete obstacles, such as semicircle, block and ramp inputs, is evaluated via direct integration of the coupled differential equations formulated in Chapter 2. Transient response of the vehicle is useful in evaluating mobility and ride performance of the vehicle. Maximum level of vibrations perceived by the driver or the crew is among the factors limiting the maximum vehicle speed (mobility), when a vehicle is

TABLE 4.5

NATURAL FREQUENCIES & ASSOCIATED DEFLECTION MODES

(a).

Dominant Deflection Modes	Undamped Natural Frequency, Hz											
	Model I			*Model II*			*Model III*			*Model IV*		
	A1	A2	A1$\frac{1}{2}$	A1	A2	A1$\frac{1}{2}$	A1	A2	A1$\frac{1}{2}$	A1	A2	A1$\frac{1}{2}$
1. Vehicle Pitch	1.1216	1.1558	1.2416	1.0605	1.0969	1.1744	1.1151	1.1517	1.2375	1.0579	1.0936	1.1711
2. Hull Bounce	1.7168	1.5869	1.7045	1.6125	1.4977	1.6018	1.7570	1.5789	1.6964	1.6034	1.4912	1.5954
3. Road Wheel Bounce	12.774	14.390	14.573	13.265	14.858	15.031	11.764	13.245	13.414	12.212	13.680	13.835
4. Road Wheel Bounce	12.761	14.384	14.565	12.700	14.040	14.218	11.740	13.243	13.409	11.693	12.926	13.090
5. Road Wheel Bounce	12.751	13.951	14.130	11.966	13.246	13.436	11.740	12.852	13.013	11.016	12.195	12.370
6. Road Wheel Bounce	12.751	13.949	14.126	11.349	12.424	12.628	11.740	12.836	12.997	10.438	11.430	11.615
7. Road Wheel Bounce	12.751	13.942	14.117	11.119	12.205	12.414	11.740	12.836	12.997	10.231	11.238	11.425

(b).

M113 A2	Damped Natural Frequency, Hz							
	Model I		*Model II*		*Model III*		*Model IV*	
Dominant Deflection Modes	C_i = 47387. N·sec/m	C_i = 5835.5 N·sec/m	C_i = 47387. N·sec/m	C_i = 5835.5 N·sec/m	C_i = 47387. N·sec/m	C_i = 5835.5 N·sec/m	C_i = 47387. N·sec/m	C_i = 5835.5 N·sec/m
1. Hull Bounce	3.2056	1.5972	2.7117	1.5025	1.5443	1.5766	1.6341	1.5037
2. Vehicle Pitch	2.5664	1.1519	2.2346	1.0983	1.1363	1.1515	1.1033	1.0918
3. Road Wheel Bounce	14.372	14.392	14.633	14.535	13.240	13.241	13.244	13.599
4. Road Wheel Bounce	14.339	14.388	13.245	13.225	13.240	13.240	12.177	12.616
5. Road Wheel Bounce	---	12.858	---	12.916	---	12.805	---	12.198
6 Road Wheel Bounce	---	12.857	---	11.595	---	12.743	---	11.505
7 Road Wheel Bounce	---	12.717	---	10.994	---	12.720	---	11.090

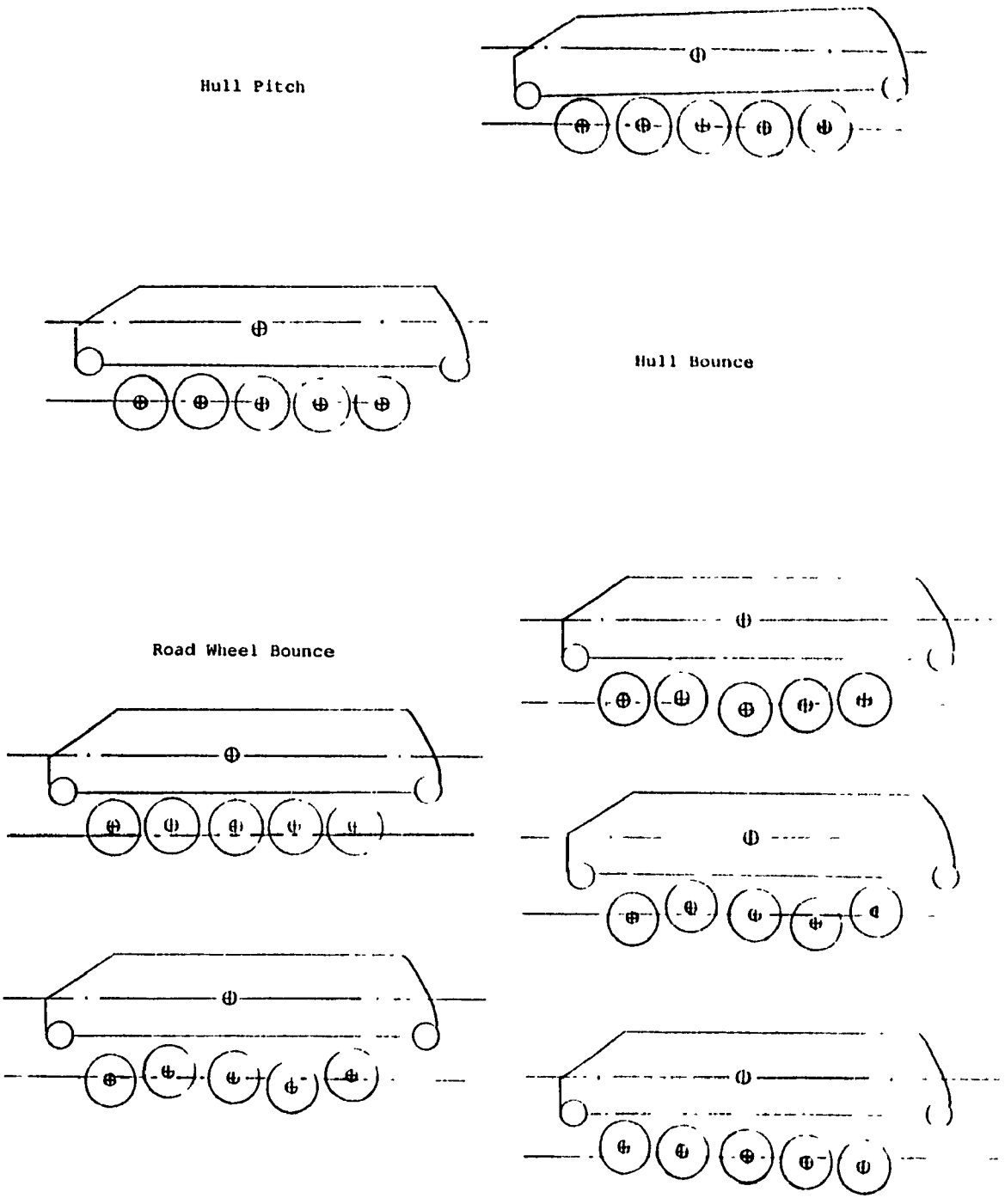

Figure 4.2 Principal Deflection Modes of the Multi-Wheeled M113 Vehicle.

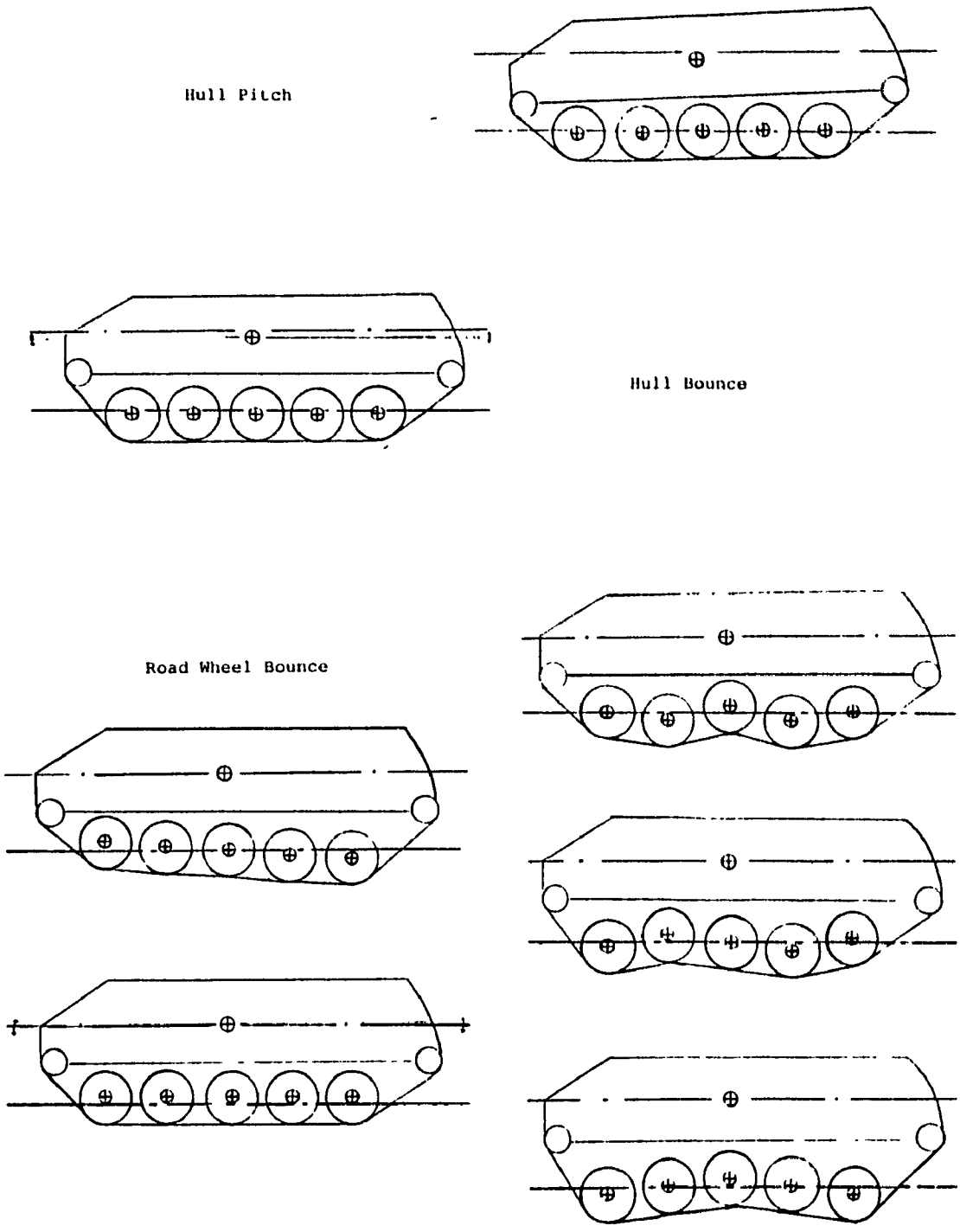

Figure 4.3 Principal Deflection Modes of the Tracked M113 Vehicle.

negotiating a specified obstacle.

4.5.1 Dynamic Response Analysis of the Multi-Wheeled/Tracked Vehicle Subjected to Semicircle Obstacle

A semicircle obstacle is characterized by its diameter and height, as shown in Figure 4.4. The displacement excitations at the road wheels (y_{oi}), and the leading (y_{oS}) and trailing (y_{oI}) segments of the track are determined from the coordinates of the obstacle, vehicle speed and initial vehicle position. The instantaneous horizontal location of a road wheel (x_{oi}), leading track segment (x_{oS}) and trailing track segment (x_{oI}), with respect to the vertical center line of the obstacle are expressed as,

$$x_{oS} = Vt - x_{st} \tag{4.17}$$

$$x_{oi} = Vt - [x_{st} + L_S/2 + (i-1)L_w] \; ; \; i = 1,2,\ldots,n \tag{4.18}$$

$$x_{oI} = Vt - [x_{st} + (L_S + L_I)/2 + 4L_w] \tag{4.19}$$

where L_S, L_w, L_I are the horizontal distances between the sprocket and the first road wheel, consecutive road wheels, and idler and the last road wheel. The horizontal positions of the road wheels, and leading and trailing portions of the track, are separated by the time delays expressed as:

$$\tau_S = L_S/(2V) \; ; \quad \tau_w = L_w/V \; ; \quad \tau_I = L_I/(2V) \tag{4.20}$$

The road wheel 'i' is considered to have a contact with the obstacle if:

$$-h_0 \leq x_{oi} \leq h_0 \quad \text{or} \quad -h_0/V \leq t_{oi} \leq h_0/V \tag{4.21}$$

where $t_{oi} = x_{oi}/V = t - t_{st} - \tau_s - (i-1)\tau_w$,

and t_{st} = is the starting time. The corresponding vertical displacement of wheel 'i' is expressed as:

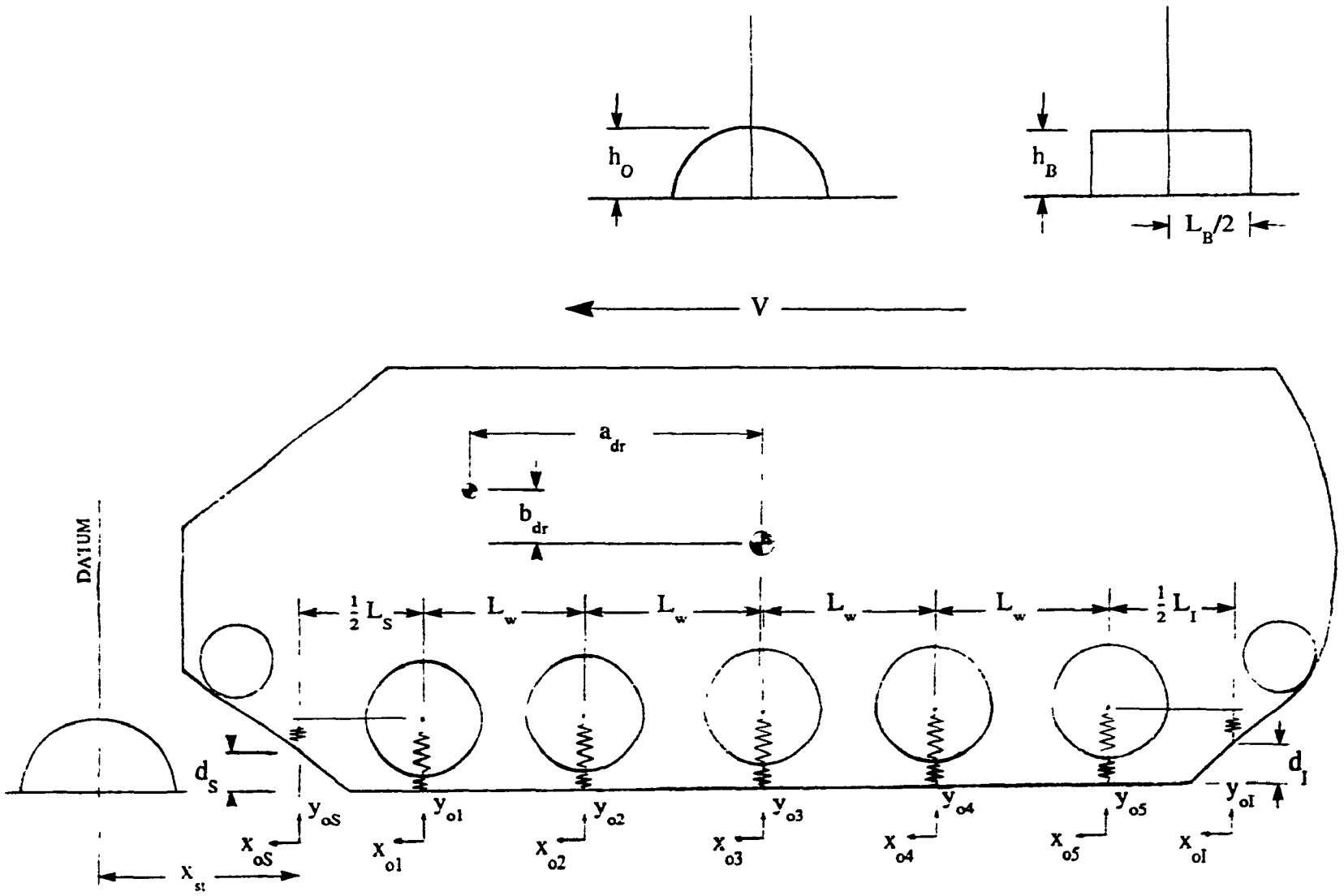

Figure 4.4 Schematic of the M113 Vehicle Models Negotiating Semicircle and Block Obstacles.

$$y_{oI} = \sqrt{h_0^2 - x_{oI}^2} \tag{4.22}$$

Similar expressions may be derived for the displacement excitations caused by the obstacle contact at the leading and the trailing portions of the track:

· Leading portion of the track

$$-h_0 \le x_{oS} \le h_0 \quad \text{or} \quad -h_0/V \le t_{oS} \le h_0/V \tag{4.23}$$

where $t_{oS} = t - t_{st}$

· Trailing portion of the track

$$-h_0 \le x_{oI} \le h_0 \quad \text{or} \quad -h_0/V \le t_{oI} \le h_0/V \tag{4.24}$$

where $t_{oI} = t - t_{st} - \tau_S - 4\tau_w - \tau_I$

The corresponding vertical displacements are expressed as:

$$y_{oS} = \sqrt{h_0^2 - x_{oS}^2} - d_S \tag{4.25}$$

$$y_{oI} = \sqrt{h_0^2 - x_{oI}^2} - d_I \tag{4.26}$$

where d_S and d_I are the clearances of the leading and trailing segments of the track, respectively, with reference to the ground.

4.5.2 Dynamic Response Analysis of the Multi-Wheeled/Tracked Vehicle Subjected to Block Obstacle

A block obstacle is characterized by its height (h_B) and width (L_B), as shown in Figure 4.4. The displacement excitations occurring at the track and the road wheels due to block excitations are determined as follows:

· Road wheels

$$-L_B/2 \le x_{oI} \le L_B/2 \quad \text{or} \quad -L_B/(2V) \le t_{oI} \le L_B/(2V) \tag{4.27}$$

· Leading portion of the track

$$-L_B/2 \le x_{oS} \le L_B/2 \quad \text{or} \quad -L_B/(2V) \le t_{oS} \le L_B/(2V) \tag{4.28}$$

• Trailing portion of the track

$$-L_B/2 \leq x_{oI} \leq L_B/2 \quad \text{or} \quad -L_B/(2V) \leq t_{oI} \leq L_B/(2V) \tag{4.29}$$

The corresponding vertical displacements of wheel 'i', and leading and trailing portions of the track are expressed as;

$$y_{oI} = h_B \tag{4.30}$$

$$y_{os} = h_B - d_s \tag{4.31}$$

$$y_{oI} = h_B - d_I \tag{4.32}$$

4.5.3 Transient Response of the M113 Vehicle Models

Transient response characteristics of the M113 vehicle models with A1, A2, and $A1\frac{1}{2}$ suspension parameters are carried out for discrete obstacles presented in sections 4.5.1 and 4.5.2, using direct integration techniques. The numerical integration is initiated at time t_{st} with the vehicle starting position at $x = -x_{st}$. At each time step, the horizontal positions of the road wheels and the track segments are evaluated and the corresponding vertical displacement excitations are computed from eqns. (4.21) thru (4.32). The dynamic response of the vehicle models is then evaluated via numerical integrations employing Runge Kutta's fourth order algorithm.

Semicircle obstacles, 20.32 cm (8 in) and 30.49 cm (12 in) high, often used in test evaluation of military vehicles, are considered as the source of excitation. Blocks of 6.35 cm (2.5 in) and 12.7 cm (5 in) are selected to compute the vehicle response to block obstacles. The transient vehicle response to discrete obstacles is expressed in terms of bounce and pitch acceleration of the hull, while the vehicle speed is held constant at 15 km/hr.

Response of Vehicle Models to Semicircle Obstacles

The bounce and pitch acceleration response characteristics of the

multi-wheeled M113 A1, M113 A2 and M113 A1$\frac{1}{2}$ vehicle models with idealized suspension (*Model I*), due to semicircle obstacle excitations, are presented in Figure 4.5. The transient response characteristics reveal large amplitude bounce and pitch acceleration at the hull c.g. as the vehicle negotiates the obstacle. The response accelerations decay gradually after the obstacle has been negotiated. The peak bounce and pitch transient accelerations of hull c.g. increase considerably with increase in obstacle size. Comparison of response characteristics of A1, A2 and A1$\frac{1}{2}$ vehicles subjected to 20.32 cm obstacle reveals that the pitch and bounce acceleration response of A2 and A1$\frac{1}{2}$ vehicles are almost identical, and slightly larger than that of the A1 vehicle. However, the A1 vehicle exhibits slightly larger amplitude transient response than its counterparts when subjected to the larger obstacle.

The bounce and pitch acceleration response characteristics of the hull c.g. of the tracked vehicle models with idealized suspension (*Model II*) negotiating semicircle obstacles, are presented in Figure 4.6. The peak transient bounce and pitch response accelerations of the A1, A2 and A1$\frac{1}{2}$ tracked vehicle configurations increase with larger obstacles. The M113 A1 vehicle exhibits faster settling times and smaller amplitudes of oscillations after negotiating the obstacles as compared with the M113 A2 and M113 A1$\frac{1}{2}$ vehicles. The bounce and pitch acceleration response characteristics of the A2 and A1$\frac{1}{2}$ tracked vehicles are quite similar, as in the case of *Model I*, and larger than that of the A1 tracked vehicle. A comparison of the transient response of the untracked (*Model I*) and tracked (*Model II*) vehicle models reveals that the addition of the track reduces vertical and pitch acceleration at the hull c.g. The initial transients to obstacle negotiation and amplitudes

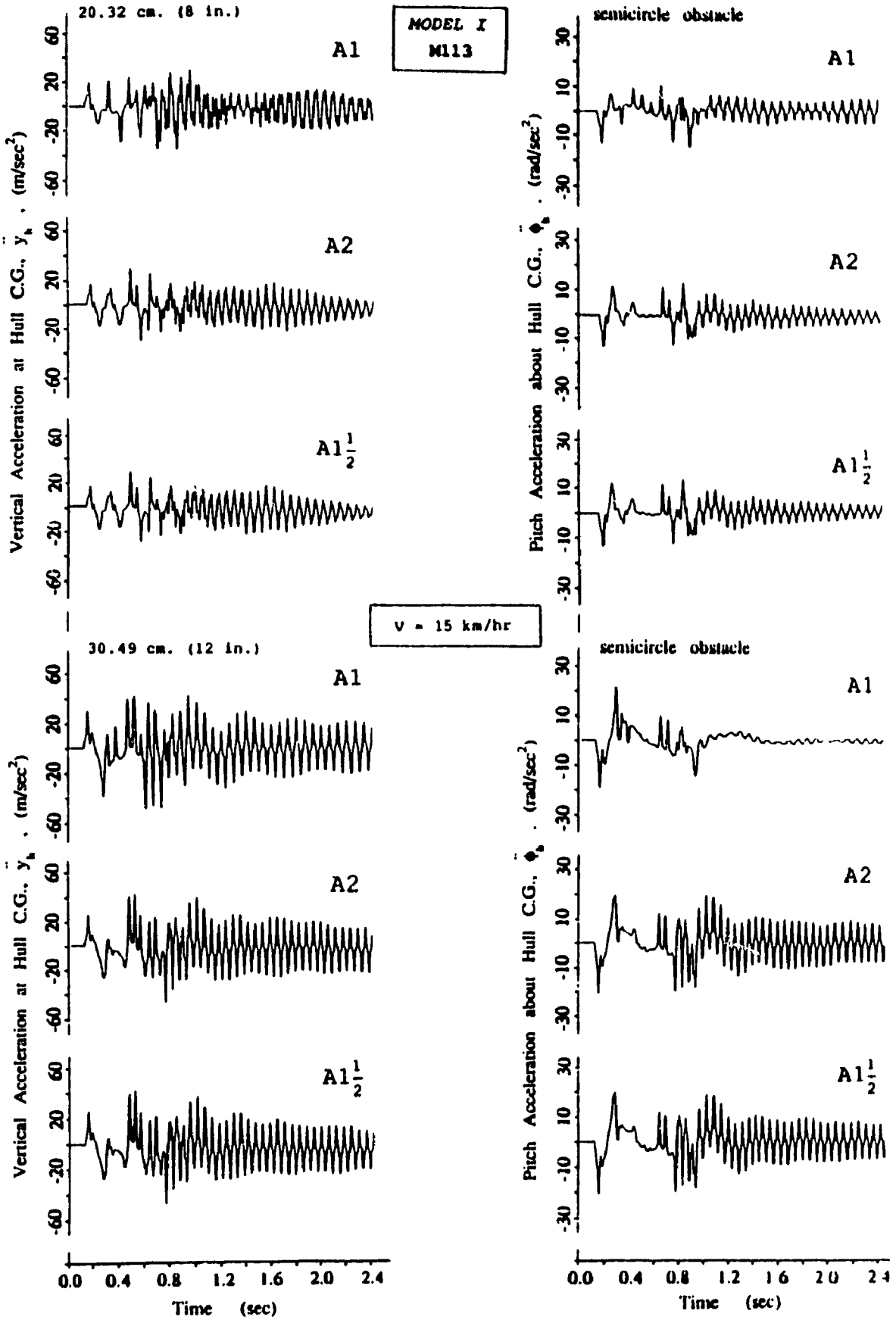

Figure 4.5 Vertical and Pitch Acceleration Response at the Hull C.G. for M113 (*MODEL I*) Negotiating Various Sizes of Semicircle Obstacles at Constant Speed.

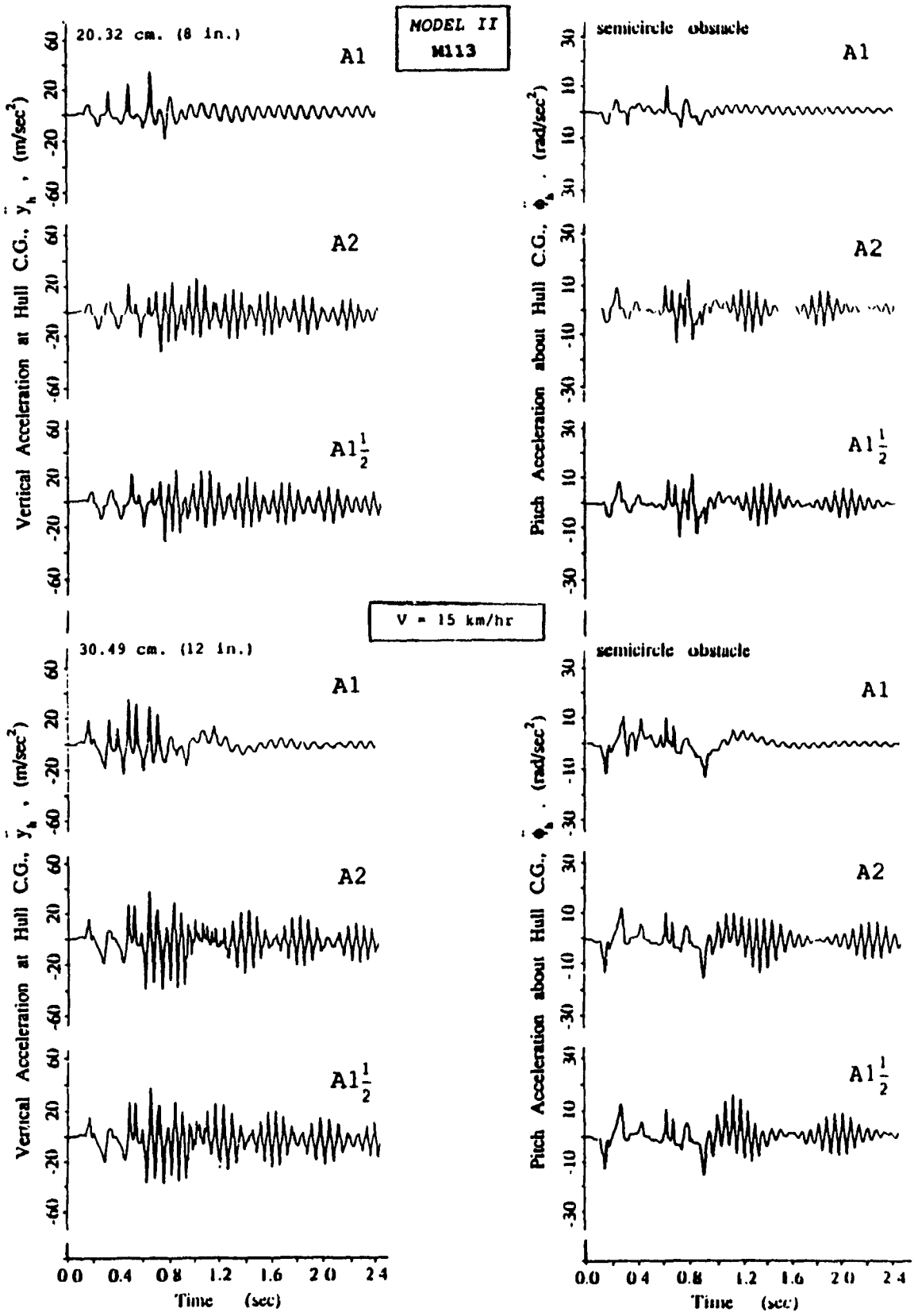

Figure 4.6 Vertical and Pitch Acceleration Response at the Hull C.G. for M113 (*MODEL II*) Negotiating Various Sizes of Semicircle Obstacles at Constant Speed.

of steady state oscillations after obstacle negotiation are significantly reduced with the addition of the track.

Figure 4.7 presents the bounce and pitch acceleration response at the hull c.g. of the M113 A1, M113 A2 and M113 A1$\frac{1}{2}$ multi-wheeled vehicles with linkage suspension (*Model III*) traversing the semicircle obstacles at constant speed. The peak transient response accelerations increase with increase in the obstacle size. Amplitudes of oscillations after the vehicle has negotiated the obstacles, vary with obstacle size and vehicle configuration. Amplitude of bounce acceleration oscillations of the M113 A1 vehicle increases with larger size obstacles while the amplitude of pitch response oscillation decreases. A comparison of transient responses of the A1, A2, and A1$\frac{1}{2}$ vehicle models, as shown in Figure 4.7, reveals almost identical results for the A2 and A1$\frac{1}{2}$, while the A1 vehicle yields high transient response. The A2 and A1$\frac{1}{2}$ vehicles exhibit significantly faster settling time than the A1 vehicle. Further comparison of the transient response characteristics of the idealized (*Model I*) and linkage (*Model III*) suspension vehicle models, reveals lower bounce transients but higher pitch transients of the linkage suspension model.

The transient hull c.g. bounce and pitch acceleration response characteristics of the tracked vehicle model with linkage suspension (*Model IV*) due to semicircle obstacle excitations are presented in Figure 4.8. The tracked vehicle models with linkage suspension provide similar transient response characteristics as the multi-wheeled vehicle model (*Model III*), however, the addition of the track yields significantly smoother transient response. A comparison of transient response of tracked vehicles with linkage suspension to those with the

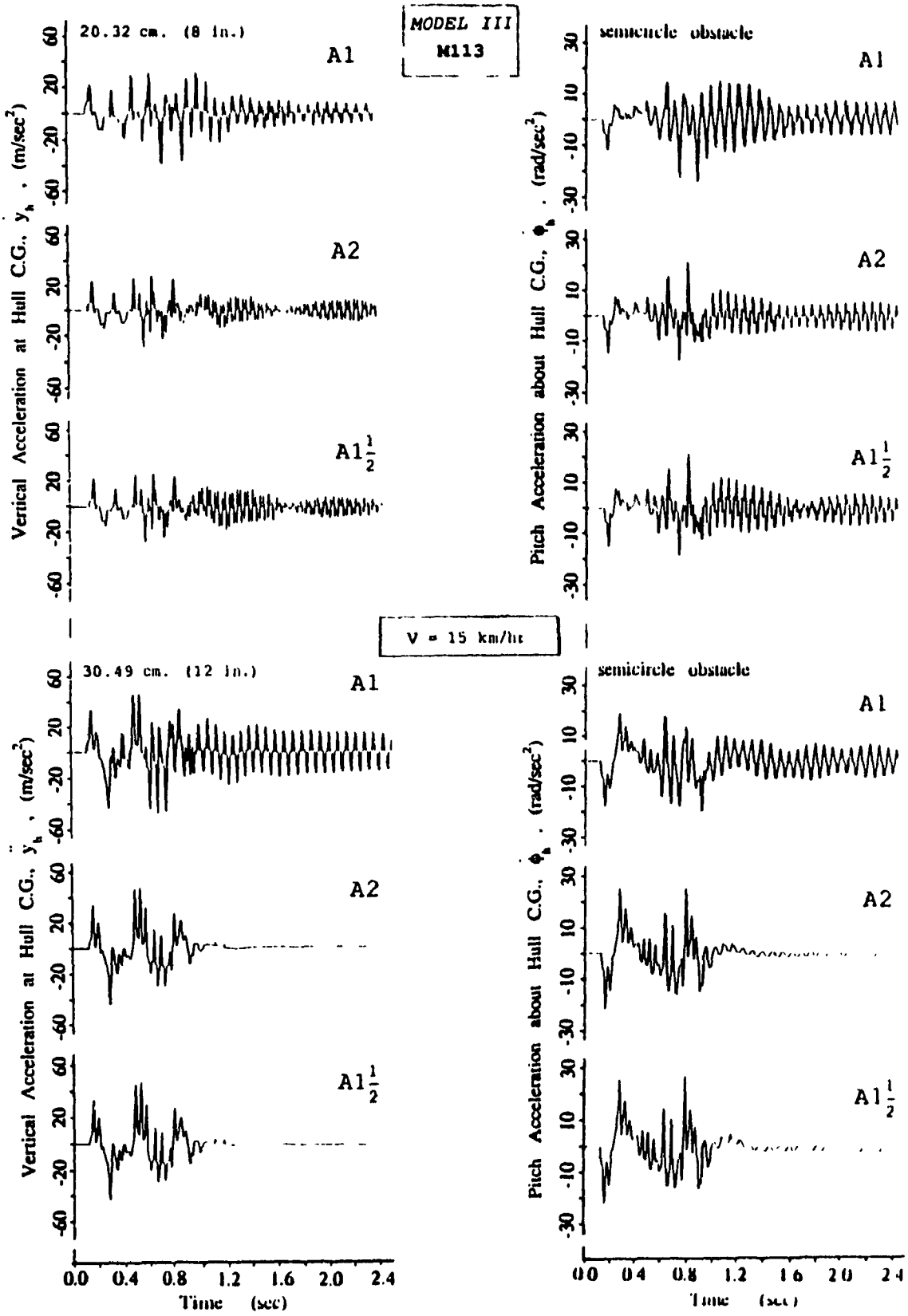

Figure 4.7 Vertical and Pitch Acceleration Response at the Hull C.G. for M113 (*MODEL III*) Negotiating Various Sizes of Semicircle Obstacles at Constant Speed.

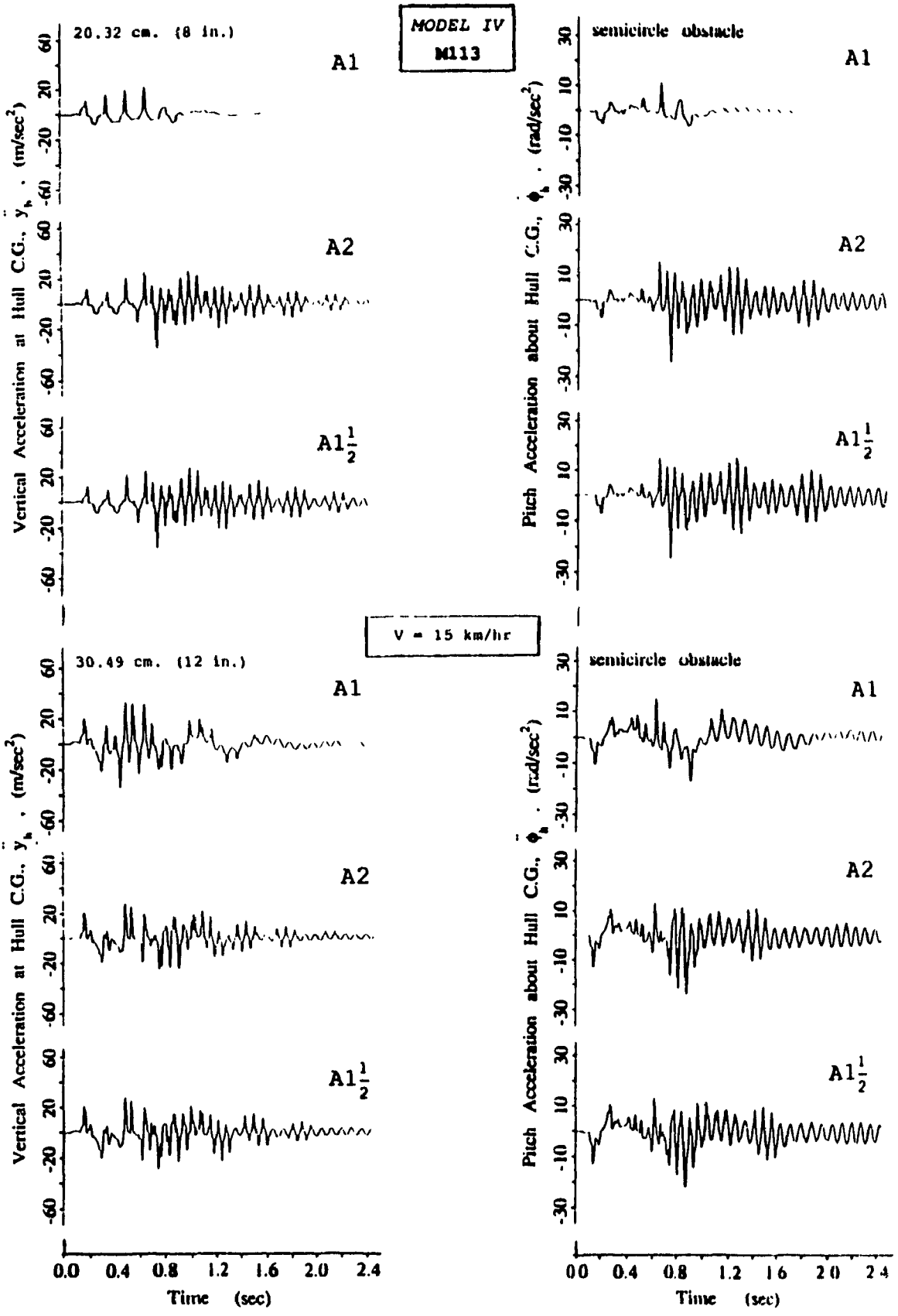

Figure 4.8 Vertical and Pitch Acceleration Response at the Hull C.G. for M113 (*MODEL IV*) Negotiating Various Sizes of Semicircle Obstacles at Constant Speed.

idealized suspension reveals that the tracked vehicle model with linkage suspension yields improved bounce response and inferior pitch response. The M113 A1 vehicle provides superior transient response as compared with its counterparts when traversing the smaller obstacle.

Response of Vehicle Models to Block Obstacles

Transient response analyses of the vehicle models with linkage suspension are carried out for excitations arising from a block obstacle. The transient bounce and pitch acceleration response at the hull c.g. of the vehicle models negotiating block obstacles at constant speed, are presented in Figures 4.9 and 4.10. The bounce and pitch response accelerations of the wheeled as well as tracked vehicle increase as the obstacle height is increased. A comparison of transient response characteristics of the wheeled (*Model III*) and tracked vehicles (*Model IV*) reveals that the tracked vehicle provides superior response than the multi-wheeled vehicle.

4.5.4 Transient Response at Driver's Location

Assessment of the vehicle ride quality requires determination of the intensity of vibrations transmitted to the driver and the crew. Assuming small rotations, vertical and longitudinal acceleration at the driver's location can be obtained from the following constraints:

$$\ddot{y}_{dr} = \ddot{y}_h - a_{dr}\ddot{\phi}_h \tag{4.33}$$

$$\ddot{x}_{dr} = b_{dr}\ddot{\phi}_h \tag{4.34}$$

where a_{dr} and b_{dr} are the horizontal and vertical coordinates of the driver with respect to the hull c.g., respectively. The longitudinal and vertical acceleration response at the driver's location of M113 vehicle models traversing the 20.32 cm high semicircle and 12.7 cm high

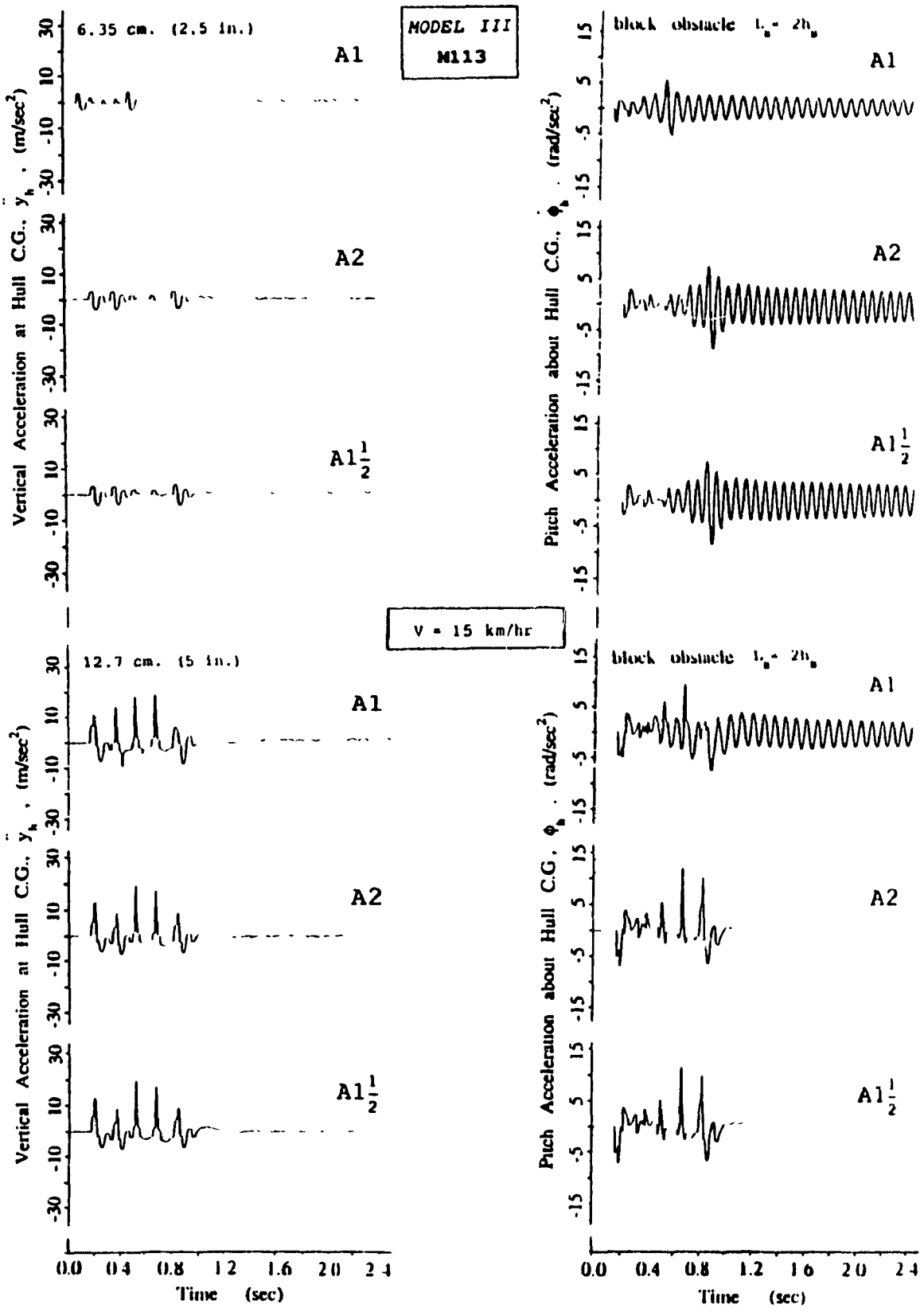

Figure 4.9 Vertical and Pitch Acceleration Response at the Hull C.G. for M113 (*MODEL III*) Negotiating Various Sizes of Block Obstacles at Constant Speed.

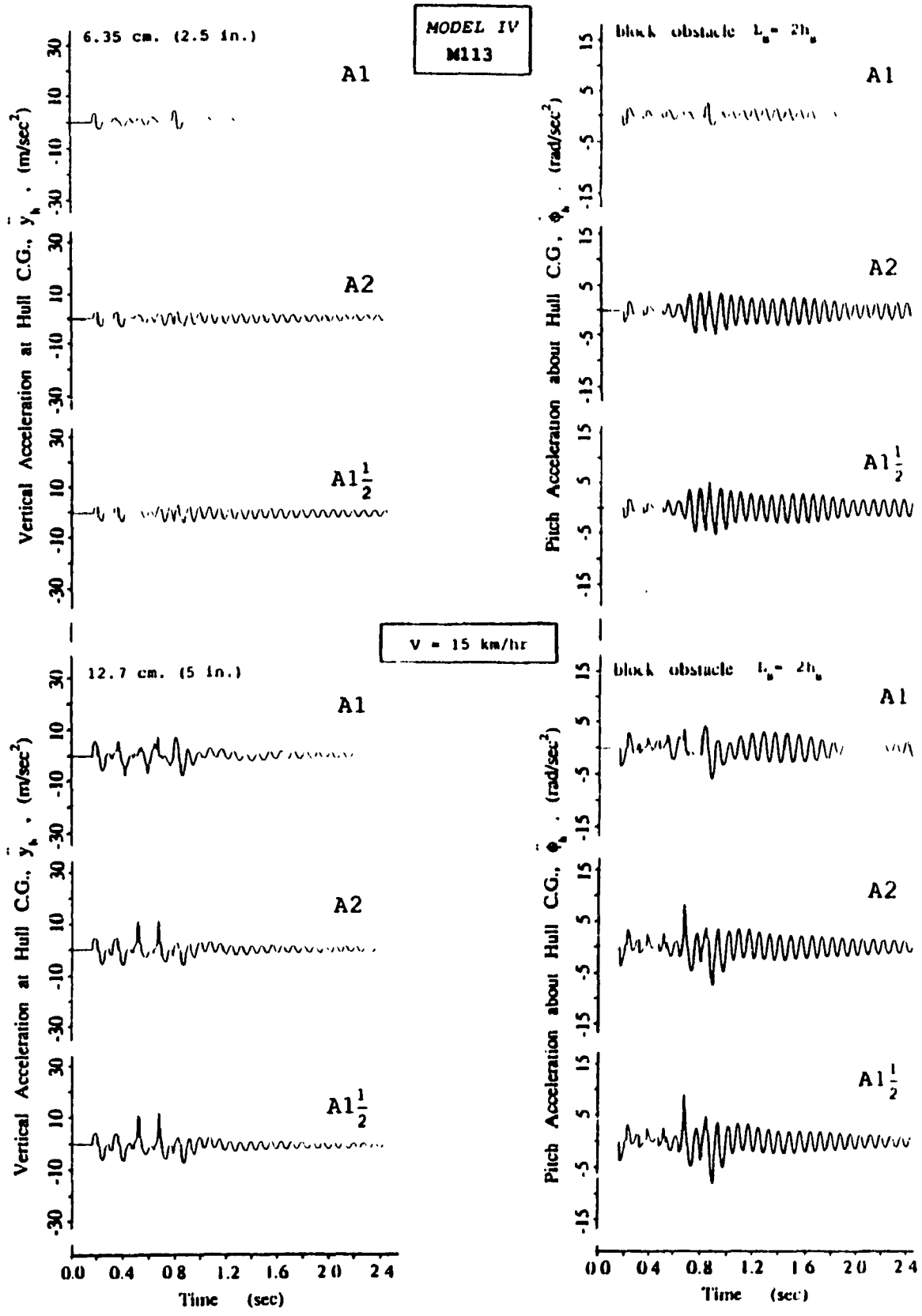

Figure 4.10 Vertical and Pitch Acceleration Response at the Hull C.G. for M113 (*MODEL IV*) Negotiating Various Sizes of Block Obstacles at Constant Speed.

block obstacles are evaluated to establish the relative ride performance of A1, A2 and A1$\frac{1}{2}$ vehicles. The transient response at the driver's location is evaluated for vehicle speeds of 15 km/hr and 25 km/hr.

Figures 4.11 and 4.12 illustrate the vertical and horizontal transient acceleration response at the driver's location of the multi-wheeled and tracked M113 A1, M113 A2 and M113 A1$\frac{1}{2}$ vehicle with linkage suspensions (*Model III & IV*), respectively traversing the semicircle obstacle (20.32 cm) at various speeds. The vertical and horizontal transient accelerations at the driver's seat location are closely related to hull c.g. bounce and pitch response characteristics. Amplitudes of initial transients and the number of oscillations of the wheeled vehicle, after the vehicles have negotiated the obstacle, increase significantly with increase in vehicle speed, with the exception of the M113 A1 vehicle which exhibits smaller bounce oscillations at higher speed, as shown in Figure 4.11. A comparison of the response characteristics of the wheeled and tracked vehicle models indicates that the tracked vehicles yield improved ride quality at the driver's seat location.

The transient response characteristics at the driver's location of the multi-wheeled and tracked vehicles subjected to block obstacle excitations are presented in Figures 4.13 and 4.14, respectively. The ride quality of the vehicle models is considerably deteriorated when the vehicle speed is increased. A comparison of the response characteristics reveals that the addition of the track deteriorates the transient response at higher vehicle speeds. The M113 A2 and M113 A1$\frac{1}{2}$ vehicles exhibit superior transient response than the M113 A1 vehicle.

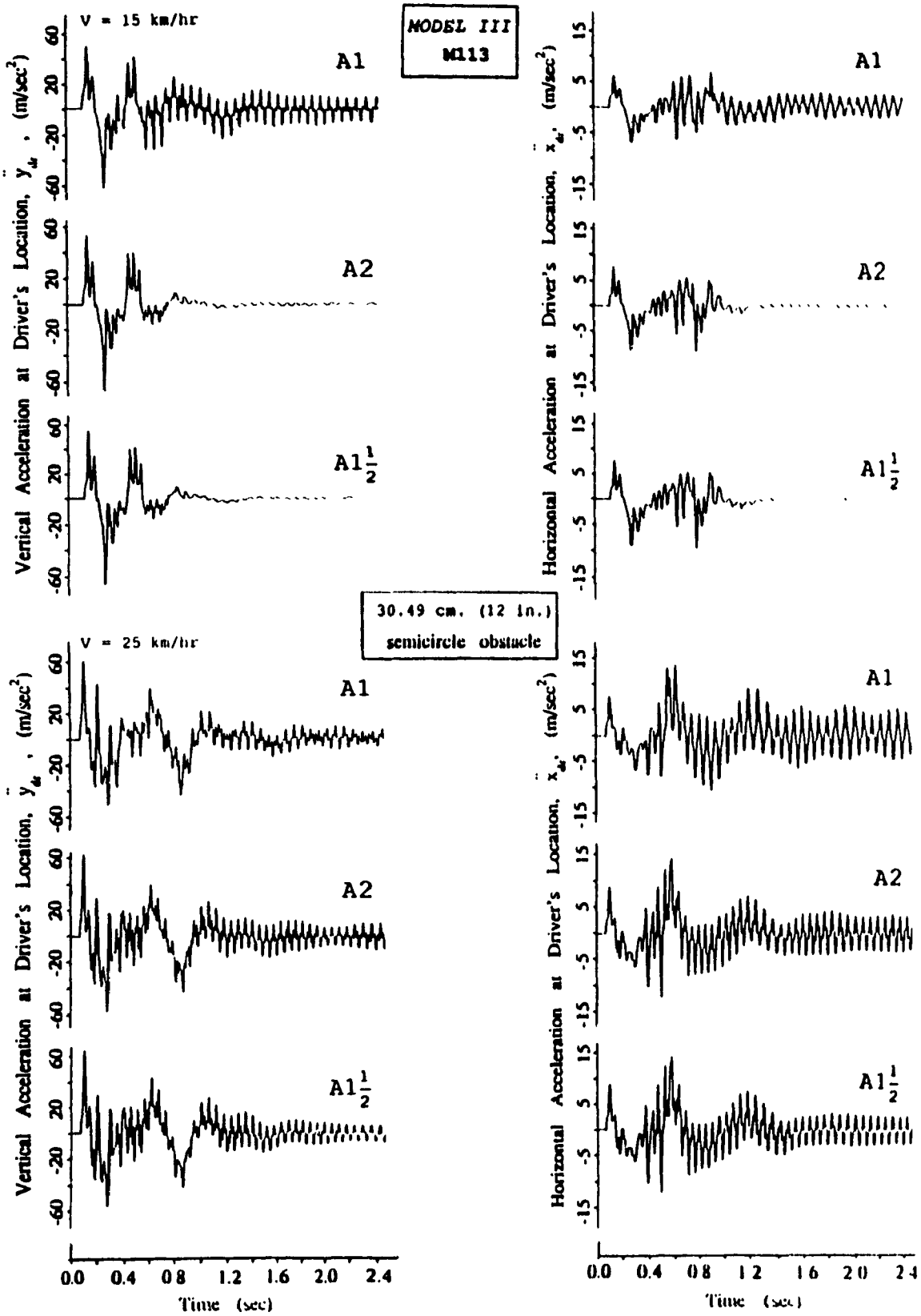

Figure 4.11 Vertical and Horizontal Acceleration Response at the Driver's Location for M113 (*MODEL III*) Negotiating Semicircle Obstacles at Various Speeds.

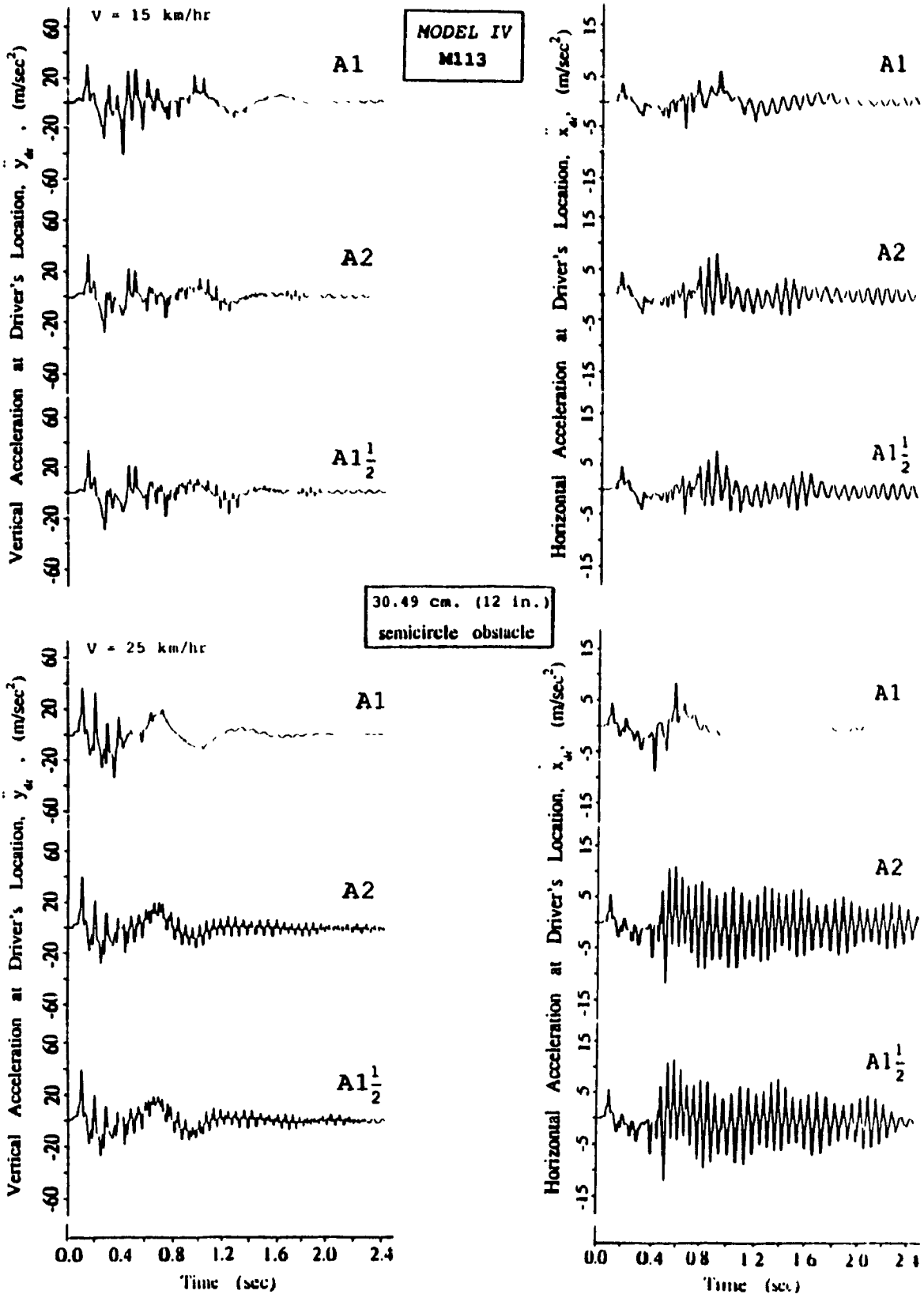

Figure 4.12 Vertical and Horizontal Acceleration Response at the Driver's Location for M113 (*MODEL IV*) Negotiating Semicircle Obstacles at Various Speeds.

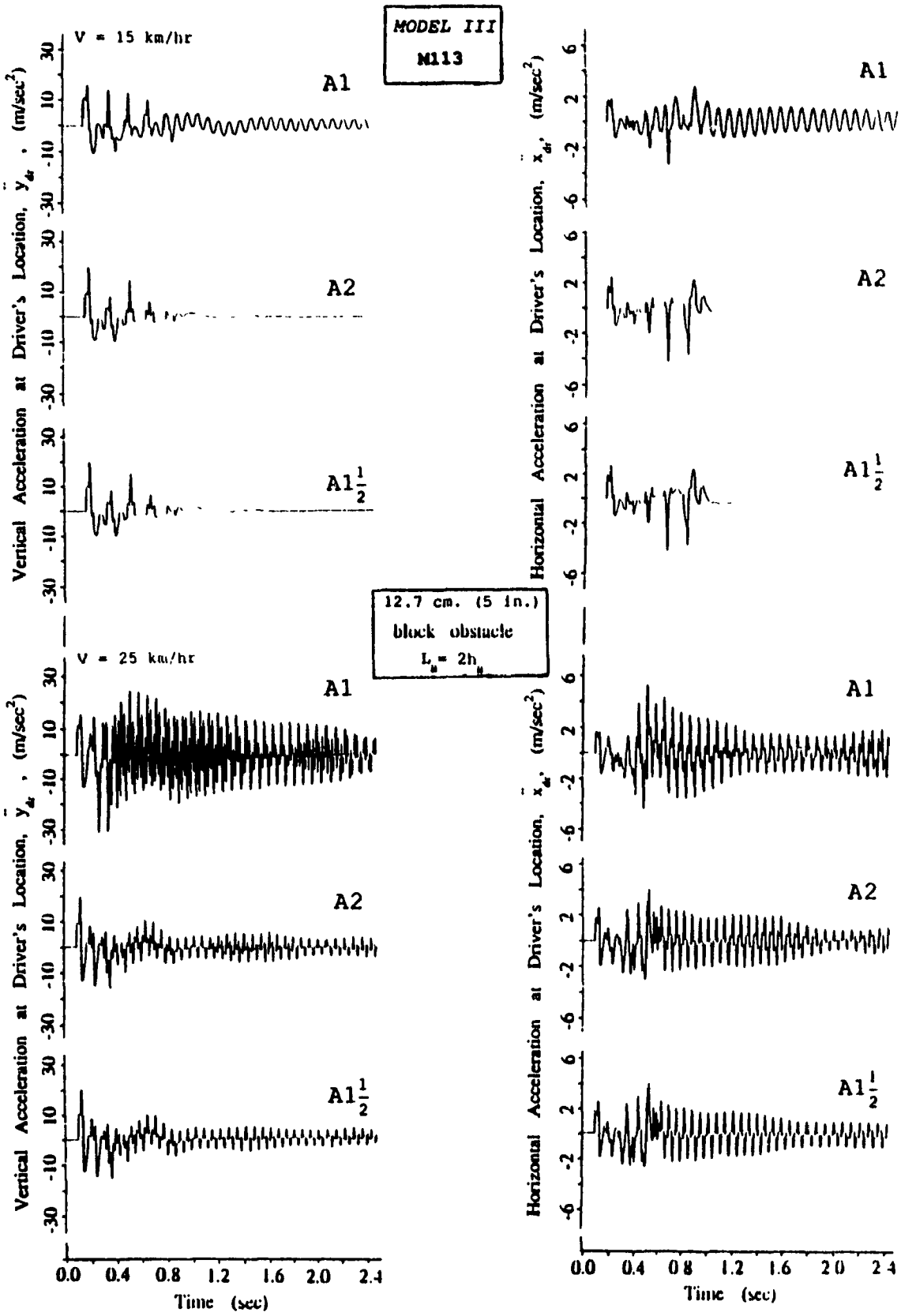

Figure 4.13 Vertical and Horizontal Acceleration Response at the Driver's Location for M113 (*MODEL III*) Negotiating Block Obstacles at Various Speeds.

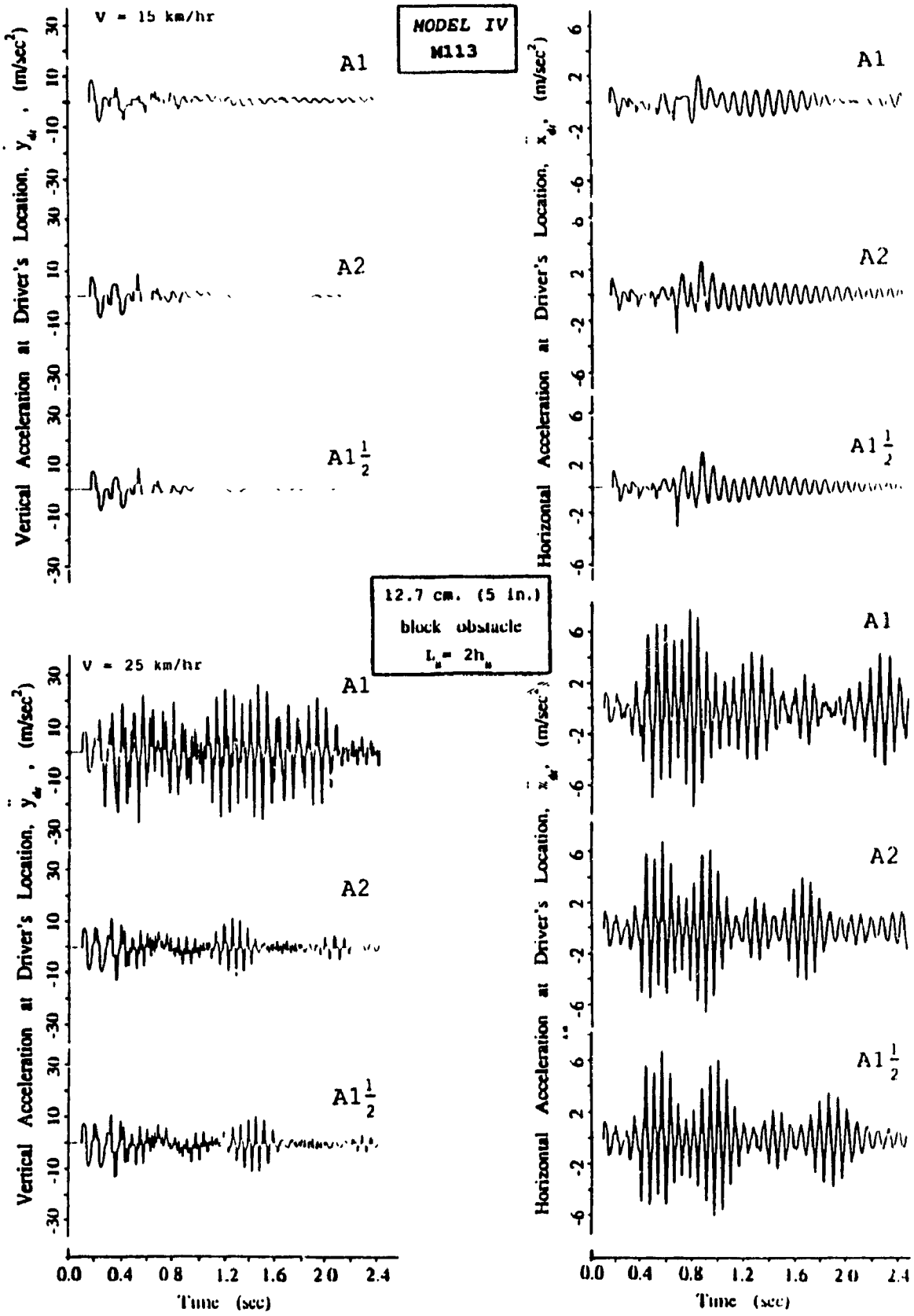

Figure 4.14 Vertical and Horizontal Acceleration Response at the Driver's Location for M113 (*MODEL IV*) Negotiating Block Obstacles at Various Speeds.

4.6 FREQUENCY RESPONSE EVALUATION OF NONLINEAR VEHICLE MODELS

Track-terrain interactions and ride dynamics of military off-road vehicles often predominate in the frequency range to which the human body is most fatigue sensitive. The frequency response characteristics of the multi-wheeled/tracked vehicle models provide the essential understanding of the sensitivity of vehicle ride response to the terrain excitation frequencies. The frequency domain technique can be applied to either linear or linearized vehicle models to evaluate their frequency response characteristics. Thus the nonlinearities arising from bump stops, Coulomb friction and force-velocity characteristics of shock absorbers, must be characterized by their linear equivalents to carry out the simulation in the convenient frequency domain.

4.6.1 Linearization of Multi-Wheeled/Tracked Vehicle Models

The nonlinear restoring and dissipative forces within a nonlinear mechanical system are expressed in terms of equivalent stiffness and damping coefficients, such that:

$$\{F_C(y,\dot{y},t)\} = [C_{eq}]\{\dot{y}\} \tag{4.35}$$

$$\{F_K(y,t)\} = [K_{eq}]\{y\} \tag{4.36}$$

where the stiffness and viscous damping coefficient matrices are computed such that the response behaviour of the linearized system does not deviate significantly from the response behaviour of the original nonlinear system. A number of linearization techniques have been developed to determine the equivalent viscous damping coefficients for randomly excited nonlinear systems [45,46]. However, often critical effects of nonlinear damping mechanisms, such as shock absorber and Coulomb friction, are not accurately characterized by the linearization theory. It has been established that the nonlinear damping mechanisms,

in general, should be expressed by a 'local constant', where each local constant is applicable only in a small frequency band centered around the excitation frequency. Thus, the local equivalent constants are determined as a function of excitation frequency, excitation amplitude, response and type of nonlinearity [47]. The local equivalent linearization technique, based upon energy balance [48], is employed to yield local damping coefficients due to the shock absorber at each excitation frequency. Nonlinearity due to elastic limit stops is also readily treated by the local equivalent linearization technique [49]. The nonlinearities due to A1 and A2 shock absorbers, Coulomb damping and bump stops are approximated by equivalent linear coefficients in the following manner.

Shock Absorber Damping

The force-velocity characteristics of shock absorbers employed in A1 and A2 suspension configurations, reveal high damping coefficient for low piston velocities and lower damping coefficients at high piston velocities, as shown in Figure 4.15. Assuming symmetric damping characteristics, the damping force due to shock absorber is expressed as:

Models I and *II*:

$$F_{d1} = \begin{cases} \bar{C}_{11} v_1 \ ; & \text{if } |v_1| \le v_p \\ \bar{C}_{11} v_p + \bar{C}_{21}(v_1 - v_p) \ ; & \text{if } |v_1| > v_p \end{cases} \qquad (4.37)$$

Models III and *IV*:

$$F_{d1} = \begin{cases} \bar{C}_{11}(v_{B1} - v_{A1}) \ ; & \text{if } |v_{B1} - v_{A1}| \le v_p \\ \bar{C}_{11} v_p + \bar{C}_{21}(v_{B1} - v_{A1} - v_p) \ ; & \text{if } |v_{B1} - v_{A1}| > v_p \end{cases} \qquad (4.38)$$

where $\bar{C}_{11}$ and $\bar{C}_{21}$ are average damping coefficients of shock absorber

corresponding to low and high values of piston velocity, respectively, and v_p is the piston velocity at which transition of damping coefficient occurs. Let $\dot{\psi}_{ij}$ represent the relative velocity across the shock absorber at roads wheel 'i' corresponding to excitation frequency ω_j:

$$\begin{aligned} \dot{\psi}_{ij} &= v_i && \text{for } \textit{Model I} \text{ and } \textit{II} \\ \dot{\psi}_{ij} &= v_{Bi} - v_{Ai} && \text{for } \textit{Model III} \text{ and } \textit{IV} \end{aligned} \tag{4.39}$$

The equivalent damping coefficient $C_i^*(\omega_j)$ corresponding to low relative velocity is given by the slope of the force-velocity curve:

$$C_i^*(\omega_j) = C_{1i} \quad ; \qquad \text{for } |\dot{\psi}_{ij}| < v_p \tag{4.40}$$

However, as the relative velocity across the shock absorber exceeds v_p, the damping force is expressed as a nonlinear function of $\dot{\psi}_{ij}$. Assuming small nonlinearity and harmonically forced vibrations, the relative displacement across the shock absorber can be expressed as:

$$\psi_{ij} = \mathcal{Y}_{ij} \sin(\omega_j t) \tag{4.41}$$

where $\mathcal{Y}_{ij}$ is the amplitude of relative displacement at excitation frequency ω_j. The shock absorber assumes a high value of damping coefficient, C_{1i} during a part of the vibration cycle when the piston velocity is less than v_p, as shown in Figure 4.16. As the piston velocity exceeds v_p, the damping coefficient is reduced to the low value, C_{2i} during the remaining part of the cycle. The relative velocity across the shock absorber approaches v_p at time t_1, given by:

$$t_1 = \frac{1}{\omega_j} \sin^{-1}\left(\frac{v_p}{v_r}\right) \tag{4.42}$$

where $v_r = \omega_j \mathcal{Y}_{ij}$

The shock absorber assumes a low value of damping coefficient, C_{2i} at time t_1 and a high damping, C_{1i} at time t_2, given by;

$$t_2 = \frac{\pi}{\omega_j} - \frac{1}{\omega_j} \sin^{-1}\left(\frac{v_p}{v_r}\right) \tag{4.43}$$

The energy dissipated per cycle by the nonlinear shock absorber is then computed as:

$$\begin{aligned}\Delta E &= \oint F_{d1}\, d\psi \\ &= 2\left\{ \int_0^{t_1} (C_{11}\dot{\psi}_{1j})\dot{\psi}_{1j}\, dt + \int_{t_1}^{t_2} \left[C_{11}v_p + C_{21}(\dot{\psi}_{1j} - v_p)\right]\dot{\psi}_{1j}\, dt \right. \\ &\quad \left. + \int_{t_2}^{\pi/\omega_j} (C_{11}\dot{\psi}_{1j})\,\dot{\psi}_{1j}\, dt \right\}\end{aligned} \tag{4.44}$$

Assuming harmonic excitations, the energy dissipated per cycle is expressed as:

$$\begin{aligned}\Delta E &= 2\omega_j^2\, y_{1j}^2 \left[\int_0^{t_1} C_{11}\cos^2\omega_j t\, dt + \int_{t_1}^{t_2} C_{21}\cos^2\omega_j t\, dt \right. \\ &\quad \left. + \int_{t_2}^{\pi/\omega_j} C_{11}\cos^2\omega_j t\, dt \right] + 2v_p y_{1j} \int_{t_1}^{t_2} (C_{11} - C_{21})\cos\omega_j t\, dt\end{aligned} \tag{4.45}$$

The equivalent viscous damping coefficient corresponding to excitation frequency, ω_j is obtained by equating the energy dissipated per cycle by the nonlinear damper to that of the linear damper.

$$C_1^*(\omega_j) = \frac{2\omega}{\pi}\left[C_{11}\int_0^{t_1} \cos^2\omega_j t\, dt + C_{21}\int_{t_1}^{t_2} \cos^2\omega_j t\, dt \right.$$

$$+ C_{11}\int_{t_2}^{\pi/\omega_j} \cos^2\omega_j t\ dt\ \Big] + \frac{2v_p(C_{11} - C_{21})}{\pi\omega_j y_{1j}}\int_{t_1}^{t_2} \cos\ \omega_j t\ dt \qquad (4.46)$$

Equation (4.46) is simplified to yield:

$$C_1^*(\omega_j) = C_{21} + \frac{1}{2\pi}(C_{11} - C_{21})\left[\sin 2\omega_j t_1 - \sin 2\omega_j t_2 + 4\omega_j t_1\right] \qquad (4.47)$$

Equation (4.47) can be solved in the frequency domain to establish the values of local damping constants using the iterative algorithm summarized below. Equation (4.47) reduces to (4.40) if the relative velocity across the damper is less than v_p.

Algorithm

The local equivalent damping algorithm may be summarized as follows:

(i) The equivalent viscous damping coefficient of the shock absorber, $C_{01}^*(\omega_j)$ is initially assumed to be high value C_{11} at an excitation frequency ω_j. The relative displacement and velocity across the shock absorbers is then computed from the linear vehicle model subject to displacement excitation $\{y_o(\omega_j)\}$.

(ii) The linearized equations of motion are then Fourier transformed to yield the frequency response function matrix;

$$[\mathcal{H}(j\omega)] = \left[[K] - \omega_j^2[m] + j\omega_j[C_{eq}(\omega_j)]^{-1}\right][K_F] \qquad (4.48)$$

(iii) The vector of relative displacement response across the shock absorbers, $\{\mathcal{Y}\}$ is computed from the constraint equations:

$$\{\mathcal{Y}\} = [T_D]\ \{Y(j\omega)\} \qquad (4.49)$$

where $[T_D]$ is a (n x N) transformation matrix relative displacement across damper to the generalized

coordinates. The damping coefficients are assumed to be true values if the relative velocities across the shock absorbers are below v_p.

(iv) The equivalent viscous damping coefficients are computed using equation (4.47) when the relative velocity exceeds v_p. The (n x 1) error vector between the assumed and computed values is given as:

$$\{\varepsilon\} = \left\{ |C_0^*(\omega_j) - C^*(\omega_j)| \right\} \qquad (4.50)$$

If the error exceeds a specified tolerance, the assumed values are updated and the iterative procedure is repeated until convergence is achieved.

The iterative methodology is carried out to establish local viscous damping constants at each discrete frequency of excitation.

Coulomb Damping

Figure 4.17 illustrates the force-velocity characteristics of the ideal Coulomb damping due to the shock absorber and suspension linkage. The Coulomb damping force in the vicinity of discontinuity is approximated by a linear viscous damper over an infinitesimal velocity band (v_f). The local equivalent damping coefficient due to Coulomb friction, F_{fi}, is determined from:

$$C_i^*(F_{fi}, \omega_j) = \begin{cases} \dfrac{F_{fi}}{v_f} ; & |\dot{\psi}_{ij}| < v_f \\ \dfrac{4F_{fi}}{\pi \omega_j Y_{ij}} ; & |\dot{\psi}_{ij}| \geq v_f \end{cases} \qquad (4.51)$$

where

$F_{fi} = F_{fLi}$; for linkage friction, and

$F_{fi} = F_{fsi}$; for shock absorber friction

Alternatively, the damping force due to friction can be expressed using equations (4.37) or (4.38) by replacing v_p by v_f and the

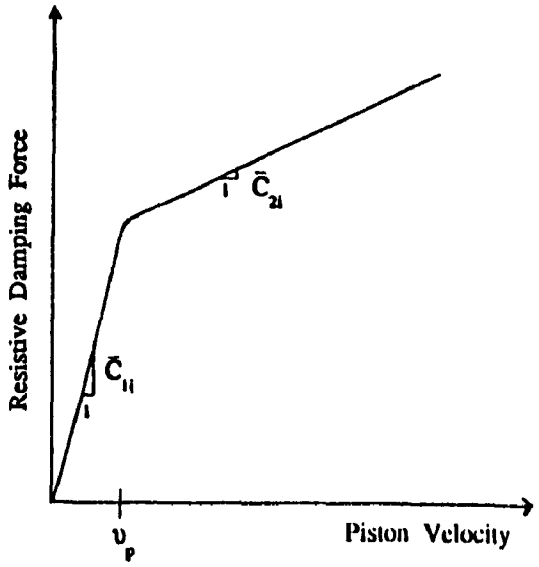

Figure 4.15 Symmetric Representation of Force-Velocity Power Curve for M113 Shock Absorbers.

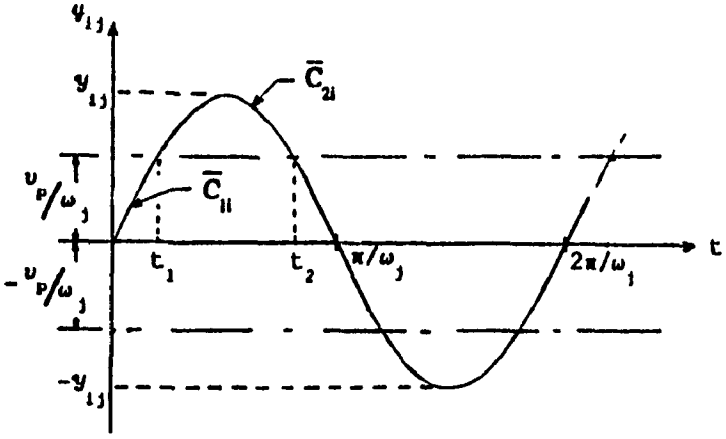

Figure 4.16 Time-Relative Displacement Characteristics of the Shock Absorber, assuming Harmonic Response.

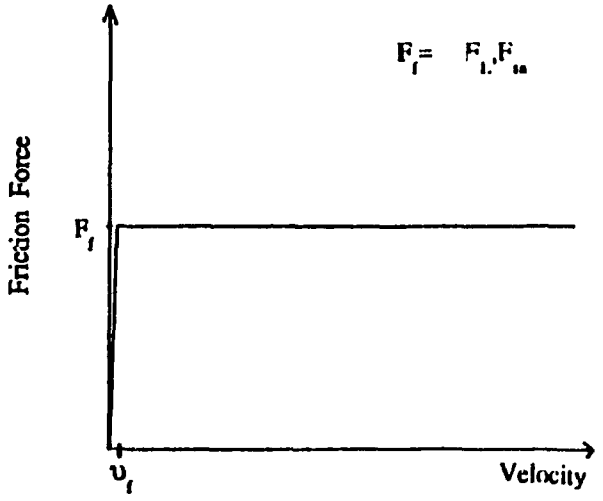

Figure 4.17 Force-Velocity Characteristics of Shock Absorber and Linkage Friction.

corresponding damping coefficients representing Coulomb friction. The local equivalent damping algorithm can be used to compute local viscous damping coefficients at each discrete excitation frequency whenever the velocity v_f is exceeded. Relative displacements across the shock absorbers are computed from equation (4.49) while the relative displacements $\{y_L\}$ across the suspension linkage are computed from:

$$\{y_L\} = [T_L]\{Y(j\omega)\} \tag{4.52}$$

where $[T_L]$ is an (n x N) transformation matrix for relative linkage displacements with respect to generalized coordinates.

Bump Stops

The trailing arm suspension of M113 vehicles is equipped with bump stops to limit the excessive motion of road wheels. The force-displacement characteristics of a typical bump stop was presented in Figure 2.9. The nonlinear symmetric force-displacement characteristics of limit stops can be readily incorporated in the local equivalent linearization technique [49]. The equations of motion of the linear equivalent multi-wheeled/tracked vehicle model are rewritten in the form:

$$[m]\{\ddot{y}\} + [C^*_{eq}(\omega_j)]\{\dot{y}\} + [K]\{y\} + [K_b]\{y\} = [K_F]\{y_o\} + [K_C]\{y_o\} \tag{4.53}$$

where $[K_b]$ and $[K_C]$ are (N x N) stiffness matrices due to bump stops The local equivalent algorithm examines the bump stop clearance at each discrete frequency and computes the bump stop contact factor $\{c_b\}$, described in equations (2.4) and (2.29). The relative displacement of the road wheels with respect to the chassis is computed at each discrete frequency using equation (4.49) for the idealized suspension models (*Model I* and *II*). The relative rotation of road arm with respect to the

chassis is computed in the following manner, for the linkage suspension models (*Model III* and *IV*):

$$\{\Theta_L\} = [T_{\theta H}]\{Y(j\omega)\} \qquad (4.54)$$

where $[T_{\theta H}]$ is an (n x N) transformation matrix relating relative rotation between road arm linkage and hull chassis to the generalized coordinates. The stiffness matrices $[K_b]$ and $[K_c]$ are suppressed when the relative displacement response remains within the permissible travel.

4.6.2 Verification of Linearized Tracked Vehicle Model

The linearized multi-wheeled/tracked vehicle models are validated for harmonic excitations by comparing its frequency response to the frequency response characteristics of the nonlinear vehicle models established via direct integration of the nonlinear differential equations of motion. The frequency response characteristics of the vehicle model is presented in terms of transmissibility, defined as the ratio of the steady state response to the excitation amplitude at the road wheels. The bounce frequency response of the tracked vehicle model is expressed as the ratio of hull bounce magnitude to a given road wheel excitation, while the hull pitch frequency response is expressed as the ratio of pitch magnitude to the static pitch deflection of the hull subjected to an excitation at the first road wheel.

The effectiveness of local equivalent linearization is demonstrated by comparing the frequency responses of the multi-wheeled/tracked vehicle models to simultaneous harmonic inputs at all five road wheels to those established via direct integration of the nonlinear vehicle models. The hull bounce, hull pitch and road wheel bounce transmissibility characteristics of the linearized tracked vehicle model

(*Model IV*) are compared to those of the nonlinear vehicle model, as shown in Figures 4.18a, 4.18b and 4.18c, respectively. Figure 4.18d illustrates the frequency response characteristics of the road arm rotation where the transmissibility ratio is normalized by road arm length, R. A comparison of the frequency response characteristics of the locally linearized and the nonlinear vehicle models demonstrates the effectiveness of the local equivalent linearization technique. The local equivalent linearization technique yields error of small magnitude in the vicinity of vehicle bounce and pitch resonant frequencies. The response characteristics of the tracked vehicle model reveal three peaks corresponding to the resonant frequencies associated with hull bounce (1.7 Hz), road wheel bounce (10.5 Hz) and the track (12.2 Hz).

4.6.3 Parametric Sensitivity Analyses

The ride dynamics of M113 vehicles is highly influenced by various vehicle parameters, such as hull mass, pitch mass moment of inertia, location of center of gravity of the sprung-mass, suspension geometry, and characteristics of the running gear. Although parametric sensitivity analyses of the vehicle model in view of its ride dynamics require computation of vehicle response to realistic random terrain excitations, the frequency response characteristics can provide a considerable insight to the frequency shaping characteristics of the vehicle as influenced by its parameters. Thus, comprehensive parametric sensitivity analyses of the vehicle models are carried out to study the vibration transmission performance of the vehicle suspension, as influenced by the force-velocity characteristics of the shock absorbers, torque-deflection of the torsion bars, track tension and suspension configuration.

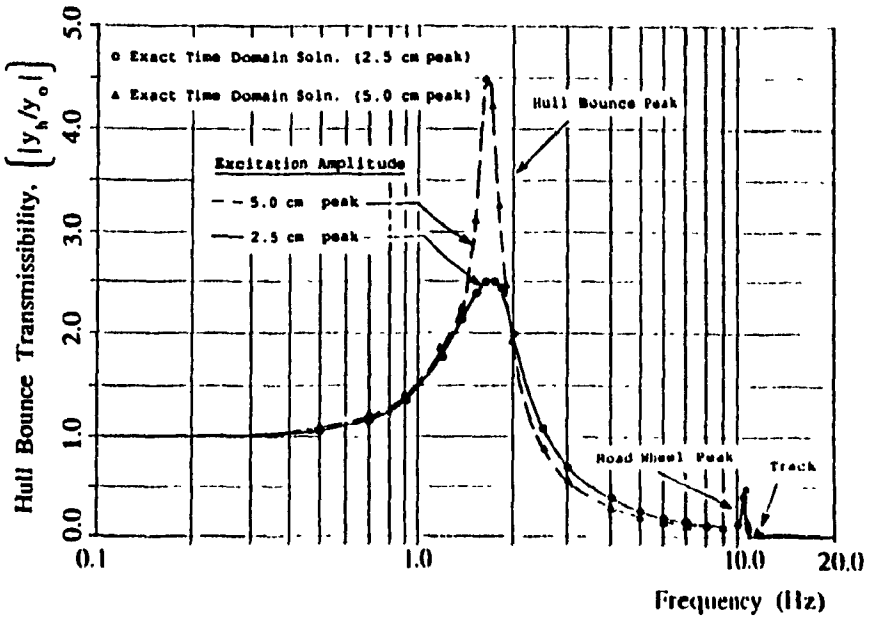

(a).

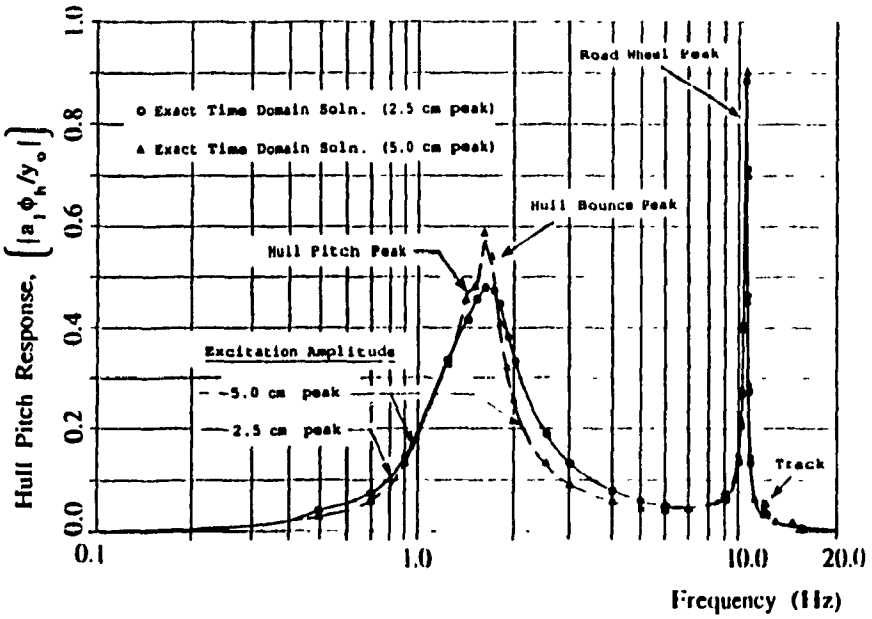

(b).

Figure 4.18 Comparison of Transmissibility Response Characteristics of the Linearized Tracked Vehicle *MODEL IV* with that of the Nonlinear Vehicle Model.

(...cont'd)

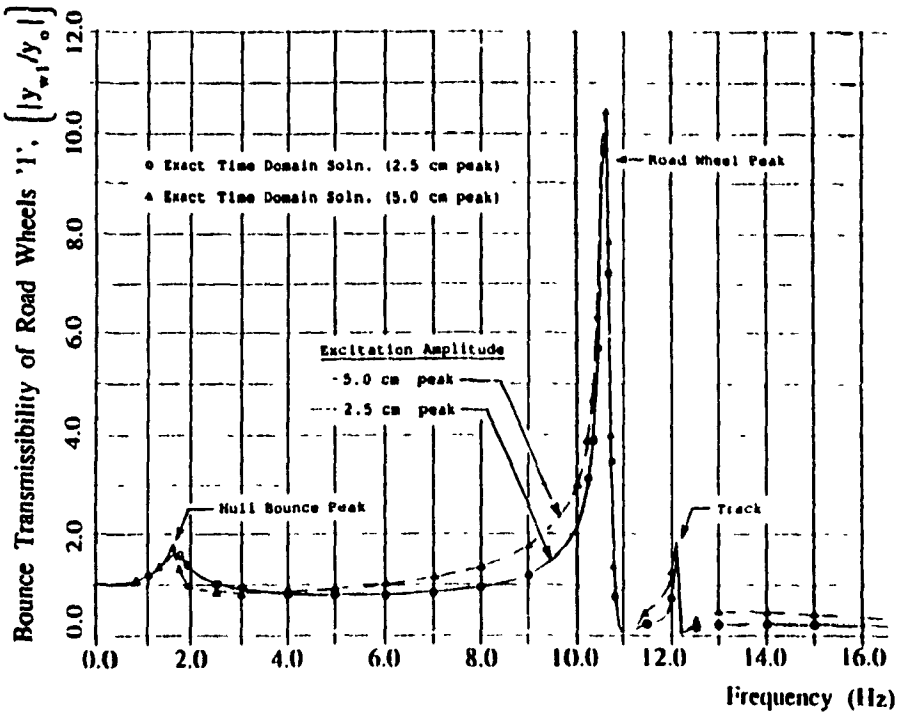

(c).

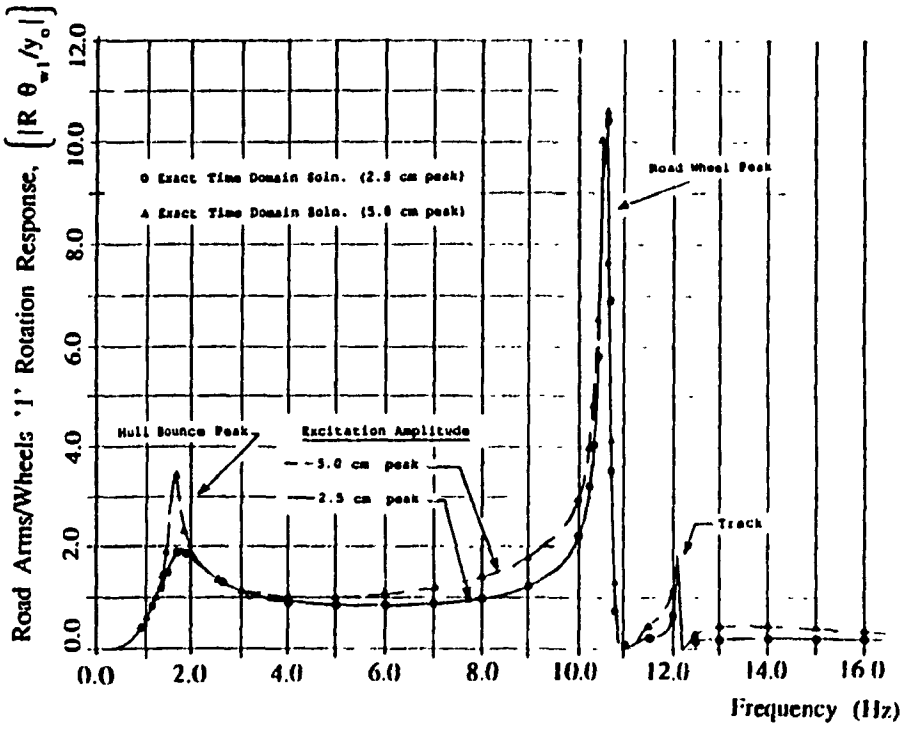

(d).

Figure 4.18 (continued)

Influence of Suspension Damping on the Frequency Response Characteristics of M113 Vehicle Models:

The sensitivity of vehicle response to variations in the damping characteristics of the road wheel suspension is initially investigated for a constant damping coefficient. The constant damping coefficient is selected as C_{11}, assuming low relative velocity response across the shock absorbers. The influence of damping parameters on the vehicle response is investigated for the following values of damping coefficients:

M113 A1

$C_{1i} = C_{2i}$ = 5, 12.5, and 22.52† kN·sec/m ; $i = 1, 5$

$C_{1i} = C_{2i} = 0.0$; $i = 2, 3, 4$

M113 A2

$C_{1i} = C_{2i}$ = 5, 22.5, and 47.3875† kN·sec/m ; $i = 1, 2, 5$

$C_{1i} = C_{2i} = 0.0$; $i = 3, 4$

Nonlinearities due to Coulomb friction and bump stops are neglected during the parametric sensitivity analyses and the transmissibility characteristics of the vehicle models are obtained for simultaneous harmonic input at the road wheels.

Figure 4.19 presents the hull bounce and pitch transmissibility response characteristics of vehicle configurations of the M113 vehicle (*Model I*) for the selected values of damping parameters. The hull bounce response characteristics of the multi-wheeled M113 A1, M113 A2 and M113 A1$\frac{1}{2}$ vehicles reveal two distinct peaks occurring in the vicinity of the hull bounce and road wheel bounce natural frequencies. The pitch response of the lightly damped A1 vehicle reveals an

† Nominal values corresponding to low relative velocity across shock absorber

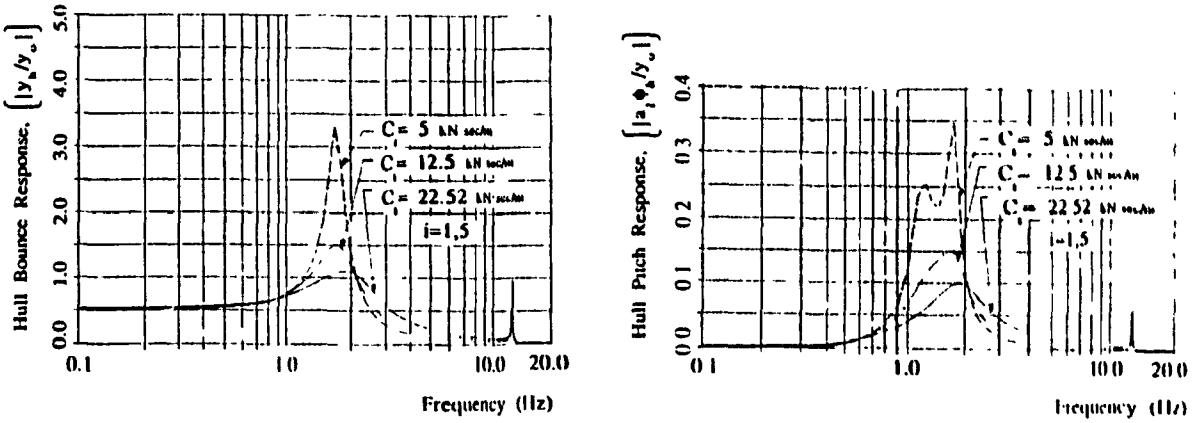

(a). M113 A1

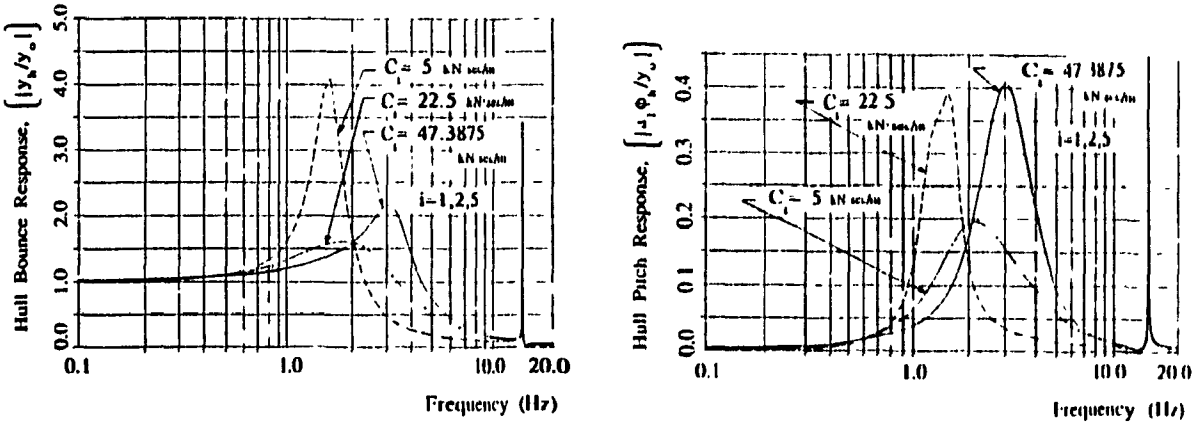

(b). M113 A2

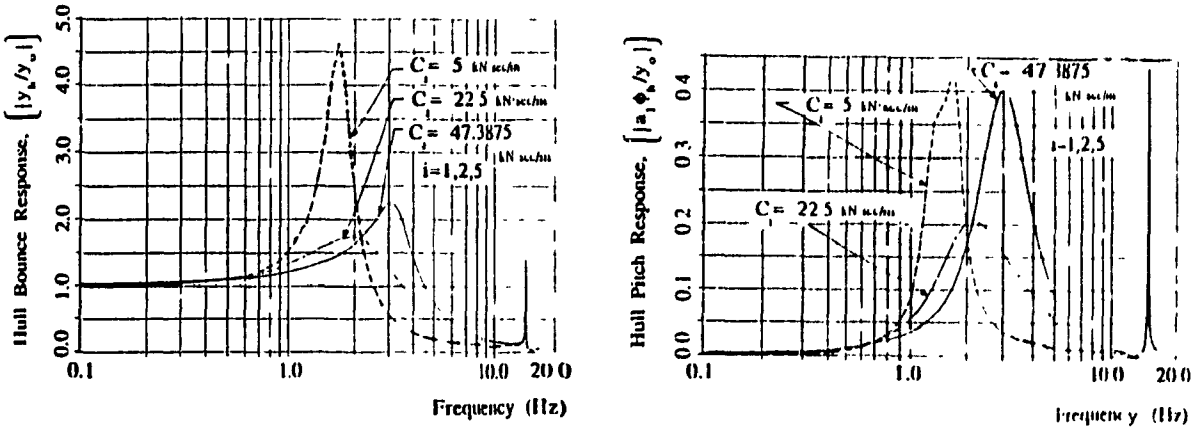

(c). M113 A1$\frac{1}{2}$

Figure 4.19 Frequency Response Characteristics of M113 Vehicles (*MODEL I*) for Various Values of Suspension Damping.

additional peak corresponding to hull pitch resonant frequency, as shown in Figure 4.19a. The bounce and pitch transmissibility response peaks of the vehicle *Model I*, for various damping values, are listed in Table 4.6. The simulation results reveal that the peak hull bounce and pitch response of the M113 A1 vehicle increase considerably in the low frequency range (< 10.0 Hz) as the damping value is decreased. The hull bounce and hull pitch response peaks corresponding to the road wheel resonant frequency is observed to be high, independent of suspension damping.

The peak hull bounce and pitch response characteristics of the M113 A2 vehicle corresponding to the hull resonant frequencies decrease considerably when the damping parameter is increased from a low to the moderate value, as shown in Figure 4.19b. However, the bounce and pitch peaks increase considerably when the damping parameter is further increased (to 47.3875 kN·sec/m). The corresponding hull bounce resonant frequency also increases considerably.

The bounce and pitch transmissibility characteristics of the M113 A1$\frac{1}{2}$ vehicle are similar to that of the M113 A2, as shown in Figure 4.19c. However, the stiffer A1$\frac{1}{2}$ suspension yields slightly higher hull bounce and pitch response than the A2 suspension at low frequencies. The bounce and pitch response around the road wheel resonance is observed to be extremely high, similar to the A2 suspension.

Figure 4.20 illustrates the hull bounce and hull pitch transmissibility response of M113 A1, M113 A2 and M113 A1$\frac{1}{2}$ vehicles with idealized track and suspension (*Model II*) for various values of damping coefficient. Variations in damping coefficients influence the response behaviour of *Model II* in a manner similar to the *Model I*. Addition of

TABLE 4.6

Peak Bounce and Pitch Transmissibility

Response of the Multi-Wheeled Vehicle (*MODEL I*)

for Various SUSPENSION DAMPING Parameters

Response Parameter		A1			A2			$A1\frac{1}{2}$		
		C_1 ; kN·sec/m			C_1 ; kN·sec/m			C_1 ; kN·sec/m		
		5 k	12.5 k	22.5 k	5 k	22.5 k	47.5 k	5 k	22.5 k	47.5 k
$\left\lvert\frac{y_h}{y_o}\right\rvert$	low freq	6.624 (1.7)	2.999 (1.7)	2.146 (1.9)	4.113 (1.6)	1.594 (1.8)	2.141 (3.0)	4.653 (1.7)	1.712 (1.9)	2.220 (3.1)
	high freq	1.883 (12.8)	1.882 (12.8)	1.882 (12.8)	3.402 (14.4)	3.398 (14.4)	3.398 (14.4)	1.380 (14.6)	1.377 (14.6)	1.377 (14.6)
$\left\lvert\frac{a_1\phi_h}{y_o}\right\rvert$	low freq	0.3473 (1.7)	0.1496 (1.7)	0.0959 (1.8)	0.3933 (1.5)	0.1935 (2.2)	0.4044 (3.0)	0.4177 (1.6)	0.2044 (2.2)	0.4000 (3.0)
	high freq	0.0581 (12.8)	0.0581 (12.8)	0.0581 (12.8)	1.049 (14.4)	1.049 (14.4)	1.049 (14.4)	0.4345 (14.6)	0.4344 (14.6)	0.4344 (14.6)

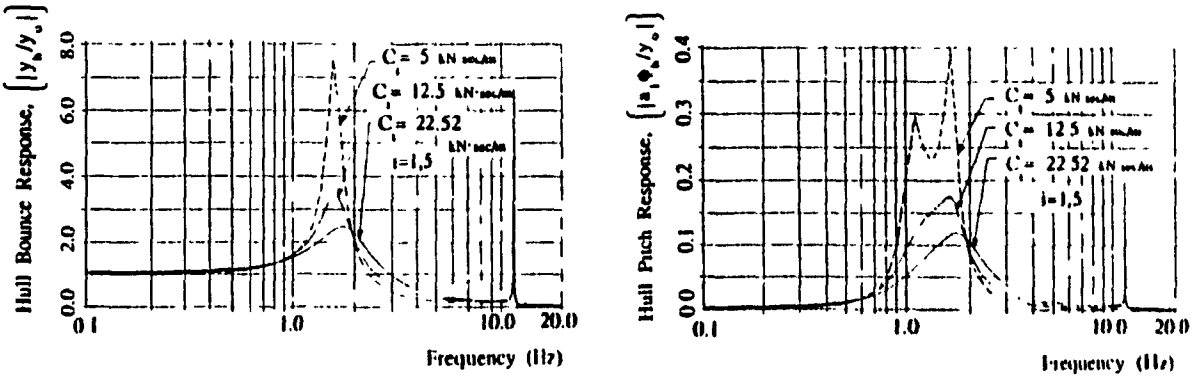

(a). M113 A1

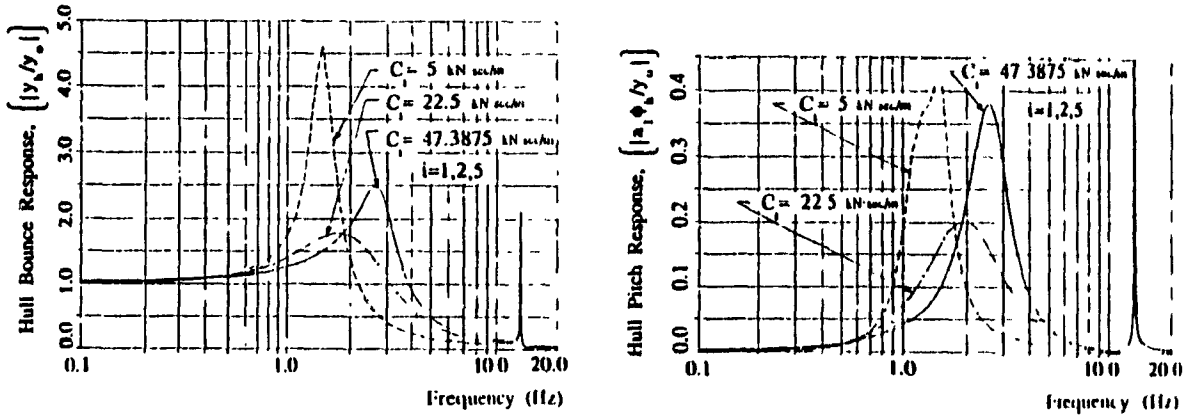

(b). M113 A2

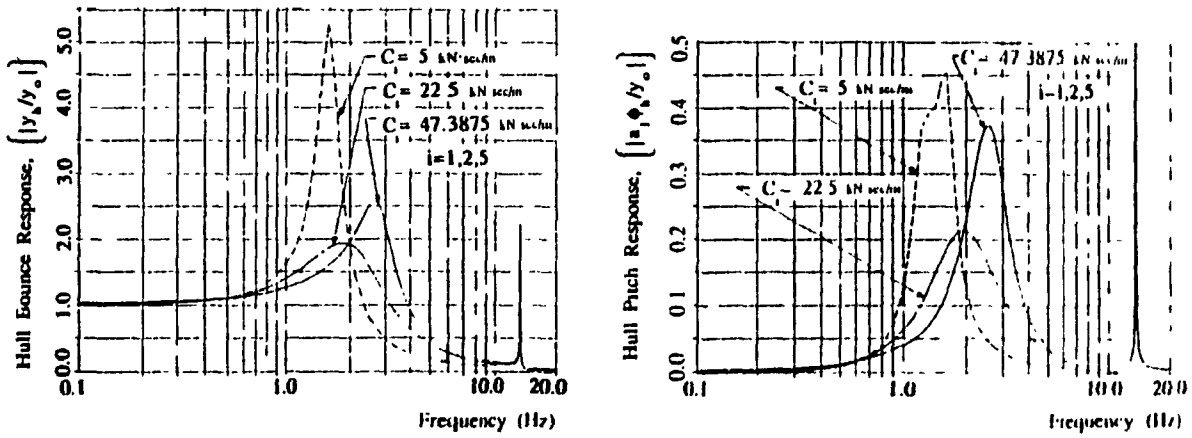

(c). M113 A1$\frac{1}{2}$

Figure 4.20 Frequency Response Characteristics of M113 Vehicles (*MODEL II*) for Various Values of Suspension Damping.

the track deteriorates the low frequency response slightly, while high frequency response is improved. The influence of the damping parameter on the tracked vehicle *Model II* with A1, A2 and A1$\frac{1}{2}$ suspension configurations is summarized in Table 4.7.

The influence of suspension damping on the frequency response characteristics of the vehicle model with linkage suspension (*Model III* and *IV*) is presented in Figures 4.21 and 4.22. The frequency response characteristics of the vehicle *Model III* and *IV* with A1, A2 and A1$\frac{1}{2}$ suspension parameters are summarized in Tables 4.8 and 4.9, respectively. Figures 4.21 and 4.22 reveal that the peak bounce and pitch response in the low frequency range are significantly suppressed with increase in suspension damping. It can be observed that the inclined shock absorbers induce severe pitching of the hull at high frequencies. Suspension damping has little effect on the hull pitch response of the vehicle model without a track (*Model III*), corresponding to high frequency. However, the pitch response of the tracked vehicle model (*Model IV*), corresponding to high frequency increases considerably when the damping parameter is increased, as shown in Table 4.9.

A comparison of the frequency response characteristics of the four vehicle models reveals that an A1 linkage suspension yields high vehicle bounce and pitch at low frequencies when compared to that of idealized A1 suspension. However, the linkage suspension suppresses the high vehicle bounce response considerably at road wheel resonant frequency. The hull bounce and pitch response of nominally damped M113 A2 and M113 A1$\frac{1}{2}$ vehicles improve considerably when the suspension kinematics is appropriately modeled. The improved performance is attributed to the reduced effective damping of the inclined shock absorbers.

TABLE 4.7

Peak Bounce and Pitch Transmissibility

Response of the Tracked Vehicle (*MODEL II*)

for Various SUSPENSION DAMPING Parameters

Response Parameter		A1			A2			$A1\frac{1}{2}$		
		C_i ; kN·sec/m			C_i ; kN·sec/m			C_i ; kN·sec/m		
		5 k	12.5 k	22.5 k	5 k	22.5 K	47.5 k	5 k	22.5 k	47.5 k
$\left\lvert\frac{y_h}{y_o}\right\rvert$	low freq	7.546 (1.6)	3.386 (1.6)	2.435 (1.8)	4.628 (1.5)	1.769 (1.8)	2.451 (2.6)	5.280 (1.6)	1.924 (1.9)	2.551 (2.6)
	high freq	1.533 (11.5)	3.743 (11.5)	6.581 (11.5)	0.4608 (13.2)	1.562 (13.2)	2.089 (13.2)	0.5073 (13.4)	1.685 (13.4)	2.217 (13.4)
$\left\lvert\frac{a_{-}\phi_h}{y_o}\right\rvert$	low freq	0.4003 (1.6)	0.1751 (1.6)	0.1167 (1.7)	0.4132 (1.4)	0.2014 (1.9)	0.3771 (2.6)	0.4557 (1.6)	0.2123 (1.9)	0.3704 (2.6)
	high freq	0.0451 (11.5)	0.1100 (11.5)	0.1933 (11.5)	0.1303 (13.2)	0.4508 (13.2)	0.6034 (13.2)	0.1438 (13.4)	0.4874 (13.4)	0.6420 (13.4)

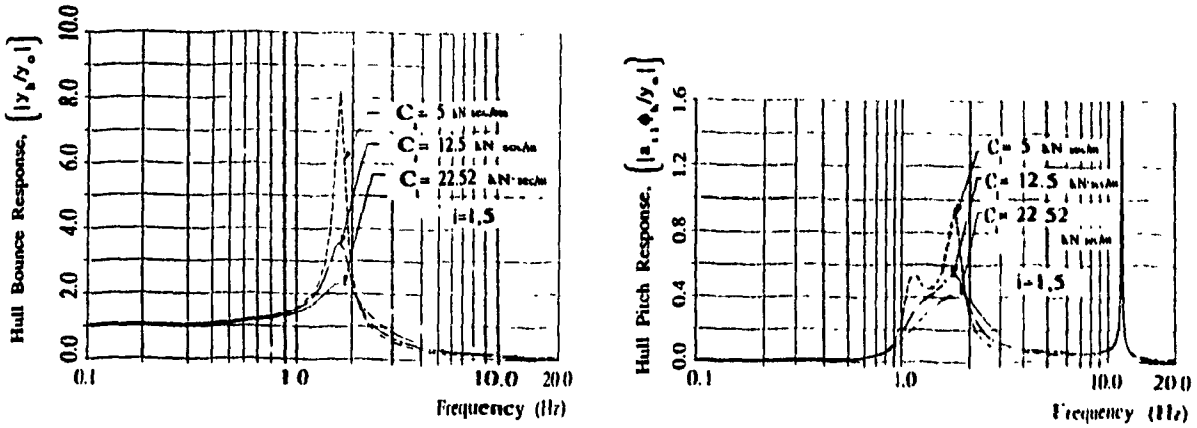

(a). M113 A1

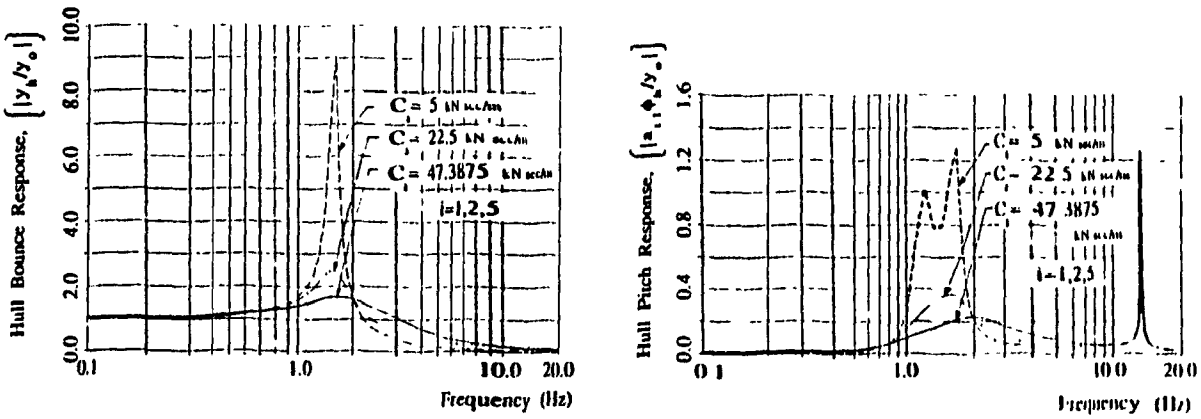

(b). M113 A2

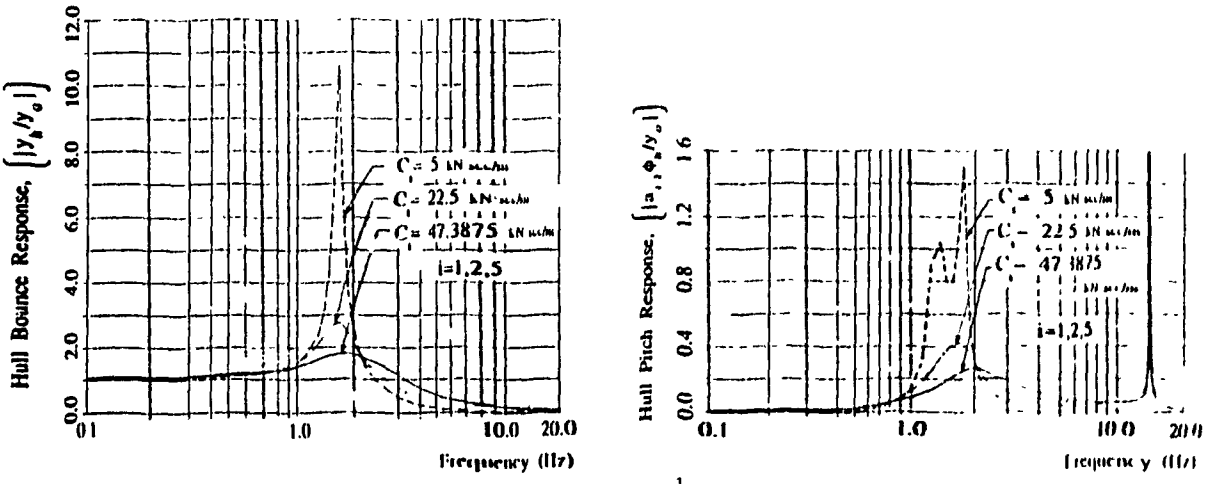

(c). M113 A1$\frac{1}{2}$

Figure 4.21 Frequency Response Characteristics of M113 Vehicles (*MODEL III*) for Various Values of Suspension Damping.

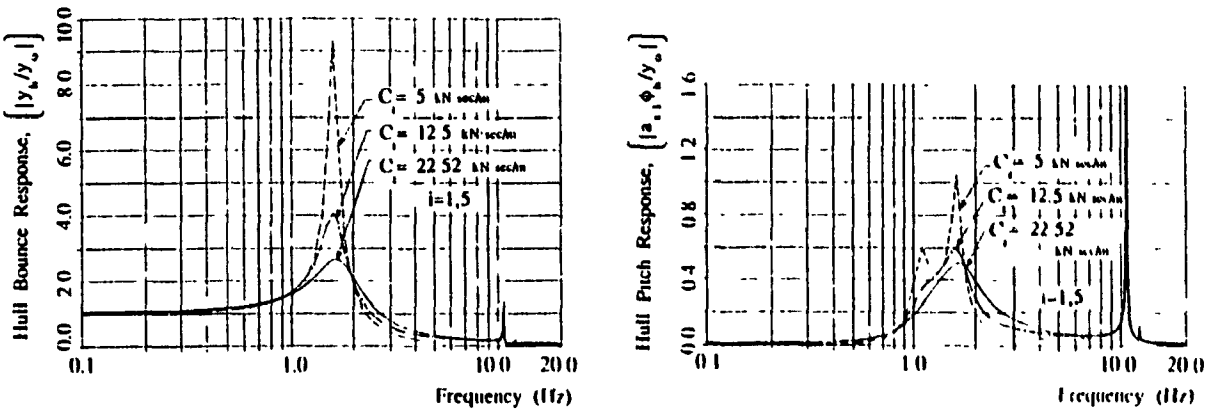

(a). M113 A1

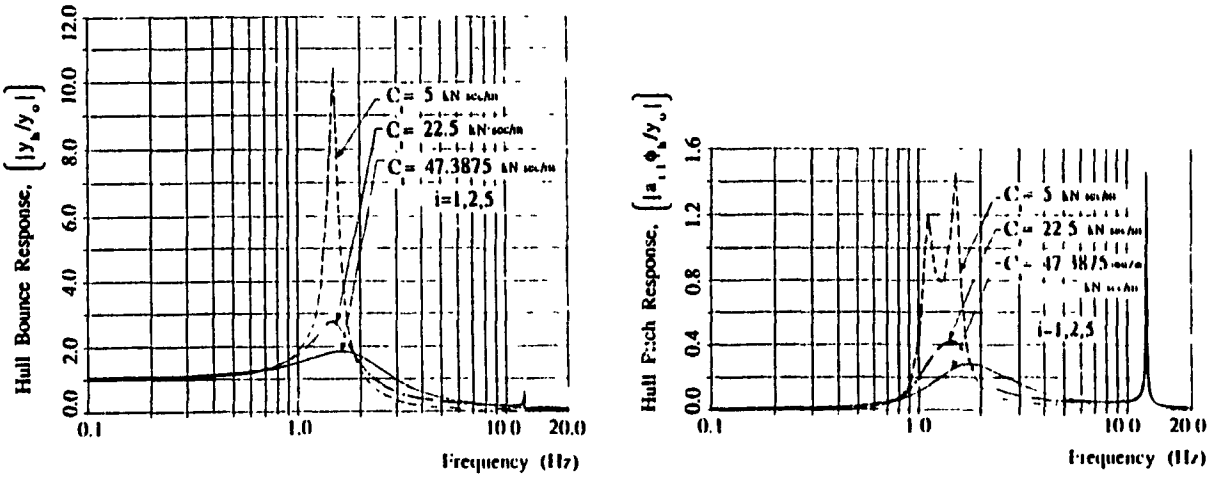

(b). M113 A2

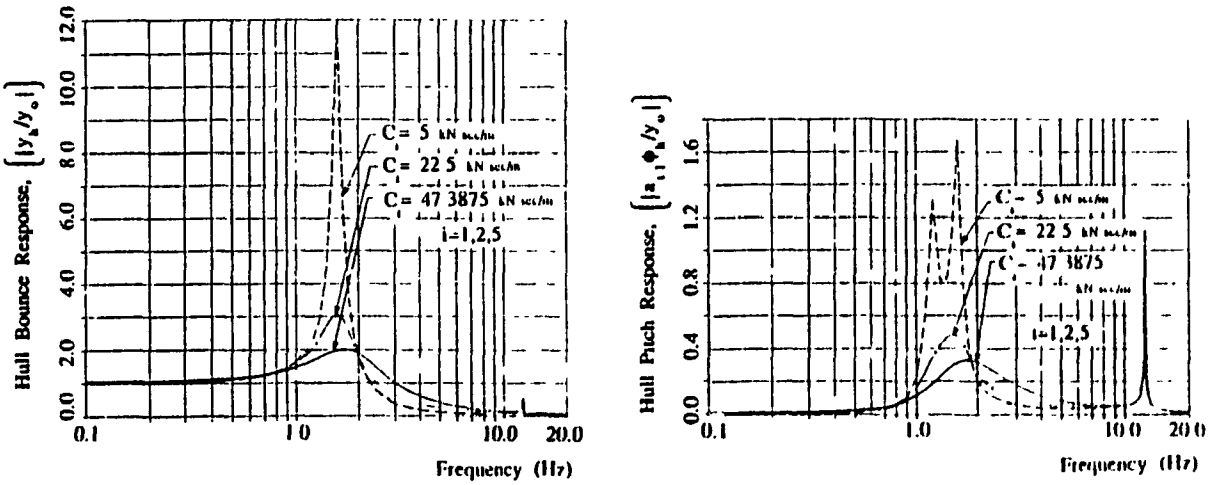

(c). M113 A1$\frac{1}{2}$

Figure 4.22 Frequency Response Characteristics of M113 Vehicles (*MODEL IV*) for Various Values of Suspension Damping.

TABLE 4.8

Peak Bounce and Pitch Transmissibility

Response of the Multi-Wheeled Vehicle (*MODEL III*)

for Various SUSPENSION DAMPING Parameters

Response Parameter		A1			A2			$A1\frac{1}{2}$		
		C_i; kN·sec/m			C_i; kN·sec/m			C_i; kN·sec/m		
		5 k	12.5 k	22.5 k	5 k	22.5 k	47.5 k	5 k	22.5 k	47.5 k
$\left\lvert\frac{y_h}{y_o}\right\rvert$	low freq	8.177 (1.7)	3.456 (1.7)	2.331 (1.7)	9.050 (1.5)	2.429 (1.6)	1.628 (1.7)	10.60 (1.7)	2.699 (1.7)	1.754 (1.8)
	high freq	0.1413 (11.7)	0.1413 (11.7)	0.1413 (11.7)	0.1435 (13.3)	0.1467 (13.3)	0.1469 (13.3)	0.1711 (13.4)	0.1725 (13.4)	0.1725 (13.4)
$\left\lvert\frac{a_{t1}\phi_h}{y_o}\right\rvert$	low freq	0.9477 (1.6)	0.5326 (1.7)	0.4315 (1.7)	1.279 (1.6)	0.3575 (1.5)	0.2178 (1.9)	1.512 (1.7)	0.4107 (1.6)	0.2526 (2.0)
	low freq	1.811 (11.8)	1.810 (11.8)	1.810 (11.8)	1.264 (13.3)	1.236 (13.3)	1.235 (13.3)	3.050 (13.4)	3.053 (13.4)	3.053 (13.4)

TABLE 4.9

Peak Bounce and Pitch Transmissibility

Response of the Tracked Vehicle (*MODEL IV*)

for Various SUSPENSION DAMPING Parameters

Response Parameter		A1			A2			$A1\frac{1}{2}$		
		C_1 ; kN·sec/m			C_2 ; kN·sec/m			C_1 ; kN·sec/m		
		5 k	12.5 k	22.5 k	5 k	22.5 k	47.5 k	5 k	22.5 k	47.5 k
$\left\lvert\frac{y_h}{y_o}\right\rvert$	low freq	9.324 (1.6)	4.016 (1.6)	2.611 (1.6)	10.45 (1.5)	2.704 (1.5)	1.794 (1.6)	12.04 (1.6)	3.036 (1.6)	1.958 (1.7)
	high freq	0.4837 (10.6)	0.9894 (10.6)	1.309 (10.6)	0.1085 (11.9)	0.3406 (12.2)	0.5710 (12.2)	0.1247 (12.2)	0.3804 (12.3)	0.4929 (12.3)
$\left\lvert\frac{a_{t1}\phi_h}{y_o}\right\rvert$	low freq	1.042 (1.6)	0.5906 (1.6)	0.4911 (1.7)	1.457 (1.5)	0.4109 (1.4)	0.2723 (1.8)	1.675 (1.6)	0.4757 (1.5)	0.3201 (1.8)
	high freq	0.8920 (10.6)	1.767 (10.6)	2.327 (10.6)	0.2560 (12.1)	0.8727 (12.2)	1.453 (12.2)	0.2656 (12.3)	0.7907 (12.4)	1.116 (12.4)

Influence of Nonlinear Force Velocity Characteristics of the Shock Absorber

The local equivalent linearization algorithm is implemented to evaluate the hull bounce and hull pitch transmissibility response characteristics of the tracked vehicle *Model II* and *IV* incorporating A1, A2 and $A1\frac{1}{2}$ parameters and Coulomb friction. Influence of nonlinear force-velocity characteristics of the shock absorbers on the vehicle response is investigated for the following variations:

M113 A1:

C_{1i} = 16.89, 22.52† and 28.15 kN·sec/m

C_{2i} = 3.49, 4.657† and 5.82 kN·sec/m ; i = 1, 5

M113 A2:

C_{1i} = 35.5, 47.3875† and 59.0 kN·sec/m

C_{2i} = 4.35, 5.8355† and 7.3 kN·sec/m ; i = 1, 2, 5

The hull bounce and pitch transmissibility response of the tracked vehicle model with idealized suspension (*Model II*) are presented in Figure 4.23. The peak vehicle response and the corresponding frequencies of vehicle *Model II* with A1, A2 and $A1\frac{1}{2}$ parameters are listed in Table 4.10. The hull bounce and pitch response of the M113 vehicle coupled with the A1 suspension decrease around the low frequency, and increase corresponding to the road wheel resonant frequency when the suspension damping is increased, as shown in Figure 4.23a and Table 4.10. In contrast, the bounce and pitch response of the vehicle model with A2 and $A1\frac{1}{2}$ suspension increase with increase in suspension damping, as shown in Figures 4.23b and 4.23c.

† Nominal damping coefficient of shock absorber

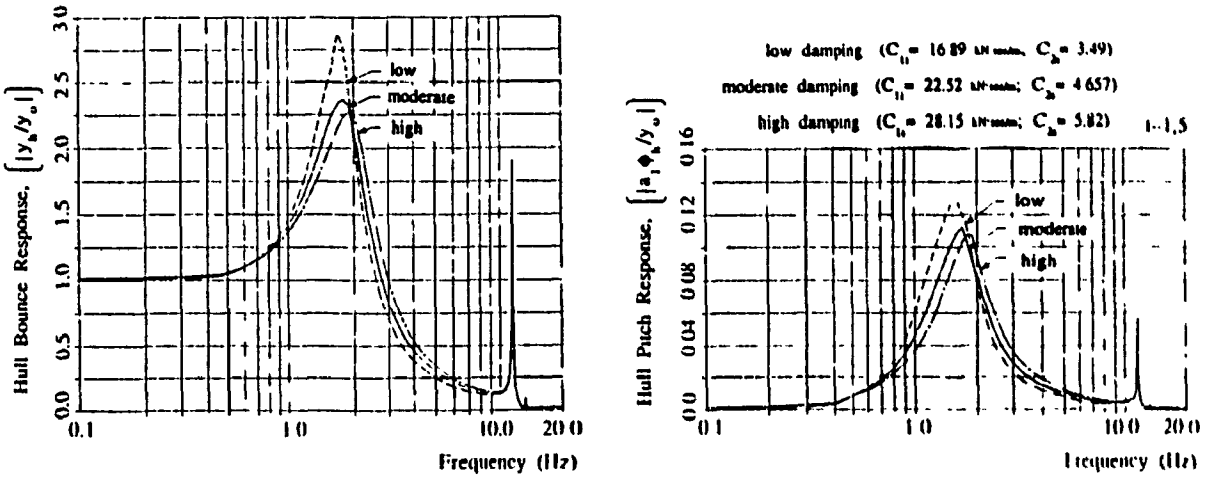

(a). M113 A1

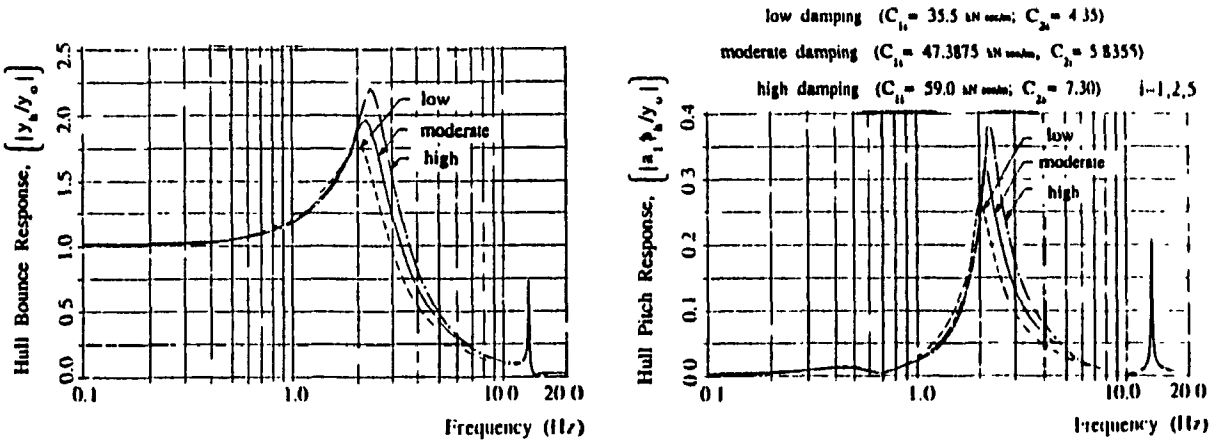

(b). M113 A2

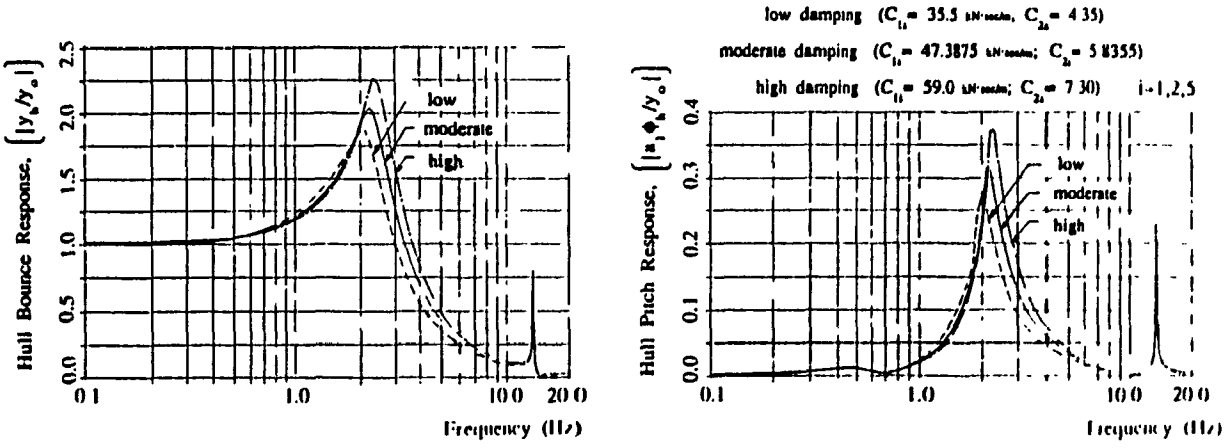

(c). M113 A1$\frac{1}{2}$

Figure 4.23 Hull Bounce and Pitch Response of Tracked M113 Vehicles (*MODEL II*) for Various Values of Nonlinear Suspension Damping.

TABLE 4.10

Bounce and Pitch Transmissibility

Response Peak Amplitudes due to

NONLINEAR SUSPENSION DAMPING VARIATION - *MODEL II*

Response Parameter		A1			A2			$A1\frac{1}{2}$		
		C_{1i}/C_{2i} ; i=1,5 ; N·sec/m			C_{1i}/C_{2i} ; i=1,2,5 ; kN·sec/m			C_{1i}/C_{2i} ; i=1,2,5 ; kN·sec/m		
		16.9/3.5 k	22.5/4.7 k	28.2/5.8 k	35.5/4.4 k	47.4/5.8 k	59.0/7.3 k	35.5/4.4 k	47.4/5.8 k	59.0/7.3 k
$\left\lvert\frac{y_h}{y_o}\right\rvert$	low freq	2.876 (1.7)	2.362 (1.8)	2.258 (1.9)	1.769 (2.0)	1.958 (2.2)	2.189 (2.3)	1.869 (2.0)	2.034 (2.2)	2.252 (2.3)
	high freq	1.160 (11.5)	1.526 (11.5)	1.893 (11.5)	0.4472 (13.2)	0.5865 (13.2)	0.7192 (13.2)	0.4912 (13.4)	0.6431 (13.4)	0.7874 (13.4)
$\left\lvert\frac{a_1\phi_h}{y_o}\right\rvert$	low freq	0.1293 (1.6)	0.1115 (1.7)	0.1066 (1.8)	0.2689 (2.0)	0.3113 (2.1)	0.3769 (2.2)	0.2797 (2.0)	0.3129 (2.1)	0.3705 (2.2)
	high freq	0.0341 (11.5)	0.0448 (11.5)	0.0556 (11.5)	0.1263 (13.2)	0.1673 (13.2)	0.2061 (13.2)	0.1391 (13.4)	0.1839 (13.4)	0.2262 (13.4)

Figure 4.24 illustrates the hull bounce and pitch transmissibility response of the tracked vehicle model with linkage suspension (*Model IV*) and the corresponding peak amplitudes are listed in Table 4.11. The peak hull bounce response corresponding to the hull resonant frequencies decreases when the damping coefficients are increased, as shown in Figures 4.24a, 4.24b and 4.24c.

Influence of Location and Number of Shock Absorbers

The frequency response characteristics of tracked vehicle models with the addition or interchanging of shock absorbers at intermediate road wheels are computed to study the influence of location and number of shock absorbers. The damping coefficients due to shock absorbers are considered to be the nominal values determined from the force-velocity characteristics. The shock absorbers are distributed over each vehicle track as follows:

Configuration I. Additional shock absorber is mounted per track at road wheel station '2' (M113 A1 only)

Configuration II. Shock absorber/track at road wheel station '2' is interchanged to station '3'.

Configuration III. Shock absorber/track at road wheel station '2' is interchanged to station '4'.

Configuration IV. Low damping (half the nominal damping) shock absorbers are mounted at intermediate road wheel stations.

Configuration V. Shock absorbers are mounted at all road wheels.

Computer simulations are carried out for the tracked vehicle models with linkage suspension (*Model IV*). Hull bounce and pitch frequency response characteristics of the tracked vehicle model with A1 linkage

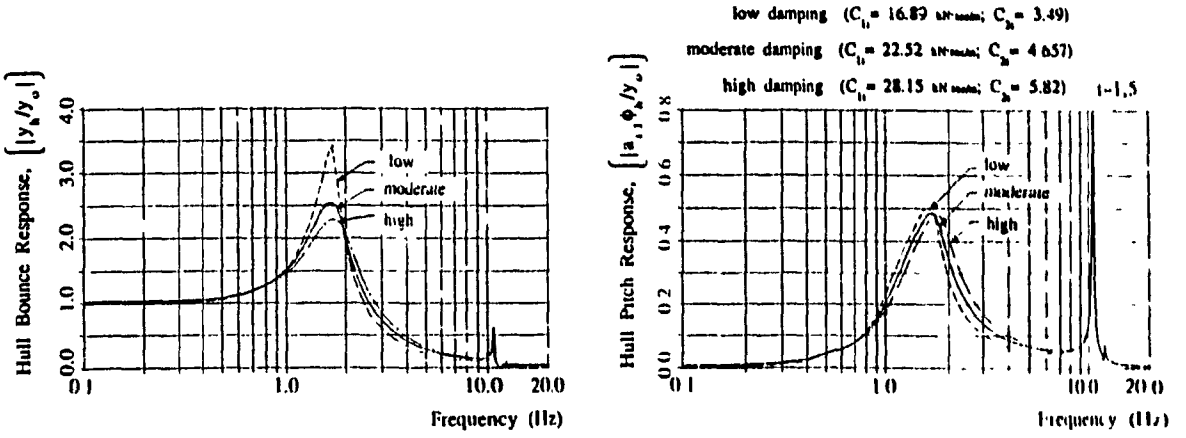

(a). M113 A1

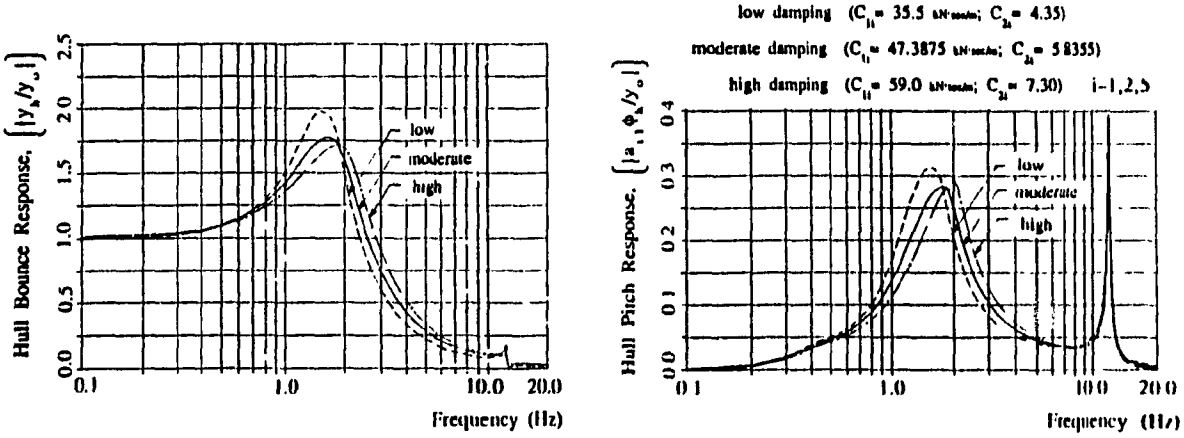

(b). M113 A2

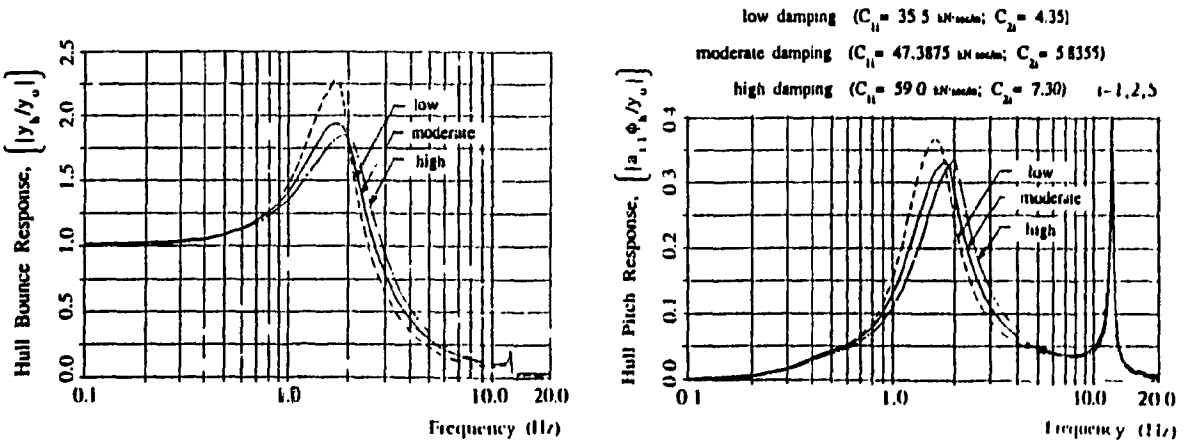

(c). M113 A1$\frac{1}{2}$

Figure 4.24 Hull Bounce and Pitch Response of Tracked M113 Vehicles (*MODEL IV*) for Various Values of Nonlinear Suspension Damping.

TABLE 4.11

Bounce and Pitch Transmissibility

Response Peak Amplitudes due to

NONLINEAR SUSPENSION DAMPING VARIATION - *MODEL IV*

Response Parameter		A1			A2			$A1\frac{1}{2}$		
		C_{1i}/C_{2i} ; i=1,5 ; kN·sec/m			C_{2i}/C_{2i} ; i=1,2,5 ; kN·sec/m			C_{1i}/C_{2i} ; i=1,2,5 ; kN·sec/m		
		16.9/3.5 k	22.5/4.7 k	28.2/5.8 k	35.5/4.4 k	47.4/5.8 k	59.0/7.3 k	35.5/4.4 k	47.4/5.8 k	59.0/7.3 k
$\left\lvert\frac{y_h}{y_o}\right\rvert$	low freq	3.434 (1.7)	2.514 (1.7)	2.265 (1.7)	1.983 (1.5)	1.764 (1.6)	1.700 (1.7)	2.302 (1.7)	1.928 (1.7)	1.839 (1.9)
	high freq	0.3831 (10.6)	0.4975 (10.6)	0.605 (10.6)	0.1147 (12.0)	0.1397 (12.1)	0.1684 (12.1)	0.1315 (12.2)	0.1627 (12.3)	0.1975 (12.3)
$\left\lvert\frac{a_{t_i}\phi_h}{y_o}\right\rvert$	low freq	0.5018 (1.6)	0.4808 (1.6)	0.4732 (1.7)	0.3142 (1.5)	0.2823 (1.7)	0.2906 (1.7)	0.3692 (1.6)	0.3330 (1.8)	0.3407 (2.0)
	high freq	0.7217 (10.6)	0.9140 (10.6)	1.093 (10.6)	0.2645 (21.1)	0.3306 (12.2)	0.3983 (12.2)	0.2740 (12.3)	0.3385 (12.4)	0.4060 (12.4)

suspension (*Model IV*) are presented in Figures 4.25 and 4.26, respectively, when additional shock absorbers are placed in each track of the vehicle at a particular road wheel station. Addition of one shock absorber per track evidently improves the hull bounce and pitch transmissibility. Addition of A1 shock absorbers at the road wheel station '4' further improves the hull bounce response corresponding to the hull bounce natural frequency, however, the hull pitch response is deteriorated considerably. The hull pitch response corresponding to the road wheel frequency increases considerably due to the damped road wheel station '4', as shown in Figure 4.26a. Addition of the shock absorbers at road wheel station '2' yields extremely superior hull pitch response, while the hull bounce response is sightly deteriorated corresponding to the hull bounce and pitch resonant frequencies, as indicated in Table 4.12.

Interchanging of intermediate A2 shock absorbers per track to selected road wheel stations on M113 A2 and M113 A1$\frac{1}{2}$ vehicles does not influence the bounce frequency response considerably, as shown in Figures 4.25b, 4.25c and Table 4.12. The vehicles with damped third road wheels exhibit slightly improved hull bounce response corresponding to the hull bounce resonance, however, the pitch response deteriorates considerably with this arrangement.

Placing shock absorbers at all the wheel stations improves the hull bounce response peak at the bounce resonance of the vehicle and eliminates the peak at high frequency resonance for all the vehicle configurations, as shown in Figures 4.25 and 4.26, and Table 4.12. However, the pitch peak response of the M113 A2 and M113 A1$\frac{1}{2}$ vehicles increases considerably due to heavily damped A2 and A1$\frac{1}{2}$ suspensions.

MODEL IV

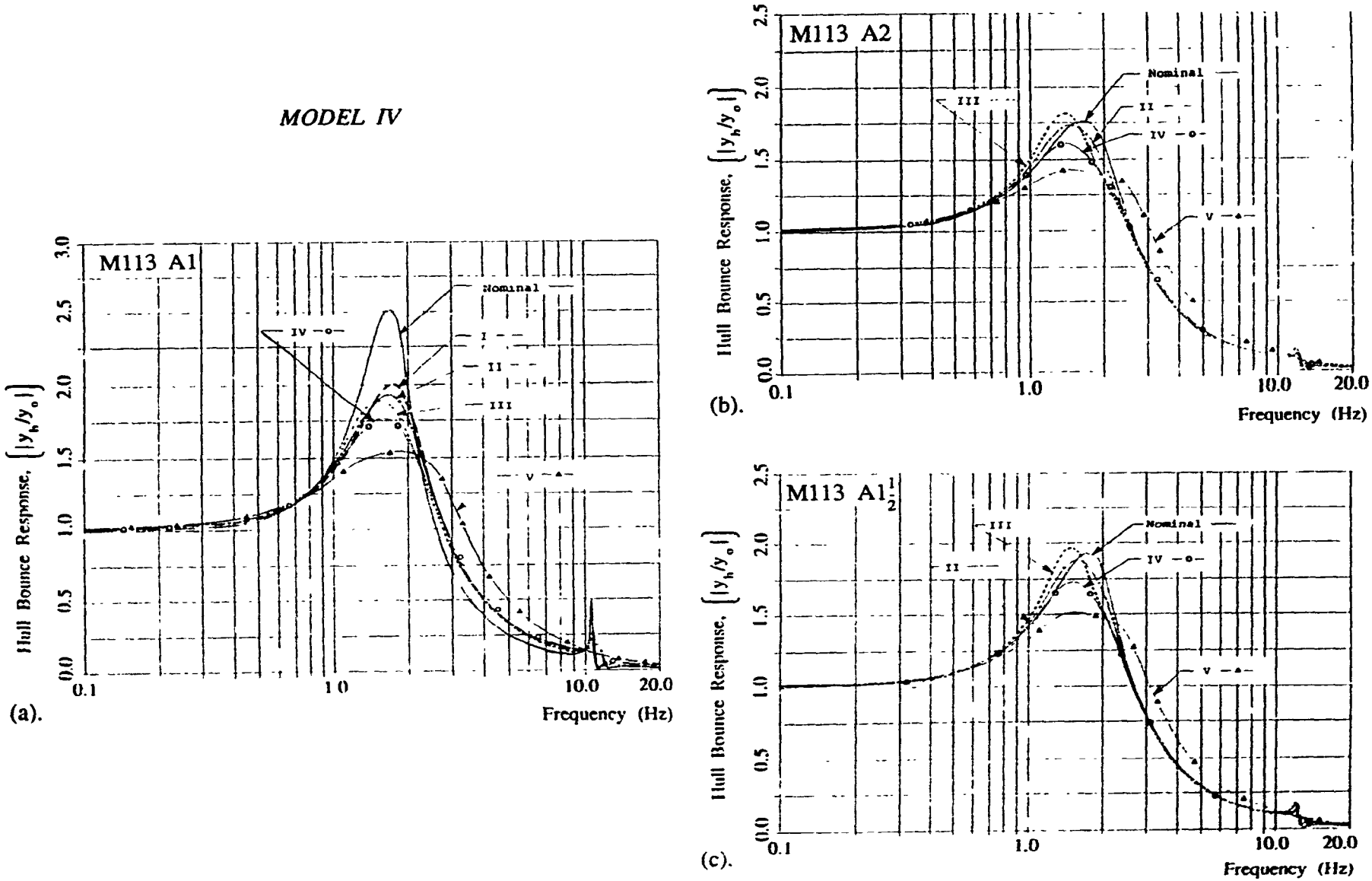

Figure 4.25 Hull Bounce Response of Tracked M113 Vehicles (*MODEL IV*) for Various Suspension Configurations on Number and Location of Shock Absorbers.

MODEL IV

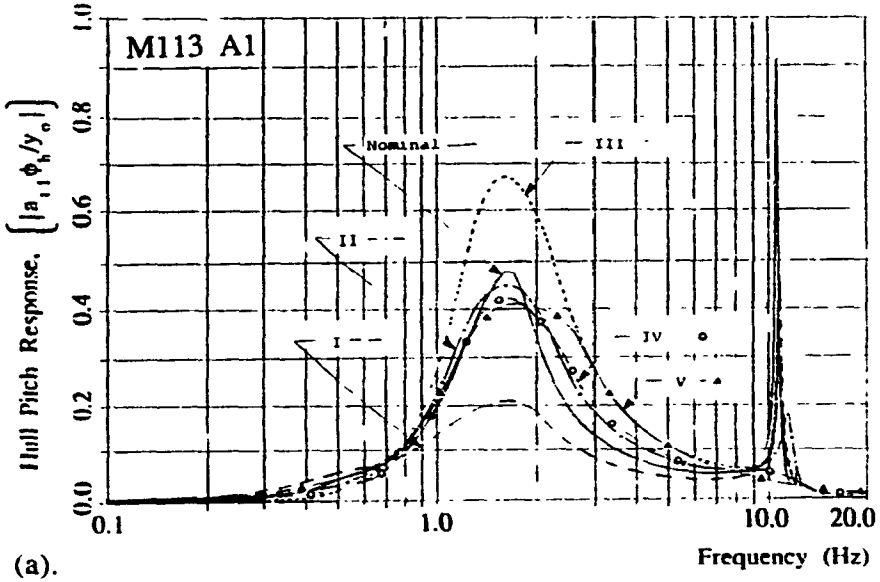

(a).

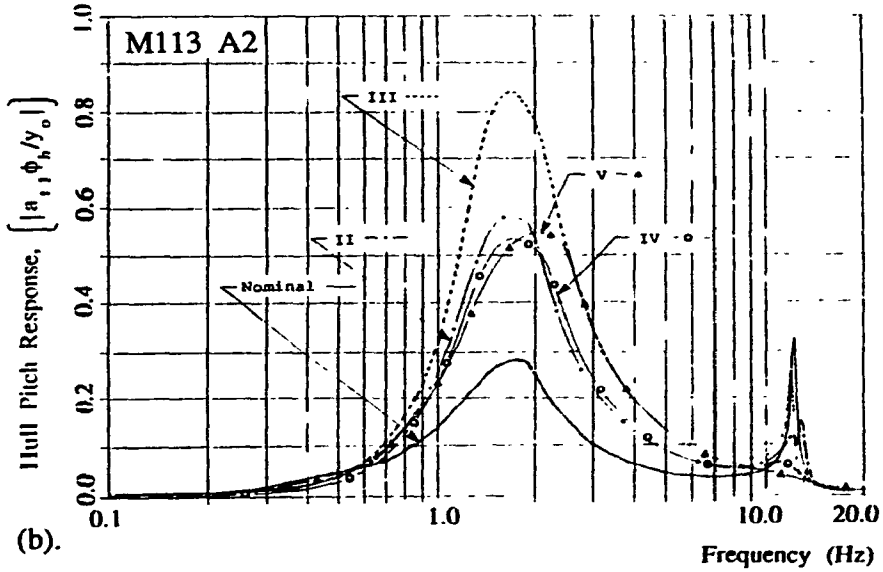

(b).

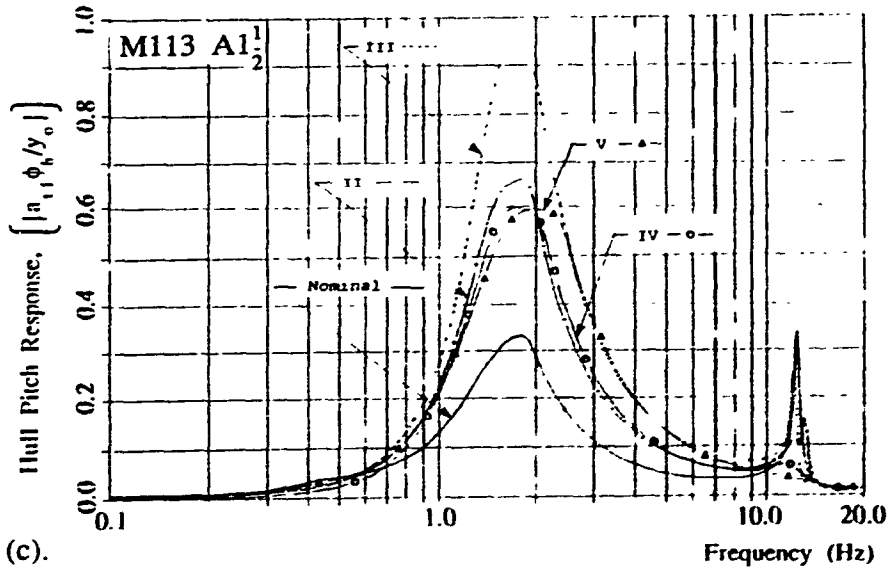

(c).

Figure 4.26 Hull Pitch Response of Tracked M113 Vehicles (*MODEL IV*) for Various Suspension Configurations on Number and Location of Shock Absorbers.

TABLE 4.12

Bounce and Pitch Transmissibility

Response Peak Amplitudes due to VARIATION IN

NUMBER AND LOCATION OF SHOCK ABSORBERS - *MODEL IV*

		Distribution of Shock Absorbers					
		Nominal	(I)	(II)	(III)	(IV)	(V)
M113 A1							
$\left\|\frac{y_h}{y_o}\right\|$	low	2.514 (1.7)	1.999 (1.7)	1.916 (1.7)	1.891 (1.5)	1.758 (1.6)	1.527 (1.8)
	high	0.4975 (10.6)	0.1535 (10.8)	0.1621 (11.2)	0.2640 (10.8)	---	---
$\left\|\frac{a_{t1}\phi_h}{y_o}\right\|$	low	0.4808 (1.6)	0.2056 (1.6)	0.448 (1.6)	0.673 (1.6)	0.4193 (1.6)	0.4036 (1.7)
	high	0.9140 (10.6)	0.2093 (10.8)	0.1751 (11.4)	0.3310 (10.8)	---	---
M113 A2							
$\left\|\frac{y_h}{y_o}\right\|$	low	1.764 (1.6)		1.723 (1.5)	1.801 (1.4)	1.607 (1.4)	1.419 (1.5)
	high	0.1397 (12.1)		0.1046 (11.8)	0.1465 (11.8)	---	---
$\left\|\frac{a_{t1}\phi_h}{y_o}\right\|$	low	0.2823 (1.7)		0.5783 (1.7)	0.8363 (1.7)	0.5344 (1.7)	0.5435 (2.1)
	high	0.3306 (12.2)		0.1168 (12.1)	0.2553 (11.9)	---	---
M113 A1$\frac{1}{2}$							
$\left\|\frac{y_h}{y_o}\right\|$	low	1.928 (1.7)		1.871 (1.6)	1.956 (1.5)	1.730 (1.5)	1.505 (1.5)
	high	0.1627 (12.3)		0.1091 (12.1)	0.1685 (12.0)	---	---
$\left\|\frac{a_{t1}\phi_h}{y_o}\right\|$	low	0.3330 (1.8)		0.6590 (1.8)	0.9708 (1.7)	0.5982 (1.7)	0.5917 (2.0)
	high	0.3385 (12.4)		0.1146 (12.3)	0.2471 (12.1)	---	---

Influence of Shock Absorber Inclination

The effective damping forces in the vertical and longitudinal axes can be varied by varying the inclination (β_o) of the shock absorber link within the trailing arm road wheel suspension. The influence of shock absorber orientation on the frequency response characteristics of the tracked vehicle model with linkage suspension (*Model IV*) is investigated for the following inclination parameters:

M113 A1: β_o = 0.619, 0.698†, 0.782 rad

M113 A2 & M113 A1$\frac{1}{2}$: β_o = 0.486, 0.524†, 0.572 rad

The hull bounce and pitch transmissibility response of the tracked vehicle model for variation in shock absorber inclination are presented in Figure 4.27. The peak transmissibility response characteristics are summarized in Table 4.13. The peak bounce and pitch transmissibility response of the A1, A2 and A1$\frac{1}{2}$ vehicle configurations corresponding to vehicle bounce resonant frequency decrease considerably when the shock absorber inclination is increased. However, the peak bounce and pitch response corresponding to road wheel resonant frequency increase with increase in shock absorber inclination. Thus an adequate inclination of the shock absorber offers considerable potentials in improving vehicle response within the low frequency region.

† Nominal shock absorber inclination angle

Influence of Suspension Stiffness Variation on the Frequency Response of Tracked Vehicles

The frequency response characteristics and thus the ride dynamics of M113 vehicles are strongly influenced by the stiffness properties of the A1, A2 and A1$\frac{1}{2}$ suspension. Variation in suspension stiffness

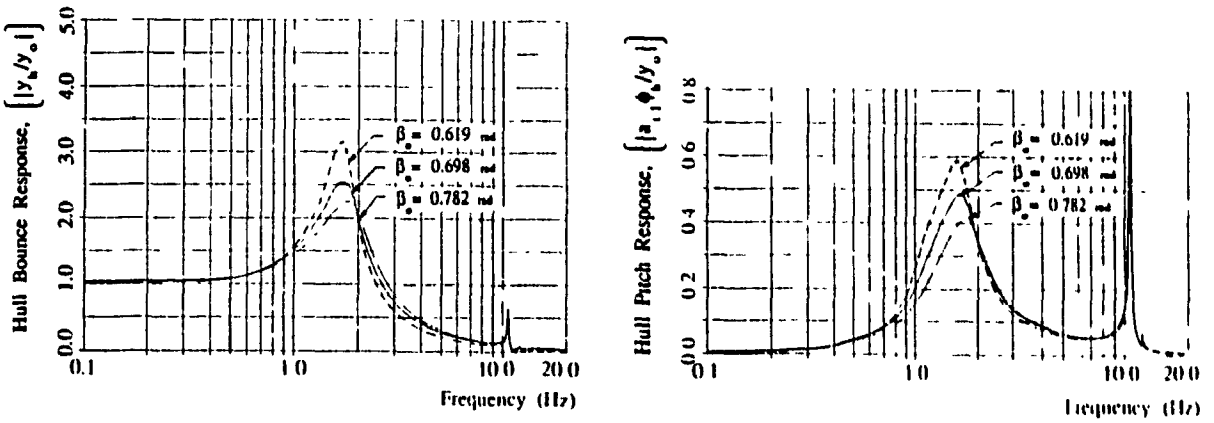

(a). M113 A1

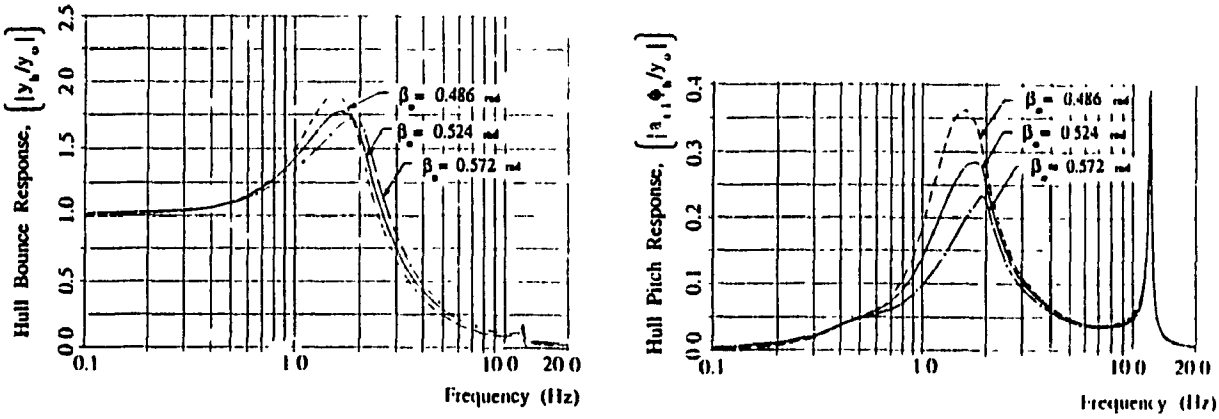

(b). M113 A2

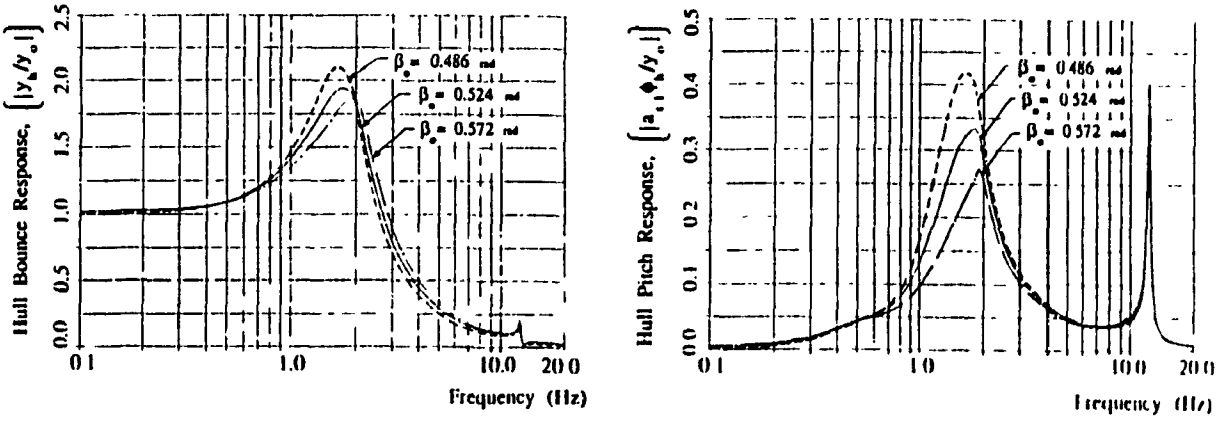

(c). M113 A1$\frac{1}{2}$

Figure 4.27 Hull Bounce and Pitch Response of Tracked M113 Vehicles (*MODEL IV*) for Various Angles of Shock Absorber Inclination.

TABLE 4.13

Bounce and Pitch Transmissibility

Response Peak Amplitudes due to VARIATION IN

SHOCK ABSORBER INCLINATION - *MODEL IV*

Response Parameter		A1			A2			$A1\frac{1}{2}$		
		β_o ; rad			β_o ; rad			β_o ; rad		
		0.619	0.698	0.782	0.486	0.524	0.572	0.486	0.524	0.572
$\left\lvert\frac{y_h}{y_c}\right\rvert$	low	3.171 (1.7)	2.514 (1.7)	2.223 (1.8)	1.914 (1.5)	1.764 (1.6)	1.710 (1.9)	2.106 (1.6)	1.928 (1.7)	1.846 (1.9)
	high	0.3797 (10.6)	0.4975 (10.6)	0.6249 (10.6)	0.1227 (12.0)	0.1397 (12.1)	0.1676 (12.1)	0.1405 (12.2)	0.1627 (12.3)	0.1966 (12.3)
$\left\lvert\frac{a_{zz}\phi_h}{y_o}\right\rvert$	low	0.5915 (1.6)	0.4808 (1.6)	0.4125 (1.8)	0.3620 (1.6)	0.2823 (1.7)	0.2306 (1.9)	0.4199 (1.6)	0.3330 (1.8)	0.2703 (1.9)
	high	0.7233 (10.6)	0.9140 (10.6)	1.122 (10.6)	0.2872 (12.2)	0.3306 (12.2)	0.3918 (12.2)	0.2948 (12.3)	0.3385 (12.4)	0.3994 (12.4)

involves varying the torsional spring rates or the linear equivalent spring rate of the torsion bars. Frequency response characteristics of the tracked vehicle *Model II* and *IV* coupled with A1 and A2 suspensions are computed for the following values of spring rates:

Model II

M113 A1: K_i = 87.8, 115.675† and 140.5 kN/m ; i = 1, ..., 5

M113 A2: K_i = 73.0, 97.722† and 123.0 kN/m ; i = 1, ..., 5

Model IV

M113 A1: $K_{\theta i}$ = 7.5, 9.884† and 12.0 kN·m/rad ; i = 1, ..., 5

M113 A2: $K_{\theta i}$ = 6.25, 8.35† and 10.5 kN·m/rad ; i = 1, ..., 5

The peak values of hull bounce and hull pitch transmissibility ratio, and corresponding frequencies of the tracked vehicle models, *Model II* & *IV* are summarized in Tables 4.14 and 4.15, respectively. The peak hull bounce and pitch response of the tracked vehicle models corresponding to vehicle bounce resonance improves considerably by employing softer torsion bars, as depicted in Tables 4.14 and 4.15. Thus, softer torsion bars offer significant potential in improving the vehicle ride bounce and pitch response. A comparison of the frequency response characteristics of the idealized and linkage suspension models reveals that the linkage suspension yields superior bounce but poor pitch response.

Influence of Track Tension on the Frequency Response of Tracked Vehicles

Variation in track tension involves varying the linear equivalent relative springs representing restoring forces due to track interaction between the adjacent road wheels. The frequency response characteristics of the tracked vehicle models with A1, A2 and A1$\frac{1}{2}$ suspension configurations (*Model II* & *IV*) are summarized in Table 4.16

TABLE 4.14

Bounce and Pitch Transmissibility

Response Peak Amplitudes due to

SUSPENSION STIFFNESS VARIATION - *MODEL II*

Response Parameter		A1			A2		
		K_i ; N/m			K_i ; N/m		
		87750	115675	140500	73000	97722	123000
$\left\|\frac{y_h}{y_o}\right\|$	low	1.968 (1.6)	2.362 (1.8)	2.878 (1.9)	1.861 (2.2)	1.958 (2.2)	2.067 (2.2)
	high	1.242 (11.2)	1.526 (11.5)	1.420 (11.7)	0.4836 (12.9)	0.5865 (13.2)	0.6800 (13.5)
$\left\|\frac{a_1\phi_h}{y_o}\right\|$	low	0.0854 (1.6)	0.1115 (1.7)	0.1316 (1.7)	0.3097 (2.2)	0.3113 (2.1)	0.3133 (2.1)
	high	0.0366 (11.2)	0.0448 (11.5)	0.0416 (11.7)	0.1341 (12.9)	0.1673 (13.2)	0.1986 (13.5)

TABLE 4.15

Bounce and Pitch Transmissibility

Response Peak Amplitudes due to

SUSPENSION STIFFNESS VARIATION - *MODEL IV*

Response Parameter		A1			A2		
		$K_{\theta i}$; N·m/rad			$K_{\theta i}$; N·m/rad		
		7500	9884	12000	6250	8350	10500
$\left\|\frac{y_h}{y_o}\right\|$	low	2.100 (1.5)	2.514 (1.7)	3.175 (1.8)	1.549 (1.5)	1.764 (1.6)	1.994 (1.8)
	high	0.3592 (10.3)	0.4975 (10.6)	0.7162 (10.8)	0.1124 (11.8)	0.1397 (12.1)	0.1701 (12.4)
$\left\|\frac{a_{t1}\phi_h}{y_o}\right\|$	low	0.4080 (1.5)	0.4808 (1.6)	0.5355 (1.7)	0.2236 (1.7)	0.2823 (1.7)	0.3557 (1.8)
	high	0.9228 (10.3)	0.9140 (10.6)	1.000 (10.8)	0.3162 (11.9)	0.3306 (12.2)	0.3464 (12.4)

TABLE 4.16

Bounce and Pitch Transmissibility Response Peak

Amplitudes due to TRACK TENSION VARIATION - *MODEL IV*

Response Parameter		*MODEL II*			*MODEL IV*		
		μ_w ; N/m			μ_w ; N/m		
		49254.	65672.	82090.	49254.	65672.	82090.
		M113 A1			M113 A1		
$\left\|\frac{y_h}{y_o}\right\|$	low	2.383 (1.8)	2.362 (1.8)	2.344 (1.8)	2.527 (1.7)	2.514 (1.7)	2.502 (1.7)
	high	2.568 (11.4)	1.526 (11.5)	1.036 (11.6)	0.7975 (10.6)	0.4975 (10.6)	0.3833 (10.6)
$\left\|\frac{a_1^{\ddagger}\phi_h}{y_o}\right\|$	low	0.1131 (1.7)	0.1115 (1.7)	0.1101 (1.7)	0.4840 (1.6)	0.4808 (1.6)	0.4778 (1.6)
	high	0.0754 (11.4)	0.0448 (11.5)	0.0305 (11.6)	0.572 (10.5)	0.9140 (10.6)	0.6168 (10.7)
		M113 A2			M113 A2		
$\left\|\frac{y_h}{y_o}\right\|$	low	1.973 (2.2)	1.958 (2.2)	1.944 (2.2)	1.768 (1.6)	1.764 (1.6)	1.760 (1.6)
	high	0.7912 (13.0)	0.5865 (13.2)	0.4247 (13.4)	0.1800 (12.0)	0.1397 (12.1)	0.1189 (12.1)
$\left\|\frac{a_1^{\ddagger}\phi_h}{y_o}\right\|$	low	0.3246 (2.1)	0.3173 (2.1)	0.3032 (2.2)	0.2853 (1.7)	0.2823 (1.7)	0.2794 (1.7)
	high	0.2214 (13.0)	0.1673 (13.2)	0.1235 (13.4)	0.5137 (12.0)	0.3306 (12.2)	0.2439 (12.3)
		M113 A1$\frac{1}{2}$			M113 A1$\frac{1}{2}$		
$\left\|\frac{y_h}{y_o}\right\|$	low	2.051 (2.2)	2.034 (2.2)	2.019 (2.2)	1.933 (1.7)	1.928 (1.7)	1.923 (1.7)
	high	0.8464 (13.2)	0.6431 (13.4)	0.4624 (13.6)	0.2192 (12.2)	0.1627 (12.3)	0.1319 (12.3)
$\left\|\frac{a_1^{\ddagger}\phi_h}{y_o}\right\|$	low	0.3253 (2.1)	0.3129 (2.1)	0.3047 (2.2)	0.3364 (1.8)	0.3330 (1.8)	0.3298 (1.8)
	high	0.2373 (13.2)	0.1839 (13.4)	0.1348 (13.6)	0.5370 (12.2)	0.3385 (12.4)	0.2517 (12.5)

$a_1^{\ddagger} = a_1$ for *MODEL II* ; $a_1^{\ddagger} = a_{t1}$ for *MODEL IV*

for the following track tension parameters:

M113 A1, M113 A2 and M113 $A1\frac{1}{2}$: μ_w = 49.254, 65.672† and 82.090 kN/m

The frequency response characteristics reveal that the track tension has negligible influence on the low frequency hull bounce and pitch peak responses. However, the increase in track tension is quite effective in reducing the peak amplitude corresponding to road wheel resonant frequencies.

4.6.4 Comparison of Frequency Response Characteristics of M113 Vehicle with A1, A2 and $A1\frac{1}{2}$ Suspension Configurations

The frequency response characteristics of the M113 vehicle models with idealized and linkage suspensions are evaluated for nominal A1, A2, and $A1\frac{1}{2}$ vehicle parameters. Hull bounce and pitch response characteristics of the vehicle models incorporating the nonlinearities due to suspension damping, Coulomb friction and bump stops are computed using the local equivalent linearization algorithm. The frequency response characteristics of vehicle models *I* thru *IV* employing A1, A2 and $A1\frac{1}{2}$ running gear parameters are presented in Figures 4.28 thru 4.31, respectively. The peak bounce and pitch transmissibility characteristics are summarized in Table 4.17. A comparison of frequency response characteristics, reveals that the M113 vehicle coupled with A2 suspension provides superior bounce and pitch transmissibility response, while the vehicle coupled with A1 suspension yields relatively high peak bounce and high pitch (linkage suspension only) response corresponding to vehicle bounce frequency. In comparison to the M113 A2, inferior vibration attenuation of $A1\frac{1}{2}$ suspension can be attributed to its stiffer suspension. In the case of M113 A1, inferior suspension performance can be attributed to two factors: (*i*) the damping coefficient of shock

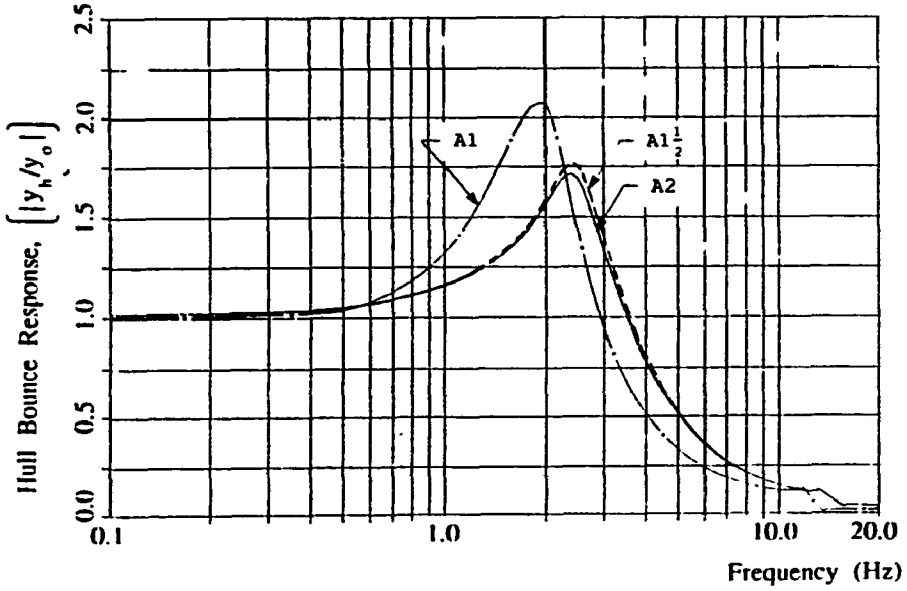

MODEL I

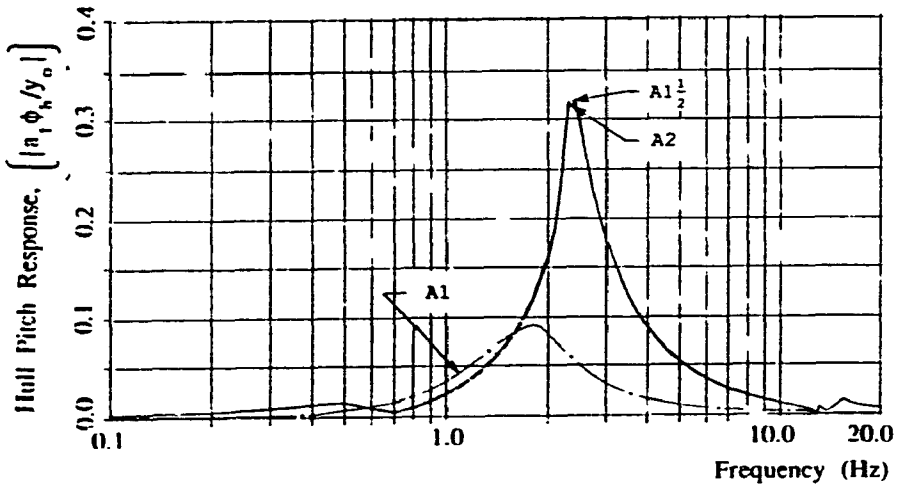

Figure 4.28 Comparison of Transmissibility Response Characteristics of M113 A1, M113 A2 and M113 A1½ Vehicles (*MODEL I*).

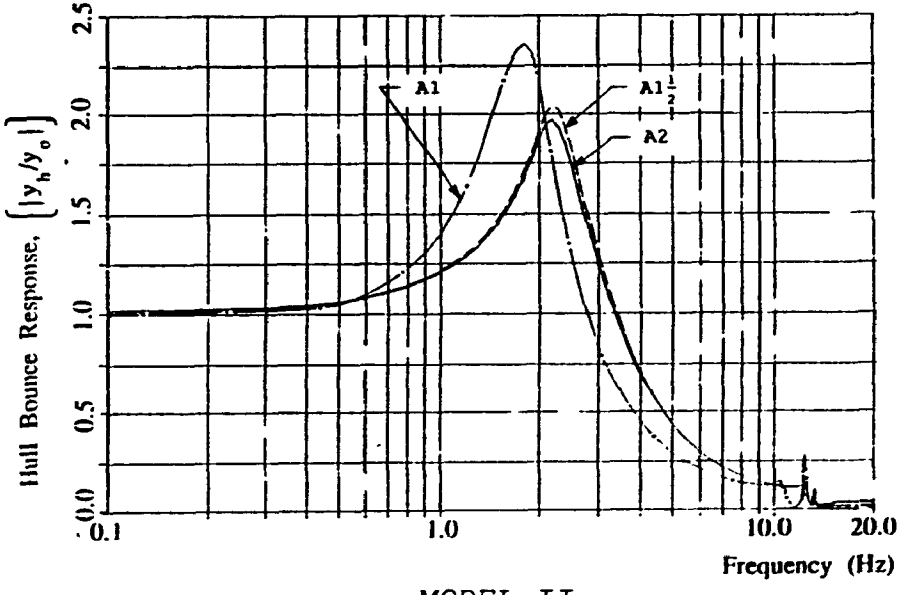

MODEL II

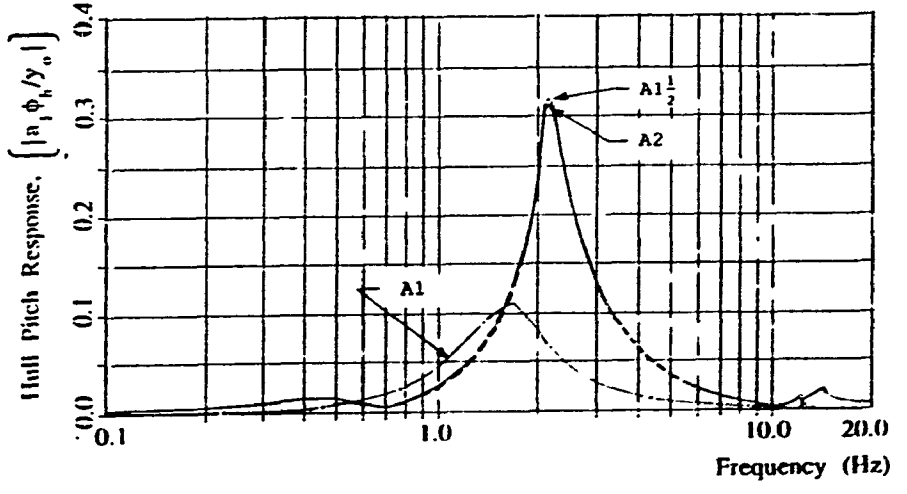

Figure 4.29 Comparison of Transmissibility Response Characteristics of M113 A1, M113 A2 and M113 A1½ Vehicles (*MODEL II*).

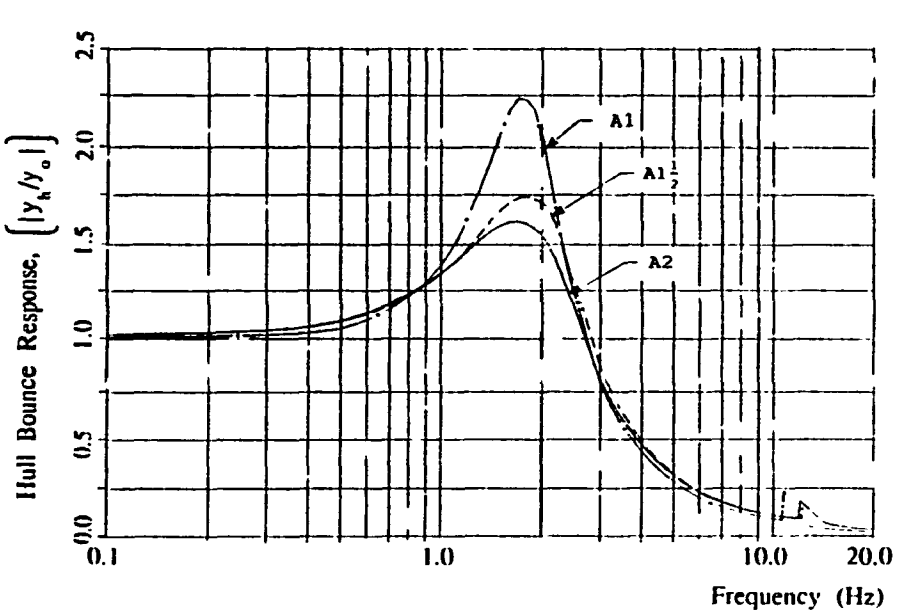

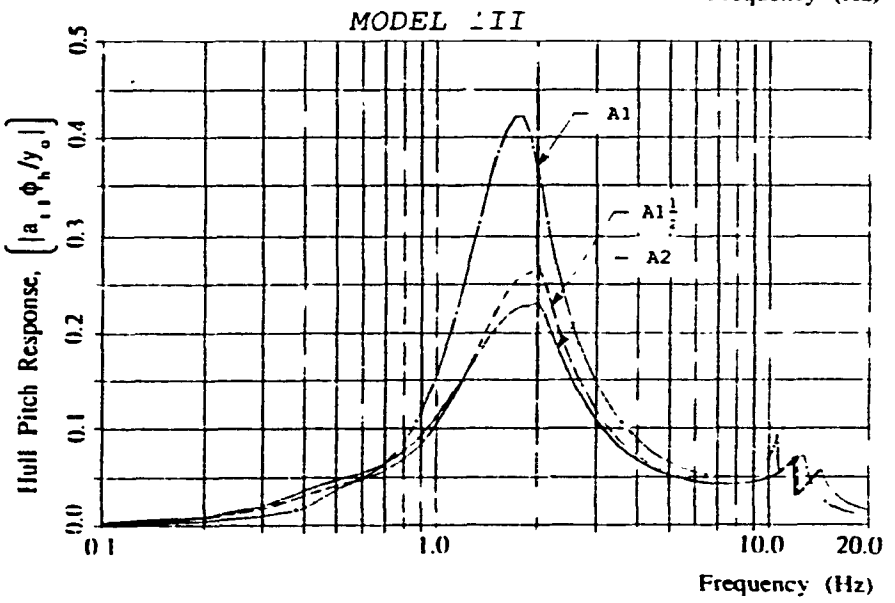

Figure 4.30 Comparison of Transmissibility Response Characteristics of M113 A1, M113 A2 and M113 A1½ Vehicles (*MODEL III*).

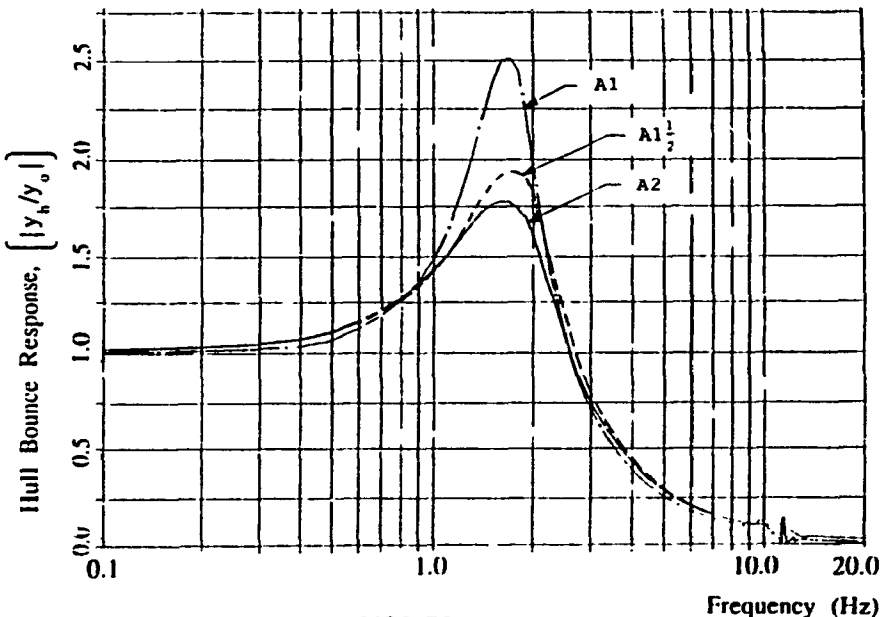

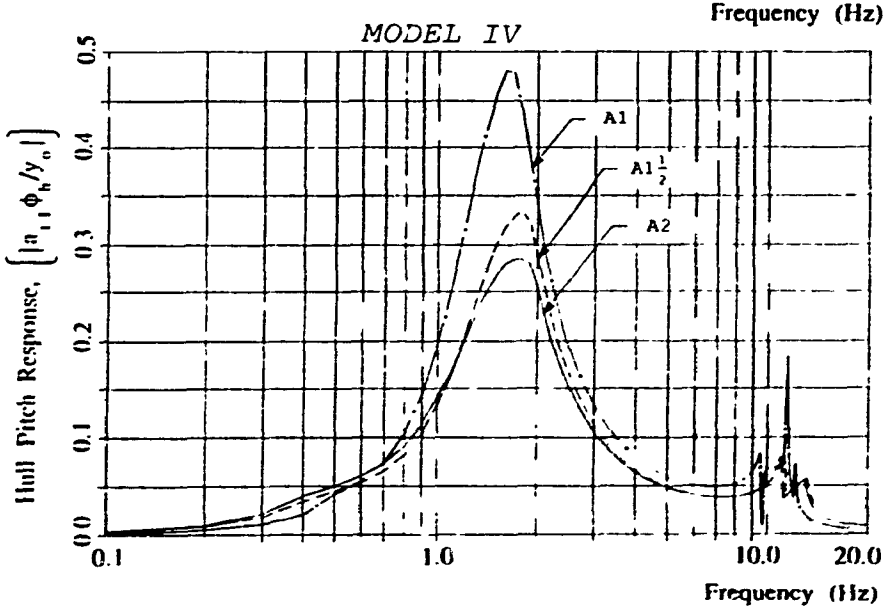

Figure 4.31 Comparison of Transmissibility Response Characteristics of M113 A1, M113 A2 and M113 A1½ Vehicles (*MODEL IV*).

TABLE 4.17

Peak Transmissibility Response Characteristics of the Multi-Wheeled/Tracked M113 A1, M113 A2 and M113 A1½ Vehicles

Vehicle Model	Peak Response Variable	Vehicle Contigurations		
		M113 A1	M113 A2	M113 A1½
MODEL I	$\left\|\frac{y_h}{y_o}\right\|$	2.071 (1.9)	1.701 (2.4)	1.759 (2.4)
	$\left\|\frac{a_1\phi_h}{y_o}\right\|$	0.0916 (1.8)	0.3139 (2.4)	0.3178 (2.4)
MODEL II	$\left\|\frac{y_h}{y_o}\right\|$	2.362 (1.8)	1.958 (2.2)	2.034 (2.2)
	$\left\|\frac{a_1\phi_h}{y_o}\right\|$	0.1115 (1.7)	0.3113 (2.1)	0.3129 (2.1)
MODEL III	$\left\|\frac{y_h}{y_o}\right\|$	2.236 (1.7)	1.602 (1.7)	1.728 (1.8)
	$\left\|\frac{a_{t1}\phi_h}{y_o}\right\|$	0.4228 (1.8)	0.2291 (2.0)	0.2676 (2.0)
MODEL IV	$\left\|\frac{y_h}{y_o}\right\|$	2.514 (1.7)	1.764 (1.6)	1.928 (1.7)
	$\left\|\frac{a_{t1}\phi_h}{y_o}\right\|$	0.4808 (1.6)	0.2823 (1.7)	0.3330 (1.8)

absorbers used in A1 suspension is considerably lower than those used in the A2 suspension; (*ii*) A1 suspension configuration uses four shock absorbers while the A2 and A1$\frac{1}{2}$ suspensions employ six.

Comparison of the frequency response behaviour further reveals that the addition of the track deteriorates the hull bounce and pitch response, slightly. Since the track tension has very little effect on hull bounce and pitch response, the deterioration of vehicle response due to track can be attributed to track pad stiffness.

4.7 EVALUATION OF VEHICLE RESPONSE TO RANDOM TERRAIN EXCITATIONS

The vehicle ride quality, in general, is assessed in view of frequency contents and amplitude of vehicle response due to random terrain excitations. The dynamic response of the multi-wheeled/tracked vehicle model is thus evaluated for random terrains, discussed in Chapter 3, in order to assess the vehicle ride quality and to determine the vehicle design factors affecting the vehicle ride quality. For linear vehicle models, the spectral density of generalized displacement coordinates is determined from the frequency response characteristics of the vehicle model and spectral density of terrain roughness. The M113 vehicle is subject to multiple inputs arising from the random track-terrain interactions and the power spectral density of the response variables is expressed as [50]:

$$\Phi_d^p(\omega) = \mathrm{Re}\left[\sum_{j=1}^{n}\sum_{k=1}^{n} h_{pj}(j\omega)\cdot h_{pk}^{*}(j\omega)\cdot \Phi_{jk}(\omega)\right] \; ; \; p = 1, \ldots, N \qquad (4.55)$$

where

$\Phi_d^p(\omega)$ = PSD of the 'p'th response variable

$h_{pj}(j\omega)$ = complex frequency response function between 'p'th output and 'j'th input variable

$h_{pk}^{*}(j\omega)$ = complex conjugate of $h_{pj}(j\omega)$

$\mathcal{S}_{jk}(\omega)$ = spectral density of input variables (CSD for 'j≠k', PSD for 'j=k')

N is the number of response variables

n is the number of excitation variables

Re designates the real part.

Equation (4.55) can be rewritten in matrix form as:

$$[\mathcal{S}_d(\omega)] = [\mathcal{H}^*(j\omega)][\mathcal{S}_w(\omega)][\mathcal{H}(j\omega)]^T \qquad (4.56)$$

where

$[\mathcal{S}_d(\omega)]$ = spectral density matrix of response variables

$[\mathcal{S}_w(\omega)]$ = spectral density matrix of input variables

$[\mathcal{H}(j\omega)]^T$ = transpose of $[\mathcal{H}(j\omega)]$

Equation (4.56) represents the power spectral density of the displacement response of the vehicle travelling over an uneven terrain. The power spectral densities of response acceleration can be determined by the relationship:

$$[\mathcal{S}_a(\omega)] = \omega^4[\mathcal{S}_d(\omega)] \qquad (4.57)$$

Response spectral densities of coordinates other than the generalized coordinates can be computed using a transformation matrix [T], defined from the constraint equations:

$$[\mathcal{S}_{dd}(\omega)] = [T]^*[\mathcal{S}_d(\omega)][T]^T \qquad (4.58)$$

where $[\mathcal{S}_{dd}(\omega)]$ is the spectral density matrix of response variables other than the generalized coordinates. The road arm rotation, longitudinal motion of the hull, and vertical and longitudinal accelerations at the driver's and crew's location can be computed from equation (4.58). Equations (4.56) thru (4.58), provide the random ride response of either linear or linearized vehicle models. The nonlinear

multi-wheeled/tracked vehicle models are linearized using the local linearization technique to carry out the ride response evaluation in the convenient frequency domain.

The multi-wheeled/tracked vehicle models are nonlinear due to nonlinear force-velocity characteristics of the shock absorbers, Coulomb damping and bump stops. The excitation amplitude at each discrete frequency is estimated from the rms value of the terrain roughness:

$$\bar{y}_{oi}(\omega_j) = \sqrt{\mathcal{S}_{wii}(\omega_j)\, d\omega} \qquad (4.59)$$

where $\mathcal{S}_{wii}(\omega_j)$ represents the 'i'th diagonal element of $[\mathcal{S}_w(\omega_j)]$. The local equivalent coefficients and thus the frequency response function is computed for the excitation amplitude estimated from equation (4.59), using the local equivalent algorithm discussed in section 4.6.1, and the random response is evaluated using equations (4.56) and (4.58).

4.7.1 Ride Dynamic Response of Multi-Wheeled/Tracked Vehicle to a Class of Random Terrains

The ride dynamic response of multi-wheeled/tracked vehicle models (*Model I-IV*), incorporating nonlinearities due to shock absorber, Coulomb friction and bump stops, is evaluated for excitations arising from Belgian pavé, pasture, plowed field and MVEE random courses. The vertical and pitch acceleration response of the hull c.g. of the multi-wheeled/tracked vehicle, coupled with A1, A2 and A1$\frac{1}{2}$ suspension, is computed assuming a constant forward speed of 15 km/hr. The hull vertical and pitch acceleration response of the multi-wheeled/tracked vehicle models with realistic linkage suspension (*Model III* and *IV*), due to various random courses, is presented in the following subsections.

Response to Belgian Pavé

The power spectral density of the hull bounce and pitch

acceleration response of the multi-wheeled vehicle, traversing on the Belgian pavé, is presented in Figure 4.32. The hull bounce and pitch acceleration response reveal acceleration peaks corresponding to the hull resonant frequencies and its multiples. Hull bounce and pitch acceleration peaks occur in the frequency range 1.-10. Hz, as shown in Figure 4.32. A comparison of the ride dynamic response of the M113 A1, M113 A2 and M113 A1$\frac{1}{2}$ vehicles, reveals that the lightly damped A1 suspension yields high acceleration response in the vicinity of hull bounce and pitch resonant frequencies (1.-1.8 Hz), while the A2 and A1$\frac{1}{2}$ suspensions which provide similar responses, suppress the peak pitch response more effectively. However, the bounce and pitch ride response of the vehicle is deteriorated in the higher frequency range. This can be attributed to the heavily dampeu A2 and A1$\frac{1}{2}$ suspension.

The bounce and pitch acceleration response of the tracked vehicle *Model IV*, is presented in Figure 4.33. Similar to the vehicle without the track (*Model III*), the tracked vehicle exhibits multiples of hull pitch and bounce acceleration peaks in the lower frequency range (1.-10. Hz). Comparison of the A1, A2 and A1$\frac{1}{2}$ vehicle configurations, reveals that M113 A1 vehicle yields higher levels of vibration at the hull c.g. in the vicinity of the hull pitch and bounce natural frequencies, while the M113 A2 and M113 A1$\frac{1}{2}$ vehicles exhibit slightly higher levels of vibration at higher frequencies.

Response to Pasture

The hull bounce and pitch acceleration response PSD of the M113 vehicle with and without the track, traversing on a pasture course, is presented in Figures 4.34 and 4.35. The PSD of bounce and pitch acceleration response due to the relatively rough pasture course is

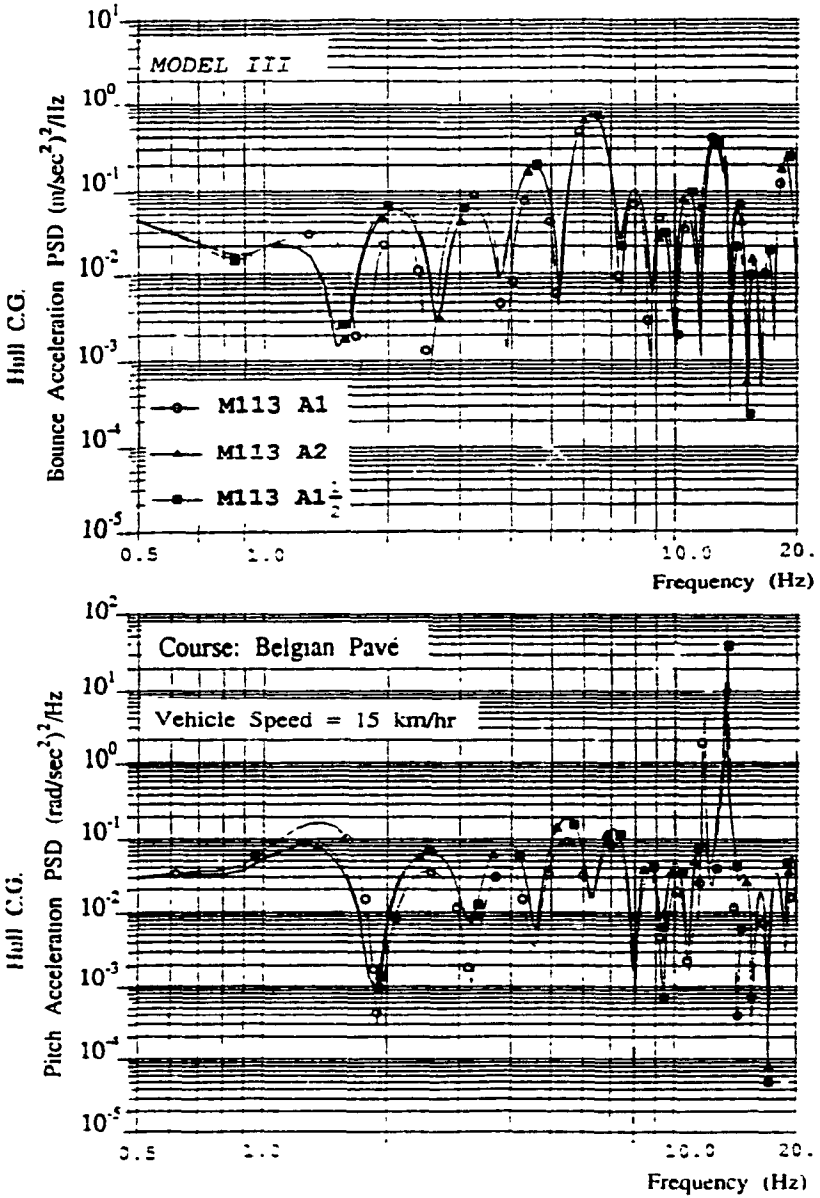

Figure 4.32 PSD of Acceleration Response at the Hull C.G. of Multi-Wheeled M113 Vehicles (*MODEL III*), Traversing Belgian Pavé at Constant Speed.

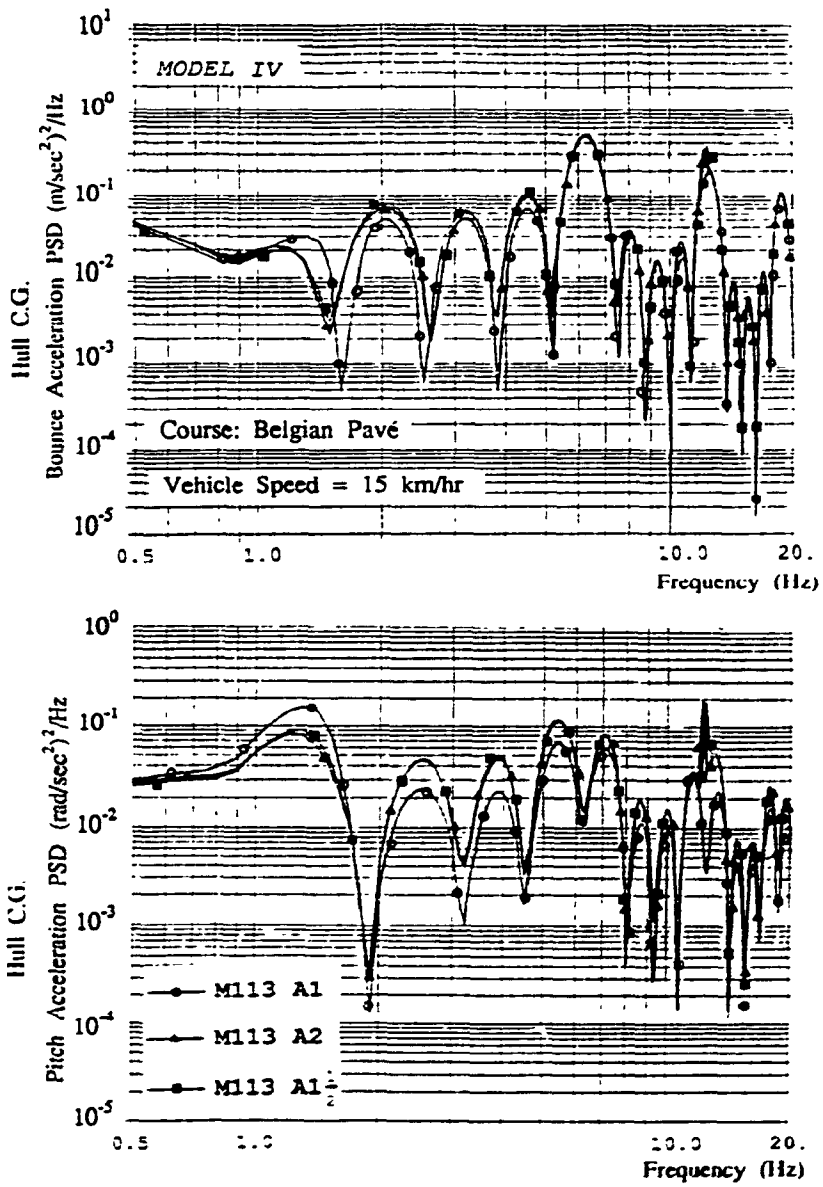

Figure 4.33 PSD of Acceleration Response at the Hull C.G. of Tracked M113 Vehicles (*MODEL IV*), Traversing Belgian Pavé at Constant Speed.

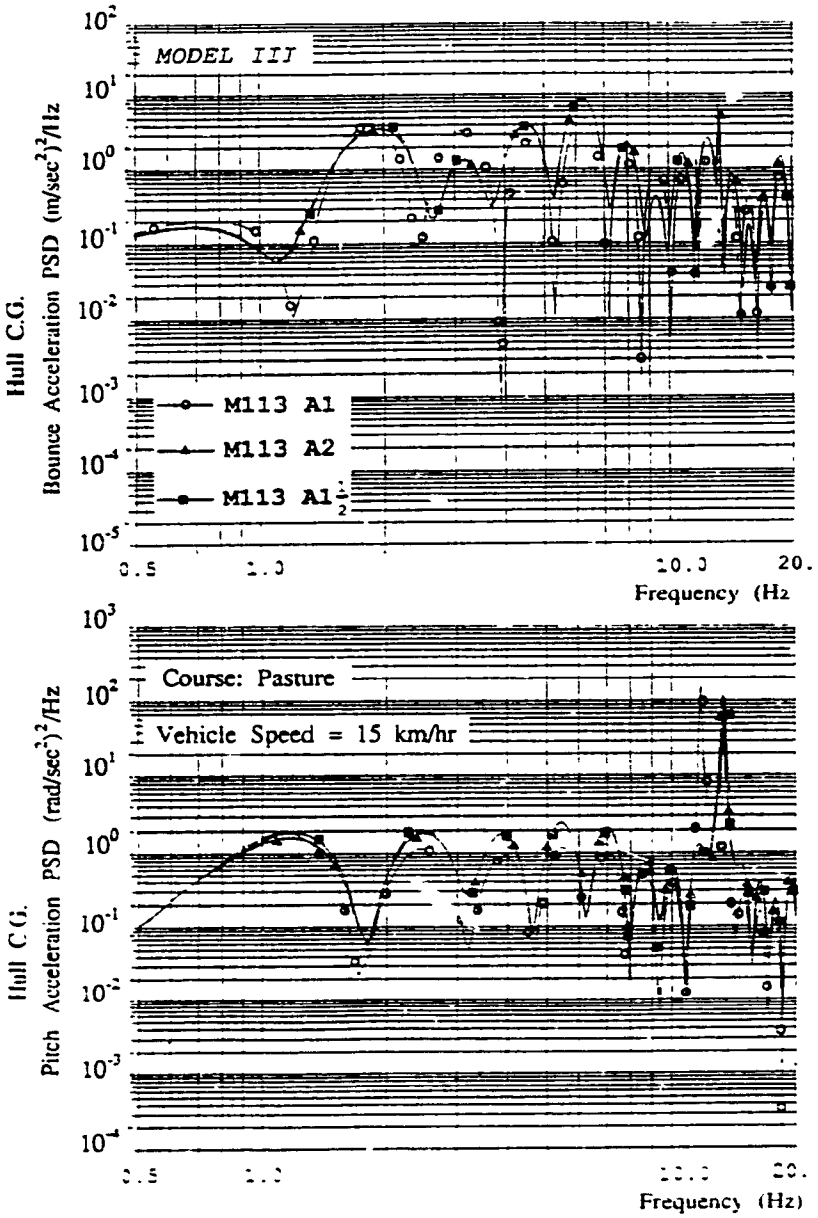

Figure 4.34 PSD of Acceleration Response at the Hull C.G. of Multi-Wheeled M113 Vehicles (*MODEL III*), Traversing Pasture at Constant Speed.

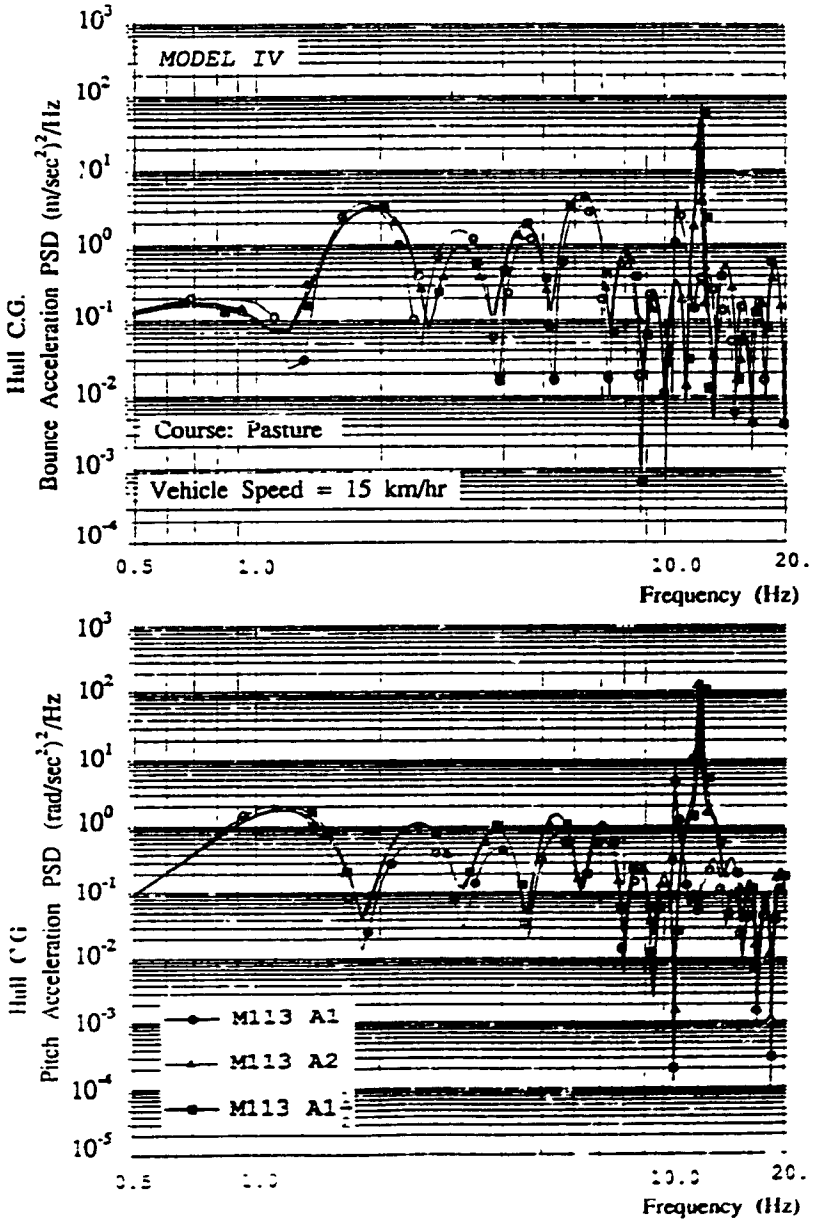

Figure 4.35 PSD of Acceleration Response at the Hull C.G. of Tracked M113 Vehicles (*MODEL IV*), Traversing Pasture at Constant Speed.

considerably larger than those caused by Belgian pave. The ride quality of the M113 vehicle is thus deteriorated considerably when traversing rougher terrains.

Comparison of PSD acceleration response of A1, A2 and A1$\frac{1}{2}$ suspended vehicles, reveals that the M113 A1 with or without a track exhibits higher hull bounce peak acceleration in the low frequency range and lower levels of pitch acceleration over the most part of the frequency range than the M113 A2 and M113 A1$\frac{1}{2}$ vehicles. The multi-wheeled and tracked M113 vehicles exhibit excessive road wheel vibration at high frequency which adversely affect hull bounce and pitch acceleration response. Extremely high peak accelerations at road wheel resonance can be attributed to bump stop contact. Further comparison of the ride response of wheeled and tracked vehicles, due to excitations arising from the pasture course, reveals that the addition of the track reduces the levels of vibration at the hull c.g.

Response to Plowed Field

The hull bounce and pitch acceleration response PSD of the multi-wheeled and tracked vehicles, traversing the plowed field, is presented in Figures 4.36 and 4.37. The ride performance of the multi-wheeled and tracked vehicles due to excitations arising from the extremely rough plowed field is quite similar to that due to the pasture. However, the high roughness values of the plowed field yield extremely high levels of vibration at the hull c.g. The A1 vehicle exhibits higher levels of low frequency bounce vibration than its counterparts, however, pitch response is suppressed more effectively by the A1 suspension. High peak accelerations due to bump stop contact occur in the vicinity of road wheel resonance.

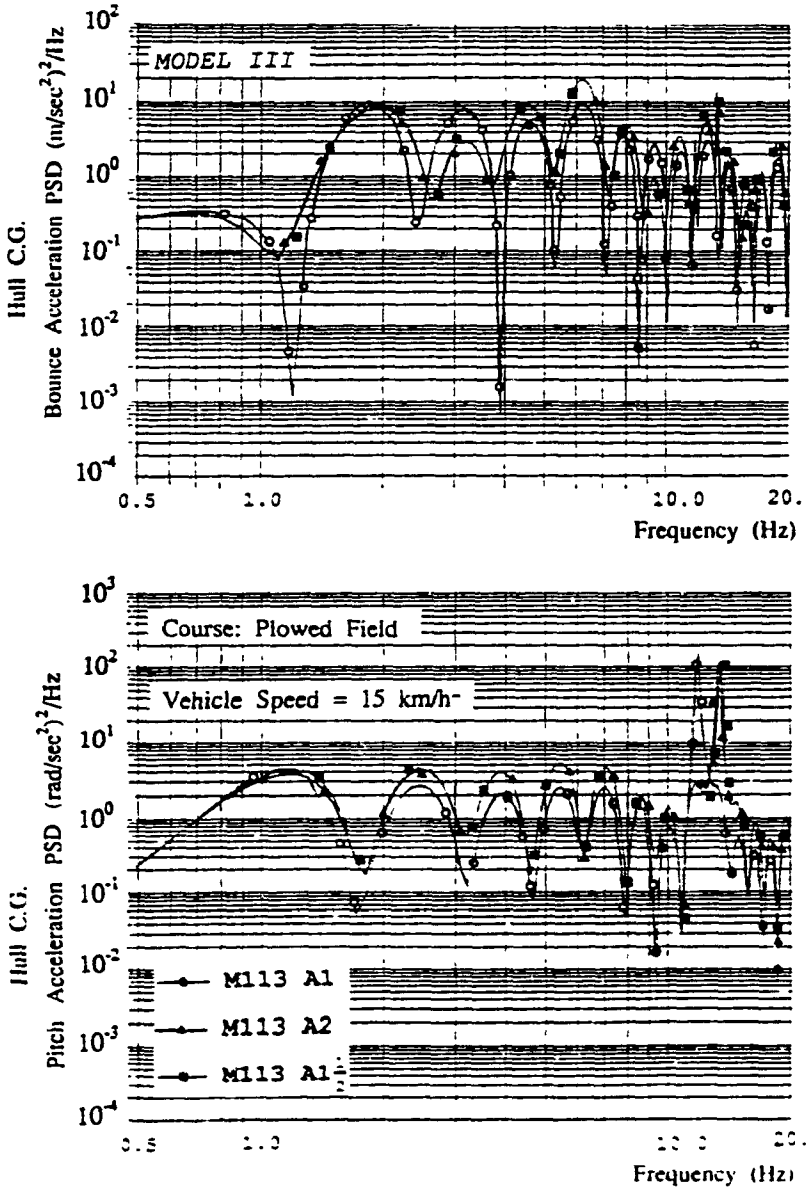

Figure 4.36 PSD of Acceleration Response at the Hull C.G. of Multi-Wheeled M113 Vehicles (*MODEL III*), Traversing Plowed Field at Constant Speed.

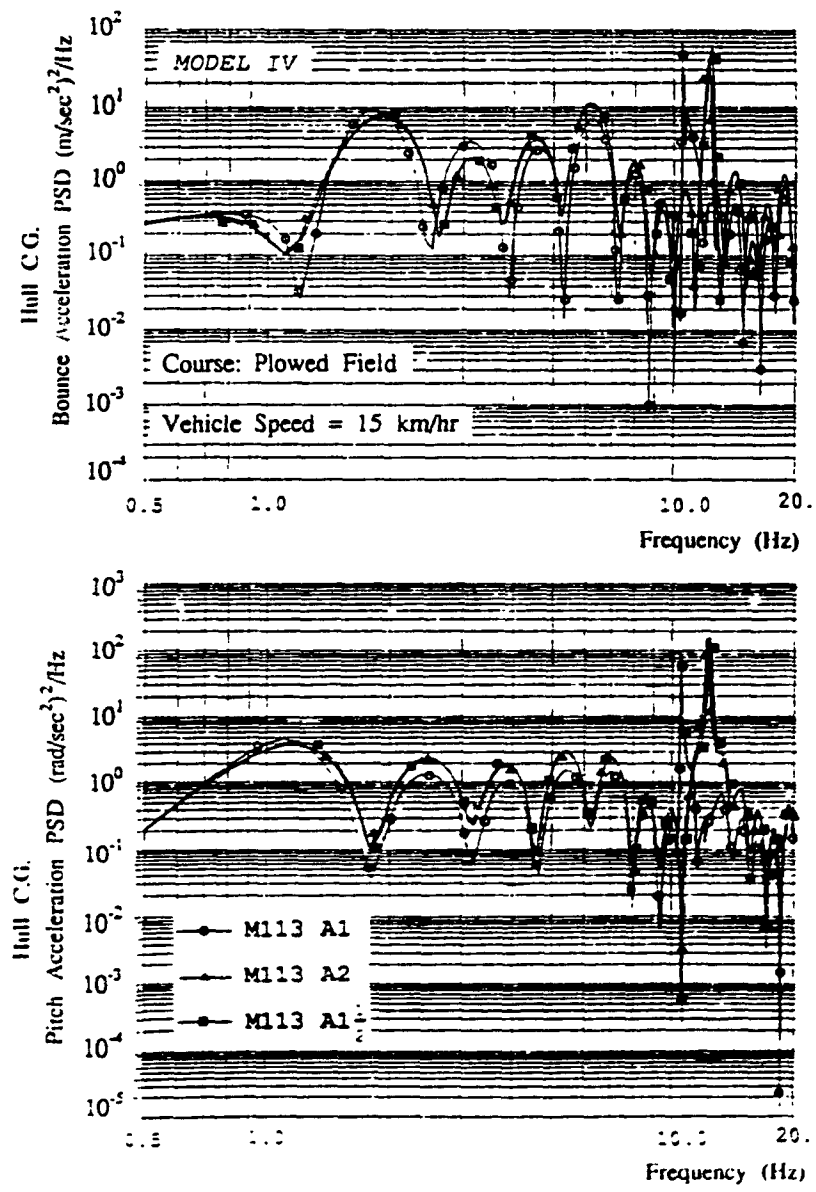

Figure 4.37 PSD of Acceleration Response at the Hull C.G. of Tracked M113 Vehicles (*MODEL IV*), Traversing Plowed Field at Constant Speed.

Response to MVEE Random Course

Figures 4.38 and 4.39 present the PSD of hull bounce and pitch acceleration response of the multi-wheeled and tracked M113 vehicles, traversing the MVEE random course. Hull bounce and pitch acceleration response dominates in the frequency range 1.-10. Hz. The multi-wheeled and tracked M113 A1 vehicles exhibit inferior hull bounce response in the frequency range 1.5-4.0 Hz, while the A1 suspension provides superior hull bounce and pitch response than its counterparts, particularly in the frequency range less than 10. Hz. The acceleration responses reveal large peaks around 11.-14. Hz due to bump stop contact Comparison of the PSD acceleration responses of multi-wheeled and tracked vehicles reveals that the track smoothens the ride response at the selected vehicle speed of 15 km/hr.

4.7.2 Ride Vibration Levels at the Driver's Location

The ride quality of the vehicle is primarily assessed with respect to the vibration levels transmitted at the driver's/passenger's location. The bounce, pitch and horizontal acceleration response at the driver's location is related to the hull bounce and pitch response of the hull through the kinematic constraint equations. The PSD of acceleration response at the driver's location is evaluated using the corresponding transformation matrix $[T_{dr}]$ and eqns. (4.57) and (4.58).

The PSD of acceleration response at the driver's location of the vehicle model without a track (*Model III*) is presented in Figures 4.40 thru 4.43. Vertical acceleration at the driver's location arises from bounce and pitch at the hull c.g., while horizontal acceleration is directly proportional to hull pitch and thus is similar to the hull pitch response. The influence of the suspension configurations and

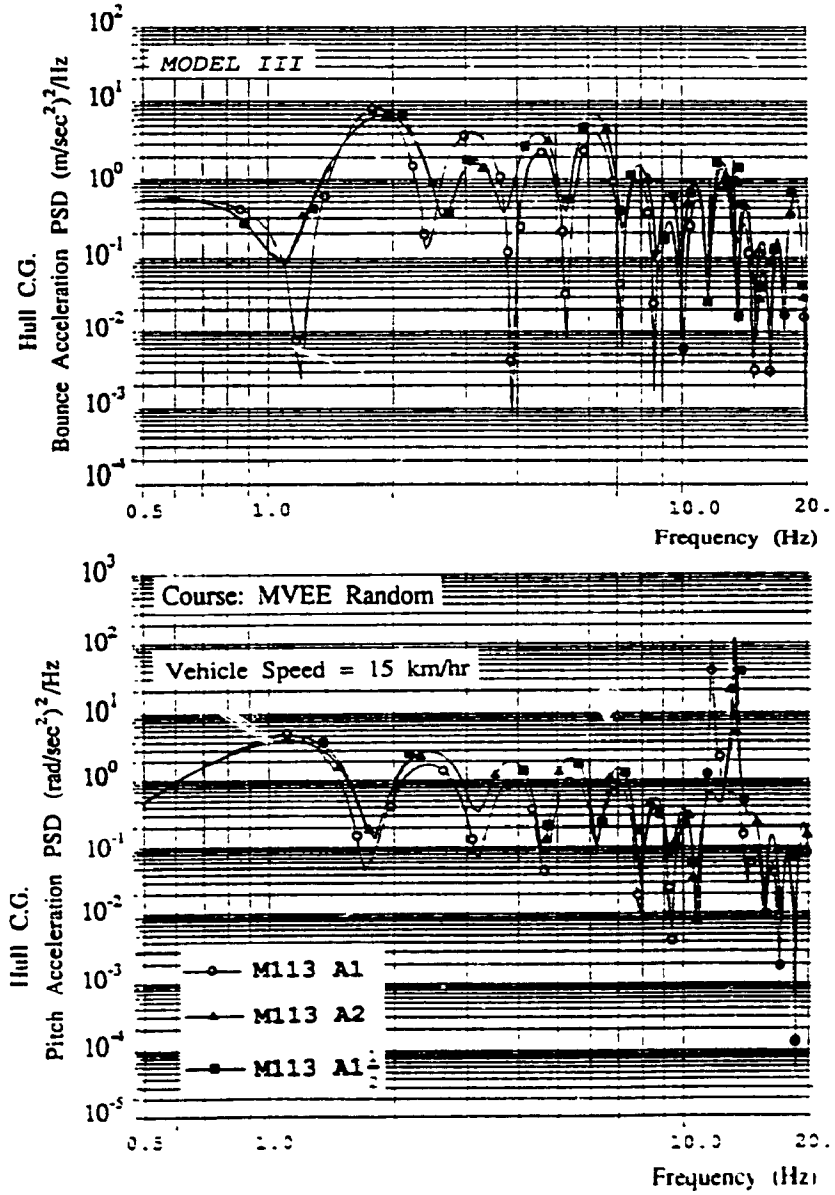

Figure 4.38 PSD of Acceleration Response at the Hull C.G. of Multi-Wheeled M113 Vehicles (*MODEL III*), Traversing MVEE Random Course at Constant Speed.

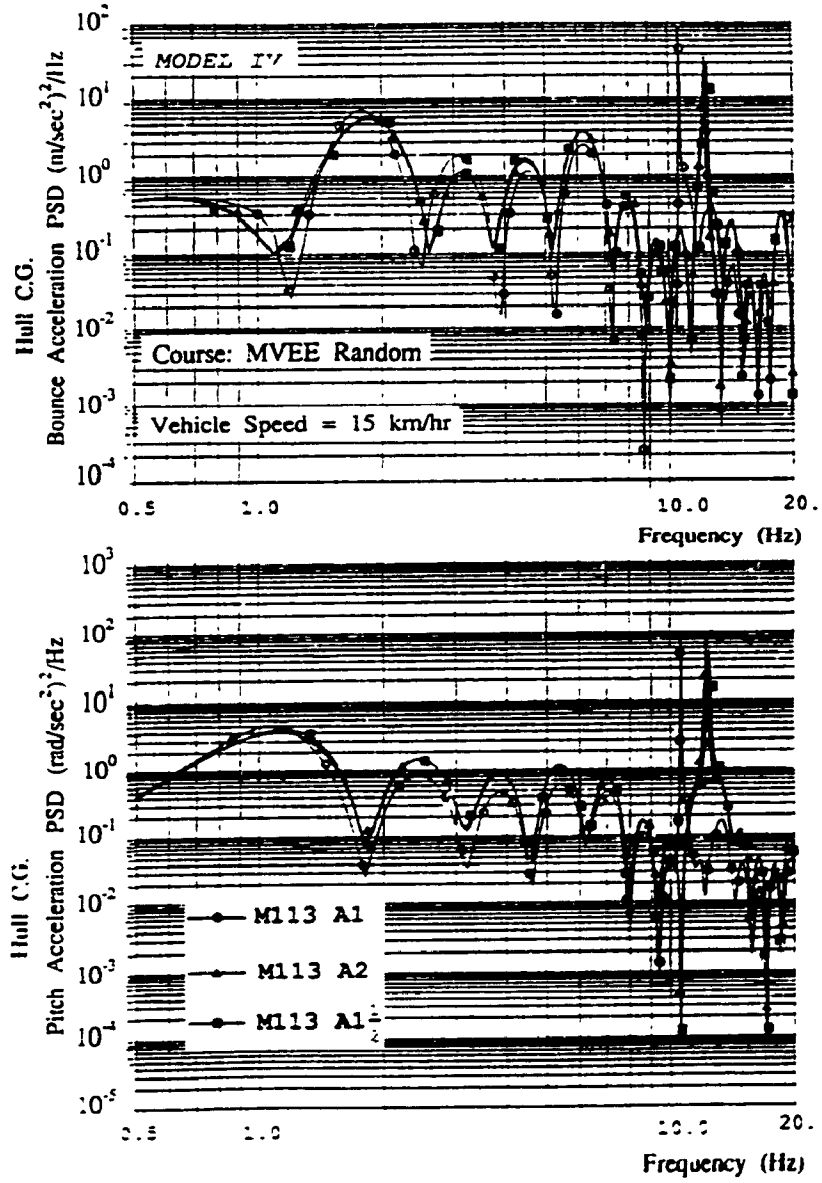

Figure 4.39 PSD of Acceleration Response at the Hull C.G. of the Tracked M113 Vehicles (*MODEL IV*), Traversing MVEE Random Course at Constant Speed.

terrain roughness on the ride vibration levels at the driver's location is illustrated in Figures 4.40 thru 4.43. It can be observed that increase in terrain roughness clearly deteriorates the ride response. The multi-wheeled M113 vehicle, coupled with A1 suspension, provides inferior bounce ride around the low frequencies, however the A1 vehicle yields better horizontal ride response than its counterparts. For the multi-wheeled vehicles traversing the smoother terrain (Figure 4.40), the A1$\frac{1}{2}$ suspension yields excessive bounce acceleration response corresponding to the road wheel resonance.

Figures 4.44 thru 4.47 present the PSD of acceleration response at the driver's location of the tracked vehicle model with trailing arm suspension (*Model IV*), traversing various terrains at constant speed. The tracked vehicles exhibit similar acceleration response as the multi-wheeled vehicles. However, the levels of vibrations at the driver's location are reduced with the addition of the track. The reduction in ride vibration response is considerable when the vehicle is traversing the rougher terrains. It is further observed that the bounce acceleration response around the road wheel resonant frequencies reduces considerably due to addition of the track.

4.8 SUMMARY

In this chapter, analytical techniques to predict the ride performance of the vehicle models are discussed. An eigenvalue analysis is carried out to establish the natural frequencies and principle deflection modes of the vehicle models. Numerical integration is utilized to determine the ride performance of the vehicle models with and without a track, traversing the discrete obstacles. The nonlinear ride dynamics models are expressed by their equivalent linear models to

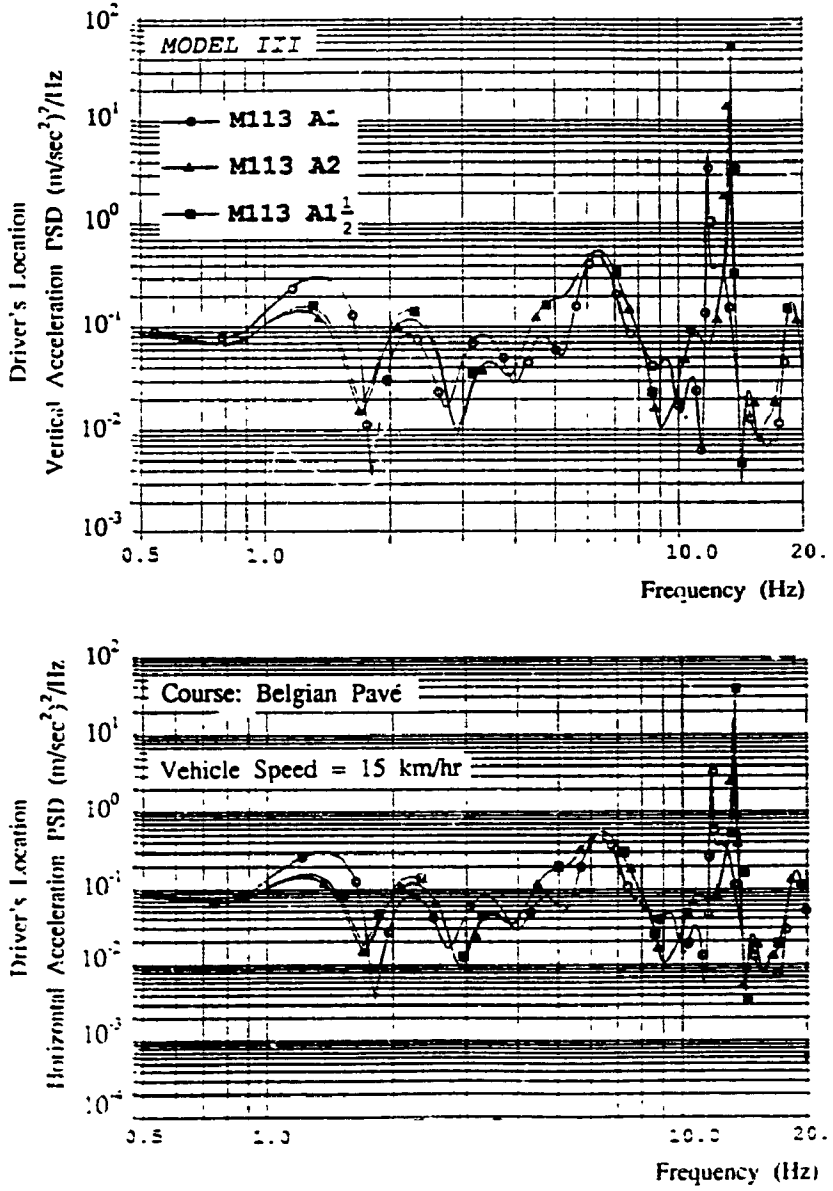

Figure 4.40 PSD of Acceleration Response at the Driver's Location of Multi-Wheeled M113 Vehicles (*MODEL III*). Traversing Belgian Pavé at Constant Speed.

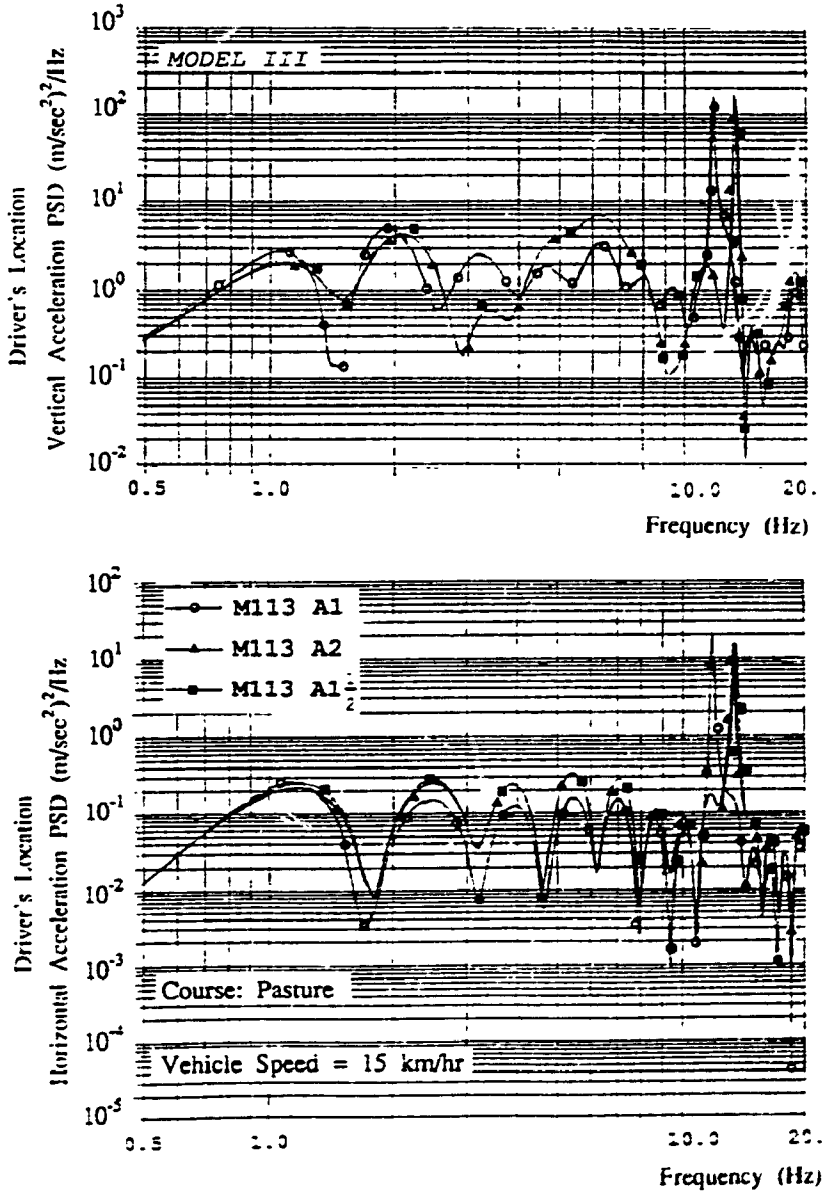

Figure 4.41 PSD of Acceleration Response at the Driver's Location of Multi-Wheeled M113 Vehicles (*MODEL III*), Traversing Pasture at Constant Speed.

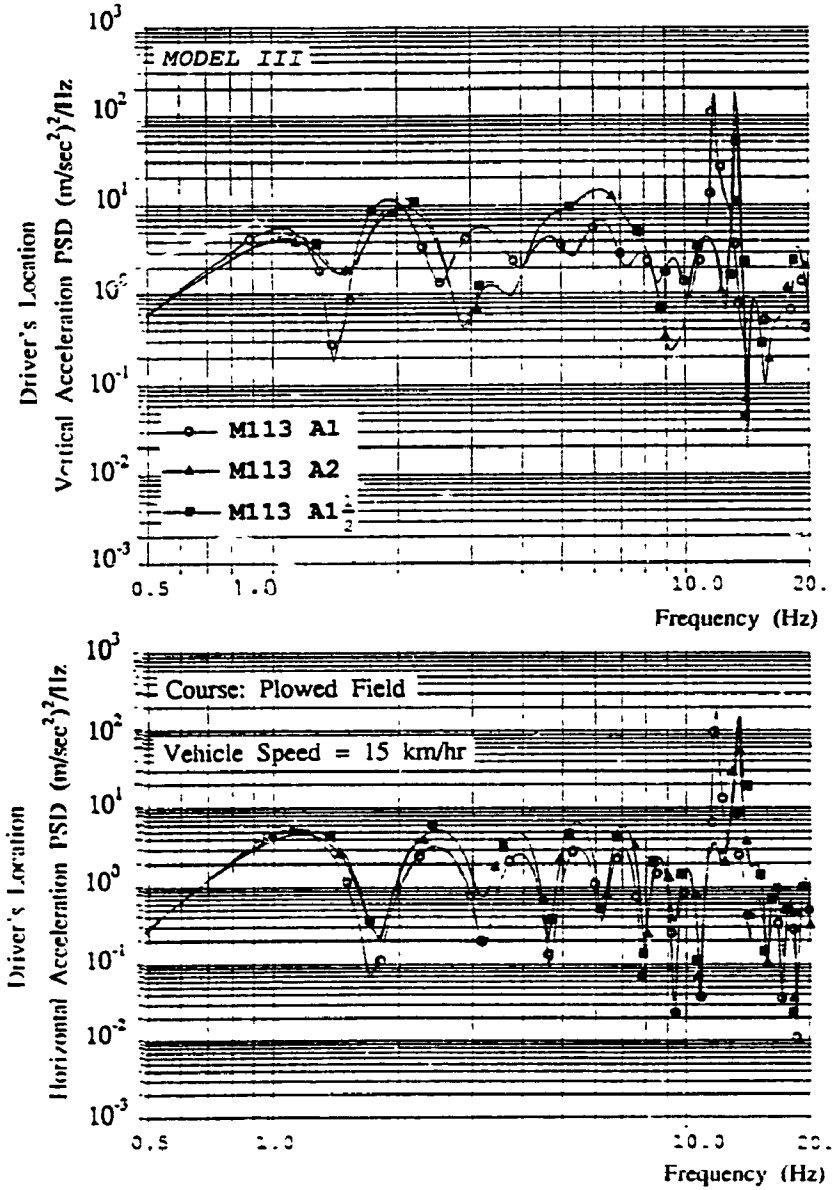

Figure 4.42 PSD of Acceleration Response at the Driver's Location of Multi-Wheeled M113 Vehicles (*MODEL III*), Traversing Plowed Field at Constant Speed.

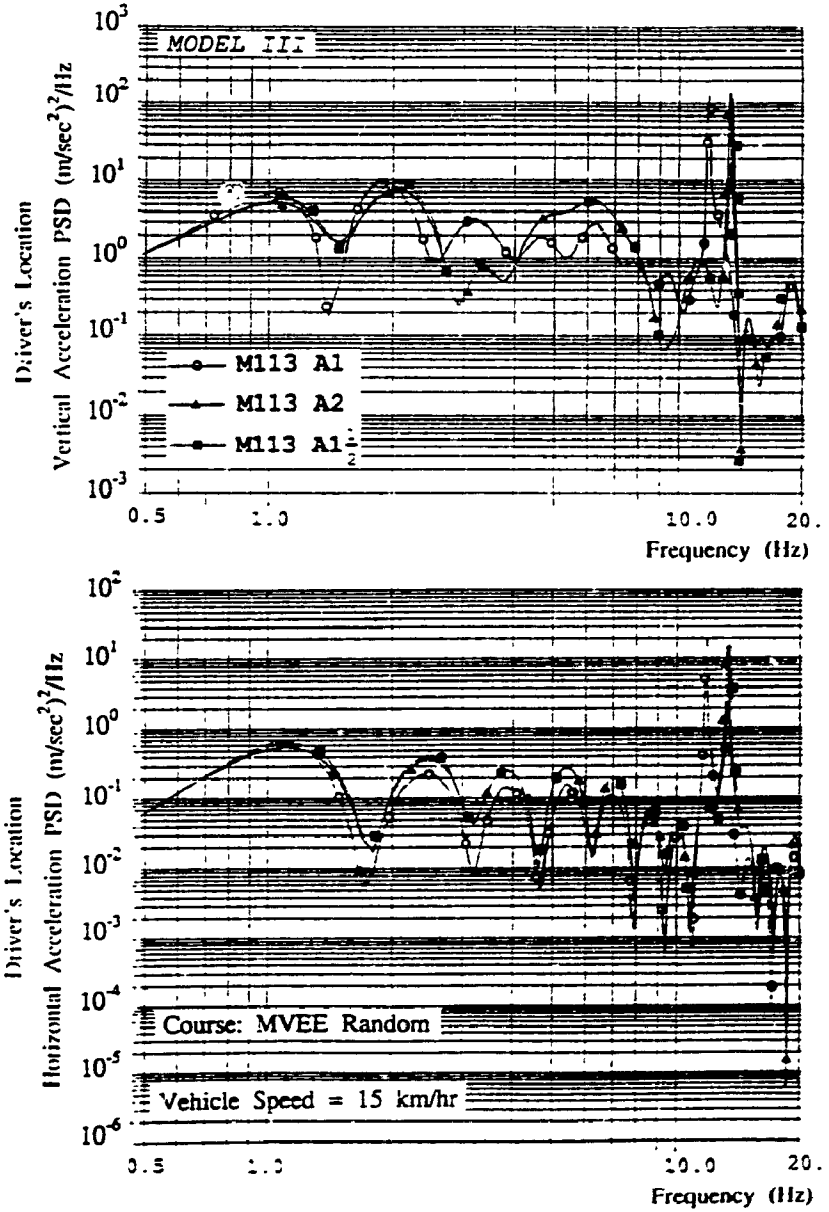

Figure 4.43 PSD of Acceleration Response at the Driver's Location of Mult-Wheeled M113 Vehicles (*MODEL III*), Traversing MVEE Random Course at Constant Speed.

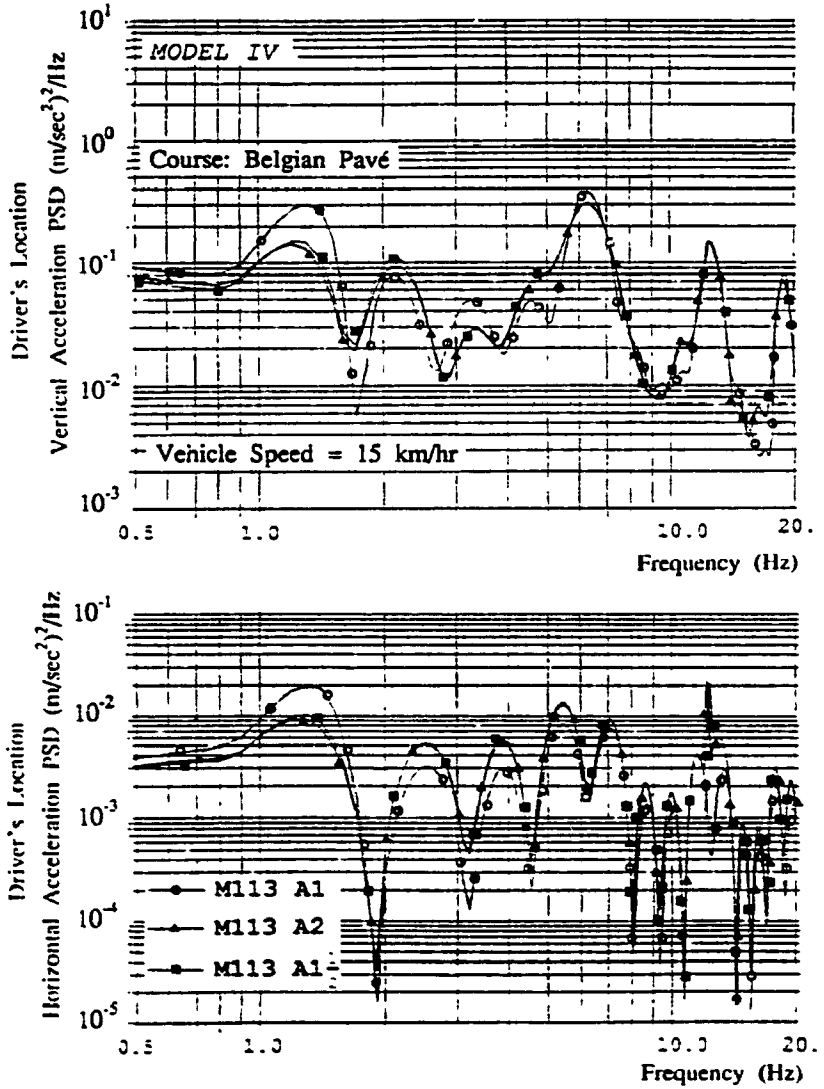

Figure 4.44 PSD of Acceleration Response at the Driver's Location of Tracked M113 Vehicles (*MODEL IV*), Traversing Belgian Pavé at Constant Speed.

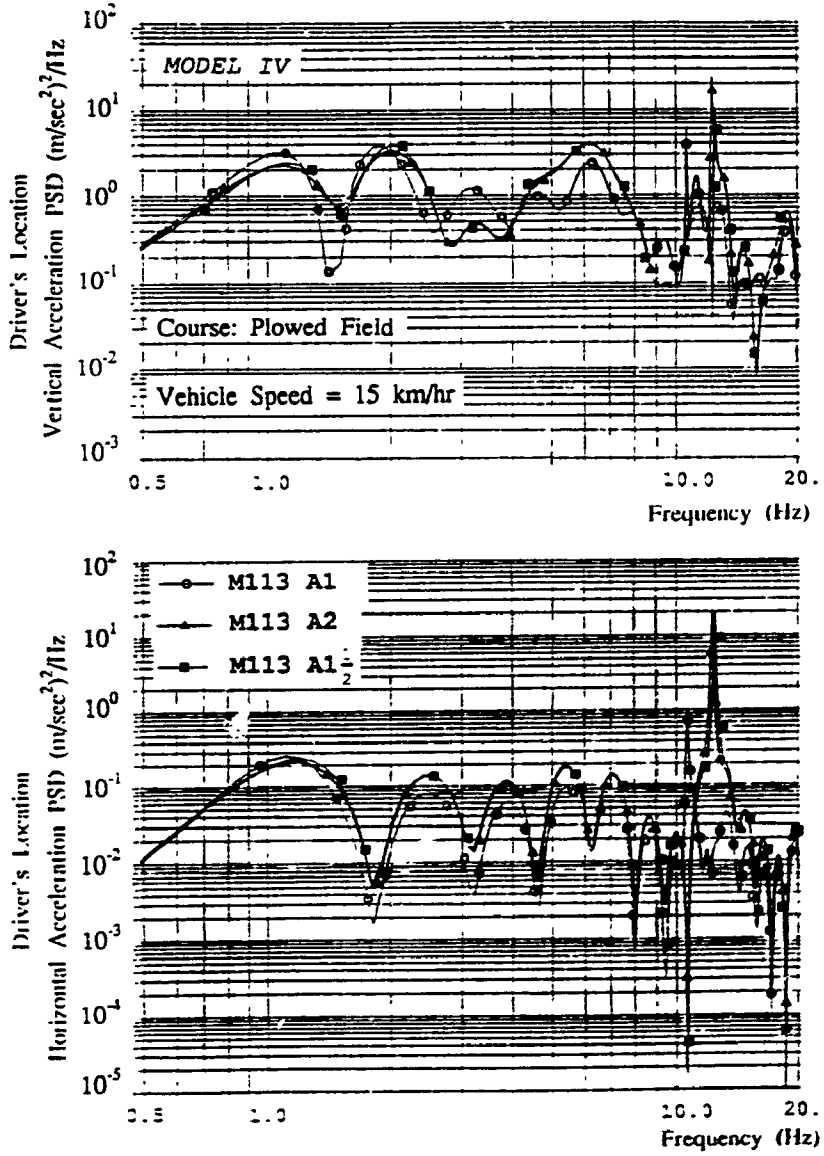

Figure 4.45 PSD of Acceleration Response at the Driver's Location of Tracked M113 Vehicles (*MODEL IV*), Traversing Pasture at Constant Speed.

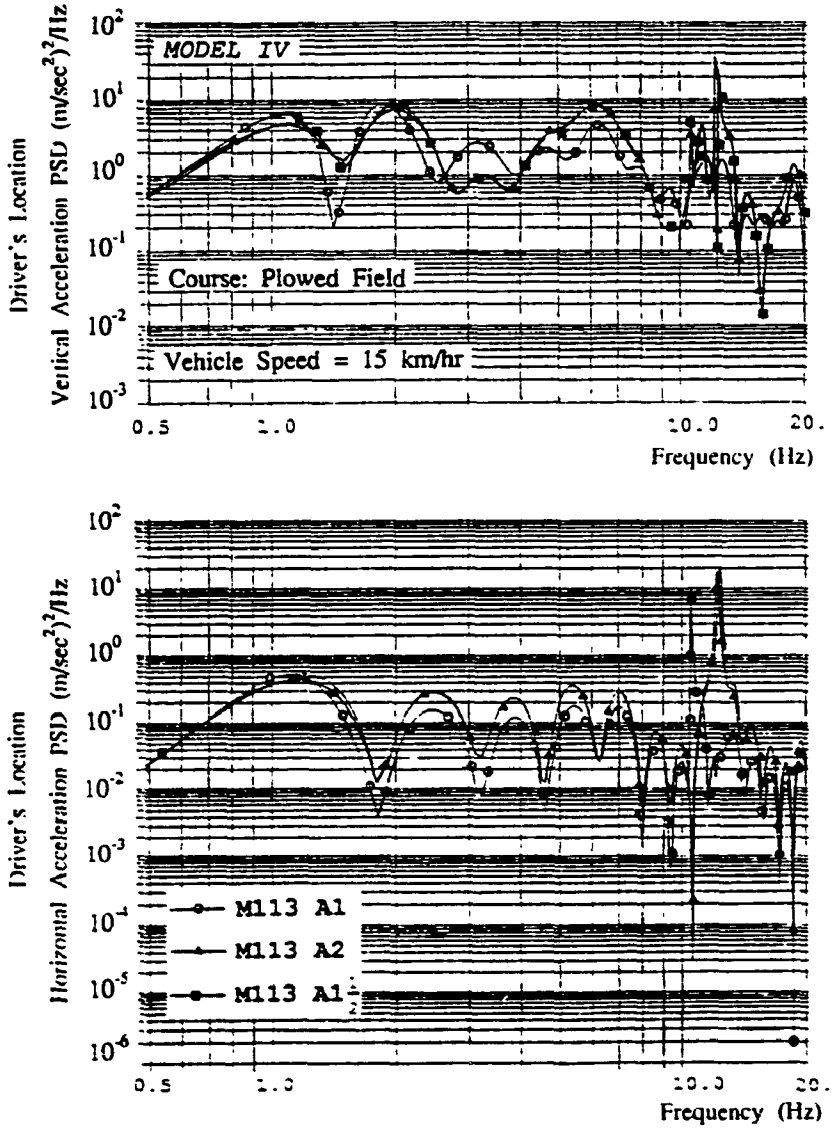

Figure 4.46 PSD of Acceleration Response at the Driver's Location of Tracked M113 Vehicles (*MODEL IV*), Traversing Plowed Field at Constant Speed.

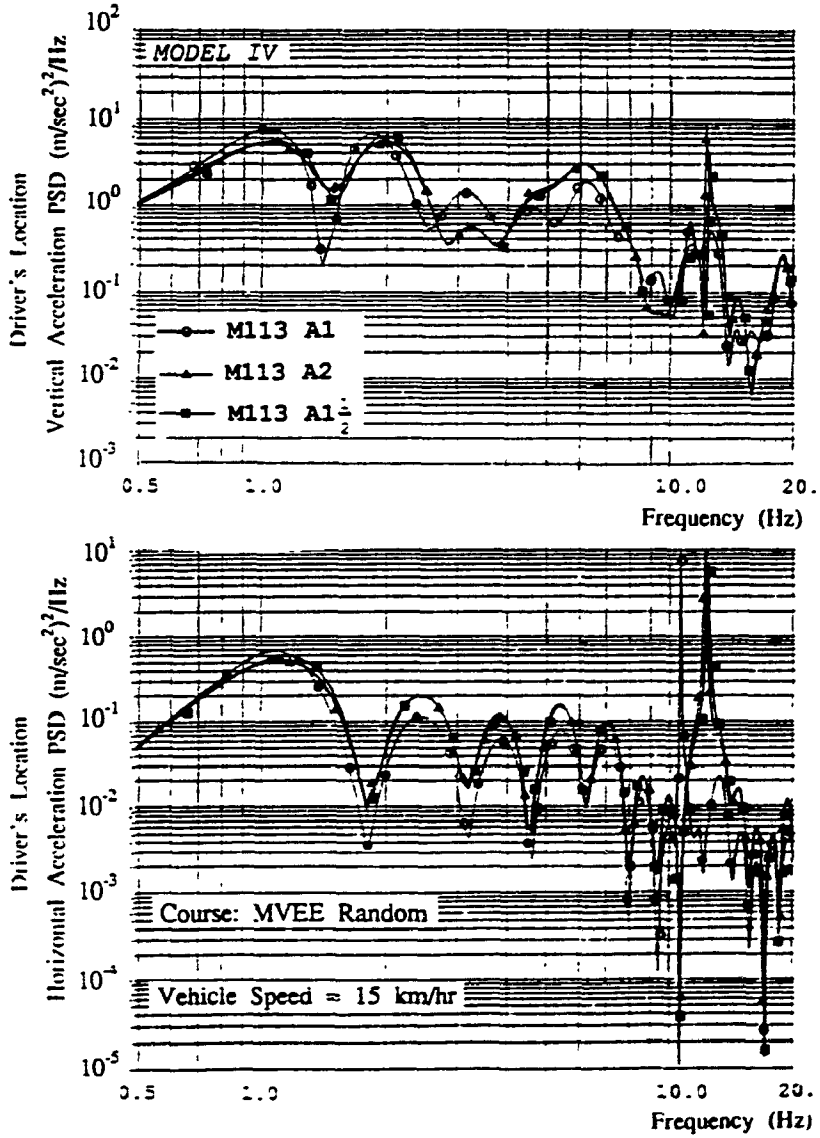

Figure 4.47 PSD of Acceleration Response at the Driver's Location of Tracked M113 Vehicles (*MODEL IV*), Traversing MVEE Random Course at Constant Speed.

carry out the ride analysis in the frequency domain. A local equivalent linearization algorithm is employed to express the nonlinear vehicle model by an array of local equivalent models. The linearization algorithm is validated by comparing the response characteristics of the linearized model to those of the nonlinear vehicle model subjected to harmonic excitations. The frequency response characteristics of the linearized vehicle models with idealized and linkage suspensions are then evaluated via computer simulation. The ride dynamics of the multi-wheeled/tracked vehicle models is investigated for a class of random courses and the ride performance characteristics of M113 vehicles coupled with A1, A2 and A1$\frac{1}{2}$ suspension systems are discussed.

CHAPTER 5

ASSESSMENT OF VEHICLE RIDE QUALITY AND PARAMETRIC SENSITIVITY ANALYSIS

5.1 INTRODUCTION

The ride quality of multi-wheeled and tracked vehicles is strongly related to the vehicle running gear parameters. Assessment of the ride quality requires identification and characterization of the dynamics associated with the vehicle running gear and an acceptable assessment tool. The ride dynamics of a vehicle may be characterized via either field measurements or analytical means. The analytical characterization of vehicle ride dynamics requires adequate representation of the random terrains and ride response evaluation of the realistic vehicle models. Numerous ride quality assessment criteria have been proposed in view of severity of ride vibration levels, dominant ride frequencies and duration of exposure [51].

In this chapter, the ride dynamic response of the M113 vehicle subjected to the non-deformable terrains is assessed using the average absorbed power criterion, widely used for ride quality assessment of military vehicles. The relative ride performance of the M113 A1, M113 A2 and M113 A1$\frac{1}{2}$ vehicle models is assessed by comparing the ride quality at the driver's location. Parametric sensitivity analyses are carried out to arrive at suspension parameters that can provide improved vehicle ride.

5.2 VEHICLE RIDE ASSESSMENT METHODS

Numerous investigations on human response to vehicle vibration have been conducted to establish the acceptable levels of ride vibration for preservation of driver comfort, health and safety, and performance. A number of standards and tolerance criteria have been proposed for

exposure to whole body vibration through subjective and objective evaluations. Subjective methods are often based upon subjective evaluations of vehicle ride comfort on an absolute scale, relative ride ranking of a group of vehicles, operator tolerance in relation to productivity, vibration interference with normal operator control tasks, health aspects to vocational exposure, competitive significance and cost/benefit ratio of potential ride improvements [51]. However, subjective methods have often been misleading due to a multitude of inconsistencies dependent upon age, preferences, and moods of the subject at the time of experiment. Alternatively, objective methods provide an assessment methodology based upon direct measure of physical quantities such as velocity, acceleration, jerk, absorbed power, etc. However, a widely acceptable objective method of ride quality assessment is yet to be established. Objective measures of mean square jerk and acceleration have shown good correlation with the subjective response [49].

Early studies on human response to vehicle vibration have lead to considerable data derived from numerous subject-shake table experiments conducted over the years [52]. Dieckmann [53] established constants related to comfort zones and fatigue time limits for passenger car vibrations. The Dieckmann's constant, k, is expressed by the following relations:

$$\begin{aligned} k &= df^2 \quad ; \quad 0 \le f \le 5 \text{ Hz} \\ k &= 5df \quad ; \quad 5 \le f \le 50 \text{ Hz} \\ k &= 200d \quad ; \quad 50 \le f \le 200 \text{ Hz} \end{aligned} \tag{5.1}$$

where d is the peak displacement amplitude in millimeters and f is the frequency in Hz. The comfort zones are defined as:

k = 0.1-1	:	imperceptible to slightly uncomfortable
k = 1-10	:	slightly disagreeable to disagreeable with a fatigue time of 1 hour
k = 10-100	:	very disagreeable to exceedingly disagreeable with a fatigue time of 1 minute

Janeway [54] recommended exposure limits to vertical vibration in terms of maximum jerk in the frequency range 0-6 Hz, maximum acceleration for middle frequency range 6-20 Hz, and maximum velocity in the high frequency range 20-60 Hz. Janeway recommended limits, J, are expressed by the formulae:

$$\begin{aligned} J &= 1/6\ df^3 \quad ; \quad \text{for f=1-6 Hz} \\ J &= df^2 \quad ; \quad \text{for f=6-20 Hz} \\ J &= 20\ df \quad ; \quad \text{for f=20-60 Hz} \end{aligned} \tag{5.2}$$

where d is the peak displacement amplitude in inches. The Janeway safe limits of vibration, which are based on research survey of subjective tolerance data, represent an attempt to set a level at which no discomfort is experienced by the most sensitive passenger. Goldmann [55] averaged vibration data from several sources and deduced three comfort levels in the vertical mode in terms of acceleration and frequency contents: perceptible, unpleasant, and intolerable. A comparison of the Dieckmann, Janeway and Goldmann limits is shown in Figure 5.1. The studies reveal that the human is most sensitive to vertical vibrations below 20 Hz. Since the above ride assessment criteria have been established for sinusoidal vibrations at a constant frequency, the validity of such methods for vehicle vibrations has been questioned.

Von Eldick Thieme [56] and Butkunas [57] have outlined methods for applying existing comfort criteria (including those mentioned above) to

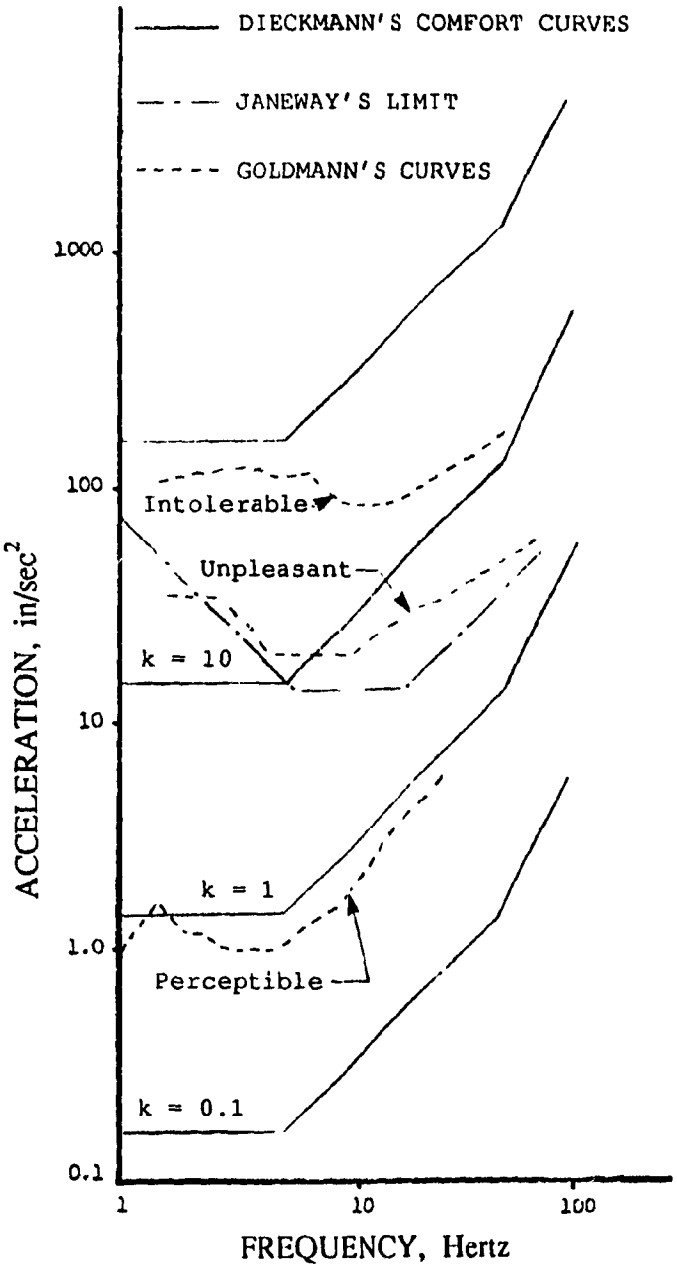

Figure 5.1 Comparison of the Dieckmann, Janeway and Goldmann Ride Comfort Assessment Criteria, [52].

random vibration environment of vehicles. The International Standards Organization (ISO) [58,59] has set forth exposure tolerance in view of preservation of health and safety, proficiency and comfort. The exposure limits are proposed for vertical and horizontal vibrations in terms of rms acceleration as a function of exposure time in the frequency range 1-80 Hz, as shown in Figure 5.2. The exposure limits, proposed in the International Standard (ISO-2631) reveal that the human body is most sensitive to vertical vibrations in the frequency range 4-8 Hz, and to horizontal vibrations in the frequency range 1-2 Hz.

In Germany, the k-factor was proposed as a measure of vibration intensity, based upon subjective assessment [60]. The k-factor can be evaluated in terms of frequency and rms acceleration, velocity or displacement amplitude as follows:

$$k = \alpha \frac{\chi_1}{\sqrt{1 + \left(\frac{f}{f_o}\right)^2}} \tag{5.3}$$

$$k = \nu \frac{\chi_2 f}{\sqrt{1 + \left(\frac{f}{f_o}\right)^2}} \tag{5.4}$$

$$k = \sigma \frac{\chi_3 f^2}{\sqrt{1 + \left(\frac{f}{f_o}\right)^2}} \tag{5.5}$$

where

α = rms acceleration in m/sec^2

ν = rms velocity in mm/sec

σ = rms displacement in mm

and the constants are given as:

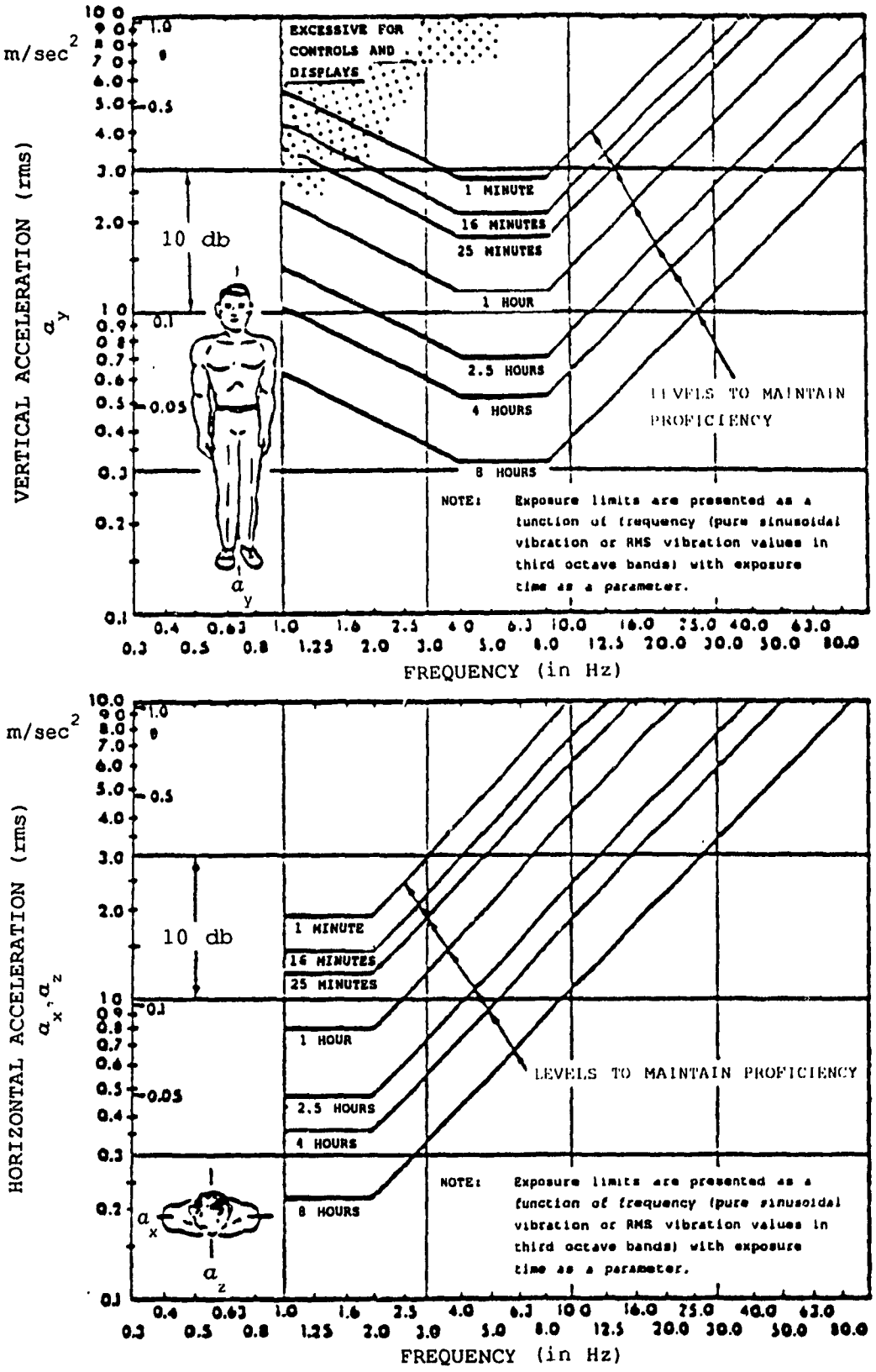

Figure 5.2 ISO *Fatigue Decreased Proficiency* Limits, for Exposure to Vertical and Horizontal Vibrations, [51].

$$f_o = 10 \text{ Hz} \qquad \chi_1 = 18 \frac{k}{m/sec^2}$$

$$\chi_2 = 0.112 \frac{k}{mm/sec^2} \qquad \chi_3 = 0.71 \frac{k}{mm/sec^2}$$

Figure 5.3 presents the acceleration limits associated with the k-factor while Table 5.1 summarizes the relationship between the k values and subjective effects. The k-factor which has been used extensively for agricultural tractors must have a value of 25 or less to be acceptable.

Lee and Pradko [61,62] proposed a scalar quantity called "absorbed power" which is a measure of the average rate of energy dissipated by the complex damped elastic properties of the human anatomy. The average absorbed power is determined from the intensity and frequency of the input vibration as:

$$\bar{P} = \sum_{j=1}^{\eta} \mathcal{K}_j \bar{a}_j^2 \qquad (5.6)$$

where

$\bar{P}$ = average absorbed power in N·m/sec or Watts

$\bar{a}_j$ = rms acceleration at frequency 'J' in m/sec^2

$\mathcal{K}_j$ = absorbed power constant of the body at frequency 'J' in $\frac{N \cdot m/sec}{(m/sec^2)^2}$

η = number of discrete frequencies

For exposure to multi-axes vibrations, ride severity is assessed by the sum of absorbed power associated with each axis of vibrations. Average absorbed power in the range 6-10 W, is considered acceptable for off-road vehicles. The absorbed power criterion is also supported by the Janeway recommended safe limits [54] particularly in the low frequency range, as shown in Figure 5.4. The 2.7 W power curve coincides very closely with the Janeway limit up to about 5 Hz.

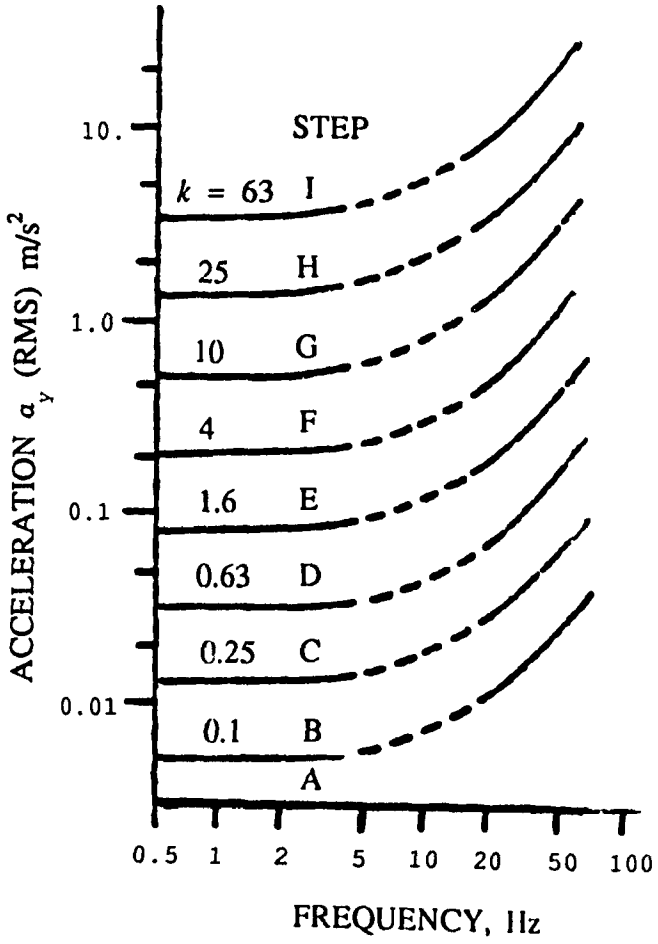

Figure 5.3 Relationship Between German *k*-Factor Values and Subjective Effects, [51].

TABLE 5.1

GERMAN k-FACTOR SUBJECTIVE TOLERANCE CRITERIA

[51]

Observed strength k	step	description of effect
	A	not noticeable
0.1		threshold
	B	
0.25		just noticeable
	C	noticeable
0.63		
	D	easily noticeable
1.6		
	E	strongly noticeable
4		
	F	
10		
	G	very strongly noticeable
25		
	H	
63		
	J	

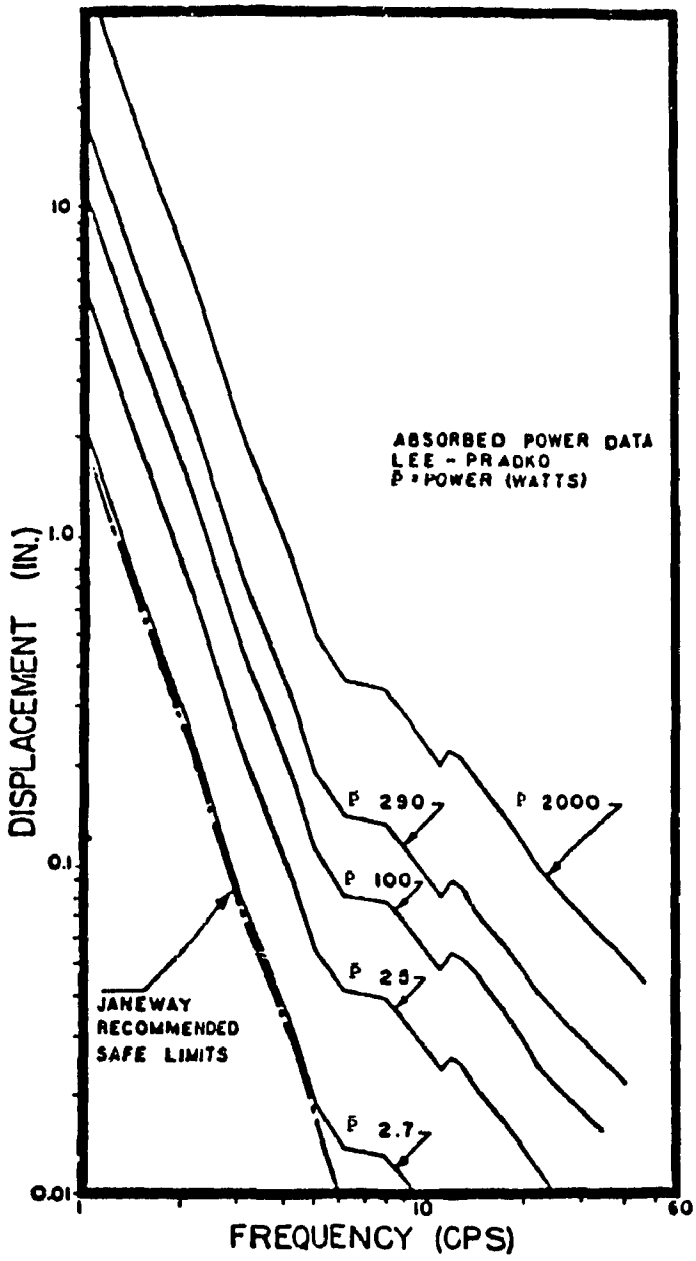

Figure 5.4 Comparison of the Lee-Pradko Absorbed Power Data with the Janeway Recommended Safe Limits, [51].

The absorbed power criterion has been extensively used to assess military vehicle ride. It has been established that subjects were better able to distinguish severe random vibration levels with increasing absorbed power than with the increasing rms acceleration input [51]. Furthermore, the implementation of absorbed power is extremely convenient, and it provides a single number rating of the ride environment, which is a function of the vibratory modes, intensities, frequency contents, body orientation, posture, etc. In view of the above, the ride dynamics of the M113 vehicle models is assessed using average absorbed power method.

5.3 COMPUTATION OF AVERAGE ABSORBED POWER

The ride dynamics of the M113 vehicle models are assessed in terms of average absorbed power associated with vertical and horizontal vibrations at the driver's location. The total absorbed power, $\bar{P}_T$ is the sum of powers associated with the vertical and fore-aft vibrations:

$$\bar{P}_T = \sum_{j=1}^{\eta} [K_{yj} \bar{a}_y^2(\omega_j) + K_{xj} \bar{a}_x^2(\omega_j)] \tag{5.7}$$

where, $\bar{a}_y(\omega_j)$ and $\bar{a}_x(\omega_j)$ are rms vertical and horizontal accelerations at the driver's location, corresponding to frequency ω_j, given by:

$$\bar{a}_y(\omega_j) = \left[\int_{\omega_L}^{\omega_U} (\omega_j)^4 \Delta_d^y(\omega_j) d\omega \right]^{\frac{1}{2}} \tag{5.8}$$

$$\bar{a}_x(\omega_j) = \left[\int_{\omega_L}^{\omega_U} (\omega_j)^4 \Delta_d^x(\omega_j) d\omega \right]^{\frac{1}{2}} \tag{5.9}$$

where $\Delta_d^y(\omega_j)$ and $\Delta_d^x(\omega_j)$ are the spectral densities of vertical and horizontal displacement response at the driver's location; ω_U and ω_L are the integration limits around the centre frequency ω_j; and K_{xj} and K_{yj} are constants determined from:

$$K_{xj},\ K_{yj} = \delta K_o K_1 \left[\frac{\mathcal{F}_1 \mathcal{F}_2 - \mathcal{F}_2 \mathcal{F}_3}{\mathcal{F}_3^2 + \omega_j^2 \mathcal{F}_4^2} \right] \qquad (5.10)$$

where $\mathcal{F}_1$, $\mathcal{F}_2$, $\mathcal{F}_3$ and $\mathcal{F}_4$ are determined from the following polynomials in frequency ω_j [61]:

For Vertical Vibrations

$$\mathcal{F}_1 = -0.102 \times 10^{-9}\omega_j^6 + 0.176 \times 10^{-5}\omega_j^4 - 0.446 \times 10^{-2}\omega_j^2 + 1$$

$$\mathcal{F}_2 = 0.129 \times 10^{-7}\omega_j^4 - 0.934 \times 10^{-4}\omega_j^2 + 0.105$$

$$\mathcal{F}_3 = -0.454 \times 10^{-9}\omega_j^6 + 0.377 \times 10^{-5}\omega_j^4 - 0.56 \times 10^{-2}\omega_j^2 + 1$$

$$\mathcal{F}_4 = -0.211 \times 10^{-11}\omega_j^6 + 0.52 \times 10^{-7}\omega_j^4 - 0.18 \times 10^{-3}\omega_j^2 + 0.105$$

$$K_o = 4.354 \ ; \quad K_1 = 1.356$$

$$\delta = 10.764$$

For Horizontal Vibrations

$$\mathcal{F}_1 = 1$$

$$\mathcal{F}_2 = 0.219$$

$$\mathcal{F}_3 = -0.0185\ \omega_j^2 + 1$$

$$\mathcal{F}_4 = -0.619 \times 10^{-3}\ \omega_j^2 + 0.219$$

$$K_o = 4.353 \ ; \quad K_1 = 1.356$$

$$\delta = 10.764$$

5.3.1 Absorbed Power of the Multi-Wheeled/Tracked Vehicle Ride Vibrations

The average absorbed power due to ride vibration levels at the driver's location of the M113 vehicle models with idealized and linkage suspensions traversing various random courses, discussed in the previous

chapters, is computed to assess the vehicle ride quality. Tables 5.2 to 5.5 summarize the averaged absorbed powers of vertical and horizontal ride vibrations at the driver's location in the frequency range 0-10 and 0-20 Hz of the vehicle *Models I-IV* with A1, A2 and $A1\frac{1}{2}$ suspension systems.

The absorbed power of ride vibrations of the wheeled vehicle model with idealized suspension (*Model I*) are summarized in Table 5.2, for random excitations arising from Belgian pavé, pasture, plowed field and MVEE random course. It can be observed that the absorbed power increases considerably with increasing terrain roughness. Significantly high values of absorbed power are obtained for the vehicle travelling on a plowed field as compared to those obtained for the vehicle travelling on a road (Belgian pavé). The relative ride performance characteristics of the A1, A2 and $A1\frac{1}{2}$ suspension systems can be established from the average absorbed power of the ride vibration at the driver's location. The absorbed power of ride vibration of the vehicle travelling at a constant forward speed of 15 km/hr indicates that the A1 suspension yields best ride while the $A1\frac{1}{2}$ and A2 suspension provide poor ride.

The absorbed power of the ride vibrations of the vehicle model with idealized suspension and the track (*Model II*), summarized in Table 5.3, reveal that introduction of the track tends to reduce the average absorbed power considerably. The absorbed power of the ride vibrations of the vehicle model without and with the track (*Model III & IV*) are presented in Tables 5.4 and 5.5, respectively. The absorbed power quantities of the vehicle vibration reveal that the linkage suspension further reduces the absorbed power at the driver's location.

The average absorbed power computed over a wider frequency range

TABLE 5.2

AVERAGE ABSORBED POWER AT DRIVER'S LOCATION

FOR MULTI-WHEELED M113 VEHICLES TRAVERSING VARIOUS TERRAINS

MODEL I

(Speed V = 15 km/hr)

Vehicle Configuration	M113 A1				M113 A2				M113 A1½			
Absorbed Power (Watts)	Vertical		Horizontal		Vertical		Horizontal		Vertical		Horizontal	
Frequency Range / Course	≤ 10 Hz	≤ 20 Hz	≤ 10 Hz	≤ 20 Hz	≤ 10 Hz	≤ 20 Hz	≤ 10 Hz	≤ 20 Hz	≤ 10 Hz	≤ 20 Hz	≤ 10 Hz	≤ 20 Hz
Belgian Pavé	2.159	2.472	0.142	0.143	4.935	5.277	0.174	0.175	4.945	5.287	0.177	0.178
Pasture	30.10	74.65	1.844	1.848	81.18	86.90	4.784	4.792	81.41	87.38	4.858	4.866
Plowed Field	66.02	117.7	4.057	4.065	177.1	188.5	10.68	10.70	177.5	188.7	10.84	10.85
WES Random	31.08	59.42	3.552	3.554	76.28	79.50	7.543	7.547	76.55	79.90	7.683	7.688

TABLE 5.3

AVERAGE ABSORBED POWER AT DRIVER'S LOCATION

FOR TRACKED M113 VEHICLES TRAVERSING VARIOUS TERRAINS

MODEL II

(Speed V = 15 km/hr)

Vehicle Configuration	M113 A1				M113 A2				M113 A1½			
Absorbed Power (Watts)	Vertical		Horizontal		Vertical		Horizontal		Vertical		Horizontal	
Frequency Range / Course	≤ 10 Hz	≤ 20 Hz	≤ 10 Hz	≤ 20 Hz	≤ 10 Hz	≤ 20 Hz	≤ 10 Hz	≤ 20 Hz	≤ 10 Hz	≤ 20 Hz	≤ 10 Hz	≤ 20 Hz
Belgian Pavé	1.415	1.551	0.110	0.111	2.137	2.282	0.138	0.139	2.143	2.288	0.140	0.141
Pasture	16.69	50.46	1.345	1.351	33.49	46.18	3.360	3.369	33.73	47.50	3.417	3.426
Plowed Field	36.02	90.90	2.946	2.955	72.78	96.07	7.427	7.443	73.30	98.20	7.549	7.566
WES Random	17.38	44.31	2.863	2.864	33.17	40.16	5.679	5.684	33.48	40.51	5.799	5.805

TABLE 5.4

AVERAGE ABSORBED POWER AT DRIVER'S LOCATION

FOR MULTI-WHEELED M113 VEHICLES TRAVERSING VARIOUS TERRAINS

MODEL III

(Speed V = 15 km/hr)

Vehicle Configuration	M113 A1				M113 A2				M113 A1½			
Absorbed Power (Watts)	Vertical		Horizontal		Vertical		Horizontal		Vertical		Horizontal	
Frequency Range / Course	≤ 10 Hz	≤ 20 Hz	≤ 10 Hz	≤ 20 Hz	≤ 10 Hz	≤ 20 Hz	≤ 10 Hz	≤ 20 Hz	≤ 10 Hz	≤ 20 Hz	≤ 10 Hz	≤ 20 Hz
Belgian Pavé	1.372	1.961	0.116	0.119	1.748	2.954	0.086	0.091	1.754	3.978	0.091	0.104
Pasture	18.39	39.41	1.529	1.630	28.35	42.23	1.855	1.910	28.60	38.26	1.982	2.035
Plowed Field	40.14	71.53	3.410	3.546	61.69	81.51	4.145	4.225	62.24	77.56	4.435	4.519
WES Random	18.93	32.33	3.269	3.347	26.23	36.19	3.570	3.614	26.69	33.00	3.806	3.900

TABLE 5.5

AVERAGE ABSORBED POWER AT DRIVER'S LOCATION

FOR TRACKED M113 VEHICLES TRAVERSING VARIOUS TERRAINS

MODEL IV

(Speed V = 15 km/hr)

Vehicle Configuration	M113 A1				M113 A2				M113 A1½			
Absorbed Power (Watts)	Vertical		Horizontal		Vertical		Horizontal		Vertical		Horizontal	
Frequency Range / Course	≤ 10 Hz	≤ 20 Hz	≤ 10 Hz	≤ 20 Hz	≤ 10 Hz	≤ 20 Hz	≤ 10 Hz	≤ 20 Hz	≤ 10 Hz	≤ 20 Hz	≤ 10 Hz	≤ 20 Hz
Belgian Pavé	0.938	1.050	0.089	0.090	0.992	1.100	0.066	0.070	0.996	1.100	0.071	0.072
Pasture	10.79	12.14	1.258	1.270	15.61	18.18	1.429	1.490	15.79	17.53	1.559	1.630
Plowed Field	23.17	25.81	2.806	2.850	33.84	39.93	3.178	3.280	34.24	38.82	3.477	3.590
WES Random	11.26	11.82	2.939	2.979	14.88	16.00	3.007	3.040	15.21	16.02	3.330	3.360

(0-20 Hz) is significantly higher than that computed over a lower frequency range (0-10 Hz). This is attributed to the considerable vehicle vibrations corresponding to the road wheel bounce resonances in the frequency range, 10-15 Hz. The A1 suspension, specifically exhibits an extremely high increase, when the absorbed power is summed over a frequency range 0-20 Hz. This considerable increase in absorbed power is attributed to six undamped road wheels, employed in the M113 A1 vehicle. The ride vibration response at the driver-seat interface, however is computed in the frequency range 0.1-10 Hz in view of the fact that the human body is most sensitive to whole body vibrations in the low frequency range (1-8 Hz) [51].

5.4 RIDE QUALITY ASSESSMENT

A comparison of absorbed power associated with the ride response of the vehicle models with idealized and linkage suspension, travelling at constant speed over the different terrains, clearly revealed the significance of the linkage suspension. Thus the further analyses and ride quality assessments are limited to vehicle models with linkage suspension (*III* & *IV*). The ride vibration response at the driver-seat interface is computed in the frequency range 0.1-10 Hz and the ride quality is presented in terms of total absorbed power associated with vertical and horizontal vibrations. The ride quality of M113 vehicle equipped with either A1, A2 or A1$\frac{1}{2}$ suspension system is assessed for various vehicle speeds and terrains of varying roughness.

5.4.1 Ride Quality of M113 Vehicle Model Without the Track (*MODEL III*)

The ride quality of tracked vehicles is strongly related to suspension configuration, force-velocity and force-displacement characteristics of the suspension system and track-terrain interactions.

The ride dynamics of M113 vehicles is investigated to study the influence of suspension system and terrain roughness, while neglecting the interactions of the track. The influence of vehicle speed and suspension parameters on the ride quality of the vehicle traversing on various undeformable terrains is presented in terms of total average absorbed power.

The average absorbed power due to vertical and horizontal vibrations at the driver's seat location in the frequency range 0.1-10 Hz, when the vehicle is traversing the Belgian pavé course, is presented in Table 5.6. The relative ride performance of A1, A2 and $A1\frac{1}{2}$ suspension systems for various vehicle speeds (5-40 km/hr) is summarized in the table. The vehicle suspension parameters affect the vehicle ride quality considerably and there exists an optimal vehicle speed that yields improved vehicle ride. The absorbed power associated with the A1 vehicle suspension exhibits slightly better vertical ride performance in the speed range 5-40 km/hr while the M113 $A1\frac{1}{2}$ vehicle provides slightly inferior ride than its counterparts. The horizontal ride response of A2 suspension is slightly superior to that of the A1 and $A1\frac{1}{2}$ suspension system. All the three suspension systems consistently provide a superior ride around 25 km/hr vehicle speed.

The ride quality of the multi-wheeled M113 vehicle deteriorates considerably when traversing on rougher terrains. The absorbed power associated with horizontal and vertical vibrations at the driver's location increase considerably when the vehicle travels on a pasture course. The total absorbed power associated with M113 A1, M113 A2 and M113 $A1\frac{1}{2}$ vehicle vibrations in the frequency range 0.1-10 Hz is summarized in Table 5.7. In the speed range 5-40 km/hr, the total

TABLE 5.6

RIDE QUALITY OF MULTI-WHEELED M113 VEHICLE MODEL WITH TRAILING ARM SUSPENSION

Course: Belgian Pavé

VEHICLE CONFIGURATION	SPEED km/hr	ABSORBED POWER		
		Vertical	Horizontal	Total
M113 A1	5.	1.239	0.105	1.344
	10.	1.538	0.050	1.588
	15.	1.372	0.116	1.488
	20.	1.106	0.183	1.289
	25.	0.875	0.263	1.138
	30.	1.010	0.383	1.393
	35.	1.386	0.610	1.996
	40.	2.048	0.910	2.958
M113 A2	5.	1.450	0.086	1.536
	10.	1.975	0.061	2.036
	15.	1.748	0.086	1.834
	20.	1.252	0.140	1.392
	25.	0 918	0.233	1.151
	30.	1.082	0.383	1.465
	35.	1.511	0.602	2.113
	40	2.206	0.887	3.093
M113 A1$\frac{1}{2}$	5.	1.479	0.095	1.574
	10.	2.001	0.064	2.065
	15.	1.754	0.091	1.845
	20.	1.266	0.154	1.420
	25.	0.951	0.259	1.210
	30.	1.121	0.430	1.551
	35.	1.577	0.684	2.261
	40.	2.328	1.019	3.347

TABLE 5.7

RIDE QUALITY OF MULTI-WHEELED M113 VEHICLE MODEL WITH TRAILING ARM SUSPENSION

Course: Pasture

VEHICLE CONFIGURATION	SPEED km/hr	ABSORBED POWER		
		Vertical	Horizontal	Total
M113 A1	5.	11.05	0.879	11.929
	10.	16.63	1.026	17.656
	15.	18.39	1.529	19.919
	20.	18.46	2.771	21.231
	25.	19.19	3.892	23.082
	30.	22.30	4.543	26.843
	35.	25.24	4.817	30.057
	40.	29.23	4.71	34.079
M113 A2	5.	17.30	1.204	18.504
	10.	28.85	1.356	30.206
	15.	28.35	1.855	30.205
	20.	22.26	3.231	25.491
	25.	20.17	4.877	25.047
	30.	24.76	6.184	30.944
	35.	32.32	7.034	39.354
	40	41.94	7.489	49.429
M113 A1$\frac{1}{2}$	5.	17.83	1.348	19.178
	10.	29.42	1.454	30.874
	15.	28.60	1.982	30.582
	20.	22.69	3.668	26.358
	25.	20.83	5.680	26.510
	30.	25.40	7.202	32.602
	35.	33.08	8.121	41.201
	40.	42.82	8.555	51.375

absorbed power ranges from 11.9 to 34.1 watts for A1 suspension, 18.5 to 49.5 watts for A2 suspension and 19.1 to 51.4 watts for $A1\frac{1}{2}$ suspension. Inferior ride quality of $A1\frac{1}{2}$ and A2 suspension systems can be attributed to heavily damped road wheel suspension used in the M113 A2 and M113 $A1\frac{1}{2}$ vehicles.

The absorbed power due to ride vibrations of the multi-wheeled M113 vehicle traversing an undeformable plowed field are summarized in Table 5.8. The ride performance of the M113 vehicle due to excitations arising from the plowed field is quite similar to that due to the pasture. However, high roughness values of the plowed field yield extremely high values of absorbed power due to vibrations at the driver's location.

The absorbed power quantities of ride vibrations of the M113 vehicle traversing the MVEE random course are summarized in Table 5.9. The absorbed power quantities of vertical and horizontal vibrations increase rapidly as the vehicle speed is increased. A comparison of ride quality of A1, A2 and $A1\frac{1}{2}$ suspension system reveals that the A1 suspension provides the best vehicle ride, while the ride quality of A2 and $A1\frac{1}{2}$ suspension systems are very similar. A comparison of Tables 5.8 and 5.9 reveals that the absorbed power of the vehicle travelling on the MVEE random course is considerably smaller than that of the vehicle travelling over a plowed field, at low vehicle speeds. However at higher speeds (specifically above 30 km/hr), the absorbed power quantities of the vehicle traversing the MVEE random course are slightly larger.

The above results demonstrate that the absorbed power quantities of vertical and horizontal vibration levels at the driver's location are

TABLE 5.8

RIDE QUALITY OF MULTI-WHEELED M113 VEHICLE MODEL WITH TRAILING ARM SUSPENSION

Course: Plowed Field

VEHICLE CONFIGURATION	SPEED km/hr	ABSORBED POWER		
		Vertical	Horizontal	Total
M113 A1	5.	23.91	1.970	25.881
	10.	35.64	2.292	37.932
	15.	40.14	3.410	43.550
	20.	40.81	6.164	46.974
	25.	42.87	8.605	51.475
	30.	49.35	9.998	59.348
	35.	55.43	10.57	66.000
	40.	63.91	10.62	74.530
M113 A2	5.	37.55	2.632	40.182
	10.	62.54	3.022	65.652
	15.	61.69	4.145	65.835
	20.	48.51	7.179	55.689
	25.	44.33	10.77	55.100
	30.	54.27	13.61	67.880
	35.	70.65	15.45	86.100
	40	91.50	16.43	107.93
M113 A1$\frac{1}{2}$	5.	38.72	2.946	41.666
	10.	63.79	3.242	67.032
	15.	62.24	4.435	66.675
	20.	49.46	8.165	57.625
	25.	45.74	12.56	58.300
	30.	55.61	15.86	71.470
	35.	72.27	17.84	90.110
	40.	93.33	18.78	112.11

TABLE 5.9

RIDE QUALITY OF MULTI-WHEELED M113 VEHICLE MODEL WITH TRAILING ARM SUSPENSION

Course: MVEE Random

VEHICLE CONFIGURATION	SPEED km/hr	ABSORBED POWER		
		Vertical	Horizontal	Total
M113 A1	5.	6.029	0.742	6.771
	10.	13.60	1.455	15.055
	15.	18.93	3.269	22.199
	20.	23.86	7.370	31.230
	25.	30.43	11.59	42.020
	30.	40.84	14.70	55.540
	35.	53.19	16.68	69.870
	40.	68.63	17.80	86.430
M113 A2	5.	8.727	0.951	9.678
	10.	22.41	1.745	24.155
	15.	26.23	3.570	29.800
	20.	25.74	7.940	33.680
	25.	31.80	13.52	45.320
	30.	47.45	18.60	66.050
	35.	69.70	22.59	92.290
	40	97.85	25.46	123.31
M113 A1$\frac{1}{2}$	5.	9.122	1.074	10.196
	10.	22.97	1.892	24.862
	15.	26.69	3.866	30.556
	20.	26.67	9.117	35.787
	25.	33.30	15.85	49.150
	30.	49.42	21.80	71.220
	35.	72.52	26.28	98.800
	40.	101.80	29.35	131.15

strongly related to vehicle speed and the suspension configuration. Figure 5.5 presents the relationship between total absorbed power and the vehicle speed for various terrain excitations. The absorbed power of the ride vibrations of the vehicle *Model III*, equipped with A1 suspension, subjected to excitations arising from Belgian pavé is well below 3.4 watts at vehicle speeds up to 40 km/hr, as shown in Fig. 5.5a. Excitations arising from a plowed field yield high values of absorbed power at low speeds, while the excitations arising from an MVEE random course yield extremely high values of absorbed power at higher speeds. The average absorbed power associated with ride vibration response of the vehicle model (*III*), equipped with A2 and A1$\frac{1}{2}$ suspension systems, is presented in Figs. 5.5b and 5.5c, respectively for various vehicle speeds. The absorbed power quantity is extremely high when the vehicle is traversing the pasture and plowed field at low speeds. The response characteristics reveal that the absorbed power associated with vehicle vibrations can be reduced by operating the vehicle in the speed range 20-25 km/hr.

The PSD of vertical and horizontal acceleration response at the driver's location of the vehicle, equipped with A1 suspension, traversing the Belgian pavé at various speeds (10-25 km/hr) is presented in Fig. 5.6. The response characteristics at 10 km/hr speed reveal high amplitude peaks around 1.2 Hz, 4.2 Hz, 8.4 Hz and 13 Hz. The frequencies corresponding to these response peaks increase as the vehicle speed is increased, as shown in Fig. 5.6a. Although the magnitudes of peak vertical acceleration at the driver's location are quite similar in the frequency range 3-10 Hz, he M113 A1 vehicle travelling at lower speed (10 km/hr) exhibits high value of absorbed

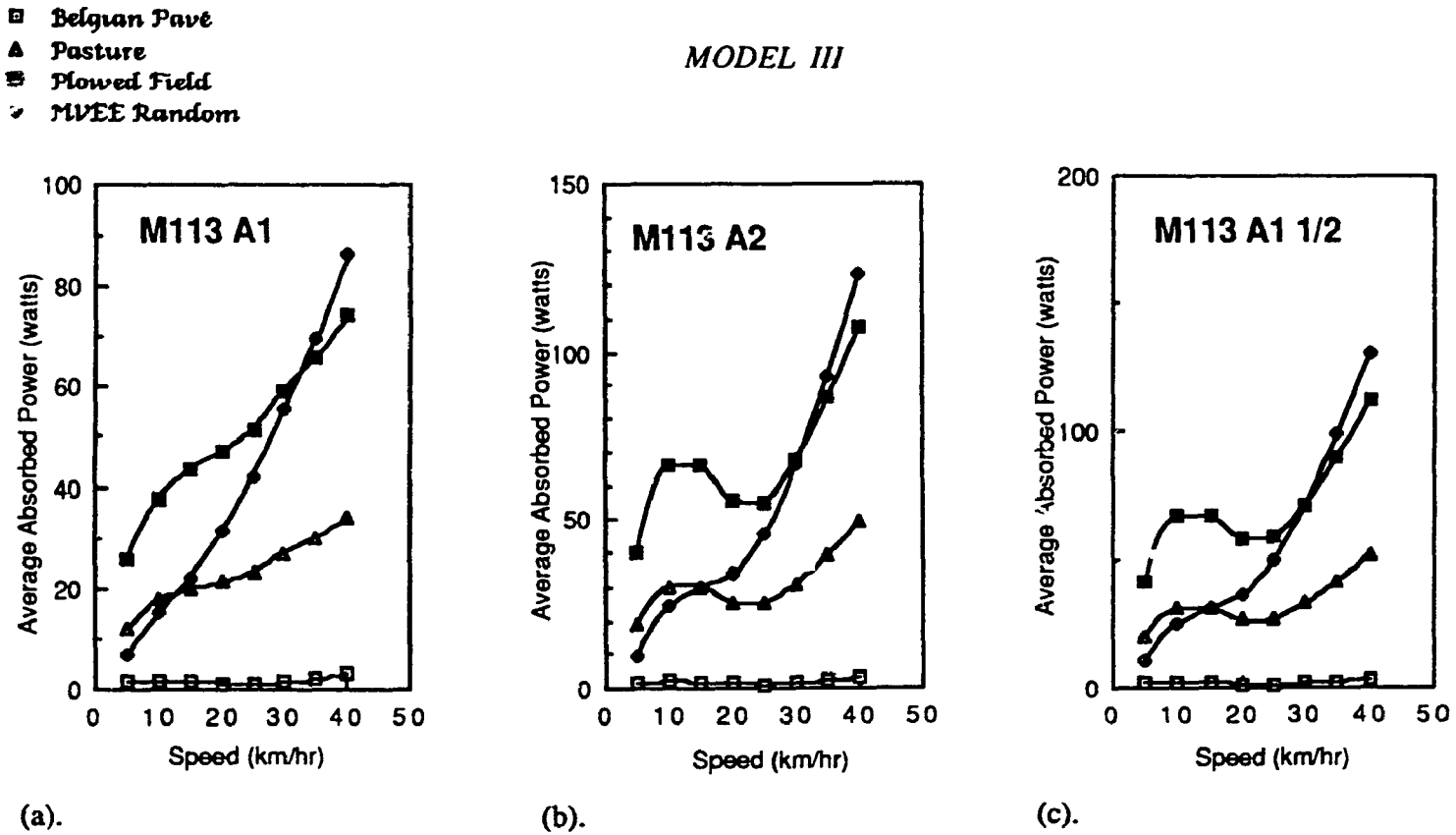

Figure 5.5 Total Average Absorbed Power at the Driver's Location of Multi-Wheeled M113 Vehicles Traversing Various Terrains.

power due to high values of absorbed power constants in the frequency range 3-5 Hz. The ride vibration response of the vehicle equipped with A2 and A1$\frac{1}{2}$ suspension reveals similar behaviour when traversing pasture and plowed fields, as shown in Figures 5.7 and 5.8, respectively. A dip in the absorbed power in the speed range 20-30 km/hr, as shown in Figures 5.5b and 5.5c can be attributed to the low values of absorbed power constants corresponding to the dominant frequencies.

Comparison of ride quality of the vehicle configurations is provided by means of bar graphs, as shown in Figures 5.9 thru 5.12. As summarized in Tables 5.6-5.9, for the random courses considered, the bar graphs clearly demonstrate that the M113 vehicle coupled with an A1 suspension provides a superior ride than the M113 A2 and M113 A1$\frac{1}{2}$. Superior ride performance of the M113 A1 can be attributed to lower damping values of the corresponding shock absorbers in the road wheel suspension system.

5.4.2 Ride Quality of the Tracked M113 Vehicle (*MODEL IV*)

The ride response characteristics of the tracked vehicle model, incorporating track dynamics and linkage suspension, (*Model IV*) are established for A1, A2 and A1$\frac{1}{2}$ suspension parameters. The ride quality of the tracked vehicle traversing the Belgian pavé, pasture, plowed field, and MVEE random course, is assessed in terms of the absorbed power of the vertical and horizontal vibrations at the driver's seat.

The absorbed power of vertical and horizontal vibrations at the seat location and the total absorbed power for the M113 A1, M113 A2 and M113 A1$\frac{1}{2}$ vehicle traversing the Belgian pavé are summarized in Table 5.10, for various vehicle speeds. The absorbed power of vertical vibrations varies only slightly for speeds below 30 km/hr, however, the

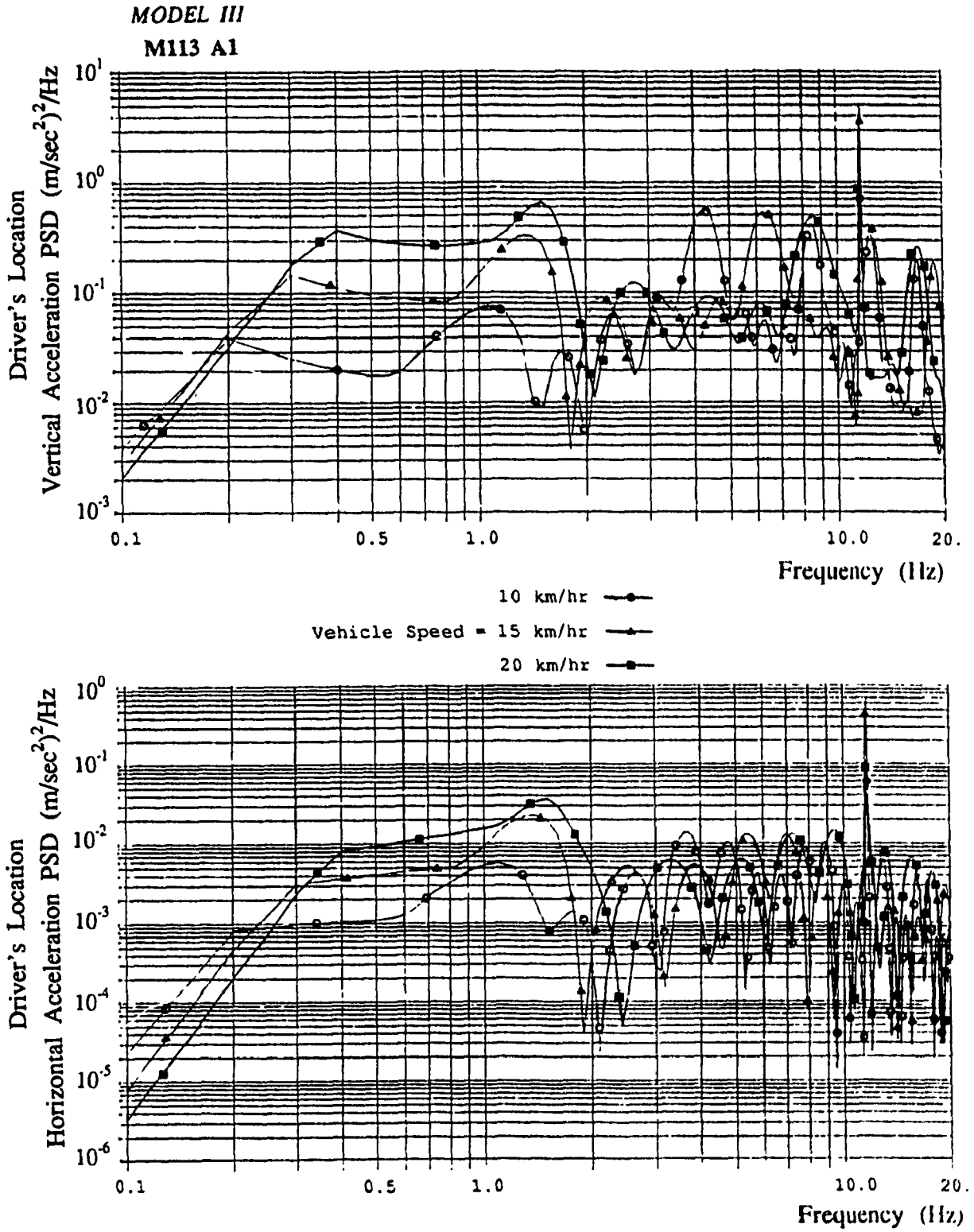

Figure 5.6 PSD of Acceleration Response at the Driver's Location of Multi-Wheeled M113 A1 Vehicle (*MODEL III*), Traversing Belgian Pavé at Various Speeds.

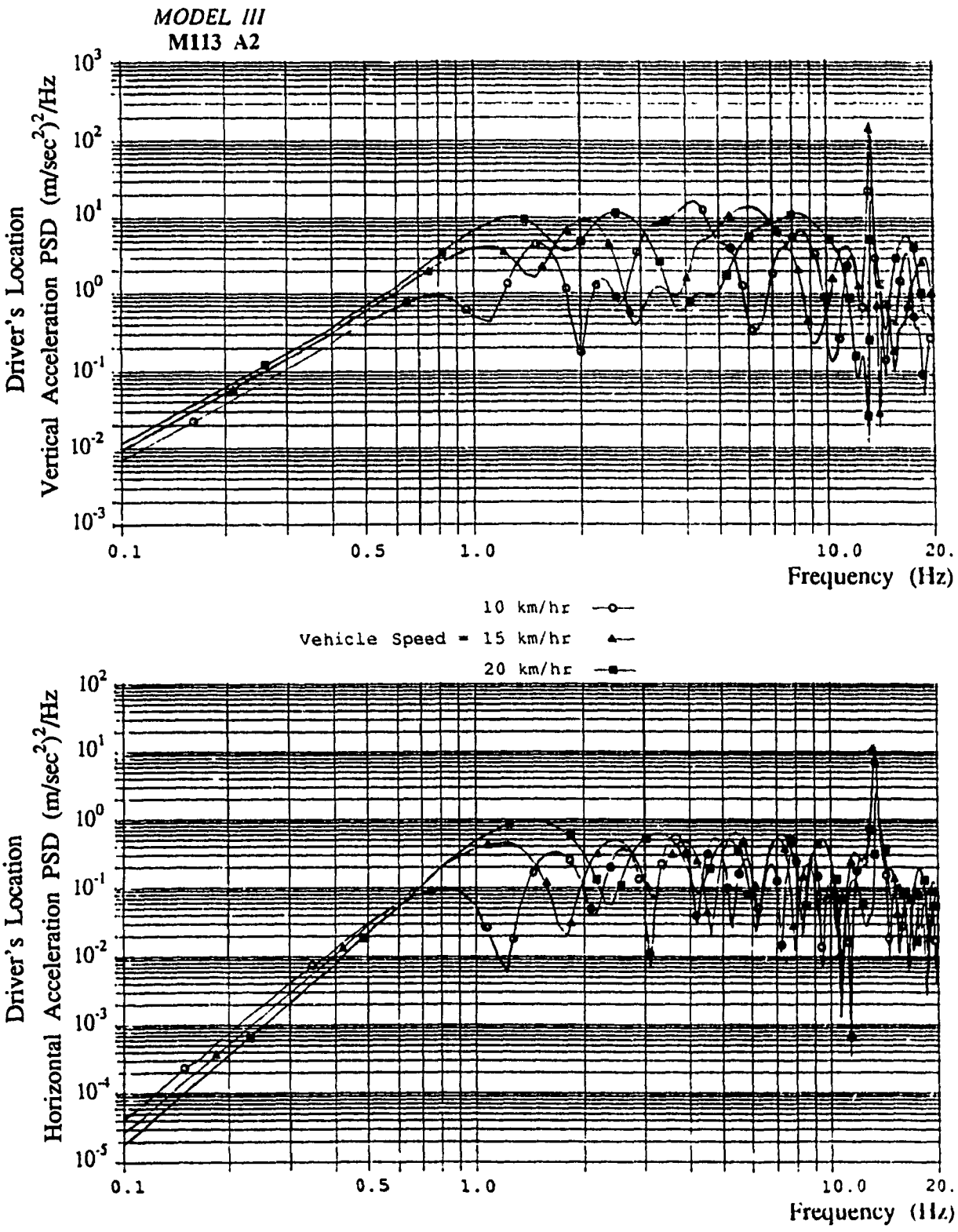

Figure 5.7 PSD of Acceleration Response at the Driver's Location of Multi-Wheeled M113 A2 Vehicle (*MODEL III*), Traversing Plowed Field at Various Speeds.

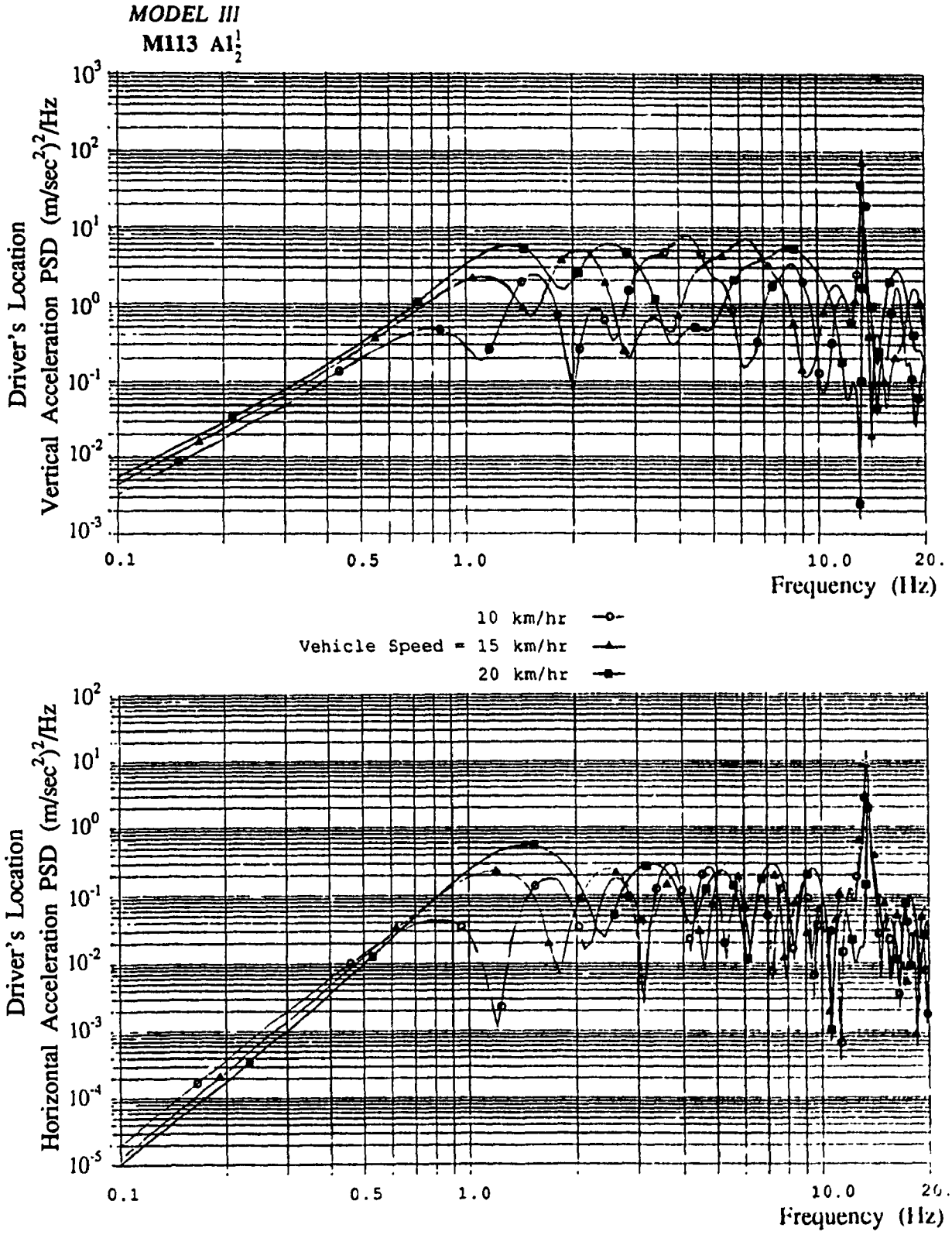

Figure 5.8 PSD of Acceleration Response at the Driver's Location of Multi-Wheeled M113 A1 Vehicle (*MODEL III*), Traversing Pasture at Various Speeds.

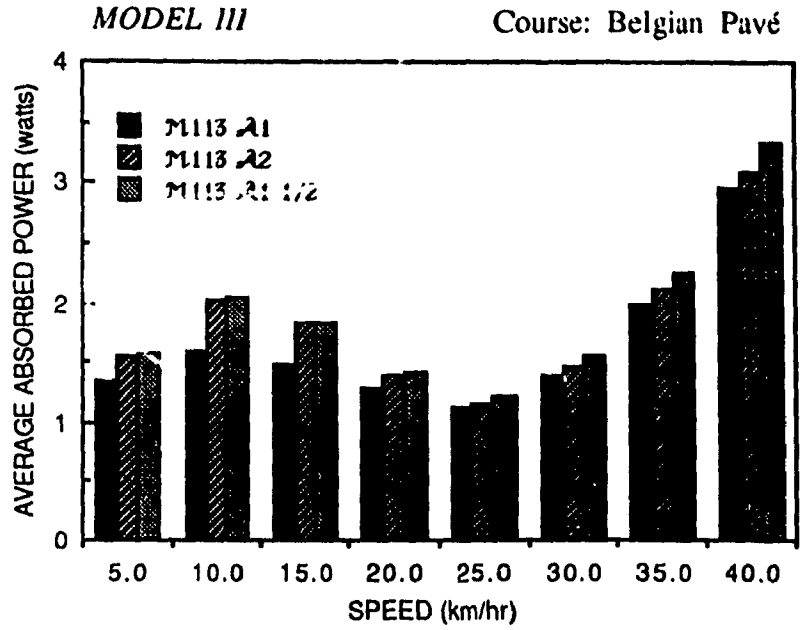

Figure 5.9 Total Average Absorbed Power at the Driver's Location of Multi-Wheeled M113 Vehicles Traversing Belgian Pavé.

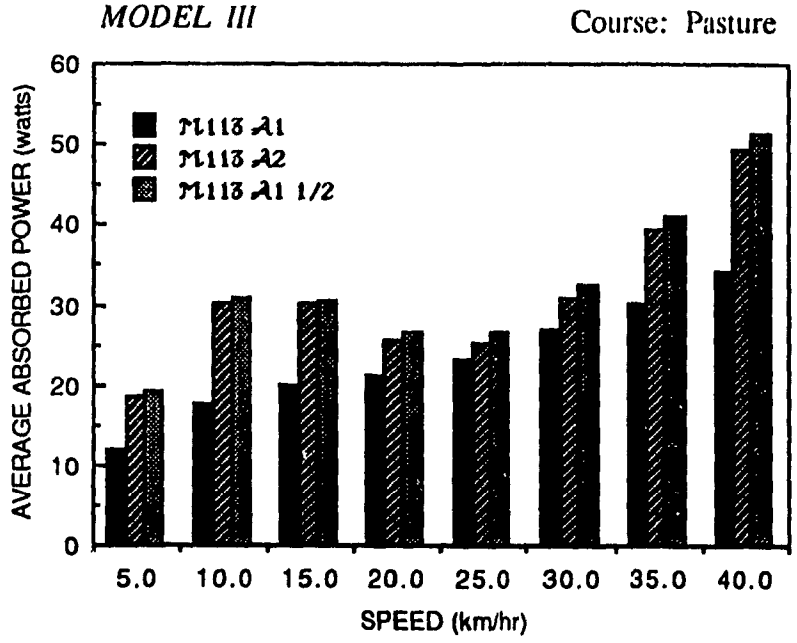

Figure 5.10 Total Average Absorbed Power at the Driver's Location of Multi-Wheeled M113 Vehicles Traversing Pasture.

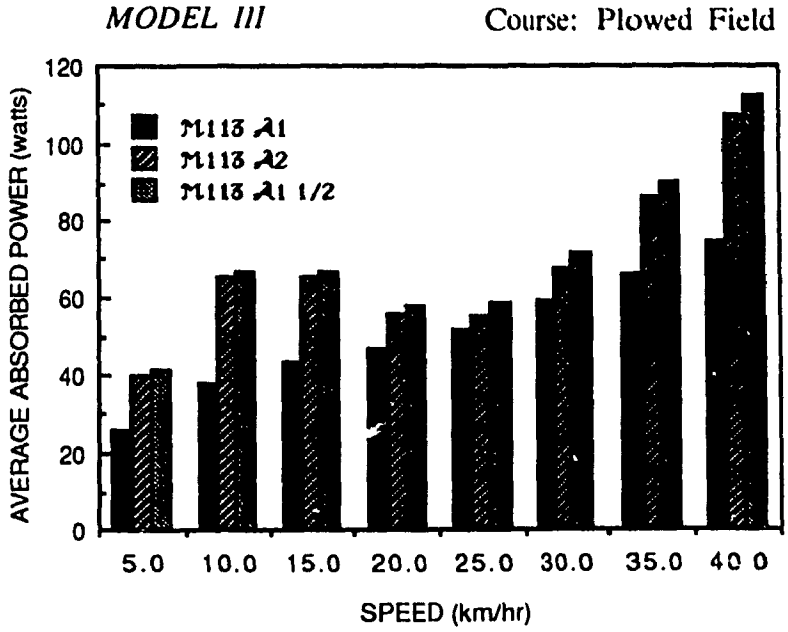

Figure 5.11 Total Average Absorbed Power at the Driver's Location of Multi-Wheeled M113 Vehicles Traversing Plowed Field.

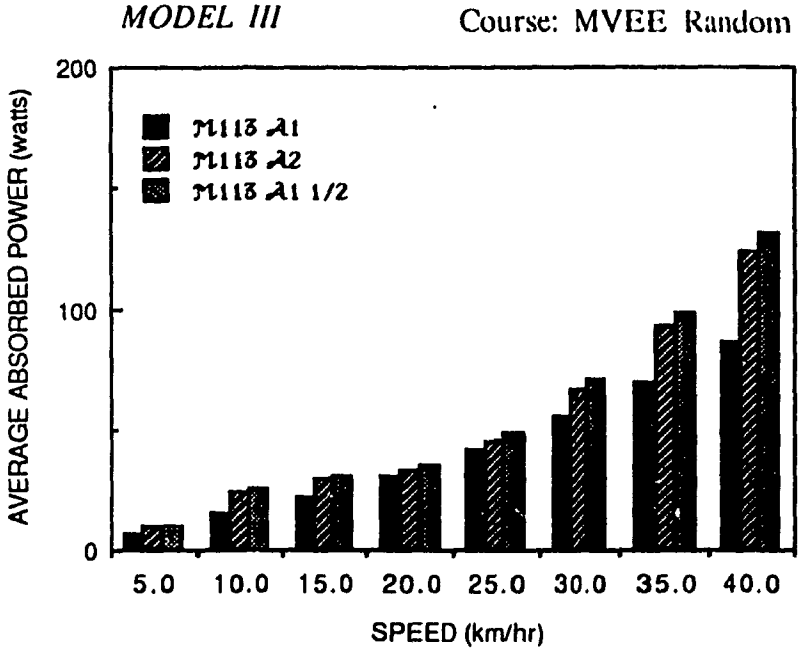

Figure 5.12 Total Average Absorbed Power at the Driver's Location of Multi-Wheeled M113 Vehicles Traversing MVEE Random Course.

absorbed power increases gradually for vehicle speeds above 30 km/hr. The absorbed power of horizontal vibrations at the driver's seat increases steadily with increase in vehicle speed. At low speeds, the M113 A1 vehicle exhibits slightly better ride quality than the M113 A2 and M113 A1$\frac{1}{2}$. The ride quality of M113 A2 vehicle, however, is slightly superior to A1$\frac{1}{2}$ and A1 vehicle configurations at higher speeds, particularly at 40 km/hr. A comparison of total absorbed power of ride vibrations of vehicle *Model III* (Table 5.6) and *Model IV* (Table 5.10) reveals that the ride quality of a tracked vehicle is superior to that of the untracked vehicle.

The absorbed power quantities of vertical and horizontal vibrations for the M113 vehicle traversing the pasture are summarized in Table 5.11, for various vehicle speeds. Absorbed power associated with the vertical and horizontal vibration response at the driver's seat location increases gradually with increase in vehicle speed. Absorbed power quantities of the M113 vehicle traversing pasture are considerably higher than those of the vehicle traversing the Belgian pavé. For the rough pasture, the M113 A1 vehicle exhibits superior ride quality than the M113 A2 and M113 A1$\frac{1}{2}$ vehicles.

The absorbed power quantities of ride vibration response of M113 vehicle configurations traversing a plowed field at various speeds are summarized in Table 5.12. Increased terrain roughness of the plowed field yields considerably large absorbed power quantities than those realized while traversing Belgian pavé and pasture. The response characteristics of M113 A1 vehicle are considerably superior to those of M113 A2 and M113 A1$\frac{1}{2}$ vehicles. The absorbed power quantity increases with increase in vehicle speed for all three suspension configurations,

TABLE 5.10

RIDE QUALITY OF TRACKED M113 VEHICLE MODEL WITH TRAILING ARM SUSPENSION

Course: Belgian Pave

VEHICLE CONFIGURATION	SPEED km/hr	ABSORBED POWER		
		Vertical	Horizontal	Total
M113 A1	5.	0.885	0.061	0.951
	10.	1.095	0.036	1.131
	15.	0.938	0.089	1.026
	20.	0.702	0.146	0.847
	25.	0.569	0.218	0.786
	30.	0.650	0.345	0.995
	35.	1.020	0.555	1.575
	40.	1.692	0.820	2.512
M113 A2	5.	0.912	0.066	0.978
	10.	1.224	0.046	1.270
	15.	0.992	0.066	1.058
	20.	0.695	0.120	0.815
	25.	0.561	0.207	0.768
	30.	0.706	0.346	1.052
	35.	1.078	0.542	1.620
	40	1.689	0.791	2.480
M113 A1$\frac{1}{2}$	5.	0.931	0.073	1.004
	10.	1.231	0.048	1.279
	15.	0.996	0.071	1.007
	20.	0.706	0.134	0.840
	25.	0.582	0.234	0.816
	30.	0.739	0.394	1.132
	35.	1.145	0.626	1.171
	40.	1.829	0.925	2.754

TABLE 5.11

RIDE QUALITY OF TRACKED M113 VEHICLE MODEL WITH TRAILING ARM SUSPENSION

Course: Pasture

VEHICLE CONFIGURATION	SPEED km/hr	ABSORBED POWER		
		Vertical	Horizontal	Total
M113 A1	5.	7.281	0.654	7.935
	10.	10.51	0.680	11.190
	15.	10.79	1.258	12.048
	20.	10.23	2.404	12.634
	25.	10.25	3.199	13.449
	30.	12.23	3.562	15.972
	35.	14.77	3.653	18.423
	40.	17.94	3.596	21.536
M113 A2	5.	10.73	0.937	11.667
	10.	17.34	0.925	18.265
	15.	15.61	1.429	17.039
	20.	12.14	2.798	14.938
	25.	11.65	4.157	15.807
	30.	14.78	5.069	19.849
	35.	19.85	5.553	25.403
	40	26.13	5.728	31.858
M113 A1$\frac{1}{2}$	5.	11.14	1.056	12.196
	10.	17.56	0.997	18.557
	15.	15.79	1.559	17.349
	20.	12.44	3.264	15.704
	25.	12.08	4.901	16.981
	30.	15.29	5.923	21.213
	35.	20.60	6.405	27.005
	40.	27.15	6.522	33.672

however a dip in absorbed power quantity is observed around the speed range 20-25 km/hr.

The absorbed power quantities of the vertical and horizontal vibration response of the M113 vehicle traversing the MVEE Random course, are summarized in Table 5.13. The absorbed power quantities associated with vertical and horizontal vibrations at the driver's seat increase rapidly with increase in vehicle speed. The M113 A1 exhibits superior ride performance to that of M113 A1$\frac{1}{2}$ and M113 A2 vehicles.

Tables 5.6 thru 5.13 demonstrate the effect of vehicle suspension properties and the track on the ride performance of the M113 vehicle. A comparison of response characteristics of the vehicle with (Tables 5.10-5.13) and without (Tables 5.6-5.9) the track, reveals that addition of the track improves the vehicle ride. Figure 5.13 presents the influence of vehicle speed on the total absorbed power of the A1, A2 and A1$\frac{1}{2}$ suspension systems for varying degree of terrain roughness. Figure 5.13 demonstrates an extremely superior ride quality, below 3.0 watts, when the vehicles are traversing the Belgian pavé at speeds ranging from 5 km/hr to 40 km/hr. The ride quality of the tracked vehicle is considerably deteriorated when traversing rougher courses, independent of the suspension type. Ride quality of the tracked vehicle traversing the MVEE random course may be considered satisfactory at low speeds. However, the MVEE random course yields highest value of total absorbed power when the vehicle is travelling at speeds greater than 25 km/hr. Total average absorbed power of ride response of A2 and A1$\frac{1}{2}$ suspension reveals considerable dip in absorbed power when the vehicle is traversing pasture and plowed field around 20 km/hr, as shown in Figures 5.13b and 5.13c.

TABLE 5.12

RIDE QUALITY OF TRACKED M113 VEHICLE MODEL WITH TRAILING ARM SUSPENSION

Course: Plowed Field

VEHICLE CONFIGURATION	SPEED km/hr	ABSORBED POWER		
		Vertical	Horizontal	Total
M113 A1	5.	15.45	1.447	16.897
	10.	22.12	1.500	23.620
	15.	23.17	2.806	25.976
	20.	22.29	5.331	27.621
	25.	22.63	7.049	29.679
	30.	26.84	7.817	34.657
	35.	32.23	8.001	40.231
	40.	39.02	7.868	46.888
M113 A2	5.	23.20	2.034	25.234
	10.	37.42	2.040	39.460
	15.	33.84	3.178	37.018
	20.	26.36	6.183	32.543
	25.	25.47	9.141	34.611
	30.	32.23	11.12	43.350
	35.	43.20	12.17	55.370
	40	56.75	12.55	69.30
M113 A1$\frac{1}{2}$	5.	24.10	2.295	26.395
	10.	37.92	2.201	40.121
	15.	34.24	3.477	37.717
	20.	27.03	7.226	34.256
	25.	26.39	10.79	37.180
	30.	33.32	13.00	46.320
	35.	44.82	14.04	58.860
	40.	58.94	14.29	73.230

TABLE 5.13

RIDE QUALITY OF TRACKED M113 VEHICLE MODEL WITH TRAILING ARM SUSPENSION

Course: NVEE Random

VEHICLE CONFIGURATION	SPEED km/hr	ABSORBED POWER		
		Vertical	Horizontal	Total
M113 A1	5.	4.249	0.568	4.817
	10.	8.752	1.007	9.579
	15.	11.26	2.939	14.199
	20.	13.63	6.666	20.296
	25.	17.87	9.846	27.716
	30.	25.73	11.90	37.630
	35.	36.12	13.06	49.180
	40.	48.99	13.62	62.610
M113 A2	5.	5.767	0.769	6.536
	10.	13.81	1.242	15.052
	15.	14.88	3.007	17.887
	20.	15.08	7.203	22.283
	25.	20.04	11.87	31.910
	30.	30.88	15.66	46.540
	35.	46.44	18.32	64.760
	40	66.20	20.01	86.210
M113 A1$\frac{1}{2}$	5.	6.086	0.874	6.960
	10.	14.05	1.355	15.405
	15.	15.21	3.330	18.540
	20.	15.72	8.466	24.186
	25.	21.15	14.08	35.230
	30.	32.67	18.45	51.120
	35.	49.39	21.35	70.740
	40.	70.65	23.08	93.730

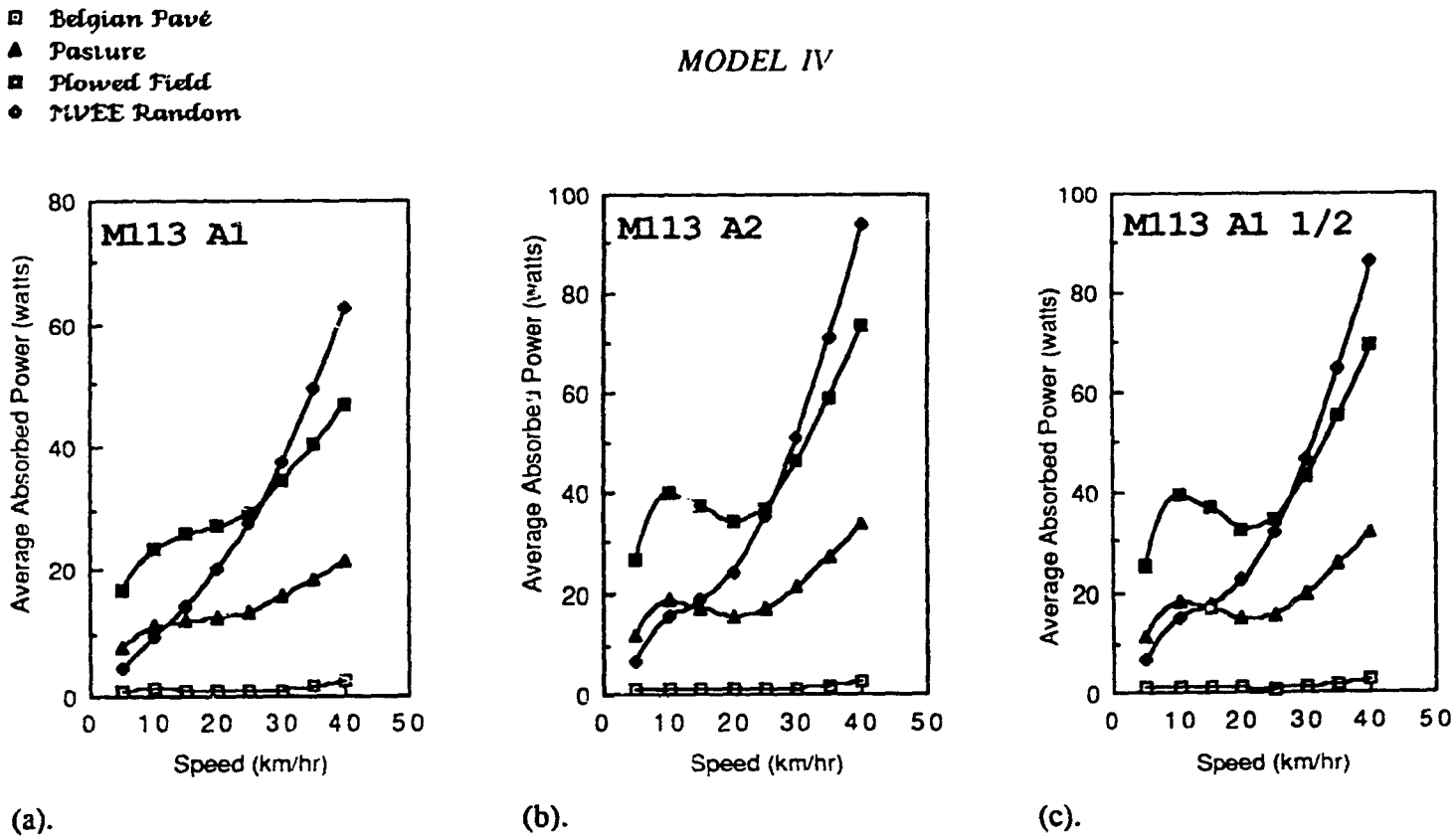

Figure 5.13 Total Average Absorbed Power at the Driver's Location of Tracked M113 Vehicles Traversing Various Terrains.

The bounce acceleration response at the driver's location of the tracked vehicle traversing Belgian pave, equipped with A1 suspension, is presented in Figure 5.14. At low speed (10 km/hr), the bounce acceleration response reveals significant peaks around 1.0 Hz, 4.2 Hz, 7.2, 12, and 16 Hz. Increase in vehicle speed causes the acceleration peak corresponding to 4.2 Hz to shift at a higher frequency, as shown in Figure 5.14. Since the human body is most fatigue sensitive to vertical vibrations in the frequency range 4-8 Hz, the shift in frequency due to increased vehicle speed yields reduced values of the average absorbed power. A similar behavior is also observed in the bounce acceleration response of A2 and A1$\frac{1}{2}$ suspension systems subjected to excitations arising from plowed field and pasture, respectively, as shown in Figures 5.15 and 5.16.

A comparison of the ride performance characteristics of A1, A2 and A1$\frac{1}{2}$ suspension configurations traversing various terrains is presented in Figures 5.17-5.20. The bar graphs clearly demonstrate the superior performance of A1 suspension for all the terrains considered in this study. It can also be observed that the tracked vehicle equipped with A1$\frac{1}{2}$ suspension yields the worst ride performance.

5.5 PARAMETRIC SENSITIVITY ANALYSIS

Total absorbed power quantities associated with ride vibrations at the driver's location of the tracked vehicle revealed the following:

(i) The ride quality of the tracked vehicle is highly influenced by vehicle speed and running gear characteristics

(ii) The interactions of the track contribute to the improvement of vehicle ride

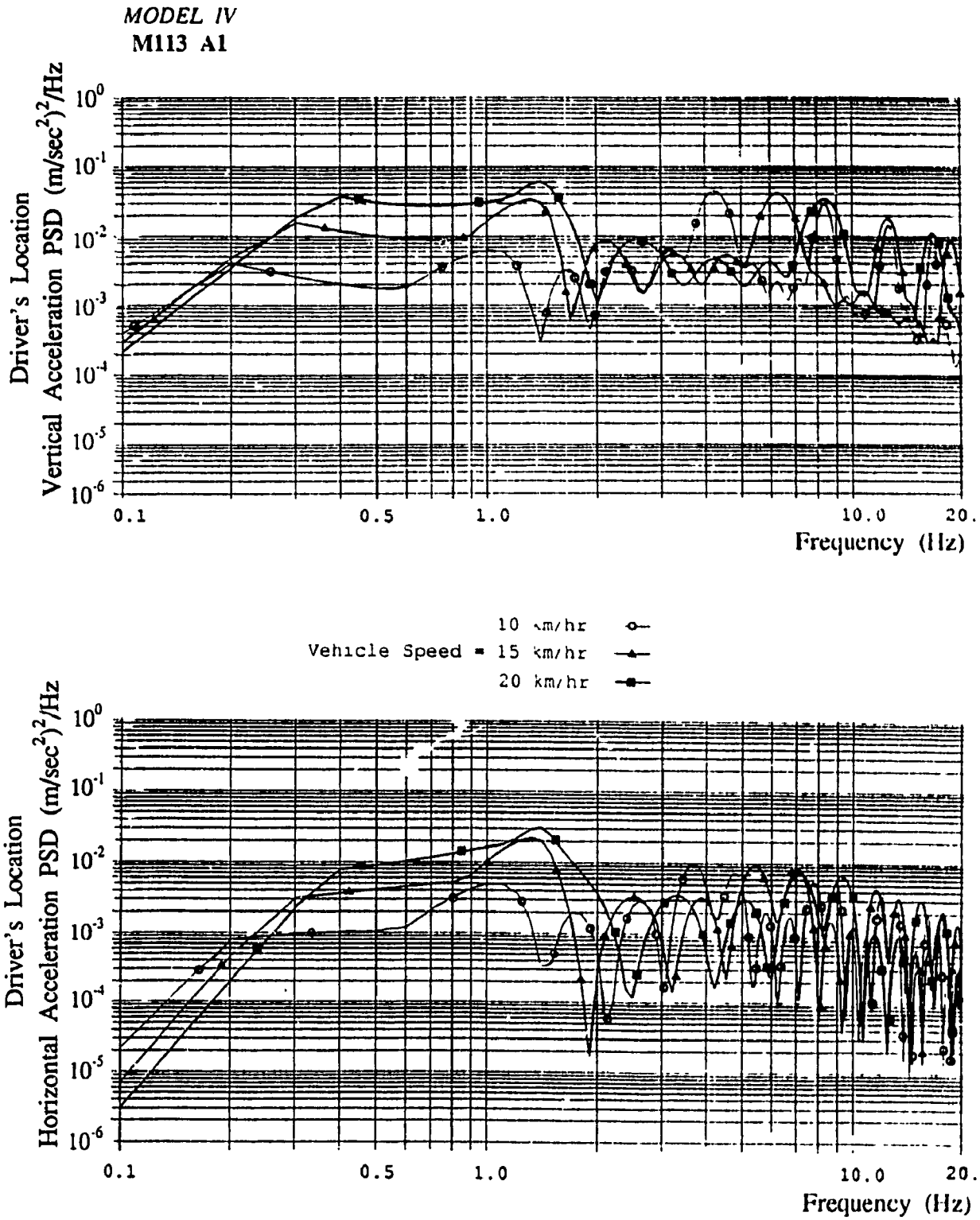

Figure 5.14 PSD of Acceleration Response at the Driver's Location of Tracked M113 A1 Vehicle (*MODEL IV*), Traversing Belgian Pavé at Various Speeds.

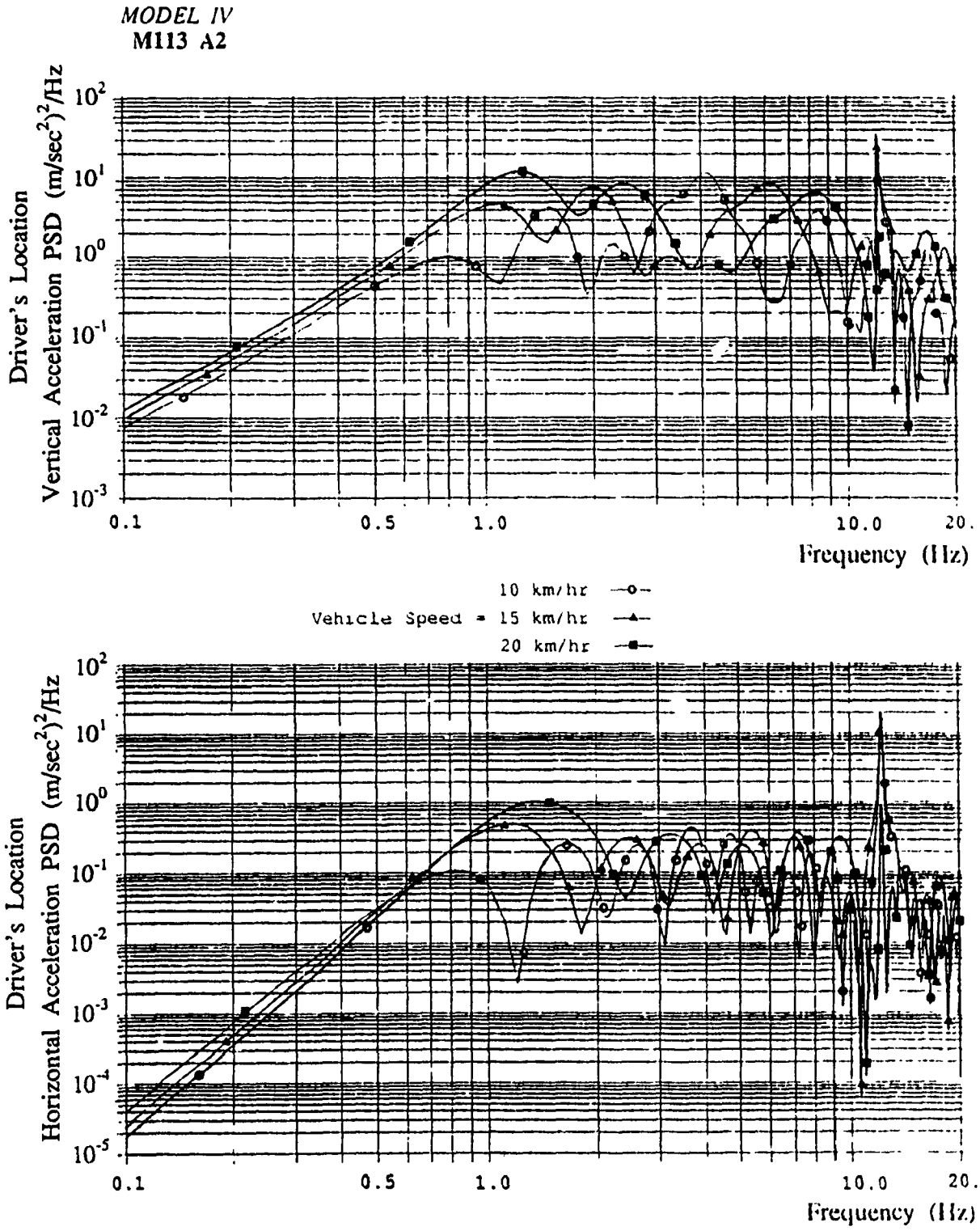

Figure 5.15 PSD of Acceleration Response at the Driver's Location of Tracked M113 A2 Vehicle (*MODEL IV*), Traversing Plowed Field at Various Speeds.

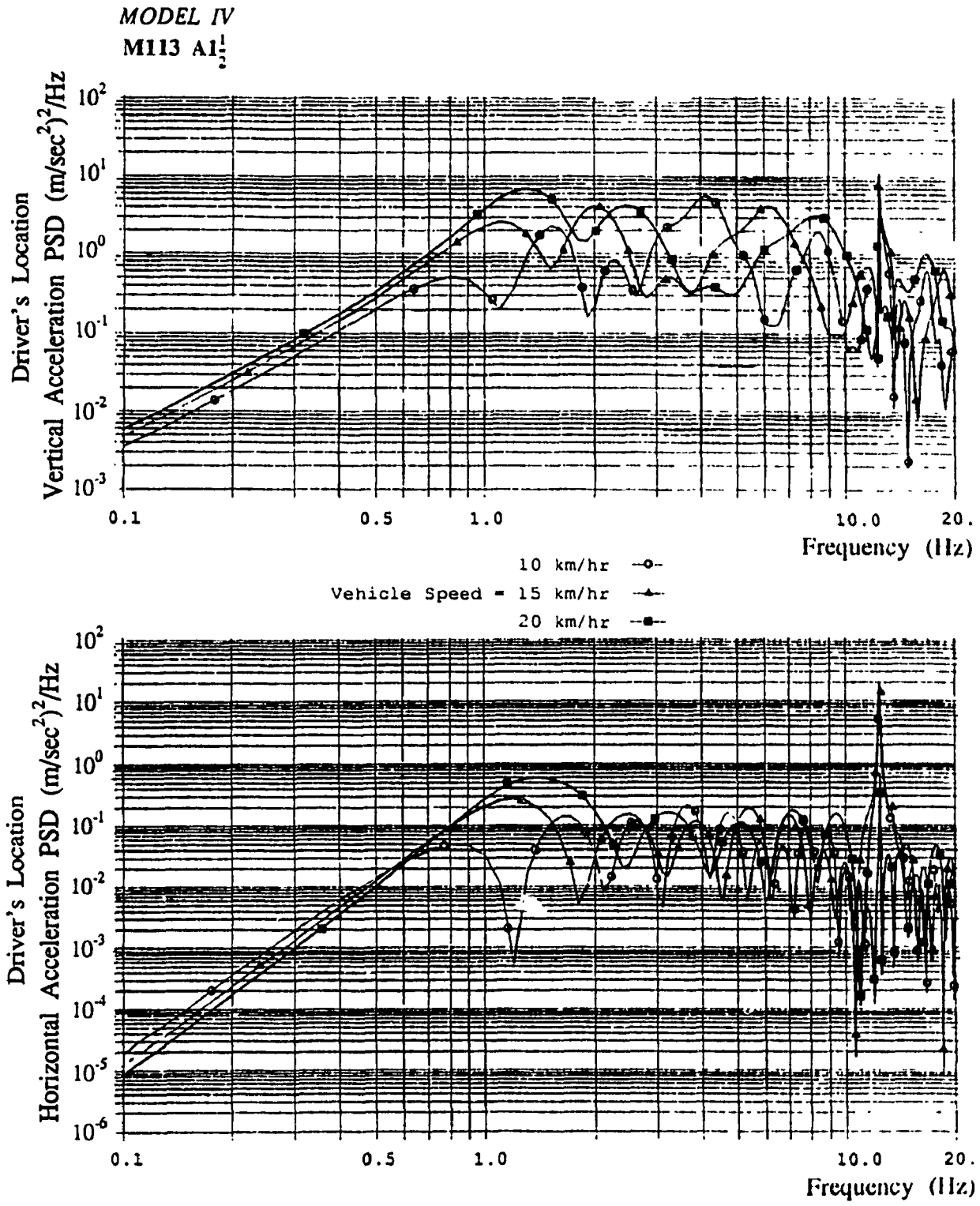

Figure 5.16 PSD of Acceleration Response at the Driver's Location of Tracked M113 A1 Vehicle (*MODEL III*), Traversing Pasture at Various Speeds.

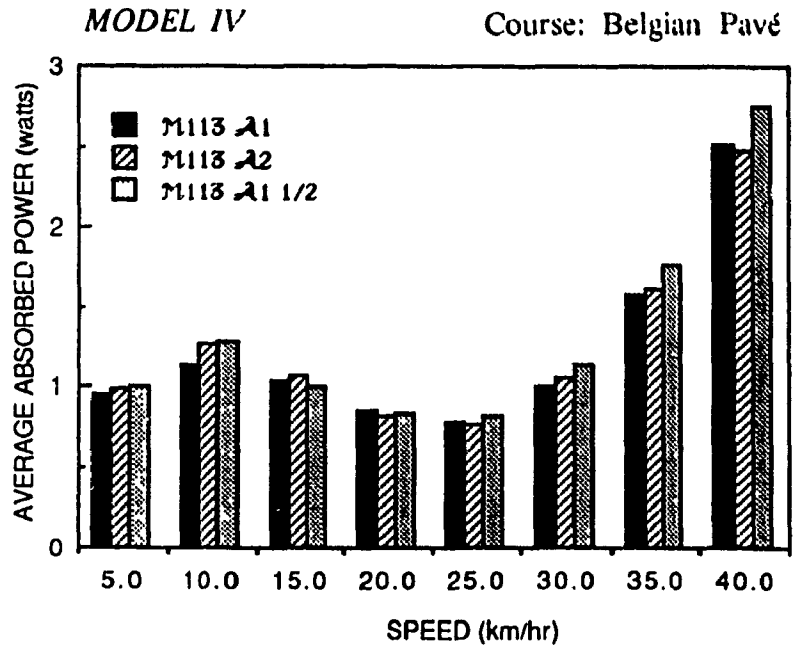

Figure 5.17 Total Average Absorbed Power at the Driver's Location of Tracked M113 Vehicles Traversing Belgian Pavé.

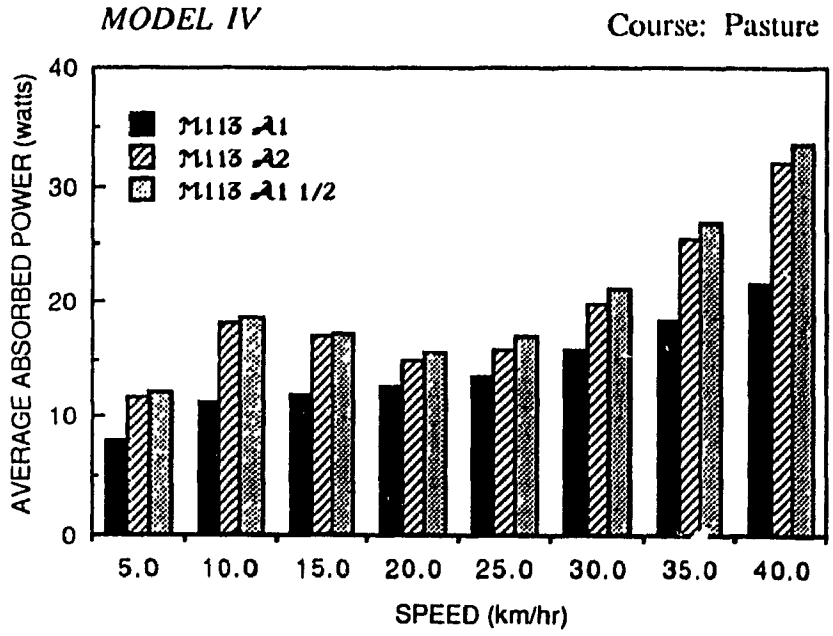

Figure 5.18 Total Average Absorbed Power at the Driver's Location of Tracked M113 Vehicles Traversing Pasture.

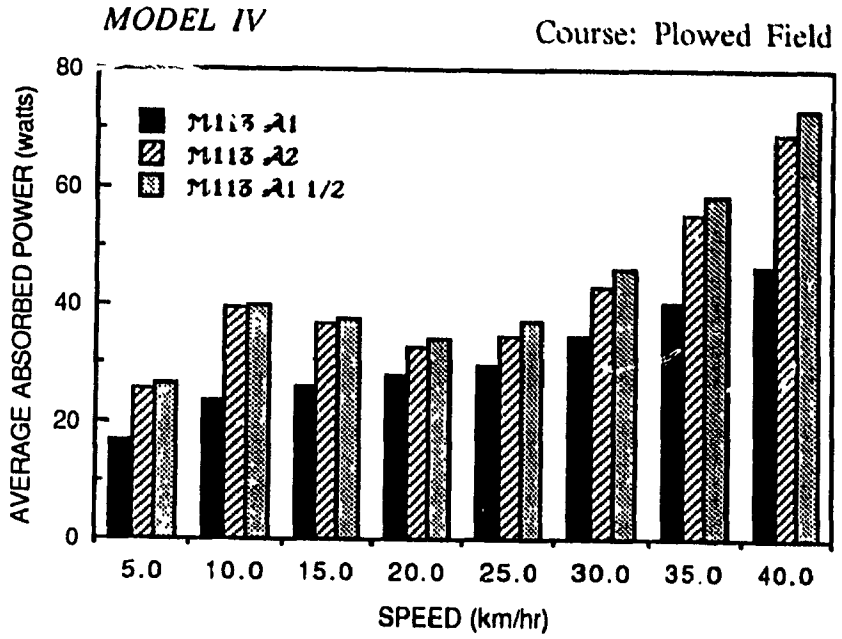

Figure 5.19 Total Average Absorbed Power at the Driver's Location of Tracked M113 Vehicles Traversing Plowed Field.

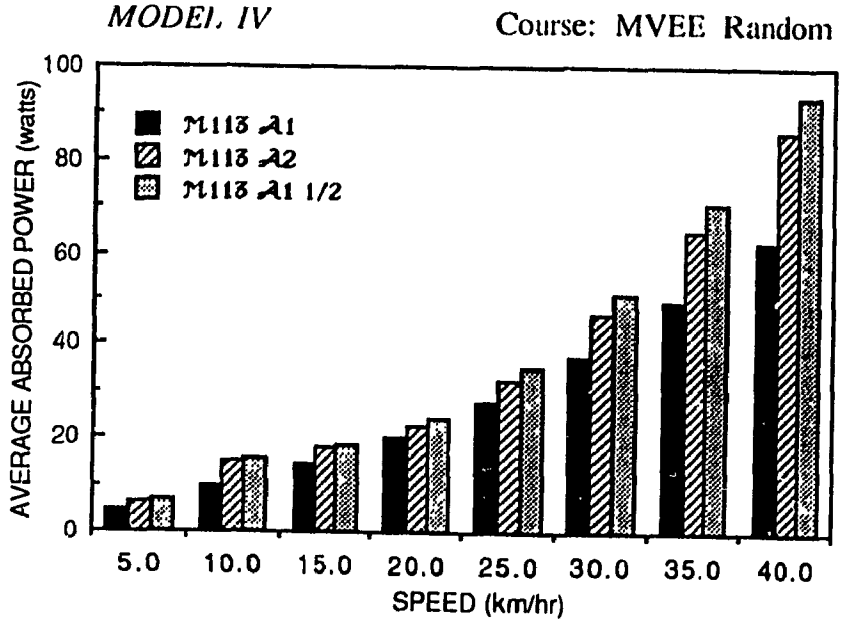

Figure 5.20 Total Average Absorbed Power at the Driver's Location of Tracked M113 Vehicles Traversing MVEE Random Course.

(iii) Heavily damped shock absorbers and stiff torsion bars within the A1$\frac{1}{2}$ suspension yield worst ride performance

In view of the above, parametric sensitivity analyses are carried out to study the influence of suspension and track parameters on the vehicle ride quality and to arrive at near optimal suspension parameters.

5.5.1 Influence of Suspension Damping on the Vehicle Ride Quality

The ride quality of the M113 vehicle is strongly influenced by the suspension damping parameter as evidenced from the absorbed power quantities of A1, A2 and A1$\frac{1}{2}$ suspension systems. The influence of suspension damping on the ride quality is investigated by varying the damping coefficients corresponding to low and high piston velocities (C_{1i} and C_{2i}) in the vicinity of nominal values for A1 and A2 suspensions.

M113 A1:

C_{1i} = 5.0, 12.5, 16.89, and 22.52† kN·sec/m

C_{2i} = 1.15, 2.5, 3.45, and 4.657† kN·sec/m i = 1, 5

M113 A2 and M113 A1$\frac{1}{2}$:

C_{1i} = 5.0, 22.5, 35.5, and 47.387† kN·sec/m

C_{2i} = 0.6, 3.25, 4.35, and 5.8355† kN·sec/m i = 1, 2, 5

The sensitivity analyses are carried out via computer simulation of the tracked vehicle model wi linkage suspension (*Model IV*), for excitations arising from the rough terrains, such as pasture and MVEE random course. The influence of suspension damping parameters on the vehicle ride quality is investigated when the vehicle is traversing pasture and MVEE random course at speeds ranging from 15-35 km/hr. The influence of damping parameter on the total absorbed power of the ride vibration levels at the driver's seat location is summarized in Tables

5.14 and 5.15.

The parametric sensitivity analyses reveal that a reduction in damping coefficients improves the ride performance of M113 A1, M113 A2 and M113 A1$\frac{1}{2}$ vehicles. However, extremely low values of damping coefficients deteriorate the vehicle ride quality considerably. The absorbed power associated with horizontal vibrations increases considerably with low damping parameter as shown in Tables 5.14 and 5.15. This increase in absorbed power can be attributed to forces arising from the bump stop contact due to extremely low damping. Excessive relative travel of the road wheels, encountered around the hull bounce resonant frequency (1.5 Hz), yields extremely high values of absorbed power associated with vertical and horizontal vibrations. Tables 5.16 and 5.17 present the excitation frequency at which the bump stop contact is encountered and the corresponding absorbed power quantities, when the vehicle traverses over pasture and MVEE random courses, respectively. Total absorbed power, as high as 252.1 watts is realized at the contact frequency (1.6 Hz) for the lightly damped M113 A1 traversing the MVEE random course at a speed of 25 km/hr. A1$\frac{1}{2}$ and A2 suspension system yield total absorbed power of 180.5 watts and 123.48 watts, respectively at the contact frequency, when the vehicle is traversing the MVEE random course at a speed of 25 km/hr. From tables 5.14 and 5.15, it is apparent that an optimal value of damping coefficients exists that will provide an improved vehicle ride. A1 shock absorbers with damping coefficients in the vicinity of C_{11} = 12.5 kN·sec/m and C_{21} = 2.5 kN·sec/m provide improved ride response, while the A2 shock absorbers with damping coefficients in the vicinity of C_{11} = 22.5 kN·sec/m and C_{21} = 3.25 kN·sec/m provide the improved ride

TABLE 5.14

INFLUENCE OF SUSPENSION DAMPING ON VEHICLE RIDE QUALITY

MODEL IV

Course: Pasture

Vehicle Configuration	Speed km/hr	Absorbed Power (Watts)							
		Damping Coefficients C_{1i} ; C_{2i} (kN·sec m⁻¹)							
		C_{1i} = 5.00; C_{2i} = 1.15 $i=1,5$		C_{1i} = 12.50; C_{2i} = 2.50 $i=1,5$		C_{1i} = 16.89; C_{2i} = 3.45 $i=1,5$		C_{1i} = 22.52; C_{2i} = 4.66 $i=1,5$	
		Vertical	Horizontal	Vertical	Horizontal	Vertical	Horizontal	Vertical	Horizontal
M113 A1	15.	4.084	3.103	6.867	1.616	8.647	1.366	10.79	1.258
	25.	7.153	5.535	6.995	3.353	8.230	3.123	10.25	3.199
	35.	20.80	5.074	11.68	3.310	12.58	3.282	14.77	3.653
		C_{1i} = 5.00; C_{2i} = 0.60 $i=1,2,5$		C_{1i} = 22.50; C_{2i} = 3.25 $i=1,2,5$		C_{1i} = 35.50; C_{2i} = 4.35 $i=1,2,5$		C_{1i} = 47.39; C_{2i} = 5.84 $i=1,2,5$	
		Vertical	Horizontal	Vertical	Horizontal	Vertical	Horizontal	Vertical	Horizontal
M113 A2	15.	8.108	21.49	8.036	1.647	12.44	1.390	15.61	1.429
	25.	33.04	93.66	6.380	3.631	8.793	3.674	11.65	4.157
	35.	41.58	82.64	9.481	3.731	14.08	4.390	19.85	5.553
M113 A1	15.	9.088	17.50	8.308	2.028	12.62	1.593	15.79	1.559
	25.	52.25	135.1	7.297	5.047	9.371	4.165	12.08	4.901
	35.	68.14	128.9	11.63	5.171	15.30	5.405	20.60	6.405

TABLE 5.15

INFLUENCE OF SUSPENSION DAMPING ON VEHICLE RIDE QUALITY

MODEL IV

Course: MVEE Random

Vehicle Configuration	Speed km/hr	Absorbed Power (Watts)							
		Damping Coefficients C_{1i} ; C_{2i} (kN·sec/m)							
		C_{1i} = 5.00; C_{2i} = 1.15 $i=1,5$		C_{1i} = 12.50; C_{2i} = 2.50 $i=1,5$		C_{1i} = 16.89; C_{2i} = 3.45 $i=1,5$		C_{1i} = 22.52; C_{2i} = 4.66 $i=1,5$	
		Vertical	Horizontal	Vertical	Horizontal	Vertical	Horizontal	Vertical	Horizontal
M113 A1	15.	42.31	23.14	7.431	4.380	9.047	3.467	11.26	2.939
	25.	86.56	203.2	14.59	11.66	15.42	10.22	17.87	9.846
	35.	161.8	207.3	36.36	13.56	33.90	12.57	36.12	13.06
		C_{1i} = 5.00; C_{2i} = 0.60 $i=1,2,5$		C_{1i} = 22.50; C_{2i} = 3.25 $i=1,2,5$		C_{1i} = 35.50; C_{2i} = 4.35 $i=1,2,5$		C_{1i} = 47.39; C_{2i} = 5.84 $i=1,2,5$	
		Vertical	Horizontal	Vertical	Horizontal	Vertical	Horizontal	Vertical	Horizontal
M113 A2	15.	11.08	34.37	7.768	4.199	11.75	3.195	14.88	3.007
	25.	48.60	133.7	11.91	11.82	15.12	11.04	20.04	11.87
	35.	143.7	232.0	26.44	14.14	34.15	15.25	46.44	18.32
M113 A1	15.	12.81	31.96	8.298	5.126	12.11	3.695	15.21	3.330
	25.	73.57	190.7	14.46	16.32	16.68	13.91	21.15	14.08
	35.	1809.	2275.	34.87	19.84	38.55	18.99	49.39	21.35

TABLE 5.16

ABSORBED POWER DUE TO BUMP STOP FORCES OF LIGHTLY DAMPED VEHICLE SUSPENSION - *MODEL IV*

Course: Pasture

Vehicle Configuration	Speed km/hr	Absorbed Power (Watts)		
		Damping Coefficients C_{1i} ; C_{2i} (kN·sec/m)		
		$C_{1i} = 5.00$; $C_{2i} = 1.15$ $i=1,5$		
		Freq.	Vertical	Horizontal
M113 A1	15.	---	---	---
	25.	---	---	---
	35.	---	---	---
		$C_{1i} = 5.00$; $C_{2i} = 0.60$ $i=1,2,5$		
		Freq.	Vertical	Horizontal
M113 A2	15.	1.5	5.122	15.20
	25.	1.5	26.85	87.06
	35.	1.5	30.96	72.24
M113 A1$\frac{1}{2}$	15.	1.6	5.260	10.06
	25.	1.6	44.26	119.5
	35.	1.6	53.20	114.5

TABLE 5.17

ABSORBED POWER DUE TO BUMP STOP FORCES OF LIGHTLY DAMPED VEHICLE SUSPENSION - *MODEL IV*

Course: MVEE Random

Vehicle Configuration	Speed km/hr	Absorbed Power (Watts)		
		Damping Coefficients C_{1i} ; C_{2i} (kN·sec/m)		
		$C_{1i} = 5.00$; $C_{2i} = 1.15$ $i=1,5$		
		Freq.	Vertical	Horizontal
M113 A1	15.	1.6	36.75	13.43
	25.	1.6	71.50	180.6
	35.	1.6	84.06	180.2
		$C_{1i} = 5.00$; $C_{2i} = 0.60$ $i=1,2,5$		
		Freq.	Vertical	Horizontal
M113 A2	15.	1.5	5.442	16.15
	25.	1.5	29.86	91.19
	35.	1.4-1.6	120.5	189.3
M113 A1$\frac{1}{2}$	15.	1.6	5.558	10.64
	25.	1.6	48.80	131.7
	35.	1.5-1.7	1175.	2210.

response. A comparison of the ride quality of vehicle suspension configurations reveals that A2 suspension with lighter damping can provide the best ride, while A1$\frac{1}{2}$ suspension continues to exhibit poor ride due to relatively stiffer suspension.

† defines nominal value of suspension damping

5.5.2 Influence of Suspension Stiffness on the Vehicle Ride Quality

Influence of suspension stiffness on the ride performance of the M113 vehicle is investigated by varying torsional stiffness of the torsion bars. The parametric sensitivity analyses are carried out for the following spring rates of A1 and A2 torsion bars.

M113 A1: $K_{\theta i}$ = 7.5, 9.884†, and 12.0 kN·m/rad $i = 1, \ldots, 5$

M113 A2: $K_{\theta i}$ = 6.25, 8.35†, and 10.5 kN·m/rad $i = 1, \ldots, 5$

The total absorbed power due to vertical and horizontal vibrations at the driver's location are computed for excitations arising from pasture and MVEE random courses, and the results are summarized in Tables 5.18 and 5.19, respectively. The sensitivity analyses revealed that softer torsion bars offer considerable improvement in vehicle ride for all vehicle speeds.

† defines nominal suspension stiffness parameter

5.5.3 Influence of Track Tension on the Vehicle Ride Quality

The influence of track tension on the ride dynamic response of the M113 vehicle is investigated by varying the track tension parameter, for excitations arising from pasture and MVEE random courses. Spring rates representing the tension of each track are selected as follows:

M113 A1, M113 A2 and M113 A1$\frac{1}{2}$: μ_w = 49254., 65672.†, and 82090. N/m

The influence of track tension on the average absorbed power associated with vertical and horizontal vibrations at the driver's seat

TABLE 5.18

INFLUENCE OF SUSPENSION STIFFNESS ON VEHICLE RIDE QUALITY

MODEL IV

Course: Pasture

Vehicle Configuration	Speed km/hr	Absorbed Power (Watts)					
		Stiffness Coefficients $K_{\theta i}$ (N·m/rad)					
		$K_{\theta i}$ = 7500. i=1,...,5		$K_{\theta i}$ = 9884. i=1,...,5		$K_{\theta i}$ = 12000. i=1,...,5	
		Vertical	Horizontal	Vertical	Horizontal	Vertical	Horizontal
M113 A1	15.	10.15	1.004	10.79	1.258	11.47	1.499
	25.	9.525	2.289	10.25	3.199	11.16	4.259
	35.	13.31	2.720	14.77	3.653	16.98	4.805
		$K_{\theta i}$ = 6250. i=1,...,5		$K_{\theta i}$ = 8350. i=1,...,5		$K_{\theta i}$ = 10500. i=1,...,5	
		Vertical	Horizontal	Vertical	Horizontal	Vertical	Horizontal
M113 A2	15.	15.45	1.251	15.61	1.429	15.87	1.609
	25.	11.20	3.312	11.65	4.157	12.28	5.229
	35.	19.31	4.168	19.85	5.553	21.00	6.790

TABLE 5.19

INFLUENCE OF SUSPENSION STIFFNESS ON VEHICLE RIDE QUALITY

MODEL IV

Course: MVEE Random

Vehicle Configuration	Speed km/hr	Absorbed Power (Watts)					
		Stiffness Coefficients K_{θ_i} (N-m/rad)					
		K_{θ_i} = 7500. $i=1,\ldots,5$		K_{θ_i} = 9884. $i=1,\ldots,5$		K_{θ_i} = 12000. $i=1,\ldots,5$	
		Vertical	Horizontal	Vertical	Horizontal	Vertical	Horizontal
M113 A1	15.	10.38	2.257	11.26	2.939	12.21	3.565
	25.	15.75	6.852	17.87	9.846	20.40	13.25
	35.	29.40	9.339	36.12	13.06	44.65	17.55
		K_{θ_i} = 6250. $i=1,\ldots,5$		K_{θ_i} = 8350. $i=1,\ldots,5$		K_{θ_i} = 10500. $i=1,\ldots,5$	
		Vertical	Horizontal	Vertical	Horizontal	Vertical	Horizontal
M113 A2	15.	14.54	2.550	14.88	3.007	15.36	3.453
	25.	18.88	9.325	20.04	11.87	21.66	15.05
	35.	43.88	14.96	46.44	18.32	50.85	22.71

location is summarized in Tables 5.20 and 5.21, for excitations arising from pasture and MVEE random course, respectively. The results reveal that variations in track tension do not alter the vehicle ride considerably. However, a slight improvement in vehicle ride can be achieved by increasing track tension. A stiffer track also limits the road wheel motion considerably.

† defines nominal track tension parameter

5.6 SUMMARY

The ride quality of the M113 vehicle configurations is investigated for excitations arising from undeformable random terrains. Various methods of ride quality assessment are discussed and a methodology based upon average absorbed power is selected to assess the ride quality of the M113 vehicles. Ride dynamic performance of the multi-wheeled/ tracked vehicle is evaluated in terms of absorbed power quantities associated with vertical and horizontal vibration at the driver's seat location. The ride quality of the M113 vehicle configurations is investigated for various vehicle speeds and selected terrains, namely; Belgian pavé, pasture, plowed field and MVEE random course. Parametric sensitivity analyses are carried out to study the influence of running gear parameters on the ride quality of the tracked vehicles.

TABLE 5.20

INFLUENCE OF TRACK TENSION ON VEHICLE RIDE QUALITY

MODEL IV

Course: Pasture

Vehicle Configuration	Speed km/hr	Absorbed Power (Watts)					
		Track Tension μ_w (N/m)					
		μ_w = 49254.		μ_w = 65672.		μ_w = 82090.	
		Vertical	Horizontal	Vertical	Horizontal	Vertical	Horizontal
M113 A1	15.	10.88	1.302	10.79	1.258	10.71	1.217
	25.	10.53	3.302	10.25	3.199	9.997	3.102
	35.	15.19	3.770	14.77	3.653	14.38	3.542
M113 A2	15.	15.69	1.488	15.61	1.429	15.54	1.375
	25.	11.90	4.299	11.65	4.157	11.42	4.023
	35.	20.33	5.734	19.85	5.553	19.40	5.381
M113 A1[illegible]	15.	15.88	1.621	15.79	1.559	15.71	1.502
	25.	12.34	5.068	12.08	4.901	11.85	4.742
	35.	21.07	6.615	20.60	6.405	20.17	6.206

TABLE 5.21

INFLUENCE OF TRACK TENSION ON VEHICLE RIDE QUALITY

MODEL IV

Course: MVEE Random

Vehicle Configuration	Speed km/hr	Absorbed Power (Watts) Track Tension μ_w (N/m)					
		μ_w = 49254.		μ_w = 65672.		μ_w = 82090.	
		Vertical	Horizontal	Vertical	Horizontal	Vertical	Horizontal
M113 A1	15.	11.46	3.037	11.26	2.939	11.09	2.847
	25.	18.44	10.18	17.87	9.846	17.36	9.535
	35.	37.00	13.50	36.12	13.06	35.32	12.63
M113 A2	15.	15.02	3.126	14.88	3.007	14.75	2.897
	25.	20.56	12.29	20.04	11.87	19.57	11.48
	35.	47.53	18.95	46.44	18.32	45.42	17.73
M113 A1E1	15.	15.37	3.457	15.21	3.330	15.07	3.211
	25.	21.68	14.58	21.15	14.08	20.67	13.62
	35.	50.48	22.09	49.39	21.35	48.38	20.66

CHAPTER 6

CONCLUSIONS AND RECOMMENDATIONS FOR FUTURE WORK

6.1 GENERAL

In this thesis, the ride dynamics of M113 personnel carrier vehicle is investigated via computer simulations. A building block simulation approach is used to develop four mathematical ride dynamic models of varying complexities. The initial model is formulated as a seven-degrees-of-freedom dynamic system with each road wheel suspension being idealized as a parallel combination of translational spring and damper, and assuming the track as a massless continuous belt. The influence of track tension on the vehicle ride is investigated by representing the forces due to each track segment as vertical restoring forces, in the second vehicle ride model. The kinematics and dynamics of the independent trailing arm road wheel suspension are incorporated in the third and fourth vehicle ride models. The dynamics due to bump stops, tire stiffness, nonlinear damping, Coulomb friction and gravity are appropriately incorporated in the vehicle models.

Transient response of the nonlinear vehicle models is evaluated for semicircle and block obstacles using numerical integration algorithm. The nonlinear vehicle models are linearized via local equivalent linearization and the linearized models are validated for harmonic excitations. The vibration transmission performance of various M113 vehicle suspensions (A1, A2 and A1$\frac{1}{2}$) is evaluated in terms of vibration transmissibility characteristics.

The random roughness of realistic terrains for military vehicles is characterized by their respective displacement and acceleration spectral

densities. Input spectral density matrix is formulated by taking into account the vehicle speed, spacing of road wheels and terrain roughness. The ride response of linearized multi-wheeled and tracked vehicle models to random terrains is evaluated and presented in terms of power spectral density of acceleration response at the driver's location. Numerous ride assessment criteria are reviewed and the tracked vehicle ride quality is assessed via average absorbed power technique, often used to assess military vehicle ride.

6.2 HIGHLIGHTS OF INVESTIGATION

The major highlights of the investigation are summarized in the following subsections.

6.2.1 Free Vibration Analysis

Free vibration analyses of the vehicle models with and without the track are carried out to establish the undamped and damped natural frequencies of the vehicle. The undamped natural frequencies associated with hull pitch and bounce are found to be in the ranges 1.0 - 1.24 and 1.49 - 1.76 Hz, respectively. The natural frequencies of the road wheel are found to be in the frequency range 11.1 - 15.1 Hz for the idealized suspension models (*Model I & II*), and in the range 10.2 - 14.0 Hz for the linkage suspension models (*Model III & IV*). The undamped natural frequencies associated with hull and road wheel bounce are slightly higher for the A1 vehicle followed by the A1$\frac{1}{2}$ and A2 configurations while pitch natural frequency is slightly higher for the A1$\frac{1}{2}$ vehicle. The undamped natural frequencies of the tracked vehicles are slightly lower than those of the multi-wheeled vehicles. The damped free-vibration analysis demonstrated overdamped road wheel bounce for the A2 vehicle with heavily damped shock absorbers.

6.2.2 Transient Response

Transient response of the multi-wheeled and tracked M113 A1, M113 A2 and M113 A1$\frac{1}{2}$ vehicles is evaluated for deterministic semicircle and block obstacles of different sizes, for various vehicle speeds. The response characteristics reveal the following:

(a) Increase in vehicle speed deteriorates the acceleration response at the driver's location.

(b) M113 vehicles crossing over large obstacles exhibit high levels of vibration at the driver's location and thus the vehicle mobility is limited.

(c) The addition of the track smoothens the transient response in the vehicle speed range 0-25 km/hr.

(d) Comparison of idealized and linkage suspensions reveals that linkage suspension yields low bounce transient response specifically when the vehicle is traversing larger obstacles. However, the tracked vehicle model with linkage suspension exhibits larger pitch transient response than its idealized counterpart. The linkage suspension model thus yields lower levels of vertical vibration and slightly higher levels of horizontal vibration at the driver's location.

(e) The multi-wheeled M113 A2 and M113 A1$\frac{1}{2}$ vehicles yield superior transient response along the hull bounce coordinate than the M113 A1 vehicle. However, the pitch response of M113 A1 vehicle is superior to that of the M113 A2 and M113 A1$\frac{1}{2}$ vehicles. The tracked M113 A1 vehicle model with idealized suspension yields superior bounce and pitch response than the corresponding M113 A2 and M113 A1$\frac{1}{2}$ vehicle models.

(f) Although the M113 A1$\frac{1}{2}$ vehicle employs a stiffer suspension than the M113 A2, both vehicles exhibit almost identical transient response.

6.2.3 Vibration Transmissibility Response of the Vehicle Models

A parametric study is carried out via transmissibility response characteristics of the vehicle models to investigate the system sensitivity to suspension parameters. Influence of parameters, such as variations in shock absorber damping, number and location of shock absorbers, shock absorber inclination, torsion bar stiffness, and track tension on the vibration transmission performance, is investigated and the following conclusions are drawn:

(a) The vibration transmissibility responses of the multi-wheeled and tracked vehicle models exhibit peak amplitudes around the low (hull bounce and pitch) resonant frequency and high (road wheels) resonant frequencies.

(b) There exists an optimal set of damping parameters, below the nominal parameters of the conventional shock absorbers utilized in the M113 vehicles. Selecting the damping coefficients below or above these optimal values deteriorates the response.

(c) Response to variations in number and location of shock absorbers showed significant improvements on hull bounce and pitch by either interchanging shock absorbers amongst intermediate road wheel stations or by placing shock absorbers at all road wheels. Best response can be achieved by applying sufficient damping at all road wheels.

(d) Increase in shock absorber inclination suppresses low frequency amplitudes. The response behaviour of linkage suspension approaches that of the idealized suspension with higher inclination angles.

(e) Increase in torsion bar stiffnesses increases resonant peak amplitudes in all cases.

(f) Variations in track tension has only little effect on the ride response. Increase in track tension can yield only slight improvement in the vibration transmission performance. The increased track tension, however suppresses the excessively high response of the undamped road wheels.

(g) A comparison of the vibration transmissibility response characteristics of the M113 A1, M113 A2, and M113 A1$\frac{1}{2}$ vehicle models, revealed that the M113 A2 provides the best vibration attenuation performance.

(h) Increase in amplitudes of harmonic input increases response amplitudes in all cases.

6.2.4 PSD Response and Average Absorbed Power

Random response simulations were carried out for the vehicle configurations traversing four types of terrain: Belgian pavé, pasture, plowed field and MVEE random course. The random response of the vehicle is presented in terms of PSD of bounce and pitch accelerations at the hull c.g., and PSD of vertical and horizontal accelerations at the driver's compartment. Ride quality is assessed in terms of average absorbed power. Absorbed power quantities are computed for vertical and horizontal vibrations at the driver's location for variations in terrain roughness, vehicle speed and running gear parameters and the following conclusions are drawn:

(a) The M113 A1 provides superior acceleration response as compared to the acceleration response of M113 A2 and M113 A1$\frac{1}{2}$ vehicles. This is clearly substantiated by the total average absorbed power quantities for the three vehicle configurations.

(b) The acceleration PSD responses of the A2 and A1$\frac{1}{2}$ suspensions are quite similar, however the A1$\frac{1}{2}$ stiffer

suspension exhibits slightly higher quantities of absorbed power at the driver's location in the frequency range 0 - 10 Hz.

(c) The linkage suspension model provides superior ride response as compared to the idealized suspensions.

(d) The addition of the track improves ride response significantly, for all the vehicle configurations.

(e) Absorbed power at the driver's location increases considerably with increasing roughness of the terrain.

(f) Absorbed power at the driver's location increases with vehicle speed. This is especially significant for vehicles traversing rough terrains at speeds over 25 km/hr. At lower vehicle speeds, the smoother terrains induce lower levels of vibration and the absorbed power quantity is strongly dependent upon the frequency range considered.

(g) Sufficient decrease in suspension damping leads to improved ride quality. However, further decrease in the damping coefficient deteriorates ride response substantially. Very low suspension damping leads to road wheel-to-bump stop contact in the low frequency range inducing extremely high response acceleration at the driver's location.

(h) Decrease in torsion bar stiffness improves the ride quality of M113 vehicles.

(i) Increase in track tension yields slight improvement in the ride response of M113 vehicles.

6.3 RECOMMENDATIONS FOR FURTHER INVESTIGATIONS

The vehicle models presented in this thesis may serve as a basis in describing the ride dynamics of multi-wheeled and tracked vehicles. The dynamic concepts and mathematical model formulations may be applied to

vehicles other than M113 vehicles such as the M60 or XM1 battle tanks, farm machinery, construction vehicles, etc.

It is recommended, however, that future work be directed to yet a much more realistic and comprehensive mathematical model describing the dynamic behaviour of the tracked vehicle. A submodel representing the driver and driver's seat should be incorporated into the main superstructure. The effect of weight of crew and cargo on the ride dynamics should be studied as well, and this can easily be done by incorporating crew and cargo properties in the hull mass and hull pitch moment of inertia. Most important is a track model involving track loads due to stretching of the track between the sprocket, road wheels, and idler; bridging effect due to track bridging over terrain concavities and finally slack between the sprocket and idler wheel. Horizontal forces on the hull chassis due to track loads occurring at the sprocket and idler should also be considered. The mathematical models can be developed under the large angle assumption. Furthermore, track dynamics due to chordal effects, tension and path, energy dissipation, tension during negotiation of an obstacle, distribution of track tension, pin/bushing stresses and deflections, temperature buildup, and end connector tightening effectiveness as can be computed from available software, should be incorporated into the vehicle models for a more comprehensive representation of the track as well as the overall vehicle dynamics.

Optimization techniques can be employed to evaluate the suspension parameters such that an optimal ride quality is achieved for a class of random terrains. Assessment of vehicle ride quality should also be carried out utilizing the alternative tolerance assessment criteria

since the absorbed power method only provides an average 'one number' rating over some frequency band not indicating actual content at a particular frequency. Finally, experimental results involving the tracked vehicle under study should be obtained to verify the analytical results. Attempts should also be made to incorporate new suspension designs such as active, semi-active or hydropneumatic suspensions onto the existing M113 vehicles.

REFERENCES

1. Hornich, R.J., "Effects of Vibrations on Operators", *Agricultural Engineering*, Dec. 1961, p.674.

2. Rula, A.A., and Nutall Jr., C.J., "An Analysis of Ground Mobility Models", *WES Technical Report No.* M-71-4, U.S. Army Engineer Waterways Experiment Station, Vicksburg, Miss., July 1971.

3. Rakheja, S., and Sankar, S., "Improved Off-Road Tractor Ride Via Passive Cab and Seat Suspension", *ASME Transactions Journal of Vibration, Acoustics, Stress, and Reliability in Design*, Vol. 24, No. 2, April 1984, pp. 305-313.

4. Glotzback, R.W., Wentz, R.A., and Mehta, N.C., "Ride Comfort in Medium and Heavy Duty Trucks", *Passenger Vibration in Transportation Vehicles*, (Eds: Berman, A., and Hannibal, A.J.) *ASME, AMD.*, Vol. 24, 1977, pp. 19-34.

5. Eppinger, R.H., King, A.I., and Lee, R.A., "Experimental and Mathematical Simulation of a Mult-Wheeled Vehicle With and Without an Elastic Track", *Proceedings of the 2nd International Conference on Vehicle Mechanics*, Paris University, Paris, France, Sept. 6-9, 1971, pp. 275-286.

6. Lessem, A.S., and Murphy Jr., N.R., "Studies of the Dynamics of Tracked Vehicles", *WES Technical Report No.* M-72-1, U.S. Army Engineer Waterways Experiment Station, Vicksburg, Miss., June 1972.

7. Hoogterp, F.B., "Interactive Vehicle Dynamics and Ride Evaluation Package", *TARADCOM Laboratory Technical Report No.* 12413, U.S. Army Tank-Automotive Research and Development Command, Warren, Mich., Nov. 1978.

8. Lee, S.M., "The Study of Vibrations Generated by the Tracks of Tracked Vehicles", Keweenaw Research Center, Michigan Technological University, Houghton, Mich., July 1976.

9. "Noise and Vibration Reduction Program on the M-109 Self-Propelled Howitzer", *Report No.* MPC-178, Allison Division Army Tank-Automotive Plant, 1966.

10. Galaitsis, A.G., "TRAXION: A Model for Predicting Dynamic Track Loads in Military Vehicles", *ASME Transactions Journal of Vibration Acoustics, Stress, and Reliability in Design*, Vol. 106, April 1984, pp. 286-291.

11. Garnich, M.R., and Grimm, T.R., "Modeling and Simulation of a Tracked Vehicle", *ASME Proceedings of the International Computers in Engineering Conference and Exhibit on Advanced Automation*, Vol. 2, Las Vegas, Nev., Aug. 12-15, 1984, pp. 591-600.

12. McCullough, M.K., and Haug, E.J., "Dynamics of High Mobility Track Vehicles", *ASME Report No.* 85-DET-95, 1985.

13. Krupka, R.M., "Mathematical Simulation of the Dynamics of a Military Tank", *SAE Technical Series Paper No.* 850416, International Congress and Exposition, Detroit, Mich., Feb. 25 - Mar. 1, 1985.

14. Wheeler, P., "Tracked Vehicle Ride Dynamics Program", *SAE Technical Series Paper No.* 770048, International Congress and Exposition, Detroit, Mich., Feb. 28 - Mar. 4, 1977.

15. Meachom, H.C. Jr., Swain, J.P., Wilcox, J.P., and Doyle, G.R., "Track Dynamics Program", *TARADCOM Laboratory Technical Report No.* 12397, U.S. Army Tank-Automotive Research and Development Command, Warren, Mich.,Oct. 1978.

16. Beck, R.R., and Wehage, R.A., "The Modeling and Simulation of Two Coupled M113 Armored Personnel Carriers", *Proceedings of the 10th Annual Conference on Modeling and Simulation,* Pittsburgh, Penn., Vol. 10, Part 2, 1979, pp. 353-359.

17. Eberle, W.R., and Steele, M.M., "Investigation of Fluidically Controlled Suspension Systems for Tracked Vehicles", *TACOM Report No.* 12072, U.S. Army Tank-Automotive Command, Warren, Mich., Sept. 1975.

18. Salemka, R.M., and Beck, R.R., "Feasibility Analysis and Evaluation of an Adaptive Tracked Vehicle Suspension and Control System", *TACOM Final Report No.* 11893 (LL-146), U.S. Army Tank-Automotive Command, Warren, Mich., June 1975.

19. Petrick, E.N., Janosi, Z.J., and Haley, R.W., "The Use of the NATO Reference Mobility Model in Military Vehicle Procurement", *SAE Technical Series Paper No.* 810373, International Congress and Exposition, Detroit, Mich., Feb. 23 - Feb. 27, 1981.

20. Creighton, D.C., "Revised Vehicle Dynamics Module: User's Guide for Computer Program VEHDYN II", *WES Technical Report No.* SL-86-9, U.S. Army Engineer Waterways Experiment Station, Vicksburg, Miss., May 1986.

21. "Effect of Design Changes on Vehicle Performance, A Limited Study of M35A2 (modified) and the M113A1", *WES Misc. Paper No.* M-72-7, U.S. Army Engineer Waterways Experiment Station, Vicksburg, Miss., April 1972.

22. Nutall Jr., C.J., Rula, A.A., and Dugoff, H.J., "Computer Model for Comprehensive Evaluation of Cross-Country Vehicle Mobility", *SAE Transactions Paper No.* 740426, 1974, pp. 1619-1642.

23. Maclaurin, B., "Progress in British Tracked Vehicle Suspension Systems", *SAE Technical Series Paper No.* 830442, International Congress and Exposition, Detroit, Mich., Feb. 28 - Mar. 4, 1983.

24. Murphy, N.R., "Comparison of Ride and Shock Responses of the M60 STB and M60 HSS/ATB Hybrid Tanks", *WES Technical Report No.* GL-79-2, U.S. Army Engineer Waterways Experiment Station, Vicksburg, Miss., Feb. 1979.

25. Austin, A.J., Hayes, N.F., and Steele, M.M., "Test and Evaluation for the Improvement of Shock Absorbers for the IFV and M113 Vehicles", *TARADCOM Laboratory Technical Report No.* 12490, U.S. Army Tank-Automotive Research and Development Command Warren, Mich., Feb. 1980.

26. Giguere, C., "M113A1 - M113A2 Suspension Comparison", *LETE Engineering Report No.* 2/82, Department of National Defence, Ottawa, Ont., Feb. 1982.

27. Giguere, C., "Maximum Average Speed Test - M113A1, M113A1-1/2, M113A2 APCs", *LETE Engineering Report No.* 77201-L099, Dept. of National Defence, Ottawa, Ont., Mar. 1982.

28. Vodyanik, I.I., "The Motion of a Tracked Vehicle on Deformable Ground", *Journal of Terramechanics,* Vol. 3, No. 1, 1966, pp. 7-11.

29. Kogure, K., "External Motion Resistance Caused by Rut Sinkage of Tracked Vehicles", *Journal of Terramechanics,* Vol. 13, No. 1, 1976, pp. 1-14.

30. Kitano, M., and Kuma, M., "An Analysis of Horizontal Plane Motion of Tracked Vehicles", *Journal of Terramechanics,* Vol. 4, No. 4, 1977, pp. 211-225.

31. Bekker, M.G., *Theory of Land Locomotion,* University of Michigan Press, 1956.

32. Bekker, M.G., "Tracked Vehicles - Terrain Damage and Economy", *SAE Transactions Paper No.* 800953, 1980, pp. 2903-2917.

33. Wong, J.Y., Garber, M., and Preston-Thomas, J., "Theoretical Prediction and Experimental Substantiation of the Ground Pressure Distribution and Tractive Performance of Tracked Vehicles", *Proceedings of the Institution of Mechanical Engineers,* Vol. 198D, No. 15, 1984, pp. 265-285.

34. Bogdanoff, J.L., Kozin, F., and Coté, L.J., "Atlas of Off-Road Ground Roughness PSDs and Report on Data Acquisition Techniques", *ATAC Components Research and Development Laboratories Technical Report No.* 9387 (LL109), U.S. Army Tank-Automotive Center, Warren, Mich., 1966.

35. LaBarre, R.P., Forbes, R.T., and Andrew, S., "The Measurement and Analysis of Road Surface Roughness", *MIRA Report No.* 1970/5, Motor Industry Research Association, 1969.

36. Dodds, C.J., and Robson, J.D., "The Description of Road Surface Roughness", *Journal of Sound and Vibration,* Vol. 31, No. 2, 1973, pp. 175-183.

37. Robson, J.D., "Road Surface Description and Vehicle Response", *International Journal of Vehicle Design,* Vol. 1, No. 1, 1979, pp. 25-35.

38. Wong, J.Y., *Theory of Ground Vehicles,* John Wiley & Sons, New York, 1978.

39. Dokainish, M.A., and Elmadany, M.M., "Dynamic Response of Tractor-Semitrailer Vehicle to Random Input", *Proceedings of 5th VSD - 2nd IUTAM Symposium on The Dynamics of Vehicles on Roads and Tracks*, Technical University Vienna, Austria, Sept. 1977, pp. 237-255.

40. Burden, R.L., Faires, J.D., and Reynolds, A.C., *Numerical Analysis*, 2nd Ed., Prindle, Weber & Schmidt, Boston, Mass., 1981.

41. Harris, C.M., and Crede, C.E., *Shock and Vibration Handbook*, 2nd Ed., McGraw-Hill, New York, 1976.

42. VEHDYN Code Data, Department of National Defence, Suffield Establishment, Ralston, Ala.,1986.

43. FMC Corporation, M113A2 Specifications, San Jose, Calif.

44. DEW Engineering and Development, Ottawa, Ont., 1981.

45. Roberts, J.B., "Response of Non-Linear Mechanical System to Random Excitations, Part 2: Equivalent Linearization and Other Methods", *Shock and Vibration Digest*, Vol. 13, No. 5, May 1981, pp. 15-29.

46. Iwan, W.D., and Yang, I.M., "Application of Statistical Linearization Techniques of Nonlinear Multi-Degrees-of-Freedom Systems", *ASME Transactions Journal of Applied Mechanics*, June 1972, pp. 545-550.

47. Rakheja, S., and Sankar, S., "Local Equivalent Constant Representation of Nonlinear Damping Mechanisms", *Engineering Computations*, Vol. 3, No. 1, Mar. 1986, pp. 11-17.

48. Su, H., "Random Response of Pressure Limited Hydraulic Damper", Technical Report, Concordia University, Montreal, Que., Feb. 1988.

49. Rakheja, S., "Computer-Aided Dynamic Analysis and Optimal Design of Suspension Systems for Off-Road Tractors", Ph.D. Thesis, Concordia University, Montreal, Que., 1983.

50. Bendat, J.S., and Piersol, A.G., *Random Data: Analysis and Measurement Procedures*, John Wiley and Sons, New York, 1971.

51. Stikeleather, L.F., "Review of Ride Vibration Standards and Tolerance Criteria", *SAE Transactions Paper No.* 760413, 1976, pp. 1460-1467.

52. Van Deusen, B.D., "Human Response to Vehicle Vibration", *SAE Transactions Paper No.* 680090, 1968, pp.328-345.

53. Dieckmann, D., "Einfluss Vertikaler Mechanischer Schwingungen auf den Menschen", *Internationale Zeitschrift Angewandte-Physiologie*, Vol. 16, 1957, pp. 519-564.

54. Janeway, R.N., "Passenger Vibration Limits", *SAE Journal*, Vol. 56, Aug. 1948, pp. 48-49.

55. Goldmann, D.E., "A Review of Subjective Responses to Vibratory Motion of the Human Body in the Frequency Range 1 to 70 cps", *Report No.* 4, Naval Medical Research Institute, Mar. 1948.

56. Von Eldik Thieme, H.C.A., "Passenger Riding Comfort Criteria and Methods of Analyzing Ride and Vibration Data", *SAE Paper No.* 295A, Mar. 1961.

57. Butkunas, A.A., "Power Spectral Density and Ride Evaluation", *SAE Transactions Paper No.* 660138, 1966, pp. 681-687.

58. ISO 2631, "Guide for Evaluation of Human Exposure to Whole Body Vibration", International Organization for Standardization, 1974.

59. Military Standard 1472A, "Human Engineering Design Criteria for Military Systems, Equipment and Facilities", Department of Defence, Washington, D.C., 1970.

60. VDI - 2057, "Assessing the Effects of Vibration on Human Beings", *Verein Deutscher Ingenieure*, translated and published by Peter Peregrinus Ltd., 1963.

61. Lee, R., and Pradko, F., "Analytical Analysis of Human Vibration", *SAE Transactions Paper No.* 680091, 1968, pp. 346-370.

62. Pradko, L., Lee, R., and Kaluza, V., "Theory of Human Vibration Response", *ASME Paper No.* 66 WA/BHF-15, 1966.

Courtesy References:

DND DEPARTMENT of NATIONAL DEFENCE of Canada

LETE LAND ENGINEERING and TEST ESTABLISHMENT Department of National Defence of Canada

FMC FORD MOTOR COMPANY San Jose, California, U.S.A.